Characterization of novel excitatory actions of α_{2A}-adrenergic receptors in the bed nucleus of the stria terminalis

By

Nicholas Andrew Harris

Dissertation
Submitted to the Faculty of the
Graduate School of Vanderbilt University
for the degree of
DOCTOR OF PHILOSOPHY
in
Molecular Physiology and Biophysics
August 31, 2018
Nashville, TN

Approved:

Sachin Patel, M.D./Ph.D. (Chair)
Roger J. Colbran, Ph.D.
Terunaga Nakagawa, M.D./Ph.D.
Colleen M. Niswender, Ph.D.
Danny G. Winder, Ph.D. (Thesis Advisor)

DEDICATION

To those struggling with addiction and its consequences

ACKNOWLEDGEMENTS

The work presented in this thesis would not have been possible without the financial support provided by the National Institutes of Health. This work was supported by grants from the National Institute of General Medical Sciences awarded to the Vanderbilt Medical Scientist Training Program (T32GM007347), from the National Institute on Alcohol Abuse and Alcoholism awarded to Danny Winder (R37AA019455), and from the National Institute on Drug Abuse awarded to Danny Winder (R01DA042475) and to me (F30DA042501). Further, thank you to the Canby Robinson Scholar Society for supporting my enrollment in the Vanderbilt Medical School.

Thank you to my advisor Danny Winder for guiding me through my development as a scientist. You have taught me more than you could know about being a great academic, role model, and person. I am lucky to have had the opportunity to work with you and look forward to continuing to learn from you for years to come.

Thank you to my thesis committee members: Sachin Patel (Chair), Roger Colbran, Teru Nakagawa, and Colleen Niswender. Your guidance and mentorship throughout the years, whether it be challenging me to think harder about my problems or enthusiastically supporting me in my endeavors along the way, have made this moment come to fruition.

Thank you to the members of the Winder lab past and present for making the lab the best place to work for the last four years. Thank you to Tiffany Wills, Yuval Silberman, Katie Holleran, Megan Williams, Stephanie Flavin and Bob Matthews for training me to be a competent scientist before I was one. Thank you to Sam Centanni for his never-ending mentorship since joining the lab and Tracy Fetterly for figuring out every single facet of this path with me along the way. Thank you to Austin Isaac, Kevin Merkel, Michelle Xu, and Eghosa Eguakun for their help with both this project and my development as a mentor. Thank you to Elana Milano for everything. Thank you to Oliver Vranjkovic, Anel Jaramillo, James Melchior, Greg Salimando, Rafael Perez, Kellie Williford, Lizzie Hale, and Jordan Brown for their support along the way.

Thank you to my family. Thank you to my parents, Tim and Cindi, for nurturing my curiosity and passion and guiding me to become who I am today. Thank you to every member of the Harris family, Robb, Sabrina, Theodore, Felicity, Dan, Elia, Ricardo, Ximena, Mike, Liz, Lana, Julian, Catie, and Sam, for keeping me grounded and happy. Thank you to the Wolenberg family, Steve, Debbie, Kristen, and Dave, for their enthusiastic love and support. Thank you to Brandy and Maxwell for doggie cuddles and long walks.

Most importantly, thank you to my wife, Kelly. This accomplishment is as much yours as it is mine. Thank you for your endless support.

TABLE OF CONTENTS

Title Page i
Dedication ii
Acknowledgements iii
Table of Contents iv
List of Figures vi
List of Tables viii
Chapter 1: Introduction 1
The physiological and psychological effects of stress 1
Addiction and stress: interactions in pathogenesis and pathophysiology 2
Withdrawal-induced negative affect and stress-induced relapse of drug seeking 4
The brain during protracted abstinence 6
The role of the extended amygdala in protracted abstinence from drug use 6
Long term potentiation of glutamatergic transmission in the dorsolateral BNST 7
LTP of excitatory transmission and intrinsic excitability in the juxtacapsular BNST 14
Expanding the scope of LTP in the BNST – effects of *in vivo* induction on behavior 16
LTP in the BNST – a summary 17
Metabotropic long term depression in the BNST – heterogeneity of stimuli 18
Metabotropic LTD in the BNST – interactions with behavioral history 19
Low frequency stimulation-induced LTD in the BNST 20
Input specificity – where to look and why 21
Cell-type specificity: projection targets and genetic markers 31
Modulation of plasticity: catecholamine receptor modulation 34
Summary of synaptic plasticity in the BNST and contributions to behavior 37
The α_{2A} adrenergic receptor as a molecular target to reverse allostatic changes in plasticity 38
Chapter 2: Dorsal BNST α_{2A}-adrenergic receptors produce HCN-dependent excitatory actions that initiate anxiogenic behaviors 40
Introduction 40
Methods 42
Results 42

Discussion 86
Conclusion 86
Chapter 3: Discussion and Future Directions 94
Contributions of auto- & heteroceptor α_{2A}-ARs to physiology, pharmacology and behavior 94
Further defining the guanfacine-activated BNST neuron and contributions to physiology 100
Pharmacology of *ex vivo* guanfacine-induced cfos expression 105
HCN channel inhibition: effects on BNST physiology and relevant behaviors 107
Postsynaptic G_i-DREADD activation effects within the BNST and the rest of the brain 110
In vivo BNST activity measurements and contributions to behavior 114
The molecular biology of guanfacine-induced cfos expression 116
The implications of competition between pre- and postsynaptic α_{2A}-ARs 117
Overall Conclusions 118
Appendix 120
Presynaptic mechanisms of guanfacine inhibition of glutamate release in the BNST 120
Electrophysiological characterization of guanfacine-activated cfos-eGFP+ BNST neurons after incubation in guanfacine or ZD7288 131
Electrophysiological effects of shRNA-mediated knockdown of BNST HCN channel subunits 138
Effects of HCN1 and HCN2 knockdown in BNST neurons on anxiety-like behavior as assessed by the elevated plus maze 141
Expression of a cAMP-insensitive HCN2 channel does not affect guanfacine-induced cfos expression 144
CNO activation of presynaptic hM4Di expressed in Calca+ parabrachial nucleus afferent terminals inhibits excitatory neurotransmission within the BNST 147
Preliminary data from mechanistic studies on *ex vivo* guanfacine-induced cfos expression 150
Guanfacine minimally affects anxiety-like behavior in the elevated plus maze but may alter BNST activity therein 154
ZD7288 does not affect electrically evoked excitatory field potentials in the BNST 165
Guanfacine enhances the amplitude of spontaneous inhibitory postsynaptic potentials in CRF+ BNST neurons 168
Full- and heteroceptor-specific α_{2A}-AR knockout mice show atypical stress-induced cfos responses relative to wildtype littermates 172
A cell type-specific analysis of transcript profiles within subpopulations of BNST neurons 176
Preliminary data suggests that non-validated ablation of CGRP+ parabrachial nucleus neurons does not affect BNST electrically-evoked field potential inhibition by guanfacine 187

Pharmacological effects on optically evoked excitatory postsynaptic and field potentials in the Thy1-COP4 transgenic mouse line…… 190

LIST OF FIGURES

Figure 1 – Anatomy of glutamatergic and catecholaminergic input to the bed nucleus of the stria terminalis..... 23

Figure 2 – Guanfacine-induced cfos expression in the dBNST is dependent on the expression of α2A-ARs in non-noradrenergic neurons..... 58

Figure 3 – Guanfacine induces cfos expression in dBNST*Adra2a* neurons..... 61

Figure 4 – Incubation of ex vivo dBNST slices with guanfacine is sufficient to induce cfos expression and can be blocked by atipamezole. 65

Figure 5 – Activation of hM4Di in dBNST neurons by clozapine-N-oxide mimics guanfacine-induced cfos expression in vivo..... 69

Figure 6 – dBNST neurons that express cfos after systemic guanfacine administration show a high prevalence of HCN activity. 71

Figure 7 – A majority of *Adra2a*+ dBNST neurons co-express *Hcn2* while a minority co-express *Hcn1*..... 73

Figure 8 – HCN channel inhibition by ZD7288 is sufficient for excitatory actions on glutamatergic transmission within the dBNST..... 77

Figure 9 – Delivery of shRNAs directed against HCN channel subunits to the dBNST occludes guanfacine-induced cfos expression 80

Figure 10 – Activation of hM4Di receptors expressed in dBNST neurons elicits anxiety-like behavior in the elevated plus maze..... 82

Figure 11 – Activation of hM4Di receptors expressed in dBNST neurons elicits GCaMP6f activity increases relative to saline-injected controls..... 86

Figure 12: SNAP25Δ3 mutation affects excitatory transmission in the BNST and its inhibition by α2A-ARs but not GABABRs..... 125

Figure 13: Preliminary data on guanfacine effects on neurotransmission in the central nucleus of the amygdala and hippocampus suggest regional differences. 127

Figure 14: Preliminary data on baclofen effects within the hippocampus of SNAP25Δ3 mice and wild-type littermates. 130

Figure 15: Guanfacine preincubation does not affect electrophysiological characteristics of cfos-eGFP+ BNST neurons after intraperitoneal guanfacine injection 134

Figure 16: ZD7288 preincubation minimally affects postsynaptic electrophysiological parameters of cfos-eGFP+ cells after intraperitoneal guanfacine injection but does affect kinetics of spontaneous transmission..... 137

Figure 17: Expression of shHCN1/2 minimally affects postsynaptic electrophysiological parameters of BNST neurons and spontaneous neurotransmission therein but does specifically affect decay kinetics of spontaneous transmission 140

Figure 18: BNST expression of shHCN1/2 does not affect anxiety-like behavior in the elevated plus maze 143

Figure 19: HCN2 mutant mice that do not show cAMP sensitivity (R591E) maintain guanfacine-induced cfos expression 146

Figure 20: CNO activation of hM4Di expressed in PBN Calca+ neurons inhibits electrically evoked EPSCs in BNST neurons 149

Figure 21: Preliminary data from experiments attempting to either mimic or block guanfacine-induced cfos-eGFP expression in ex vivo BNST brain slices 153

Figure 22: Guanfacine does not affect behavior in the elevated plus maze but does inhibit BNST Ca2+ transients 156

Figure 23: Preliminary data suggests minimal effects of guanfacine injections on transitions during the elevated plus maze relative to saline-injected control animals..... 159

Figure 24: Guanfacine appears to have inhibitory effects on BNST during transitions into the various compartments of the EPM when quantified as imputed calcium transients 161

Figure 25: Inhibitory effects of hM4Di on BNST activity during transitions in the EPM is evident from imputed calcium transients but not raw photometry signal..... 165

Figure 26: Preliminary data suggests that HCN inhibition by ZD7288 minimally affects electrically-evoked excitatory field potential responses recorded in the BNST..... 168

Figure 27: Guanfacine enhances inhibitory tone in CRF+ BNST neurons. 170

Figure 28: Responsivity to guanfacine and stress are dysfunctional in full- and heteroceptor-specific α_{2A}-AR knockout mice 175

Figure 29: Transcript analysis in BNST neuronal subpopulations 184

Figure 30: Guanfacine-initiated changes in transcription across different BNST subpopulations 186

Figure 31: Ablation of CGRP+ parabrachial nucleus does not affect guanfacine-induced inhibition of electrically evoked excitatory field potentials in the BNST 189

Figure 32: Pharmacological investigations of optically evoked field potentials in the BNST of Thy1-COP4 transgenic mice.....195

LIST OF TABLES

Table 1: Overview of LTP studies in the BNST……..7
Table 2: Overview of LTD studies in the BNST……...10

Chapter 1

Introduction

The physiological and psychological effects of stress

Stress is broadly defined as the typical response of an organism to nocuous agents (Selye, 1936). These stimuli, which can be physical, psychological or pharmacologic, induce a typical syndrome that can be separated into two phases: acute response and chronic habituation. The first phase, also known as a general alarm or adaptation reaction, involves a concerted effort by the body to limit bodily harm and release of neuroactive chemicals such as the catecholamines and steroid hormones. Depending on the severity of the acute stressor, the concerted adaptation reaction can either enhance or reduce the ability of an organism to persevere through the experience. This is described by the Yerkes-Dodson Law, which states that arousal affects performance in a difficult task in an inverted U-shaped curve (Dodson, 1915). The second phase of the typical stress response involves invoking allostasis, defined as achieving stability through change, to mitigate potentially damaging effects of continued acute stress responses (Sterling and Eyer, 1981, 1988; Ganzel et al., 2010). While acute stress responses can be adaptive, chronic stress responses are more likely to be maladaptive (McEwen, 2007). Chronic stress can elicit negative effects on the body through a variety of mechanisms. These include direct damage from frequent stress, a lack of adaptation to repeated stress, continued allostatic responses after termination of stress, and compensation in other systems (McEwen, 1998, 2012). Each of these response patterns can perpetuate maladaptive behaviors and increase risk for the development of neuropsychiatric pathology related to stress (Flügge et al., 2004; Arnsten, 2009).

Stress increases risk for the development of neuropsychiatric disorders such as depression, anxiety, and substance abuse, and worsens outcomes for primary medical disorders

such as cardiovascular disease, HIV/AIDS and cancer (Heim and Nemeroff, 2001; Turner and Lloyd, 2003; Cohen et al., 2007; Larzelere and Jones, 2008; Lloyd and Turner, 2008; Scott et al., 2008; Lampert et al., 2016). In the context of primary medical disorders, stress either directly related to the medical condition or due to other factors can also increase the likelihood of developing a secondary psychiatric diagnosis. When quantified as adverse life events, there is a positive correlation between number of these events and likelihood of diagnoses of depression (Kendler et al., 1999) and panic disorder (Faravelli, 1985), especially if the event is dependent on and a result of the subject's own actions. Due to the complexity of the outcomes on pathogenesis and pathophysiology, in addition to the widespread effects of stress on the body and the brain, the mechanism underlying this interaction is unclear but is hypothesized to be the result of allostatic overload after exposure to chronic stress. If broken down into different causative factors, the data suggests that both genetics and environment influence the development of stress and anxiety disorders (Sharma et al., 2016). A better understanding of the neural underpinnings of chronic stress and allostatic overload could have significant effects on the morbidity and mortality of several disease processes. One such disease process is addiction, where stressful life events not only influence development of the disease but can also act as disease-modifying in that it can trigger relapse to drug use after extended periods of abstinence.

Addiction and stress: interactions in pathogenesis and pathophysiology

Addiction is a highly prevalent, chronically relapsing disease (Kessler et al., 2005b). Lifetime prevalence for substance use disorders as defined by the Diagnostic and Statistical Manual (Version IV) is estimated at 14.6% for substance use disorders of any kind and 13.2% for alcohol abuse specifically (Kessler et al., 2005b). Early life and chronic exposure to stress increases the risk of development of addiction to nearly all drugs of abuse. In nicotine addiction,

for example, increased risk for smoking occurs as a result of childhood abuse and household dysfunction, adverse childhood experiences, parental divorce, negative life events, acute and chronic stressors, and perceived stress (Felitti, 1998; Reynolds and Frank, 2000; Kassel et al., 2003). Similar effects have been observed in a number of rodent models of addiction, where acquisition of self-administration for nicotine, amphetamine, cocaine, or heroin is increased after exposure to tail pinch, social defeat, neonatal isolation, or electric footshock (Piazza et al., 1990; Shaham and Stewart, 1994; Haney et al., 1995; Tidey and Miczek, 1997; Will et al., 1998; Kosten et al., 2000; Kabbaj et al., 2001; Goeders, 2003). Thus, stress exposure is permissive in the development of substance use disorders and addiction-like behaviors.

In addition to increasing likelihood of addiction development, stress also impacts likelihood of success in treating the disease as measured by rates of remission and relapse. As diseases, addiction and alcoholism are characterized by bouts of remission and relapse (Lopez-Quintero et al., 2011). Only a minority of patients receive treatment, and for those that do, relapse to use is a common event and susceptibility to relapse can last for years into abstinence (Degenhardt et al., 2013). These high rates of eventual relapse occur in patients with substance use disorders to all drugs of abuse, including cocaine, alcohol, opiates, nicotine, and others, and even in behavioral addictions such as gambling disorder (Ledgerwood and Petry, 2006). Therefore, we consider that the biology underlying these processes have overlapping neural substrates. During the transition from casual drug use to pathologic addiction, brain changes occur that prime those with a substance use disorder to reengage in drug use and relapse to addiction (Koob and Volkow, 2010; George et al., 2012). The process of protracted abstinence after extensive drug use has been effectively modeled in rodents as either extinction training or incubation of drug craving after self-administration or other drug conditioning procedures

(Shalev, 2002; Lu et al., 2004). In both humans and rodents, relapse can be triggered by stressful life events (Brown et al., 1995; Shaham et al., 2000a; Sinha et al., 2011), re-exposure to the drug (De Vries et al., 1998), or even exposure to the environment of or cues associated with drug use (Shaham et al., 2003; Crombag et al., 2008). Here we will focus on the neural basis of stress-induced reinstatement, its neural underpinnings, and potential means of treatment.

Withdrawal-induced negative affect and stress-induced relapse of drug seeking

Addiction is a multifaceted disease with several factors contributing to both development and maintenance of substance dependence and abuse. To tackle this complexity, the addiction cycle can be broken down into three separate phases: 1) a binge-intoxication phase characterized by heavy use and increased drug salience, 2) a withdrawal-negative affect phase characterized by negative emotionality and increased susceptibility to stress, and 3) a preoccupation-anticipation phase characterized by loss of executive control (Koob and Volkow, 2010). Interactions between the stress system and addiction-like behaviors are strongest during the withdrawal and negative affect stage, highlighting the potential for treatments specifically tailored to this phase. For this reason, we will focus on this phase and the changes in neural circuitry that occur therein.

As drug use becomes habitual and withdrawal-induced negative affect becomes prominent, the brain recalibrates such that the homeostatic set point of "normalcy" is not reached in the absence of drug and a new allostatic set point is only reached in the presence of drug. After development of physical dependence and voluntary or involuntary abstinence from drug use, an acute abstinence syndrome occurs which lasts for 4-5 days after development of physical dependence and includes symptoms such as tremors, feelings of tension, restless and insomnia. This syndrome typically precedes a transition to a secondary or protracted abstinence syndrome after acute physical symptoms have subsided. At this time, patients commonly report increased

symptoms of anxiety and depression such as emotional instability, autonomic overactivity, restlessness, and sleep impairment. These psychiatric symptoms can become clinically significant, as severe depression prevalence in alcohol dependence can be as high as 30-70% (Schuckit and Monteiro, 1988) and 80-98% of alcohol-dependent men have repetitive panic attacks or anxiety during withdrawal (Schuckit et al., 1990; Schuckit and Hesselbrock, 1994). The negative emotional states highly prevalent in this phase of the addictive cycle are hypothesized to contribute to relapse susceptibility, specifically in response to stress in the environment (Brownell et al., 1986; Heilig et al., 2010).

Stress-induced relapse to drug-seeking is a well-validated phenomenon in people with substance use disorders that has been extensively and effectively modeled in rodents. Alcoholics and smokers have both been shown to increase consumption in response to stressful situations as compared to situations with low anxiety provocation (Miller et al., 1974; Pomerlau and Pomerlau, 1991; Pelham et al., 1997). In the laboratory, stress imagery induces both cocaine craving and anxiety symptoms such as increased heart rate, salivary cortisol, and subjective anxiety, in cocaine-dependent subjects (Sinha et al., 2000). In rodents, exposure to a brief footshock reinstates previously extinguished drug-seeking behavior in animals dependent on heroin, cocaine, alcohol, and nicotine (Shaham and Stewart, 1995; Erb et al., 1996; Ahmed and Koob, 1997; Buczek et al., 1999), effectively modeling the human conditions. A better understanding of the neural substrates associated with the priming of the brain to respond to these stimuli with drug-seeking will allow for better treatment of people with substance use disorders in the context of stress-induced relapse prevention. We hypothesize that chronic drug use and cycles of relapse induce structural and molecular changes that underlie this increased

susceptibility to relapse and aim to investigate their neural underpinnings and treatment modalities focused on reversing these changes.

The brain during protracted abstinence

The effects of abstinence from drug use on structural changes in the brain have been studied in a number of brain regions. The classical neural pathway for these and related studies is the mesolimbic dopamine system consisting of the projection from the ventral tegmental area (VTA) to the nucleus accumbens (NAc). This projection is engaged during use of all drugs of abuse and leads to dopamine release in the NAc that is critical for reinforcement of drug use, reinstatement of drug-seeking and other drug-related behaviors (Pierce and Kumaresan, 2006). Compelling evidence supports the notion that drug exposure elicits robust changes in plasticity in projection neurons within the mesocorticolimbic dopamine system (Nestler et al., 1993; Kauer and Malenka, 2007; Lüscher and Malenka, 2011). However, the long-term changes in synaptic plasticity in amygdalar and other regions that project into the mesolimbic dopamine system are likely important in the longer-term effects of protracted use and abstinence-related relapse but much less studied. Here we will focus on such changes that occur in the extended amygdala that may contribute to increased relapse propensity in this phase of the addiction cycle.

The role of the extended amygdala in protracted abstinence from drug use

The extended amygdala is a collection of nuclei known to play a key role in addiction-related behaviors (Epping-Jordan et al., 1998; Carboni et al., 2000; Eiler et al., 2003). Composed of the anatomically-related central nucleus of the amygdala (CeA), the bed nucleus of the stria terminalis (BNST), and the shell of the NAc (Alheid and Heimer, 1988; Alheid, 2003), the extended amygdala functions as an integrator of stress and reward information within the brain and is implicated in the withdrawal and negative affect stage of the addictive cycle described

above (Walker and Davis, 2008; Koob, 2009; Jennings et al., 2013; Adhikari, 2014). Specifically, the BNST has a direct projection to the VTA that is critical for and engaged during drug-seeking behavior as well as withdrawal from drugs of abuse (Sartor and Aston-Jones, 2012). In addition, activity in the BNST is critical for both cue- and stress-induced reinstatement of drug-seeking and has been shown to undergo plastic changes during abstinence from drugs of abuse after extended use (Delfs et al., 2000; Shalev et al., 2001; Olive et al., 2002; McFarland et al., 2004). Extensive work has been to characterize synaptic plasticity in the rodent BNST and detail interactions with stress and drug use in animal models. For this reason, it will be the subject of the remainder of this chapter, extending prior analyses of this literature (McElligott and Winder, 2009; Lovinger and Kash, 2015; Normandeau and Dumont, 2017).

Long term potentiation of glutamatergic transmission in the dorsolateral BNST

Early work on synaptic plasticity in the BNST utilized *ex vivo* brain slices to study changes in neurotransmission after electrical stimulation of glutamatergic afferents within coronal sections. Different stimulation protocols can elicit different changes in activity, with long term potentiation (LTP) representing enhanced effect to the same stimulation parameters and long term depression (LTD) diminished effect. Here we will summarize work done on LTP in the BNST before transitioning to LTD. An overview of both LTP and LTD experimental results in the BNST can be seen in Table 1 and Table 2 below, respectively.

Table 1: Overview of LTP studies in the BNST

Type of LTP	Notes	Reference
LTP of excitatory transmission in dlBNST	• Induced by HFS (2x 100 Hz for 1s) • Recorded by field potentials or sharp electrode recordings in *ex vivo* BNST slices (mouse) • Blocked by: NMDAR inhibition, GluN2B KO, GluN2B inhibition • Inhibited by: pre-stimulation 100 mM ethanol (only 0-5 minutes)	• Weitlauf et al 2004 • Weitlauf et al, 2005 • Wills et al 2012

	• Unaffected by: L-type Ca^{2+} channel inhibition, $GABA_A$ inhibition, GluN2A KO, post-stimulation 100 mM ethanol	
CIE-induced enhancement of LTP of excitatory transmission in dlBNST	• Induced by HFS (2x 100 Hz for 1s) • Recorded by field potentials in *ex vivo* BNST slices (mouse) • Blocked by: GluN2B KO, GluN2B inhibition, chronic or acute social isolation, simultaneous chronic social isolation and chronic unpredictable stress • Unaffected by: acute corticosterone administration	• Conrad et al 2011 • Conrad et al 2011 • Wills et al 2012
DA-induced enhancement of STP of excitatory transmission in dlBNST	• Induced by HFS (2x 100 Hz for 1s) • Recorded by field potentials in *ex vivo* BNST slices (mouse) • Blocked by: NMDAR inhibition, CRFR1 antagonist, pan-dopamine receptor antagonist (flupenthixol), D1R KO	• Kash, Nobis et al 2008
LTP of excitatory transmission in oval BNST CRF cells	• Induced by HFS (5x 100 Hz 1s, interval=20s) • Recorded by whole cell electrophysiology in *ex vivo* BNST slices (rat) • Occurs in: all CRF+ BNST neurons • Enhanced by: repeated restrain stress (only in Type III) • Blocked by: intracellular STEP (only in Type III)	• Dabrowska et al 2013
LTP of VSub-amBNST projections	• Induced and recorded *in vivo* by HFS (500 pulses at 400 Hz, 250 us duration) in VSub and electrophysiological recordings in amBNST (rat) • Blocked by: NMDAR inhibition • Induces: potentiation of cocaine-induced locomotor activity (via BNST-VTA projections), anxiolysis (NMDAR-dependent)	• Glangetas et al 2015 • Glangetas et al 2017
LTP of ILC-BNST projections in nicotine self-administration	• Induced and recorded *in vivo* by LFS (10 Hz for 1 minute) in ILC and electrophysiological recordings in BNST (rat) during protracted abstinence • Does not occur in saline self-administration or yoked nicotine controls • Blocked by: NMDAR inhibition, extinction training, CB1R antagonism • Results in: enhanced nicotine seeking	• Reisiger et al 2014

Increased AMPAR/NMDAR ratio in vlBNST	• Observed after cocaine self-administration or with chronic subcutaneous morphine pellet implant in whole-cell recordings from *ex vivo* rat BNST slices • Not seen after: acute cocaine injection, passive administration of cocaine or food	• Dumont et al 2005 • Dumont et al 2008
Increased AMPAR/NMDAR ratio in ovBNST	• Observed after acquisition in cocaine and sucrose self-administration in whole-cell recordings from *ex vivo* rat BNST slices. • Blocked by: *in vivo* GluN2B inhibition (cocaine only) • Results in: no effects on lever pressing for sucrose or cocaine, potentially disrupts reinstatement behaviors.	• deBacker et al 2015
HFS LTP of excitatory transmission and intrinsic excitability of jcBNST neurons	• Induced by HFS (100 Hz for 1s at 10s intervals) in *ex vivo* BNST slices (rat) • LTP-IE characteristics: reduced inward rectification, depolarized RMP, increased membrane resistance, decreased rheobase, decreased firing threshold, increased temporal fidelity of firing • Blocked by: NMDAR inhibition, mGluR5 inhibition, D1R inhibition, alcohol dependence and 4-6 week protracted withdrawal (see below), long-access cocaine self-administration, long-access heroin self-administration • Enhanced by: $GABA_A$ and $GABA_B$ inhibition • Unaffected by: D2R inhibition, alcohol dependence and 0-4 week protracted withdrawal, short-access cocaine self-administration, short-access heroin self-administration	• Francesconi et al 2009 • Francesconi et al 2009
Ethanol withdrawal-induced disruption of LTP of excitatory transmission in jcBNST	• Induced by HFS (100 Hz for 1s at 10s intervals) in *ex vivo* BNST slices (rat) • Observed in animals with escalated dependent alcohol intake induced by exposure to alcohol vapors • Mimicked by: chronic ICV CRF (alcohol naïve animals) • Blocked by: CRFR1 antagonist • Unaffected by: CRFR2 antagonist	• Francesconi et al 2009
LTP-IE in jcBNST neurons	• Observed after self-administration of opioids in *ex vivo* rat BNST slices (only in Type III jcBNST neurons)	• Francesconi et al 2009

	• Does not occur in Type I or Type II jcBNST neurons	

amBNST=anteromedial BNST;BNST=bed nucleus of the stria terminalis; CIE-chronic intermittent ethanol, CRF=corticotropin releasing factor, CRFR1=CRF receptor 1; CRFR2=CRF receptors 2; DA=dopamine; D1R=DA receptor 1; D2R=DA receptor 2; dlBNST=dorsolateral BNST; $GABA_A$=gamma-aminobutyric acid receptor A; $GABA_B$=GABA receptor B; GluN2A=Glutamate NMDAR subunit 2A; GluN2B=Glutamate NMDAR subunit 2B; HFS=high frequency stimulation; ; ICV=intracerebroventricular KO=knockout; LTP=long-term potentiation; LTP-IE=LTP of intrinsic excitability; mGluR5=metabotropic glutamate receptor 5; NMDAR=N-methyl-D-aspartate receptor; RMP=resting membrane potential; STEP=striatal enriched protein tyrosine phosphatase; STP=short-term potentiation; vlBNST=ventrolateral BNST; VTA=ventral tegmental area

Table 2: Overview of LTD studies in the BNST

Type of LTD	Notes	References
Group I mGluR-LTD in dlBNST	• Observed in whole-cell recordings from *ex vivo* BNST mouse slices • Blocked by: CB1R inhibition (mGluR1/5), ERK1 inhibition (mGluR5-only), single injection of cocaine (blocked by *in vivo* mGlu5 antagonism), bath application of cocaine, chronic intermittent ethanol exposure • Unaffected by: ERK2 inhibition, GluA1 inhibition, 10 days withdrawal from single cocaine injection, restraint stress, α_{2A}-AR KO	• Grueter et al 2006 • Grueter et al 2008 • McElligott et al 2010
α_1-AR-LTD in dlBNST	• Observed in whole-cell recordings from *ex vivo* mouse BNST slices • Blocked by: clathrin-dependent endocytosis inhibition, GluA1 inhibition, L-type VGCC, restraint stress, continuous or intermittent ethanol exposure, NET KO, α_{2A}-AR KO • Unaffected by: NMDAR inhibition, mGluR5-inhibition, single exposure to cocaine • Mimicked by: 20 minute (but not 10 minute) 100 uM norepinephrine application	• McElligott et al 2010 • McElligott and Winder 2008
hM3Dq-LTD in dlBNST	• Observed in whole-cell recordings from *ex vivo* mouse BNST slices • Blocked by: PLC inhibition, CB1R inhibition • Results in: anxiogenesis, activation of VTA/PBN/LC	• Mazzone et al 2016
LFS of ILC-aBNST	• Induced by 5 minute 10 Hz stimulation of prefrontal cortex cell bodies *in vivo* and recorded in aBNST neurons (mouse)	• Glangetas et al 2013

projection-induced LTD	• After stress, switches to LTP (glucocorticoid-independent) • Blocked by: NMDAR inhibition, CB1R antagonism, CB1R KO, glutamatergic neuron-specific CB1R KO (both LTD alone and LTD transition to LTP) • Occurs in: VTA-projection neurons as well as unidentified BNST neurons	
HFS of ILC-BNST projection-induced LTD	• Induced and recorded *in vivo* by HFS (500 pulses at 400 Hz, 250 us duration pulse) in ILC and electrophysiology recordings in BNST (rat) • Same protocol induces LTP of VSub-BNST projections • Enhanced by: NMDAR inhibition	• Glangetas et al 2017
LFS LTD in BNST neurons	• Induced by LFS (10 minute 10 Hz) and recorded by whole cell electrophysiology in *ex vivo* BNST neurons (rat) • Blocked by: CB1R antagonism, mGluR5 inhibition, TRPV1 inhibition, MAGL inhibition, PLC inhibition, sarcoplasmic/endoplasmic Ca^{2+} channel blockade • Occluded by: TRPV1 agonism • Enhanced by: FAAH inhibition (subthreshold induction protocol) • Unaffected by: NMDAR inhibition, L-type Ca^{2+} channel inhibition, DAGL inhibition	• Puente et al 2011
LFS LTD in ovBNST neurons	• Induced by LFS (15 minute 1 Hz) and recorded by whole cell electrophysiology in *ex vivo* BNST neurons (rat) • Blocked by: NMDAR inhibition, GluN2B inhibition, cocaine self-administration (maintenance) • Rescued by: GluN2B inhibition (rescue blocked by NMDAR inhibition) • Unaffected by: Sucrose self-administration (maintenance)	• deBacker et al 2015
DSE/STD in BNST neurons	• Induced by 10-second depolarization in whole cell electrophysiology recordings of *ex vivo* BNST neurons (rat) • Blocked by: CB1R antagonism, DAGL inhibition, L-type Ca^{2+} channel inhibition, PLC inhibition, sarcoplasmic/endoplasmic Ca^{2+} channel blockade • Enhanced by: MAGL inhibition • Unaffected by: FAAH inhibition, TRPV1 inhibition, mGluR5 inhibition, mGluR1 inhibition	• Puente et al 2011

2AG=2-arachidonyl glycerol; aBNST=anterior BNST; α_1-AR=alpha1-adrenergic receptor; α_{2A}-AR=alpha2a-adrenergic receptor; BNST=bed nucleus of the stria terminalis; CB1R=cannabinoid receptor 1; DAGL=diacylglyercol lipase; DSE=depolarization-induced suppression of excitation; ERK1=extracellular related kinase 1; FAAH=fatty acid amide hydrolase; GluA1=glutamate AMPAR subunit A1; hM3Dq=human M3 muscarinic receptor Gq-coupled DREADD; LC=locus coeruleus; LFS=low frequency stimulation; LTD=long-term depression; KO=knockout; MAGL=monoacylglycerol lipase; mGluR=metabotropic glutamate receptor; NET=norepinephrine transporter; NMDAR=N-methyl-D-aspartate receptor; PBN=parabrachial nucleus; PLC=phospholipase C; STD=short-term depression; TRPV1=transient receptor potential cation channel subfamily V member 1; VGCC=voltage-gated Ca^{2+} channel; VSub=ventral subiculum; VTA=ventral tegmental area.

Mechanism of LTP in dlBNST

LTP can be induced in BNST slices using high frequency stimulation (HFS) protocols, often involving two bouts of 100 Hz stimulation for 1 second each, while recording changes in either the synaptic component of field potential responses to stimulation or intracellular recordings using sharp electrodes. Early studies aimed to uncover the molecular mechanisms underlying this effect in *ex vivo* mouse BNST slices, and showed that this LTP was sensitive to NMDAR (N-methyl-D-aspartate receptor) inhibition by AP5 and insensitive to inhibition of L-type calcium channels by nimodipine or $GABA_A$ receptors by picrotoxin (Weitlauf et al., 2004). Subunit specificity of the effects of NMDAR inhibition was later shown, as GluN2A knockout did not affect LTP (Weitlauf et al., 2005) but GluN2B knockout and pharmacological inhibition by Ro25-6981 both reduced LTP (Wills et al., 2012). Interestingly, the early phase of LTP (0-5 minutes post-HFS) was sensitive to bath application of 100 mM ethanol before but not after HFS through an NMDAR-dependent process (Weitlauf et al., 2004). The effects of ethanol on NMDAR-dependent transmission were again later shown to be GluN2B-dependent but GluN2A-independent (Kash et al., 2008a; Wills et al., 2012).

Drug exposure interactions with dlBNST LTP

Although ethanol appeared to have an inhibitory effect on LTP in mouse BNST slices when bath applied, chronic exposure to alcohol using the chronic intermittent ethanol (CIE) paradigm was shown to upregulate GluN2B expression (Kash et al., 2009) and enhance LTP induction in the BNST through an GluN2B-dependent process (Wills et al., 2012). This enhancement was prevented by chronic but not acute corticosterone administration, chronic or acute social isolation (Conrad et al., 2011), and simultaneous chronic social isolation and chronic unpredictable stress (Conrad and Winder, 2011). The CIE paradigm consists of two cycles of four days with 16-hour ethanol exposure and 8-hour recovery with three days in between each cycle. This suggests that repeated exposure to ethanol and withdrawal induces structure and molecular changes in the BNST that increase the potential for LTP induction. Similarly, a single injection of cocaine or bath application of cocaine enhances the early phase of high frequency stimulation-induced LTP, defined here as short-term potentiation (STP), in a dopamine- and CRF-dependent process (Kash et al., 2008b). However, each of these recordings were done on the population level as a field potential and do not give information regarding cell-specific effects on plasticity, which is important in the heterogeneity of the BNST. Parallel cell-specific results were observed, though, in rats undergoing a self-administration procedure for cocaine or food. In both cases, self-administration increased the excitability of anterolateral BNST neurons via an increased AMPAR/NMDAR ratio, an electrophysiological measurement that compares the current passing through the two receptors and is increased upon the synaptic AMPAR insertion that commonly occurs in LTP (Dumont et al., 2005). This increased excitability is not seen after either acute cocaine injection or passive administration of cocaine or food (Dumont et al., 2005). Similar results were also obtained in the oval BNST, a subnucleus located within the dorsal aspect of the dorsolateral BNST well-delineated by genetic markers like CRF in the rat

but less so in the mouse (Daniel et al., 2017). Here, sucrose and cocaine self-administration increased AMPAR/NMDAR ratios during the acquisition phase (Debacker et al., 2015). Interestingly, cocaine-induced excitability changes persisted throughout maintenance and withdrawal and were sensitive to GluN2B blockade, while sucrose-induced changes diminished during maintenance and resulted in increased NMDAR current decay rates, suggesting mechanistic differences. Increased AMPAR/NMDAR ratios were also seen in ventrolateral BNST neurons after chronic treatment with a subcutaneous morphine pellet implant (Dumont et al., 2008). This effect was specific to VTA-projecting BNST neurons and was only elicited by electrical stimulation of afferents in dorsolateral BNST and not medial stimulation, suggesting input and output specificity.

Long term potentiation of excitatory transmission and intrinsic excitability in the juxtacapsular BNST

The juxtacapsular nucleus (jcBNST) is a subnucleus of the BNST located on the lateral aspect of the dorsal BNST and runs parallel to the internal capsule that has received specific focus due to its input from the basolateral amygdala alongside lesser input from the CeA (Dong et al., 2000; Larriva-Sahd, 2004). Upon high frequency stimulation of the stria terminalis in *ex vivo* rat brain slices, LTP of excitatory transmission is observable within the jcBNST as in the dlBNST (Francesconi et al., 2009a). This LTP is inhibited by NMDAR, D1R and mGluR5 inhibition, is enhanced by $GABA_A$ and $GABA_B$ inhibition, and is unaffected by D2R inhibition. In addition, the same stimulation protocol elicits an alternative form of LTP known as LTP of intrinsic excitability (LTP-IE), which consists of reduced inward rectification, depolarized resting membrane potential, and increased membrane resistance, together decreasing the rheobase and firing threshold and increasing temporal fidelity of firing and overall cellular

excitability. The mechanism underlying the changes in cellular excitability were shown to involve the postsynaptic D-type K^+ current (I_D). Both forms of LTP are disrupted by long-term drug exposure in rats during protracted withdrawal after alcohol dependence, as well as rats self-administering cocaine or heroin with long (23 hour) access to the self-administration chamber. LTP is unaffected in a variety of control groups including non-dependent rats in protracted withdrawal from ethanol as well as self-administering rats on a short-access schedule of drug access. Occlusion of jcBNST LTP induction by withdrawal is suggested by recent data showing that opioid dependence in self-administering rats elicits LTP-IE specifically in the electrophysiologically-defined Type III neurons of the jcBNST but not Type I or Type II neurons (Hazra et al., 2011; Francesconi et al., 2017). Briefly, in an effort to combat the heterogeneity of the BNST, Hammack et al developed a classification system whereby neurons are sub-divided based on their electrophysiological response to positive and negative current injections (Type I: hyperpolarization sag and regular firing pattern; Type II: hyperpolarization sag and burst firing pattern; Type III: no hyperpolarization sag and fast inward rectification) (Hammack et al., 2007). This schema was confirmed with follow-up transcriptomic analyses (Hazra et al., 2011), and has proven useful in classifying otherwise unidentified BNST neurons and will thus be used here as appropriate.

In contrast to the observed LTP-IE in Type III jcBNST neurons, protracted withdrawal from four weeks of intermittent alcohol vapor exposure reduces excitability of all three types of rat jcBNST neurons (Szücs et al., 2012), suggesting a complex interaction between drug exposure and contingency of administration that needs to be further explored. Interestingly, LTP impairment in protracted abstinence can be mimicked by chronic intracerebroventricular (ICV) administration of corticotrophin releasing factor (CRF) and is blocked by the CRFR1 antagonist

R121919 but not the CRFR2 antagonist astressin$_2$-B (Francesconi et al., 2009b), suggesting a role for this neuropeptide in withdrawal-associated changes in plasticity in the rat BNST. As described above, it was later shown that CRF neurons in the oval subnucleus of the rat BNST can undergo LTP after high frequency stimulation, and that this LTP was enhanced by repeated restraint specifically in Type III CRF neurons via a striatal-enriched tyrosine phosphatase (STEP)-dependent mechanism (Dabrowska et al., 2013a), providing a possible source of the CRF for the observed changes in plasticity within the jcBNST. Future work should aim to determine whether or not changes in plasticity observed in the jcBNST are specific to this subnucleus and, if so, how this system interacts with the other subnuclei of the BNST as well as other nuclei of the extended amygdala and the rest of the brain.

Expanding the scope of LTP in the BNST – effects of *in vivo* induction on behavior

Two of the limitations of the work on LTP in the BNST described thus far are 1) the lack of input specificity during high frequency stimulation of afferents in *ex vivo* brain slices, and 2) a lack of connection to behavioral outcomes in addition to the well-established connection to behavioral history. In two recent rat studies, high frequency stimulation of the ventral subiculum and CA1 subregion of the hippocampus were shown to induce LTP in the BNST via an NMDAR-dependent mechanism (Glangetas et al., 2015, 2017). This elicited anxiolysis that was reversed by the NMDAR antagonist AP5 in one study and potentiation of cocaine-induced locomotor activity at a sub-threshold dose via LTP in VTA-projecting BNST neurons in the other. Unexpectedly, when the same stimulation protocol was used to stimulate the infralimbic cortex, it induced LTD in the BNST, suggesting that this stimulation protocol differentially affects glutamatergic inputs to the BNST and highlighting the importance of input specificity in studies on BNST plasticity. These two studies provide a framework for future work on BNST

LTP *in vivo*, where the electrophysiological and behavioral effects of high frequency stimulation of cell bodies projecting to the BNST and recording of neuronal effects can inform our understanding of the relevant neural circuitry.

LTP in the BNST – a summary

LTP has been shown to occur in BNST neurons after either high frequency stimulation (HFS) of afferent populations or after long-term drug exposures. In both the dorsolateral and juxtacapsular subnuclei of the BNST, HFS-induced LTP is sensitive to NMDAR inhibition. However, the two types of LTP differ in that dlBNST LTP is enhanced by exposure to alcohol in a chronic intermittent ethanol (CIE) paradigm and cocaine *in vivo* or *ex vivo* while jcBNST LTP is disrupted by long-term exposures to alcohol, cocaine and heroin, suggesting regional differences. In the dlBNST, LTP is disrupted by chronic stressors including corticosterone, social isolation, and combined isolation with unpredictable stress, while the effects of these stressors have not been evaluated in the jcBNST. In the jcBNST, LTP of intrinsic excitability is also observed after HFS and during protracted abstinence in opioid withdrawal specifically in Type III neurons, driven by changes in the D-type K^+ current I_D. LTP-IE has not been studied in dlBNST neurons, but anterolateral and ventrolateral BNST neurons show enhanced AMPA/NMDA ratios after cocaine self-administration or chronic morphine pellet implant, which suggest increased excitability to synaptic inputs through a parallel mechanism. Future work should aim to further compare these types of LTP as well as continue to uncover molecular correlates underlying this change in synaptic plasticity. In addition, a future focus on species differences in these forms of LTP would inform this literature due to a lack of direct comparison and substantial points of divergence between rat and mouse BNST (Daniel et al., 2017; Kaufling et al., 2017).

Metabotropic long term depression in the BNST – heterogeneity of stimuli

Plasticity is bidirectional, with LTP resulting in increased activity and LTD resulting in decreased activity. Classically, the intracellular levels of Ca^{2+} that initiate LTD are lower than the high levels required to initiate LTP (Winder and Sweatt, 2001). The two most common means of LTD induction are low frequency stimulation protocols or activation of metabotropic signaling cascades, the latter of which has been more extensively studied in the BNST again in *ex vivo* brain slices. Specifically, LTD of excitatory transmission in the BNST can be initiated by G_q-coupled GPCR signaling cascades downstream of metabotropic glutamate receptors (mGluR) (Grueter and Winder, 2005; Grueter et al., 2006, 2008b, 2008a), the α_1-adrenergic receptor (α_1-AR) (McElligott and Winder, 2008; McElligott et al., 2010), and the chemogenetic receptor hM3Dq (Mazzone et al., 2018).

Metabotropic glutamate receptors can be functionally split into three classes: 1) Group I consists of mGluR1 and mGluR5, which are predominantly postsynaptic and stimulate G_q-GPCR signaling cascades, 2) Group II consists of mGluR2 and mGluR3, which are both presynaptic and postsynaptic and stimulate G_i-GPCR signaling cascades, and 3) Group III consists of mGluR4, mGluR6, mGluR7, and mGluR8, all of which are both presynaptic and postsynaptic and also stimulate G_i-GPCR signaling cascades (Niswender and Conn, 2010). Both Group I mGluRs and α_1-ARs are G_q-coupled GPCRs. The processes by which they elicit LTD share some features but differ in others. In the mouse BNST, Group I mGluR-dependent LTD was shown to occur via two distinct pathways: 1) an mGluR1 and mGluR5-dependent process that involves presynaptic cannabinoid receptor 1 (CB1R) signaling, and 2) an mGluR5-dependent pathway involving postsynaptic extracellular related kinase 1 (ERK1) but not ERK2 activation (Grueter et al., 2006). mGluR5-LTD was unaffected by GluA1 inhibition and did not result in a change in

calcium-permeable AMPA receptor expression (McElligott et al., 2010). On the other hand, α_1-AR-dependent LTD was shown to be postsynaptic and dependent on clathrin-dependent endocytosis, GluA1 activity, and L-type voltage-gated calcium channel (VGCC) activation (McElligott and Winder, 2008; McElligott et al., 2010). α_1-AR-LTD was independent of NMDAR and mGluR5 activation (McElligott and Winder, 2008) and resulted in loss of sensitivity to calcium-permeable AMPA receptors (McElligott et al., 2010). Norepinephrine (100 μM) initiates α_1-AR-dependent LTD after 20 minute but not 10 minute bath application.

To determine if G_q-GPCR-initiated LTD was translatable beyond the mGluR5 and α_1-AR, hM3Dq-dependent LTD was tested and confirmed in mouse VGAT+ BNST neurons (Mazzone et al., 2018). hM3Dq is a modified form of the M3 muscarinic receptor that does not respond to its endogenous ligand acetylcholine but instead responds to the otherwise inert ligand clozapine-N-oxide (CNO). In this study, hM3Dq-LTD was sensitive to phospholipase C (PLC) inhibition and CB1R antagonism, induced anxiogenesis not seen with activation of the chemogenetic G_i-coupled hM4Di receptor, and led to downstream recruitment of the VTA, parabrachial nucleus (PBN) and locus coeruleus (LC) as seen by DREADD-associated metabolic mapping (DREAMM). In addition to extending mGluR5- and α_1-AR-LTD to hM3Dq, this work also highlighted the potential for alternative G_q-GPCR-LTD pathways as VGAT+ BNST neurons also expressed the acetylcholine M_1 muscarinic receptor and the serotonin 5-HT_{2C} receptor.

Metabotropic LTD in the BNST – interactions with behavioral history

Analogous to BNST HFS-induced LTP, LTD initiated by G_q-GPCR agonism is also highly sensitive to behavioral and pharmacological history of the animal. mGluR5/ERK1-dependent LTD in mouse BNST is sensitive to a single injection of cocaine, bath application of cocaine, and chronic intermittent ethanol (CIE) exposure (Grueter et al., 2006, 2008a). The

duration of disruption of mGluR5/ERK1-LTD is extended with repeated injections of cocaine but is not permanent, as LTD is observable 10 days after final cocaine injection (Grueter et al., 2008a). Cocaine-induced disruption of mGluR5/ERK1-LTD can also be prevented by *in vivo* mGluR5 antagonism (Grueter et al., 2008a). α_1-AR-dependent LTD is absent after restraint stress or exposure to either continuous or intermittent alcohol, and in various genetic models of affective disorders including the norepinephrine transporter (NET) and α_{2A}-adrenergeric receptor (α_{2A}-AR) knockout mice (McElligott and Winder, 2008; McElligott et al., 2010). While there are many similarities in processes that affect these types of LTD, there are differences. For example, mGluR5-dependent LTD is not affected by restraint stress or by α_{2A}-AR knockout, while α_1-AR-dependent LTD is not affected by a single exposure to cocaine (McElligott and Winder, 2008; McElligott et al., 2010).

Low frequency stimulation-induced LTD in the BNST

Low frequency stimulation (LFS; 15 minute 10 Hz stimulation) of glutamatergic afferents in *ex vivo* rat BNST slices is also capable of inducing LTD of excitatory transmission (Debacker et al., 2015). This LTD is NMDAR- and GluN2B-dependent and is unaffected by sucrose self-administration but is occluded by cocaine self-administration in a GluN2B-dependent process, again connecting plasticity changes with drug history. Honing in on a specific population of afferents, a similar stimulation protocol (5 minute 10 Hz stimulation) within prefrontal cortex *in vivo* has also been shown to lead to LTD of firing in mouse BNST neurons (Glangetas et al., 2013). After stress, though, this LTD switches to LTP in a glucocorticoid receptor-independent fashion. In both cases, CB1R antagonism, full knockout, or glutamatergic neuron-specific knockout blocks both the LTD and the stress-induced transition to LTP. Similarly, after extended nicotine self-administration in rats, LTP is observed broadly in

BNST neurons and specifically in VTA-projecting BNST neurons after stimulation of infralimbic cortex (Caille et al., 2009; Reisiger et al., 2014). This LTP was NMDAR- and CB1R-dependent and was absent in extinguished but not abstinent mice, and induced nicotine-seeking in trained animals. Prior rat *ex vivo* work highlighted the role of CB1R agonism in the BNST in both depolarization-induced suppression of excitation (DSE) and LTD, dissociating the 2-arachidonylglycerol-mediated L-type calcium channel-dependent short-term depression (STD) and the mGluR5-initiated anandamide-mediated TRPV1-dependent LFS LTD (Puente et al., 2011). More mechanistic work on *in vivo* endocannabinoid modulation of BNST plasticity will inform our understanding of endocannabinoid-mediated LTD and the molecular correlates underlying the transition from LTD to LTP.

As can be seen here, BNST neurons are highly susceptible to long term depression after activation of subtypes of metabotropic receptors to glutamate and norepinephrine or low frequency stimulation of afferent populations, and that these forms of plasticity are differentially affected by stress and drug exposure. The behavioral correlates and molecular underpinnings, in addition to species differences, alternative targets and effect specificity, remain to be fully elucidated.

Input specificity – where to look and why

Through the processes of LTP and LTD detailed above, BNST neurons increase or decrease their response to glutamatergic input. However, in most cases, it is unclear whether these effects occur in response to all glutamatergic afferents or whether it is input- and synapse-specific. In the basolateral nucleus of the amygdala (BLA), for example, auditory fear conditioning initiates changes in plasticity in an input-specific manner (Sigurdsson et al., 2007). In auditory fear conditioning, an auditory stimulus functions as the conditioned stimulus (CS)

that is eventually learned to be a signal of a forthcoming footshock, which is the aversive unconditioned stimulus (US). After learning has taken place, LTP of input from the auditory thalamus and auditory cortex to the BLA is specifically observed, consistent with the strengthened connection between the CS and US-mediated behaviors such as freezing (Tully et al., 2007). In the context of protracted abstinence-induced plasticity in the BNST, the corollary of these inputs is unclear, as the source of withdrawal stimuli-associated activity has not been clearly elucidated. In addition, one of the key points of differentiation between the amygdala and the BNST in stress and anxiety is that the former is engaged during acute, predictable stressors while the latter is engaged during chronic, diffuse stressors that may lack a specific unitary source (Walker and Davis, 2008). However, with projection-specific optogenetic technology and other recently developed tools that can differentiate specific inputs to or populations of neurons of interest, this is an experimentally testable hypothesis. Here, we will provide rationale for investigations of plasticity at specific glutamatergic inputs to the BNST that play a role in reinstatement behaviors and attempt to connect these inputs to the LTP and LTD experiments described above. For an overview of the anatomy of these inputs with respect to subnucleus divisions of the BNST as well as relationships to catecholamine input (to be discussed below), see Figure 1.

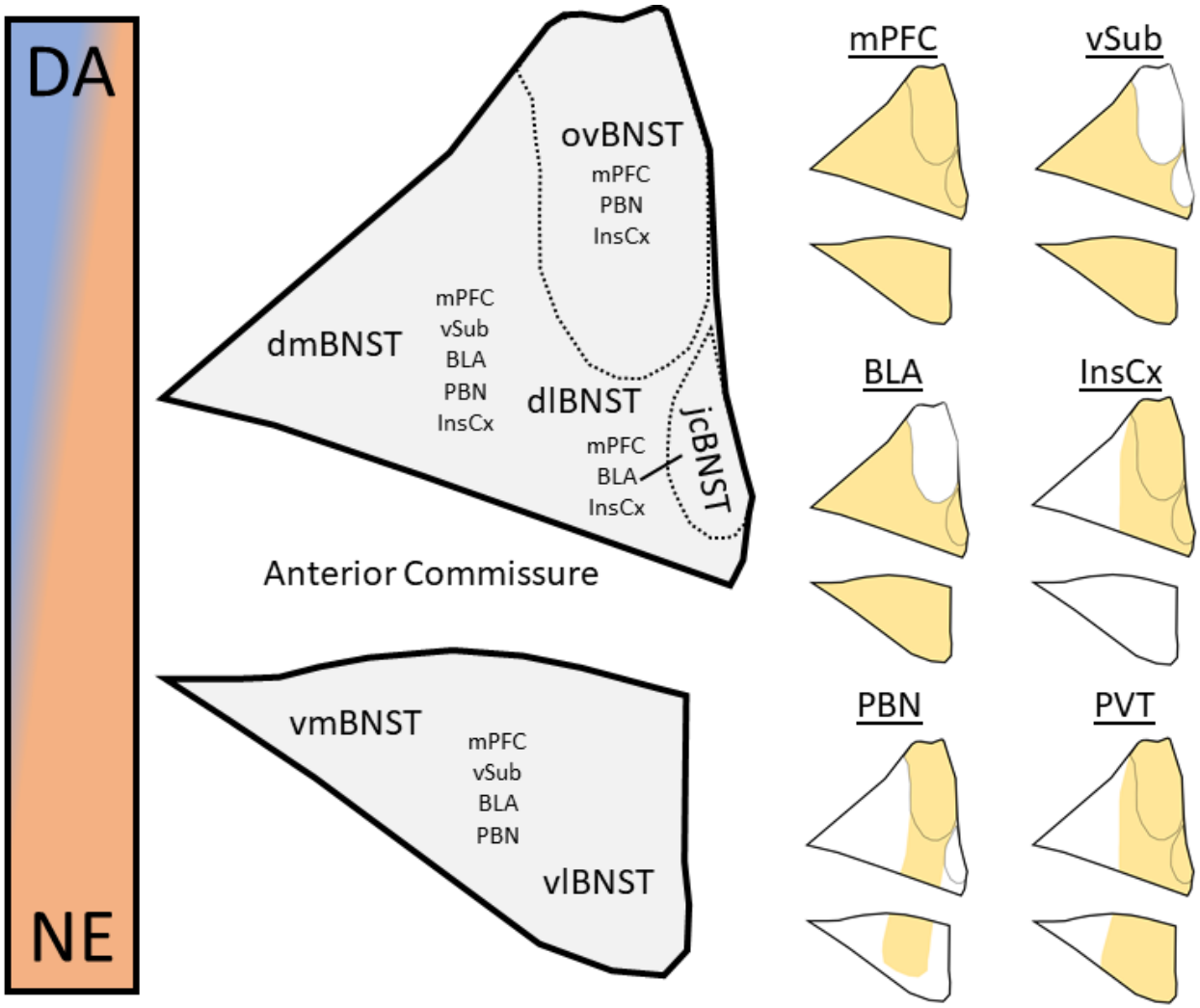

Figure 1 – Anatomy of glutamatergic and catecholaminergic input to the bed nucleus of the stria terminalis. (Left) Anatomical depiction of BNST subnuclei shows location of the oval (ovBNST), juxtacapsular (jcBNST), dorsomedial (dmBNST), dorsolateral (dlBNST), ventromedial (vmBNST) and ventrolateral (vlBNST) subnuclei (Allen Reference Atlas). In addition, glutamatergic afferent populations are noted within the subnuclei and catecholaminergic input is represented as a gradient from high prevalence of dopaminergic (blue) to noradrenergic terminals (orange). (Right) Terminal field afferent populations from each of the six glutamatergic inputs, including the ventral subiculum (VSub), medial prefrontal cortex (mPFC), parabrachial nucleus (PBN), basolateral amygdala (BLA), insular cortex (InsCx), and paraventricular nucleus of the thalamus (PVT). The topography of afferent population terminal fields are adapted from McDonald et al 1996 for the mPFC, Dong et al 2001 for the VSub, Kim et al 2013 for the BLA, Yasui et al 1991 for the InsCx, Saper & Loewy 1980 for the PBN, and Li & Kirouac 2008.

Medial prefrontal cortex

Input-specificity of abstinence-associated changes in synaptic plasticity has been performed on infralimbic cortical input to the BNST as previously described. LTP of this input occurs in nicotine self-administration in rats and low frequency stimulation in drug-naïve mice elicits LTD of this input that transitions to LTP with stress exposure in a CB1R-dependent fashion (Glangetas et al., 2013; Reisiger et al., 2014). This suggests that drug exposure correlates with a strengthening of this input and thus may underlie some of the behavioral changes associated with increased drug exposure. Indeed, in humans, increased glucose metabolism is observed in the related orbitofrontal cortex (OFC) one week into withdrawal, and metabolism within the OFC and the prefrontal cortex (PFC) correlates with drug craving in abstinent patients (Volkow et al., 1991). In the context of stress, stress-induced changes in PFC activity by functional magnetic resonance imaging (fMRI) was associated with greater number of days since last cocaine exposure and shorter time to relapse (Sinha and Li, 2007). In rodent models, prefrontal cortex activity has been shown a number of times to be critical for stress-induced reinstatement of drug-seeking and incubation of drug craving (Capriles et al., 2003; Koya et al., 2009; Willcocks and Mcnally, 2013). PFC neurons have also been shown to undergo changes in plasticity and enhancement of activity during either protracted abstinence from drugs of abuse or after acute or chronic stress exposure (Ostrander et al., 2003; Koya et al., 2009; Lu et al., 2010; Flak et al., 2012; Pleil et al., 2015a). The BNST mediates an interaction between medial PFC activity and recruitment of the paraventricular nucleus of the hypothalamus (PVN) during psychological stressors, suggesting a role of this nucleus as a relay between cortical input and behavioral output that may translate from stress circuitry to drug and reward circuitry (Spencer et al., 2005; Radley et al., 2009, 2013; Johnson et al., 2016). This collection of work highlights the

potential for a PFC-BNST circuit to mediate aspects of stress-induced reinstatement of drug- and alcohol-seeking behaviors. However, the PFC is a heterogeneous collection of nuclei consisting of at least the infralimbic cortex, prelimbic cortex, and orbitofrontal cortex, each of which project to the BNST (Mcdonald et al., 1996) and are known to engage differently in addiction-related and other behaviors. It will be important to parse out these differences as plasticity in this circuit is investigated.

Ventral subiculum

Long-term potentiation induced by *in vivo* high frequency stimulation of the ventral subicular (VSub) input to the BNST was determined to be anxiolytic in mice and potentiating of the locomotor response to cocaine via BNST-VTA projections in rats (Glangetas et al., 2013, 2015). Similar to the input to the BNST from the PFC, this projection is known to act as an inhibitory relay between the ventral hippocampus and the PVN to dampen the stress response (Cullinan et al., 1993; Radley and Sawchenko, 2011). This suggests that engagement of this pathway, as occurs during stressful stimuli, would attempt to counteract the effects of stress. Chronic engagement of this pathway, though, could lead to loss of potential for plasticity. However, with chronic or juvenile exposure to stress, we see enhanced LTP within the ventral hippocampus, suggesting otherwise (Thompson et al., 2004; del Olmo et al., 2006; Keralapurath et al., 2014; Grigoryan et al., 2015). The cocaine-potentiating effects of high frequency stimulation of the ventral subicular input to the BNST via projections to the VTA suggests that interactions between stress and cocaine may also occur via this circuit. Supporting this hypothesis, cocaine conditioning also increased (Keralapurath et al., 2014) and induced structural changes that support increased activity in the region (Caffino et al., 2014; Keralapurath et al., 2017). These data suggest that protracted abstinence may lead to increased plasticity at VSub-

BNST projections, and that this projection may contribute to susceptibility to reinstatement. Specifically, the ventral subiculum is critical for cocaine-, cue- and context-induced reinstatement of cocaine-seeking behaviors (Sun and Rebec, 2003; Rogers and See, 2007; Atkins et al., 2008; Lasseter et al., 2010). Interestingly, electrical stimulation of the ventral subiculum itself is capable of reinstating drug-seeking behaviors (Taepavarapruk and Phillips, 2003). In human patients, though, we see decreased hippocampal volume in alcoholics (De Bellis et al., 2000) and after childhood maltreatment (Teicher et al., 2012), suggesting a loss of activity with these chronic stressors. Future studies will inform whether changes in plasticity occur at VSub-BNST projections during protracted abstinence and, if they do, whether the projection still elicits anxiolysis as it does in naïve animals.

Basolateral Amygdala

The BLA sends a glutamatergic projection to the BNST that has also previously been shown to induce anxiolysis and decrease respiratory rate (Kim et al., 2013). Although this projection has not been directly investigated in the context of abstinence-induced changes in plasticity, the BLA sends a portion of its BNST projections to the juxtacapsular subnucleus (jcBNST) (Dong et al., 2001) where high frequency stimulation of the stria terminalis induces LTP-IE that is occluded by prolonged drug exposure. Consistent with a potential role in abstinence-induced changes in plasticity, extensive evidence has linked the BLA with reinstatement of drug-seeking behaviors. Specifically, the BLA is shown to be critical for context-, cue- and drug-induced reinstatement of drug-seeking behaviors in some but not all studies (Meil and See, 1997; Grimm and See, 2000; Kantak et al., 2002; Fuchs et al., 2005). Furthermore, a history of drug exposure and re-exposure to drug-associated stimuli leads to robust activation and activity-dependent changes in the BLA in both rodent models

(Neisewander et al., 2000; Meredith et al., 2002) and humans (Bonson et al., 2002; Moaddab et al., 2017), supporting the hypothesis that BLA-BNST connectivity may be enhanced in protracted abstinence. However, given the anxiolysis induced by stimulation of this pathway and the fact that withdrawal induces anxiogenesis in patients with substance use disorders, it is also a candidate pathway for input-specific LTD of glutamatergic transmission in the BNST. Consistent with this hypothesis, BLA lesions did not affect footshock-induced reinstatement of cocaine-seeking behavior dependent on BNST activity (McFarland et al., 2004) and direct administration of NMDAR antagonists into the BLA to block development of NMDAR-dependent plasticity did not affect conditioned reward or reinstatement of cocaine self-administration (See et al., 2001). In addition, human imaging studies show that a reduced amygdalar volume is consistent with high risk for the development of alcoholism and other neuropsychiatric disorders (Hill et al., 2001; Benegal et al., 2007). It will be important for future studies to determine the presence, directionality, behavioral relevance, and subnucleus specificity of plasticity at glutamatergic synapses originating in the BLA projecting to the BNST.

Insular cortex

The insular cortex is another glutamatergic input to the BNST, including but not limited to the jcBNST (Yasui et al., 1991), that has the potential to either enhance or inhibit reinstatement of drug-seeking behaviors and thus could undergo bidirectional changes in plasticity with increased drug exposure and protracted abstinence. Broadly, the insular cortex functions in integrating interoceptive processes and translating that information into conscious feelings and behavioral decisions regarding risk and reward (Naqvi et al., 2007). The insula has received substantial interest since the observation that nicotine-dependent patients who had stroke-associated damage to the insula reported substantially decreased craving and high rates of

success in quitting smoking (Naqvi et al., 2007). This clinical finding has been well-replicated in humans (Abdolahi et al., 2015a, 2015b) and modeled in rodents (Forget et al., 2010; Pushparaj et al., 2015). Insular activity is also critical for addiction-like behaviors to other drugs of abuse, as inactivation blocks conditioned place preference (CPP) for amphetamine (Contreras et al., 2007, 2012), cue-induced reinstatement to cocaine-seeking (Cosme et al., 2015), and operant responding for alcohol (Pushparaj and Le Foll, 2015). Consistent with a potentiating role in the development and maintenance of addiction-like behaviors during abstinence, the insula is engaged during cue or context presentations in humans (Janes et al., 2017) and rodents (Contreras et al., 2007), and shows increased dendritic complexity after chronic nicotine exposure and withdrawal in rodents (Ehlinger et al., 2012). Although the case for a hyperactive insula in addiction is compelling, there is also a case for loss of insular activity with chronic drug exposure and abstinence. Reduced gray matter volume is observed in the insula cortex of drug users as well as decreased regional activity during decision-making processes (Droutman et al., 2015), and stimulation of the insula in rodent models decreases nicotine self-administration (Pushparaj et al., 2013). The only study to evaluate the potential function of insula-BNST connectivity shows that inactivation of either population blocks the ability of safety signals to decrease stress-associated decrements in social interaction (Christianson et al., 2011), although the authors do not test the projection directly and posit that it occurs via a relay in the BLA. This hypothesis will need to be tested in future studies.

Parabrachial nucleus

The parabrachial nucleus (PBN) provides a dense glutamatergic input to the BNST that extends from the oval to the ventrolateral subnuclei but remains largely unexplored (Saper and Loewy, 1980). These synapses tend to be axosomatic in structure and likely instructive in

functionality (Shimada et al., 1989; Dobolyi et al., 2005), as introduction of channelrhodopsin and elicitation of light-evoked currents is capable of initiating action potentials or hyperpolarizing BNST neurons recorded in whole-cell electrophysiology (Flavin et al., 2014). The behavioral relevance of PBN-BNST projections has yet to be evaluated, yet PBN neurons and specifically those projection neurons positive for the neuropeptide calcitonin-gene related peptide (CGRP) have been implicated in a number of behaviors, including pain, thirst, taste and other physiologic processes (Palmiter, 2018). Specifically, CGRP+ PBN neurons are activated by diverse events such as noxious stimulation (both internal and external), satiation, consumption of novel foods, and auditory cues in a fear conditioning paradigm, and are critical for food neophobia and conditioned fear responses (Campos et al., 2018). Together, these data suggest that the PBN plays a role both in the processing of danger signals and engaging those adaptive responses that will limit resultant harm (Campos et al., 2018). CGRP co-release with glutamate from PBN afferents in the BNST mimics the actions of intracerebroventricular (ICV) administration of CGRP in the induction of anxiety and leads to recruitment of other brain regions involved in the stress response (Sink et al., 2011), suggesting relevance to abstinence-induced negative affect and stress-induced reinstatement. The parallel CGRP+ projection from the PBN to the CeA encodes the affective components of pain (Han et al., 2015) and is critically involved in pain-associated plasticity and excitatory transmission in this region (Han, 2005; Han et al., 2010; Okutsu et al., 2017; Shinohara et al., 2017), providing a framework for PBN circuits in the extended amygdala interacting with chronic stressors. Interestingly, though, CGRP appears to have excitatory actions in the CeA but potentiate $GABA_A$-mediated currents in the BNST potentially leading to increased inhibition, highlighting potential regional differences (Gungor and Pare, 2014).

Paraventricular nucleus of the thalamus

The paraventricular nucleus of the thalamus (PVT) also provides a dense glutamatergic input to the lateral BNST that has been extensively studied by anatomical methods but minimally by functional methods (Dong et al., 2017). Preclinical data supports a role for the PVT in drug-seeking behaviors, as activity within the subnucleus has been shown to be critical for expression of cocaine conditioned place preference, as well as cue- and drug-induced reinstatement of cocaine-seeking (Browning et al., 2014; Matzeu et al., 2015; Wunsch et al., 2017; Kuhn et al., 2018). In humans, the thalamus is activated by drug cues but shows reduced activity during response inhibition (Huang et al., 2018), suggesting a role in addiction-related processes. The projection from the PVT to the nucleus accumbens (NAc) has been heavily investigated as the nexus for connections between PVT activity and drug-seeking behavior. Consistent with this notion, drug exposure increases excitability and induces synaptic plasticity in neurons projecting from PVT to NAc (James et al., 2010; Joffe and Grueter, 2016; Neumann et al., 2016), and *in vivo* depotentiation of this pathway by an LTD protocol can limit the expression of withdrawal-associated symptomatology (Zhu et al., 2016). Interestingly, there is heavy collateralization between PVT projections to the NAc, the BNST, and the central nucleus of the amygdala (CeA), suggesting that the same synaptic plasticity that is occurring in projections from the PVT to the NAc might also be occurring in projections to the BNST (Dong et al., 2017). Furthermore, PVT fibers appose with extended amygdala neurons positive for the neuropeptide corticotropin releasing factor (CRF), suggesting an interaction that may underlie abstinence-induced changes in plasticity and behavior (Li et al., 2008). Future studies should aim to explore the function of this projection in the context of reinstatement behaviors.

Together, the glutamatergic inputs from the prefrontal cortex, ventral subiculum, basolateral amygdala, insular cortex, parabrachial nucleus, and paraventricular nucleus of the thalamus are potential candidates for mediating the changes in input-specific synaptic plasticity in the BNST that occur with protracted abstinence from drugs of abuse that prime the brain for relapse to drug-seeking behaviors. Future experiments should aim to connect changes in the strength of these inputs to the different types of plasticity observed in the BNST and determine the directionality (i.e. LTP or LTD) and behavioral relevance of these effects. This increased understanding of the input specificity underlying abstinence-induced changes in plasticity will open the door to more focused pharmacological studies aimed at protecting against these maladaptive changes.

Cell-type specificity: projection targets and genetic markers

Studies of plasticity in the BNST have mostly focused on effects within neuronal populations through field potential recordings or unidentified neurons through *in vivo* or *ex vivo* electrophysiology. Although determining the source of input to a defined neuronal population will be important for circuit-based interventions, the outcome of LTP or LTD will converge on increased or decreased likelihood of neuronal firing and neurotransmitter release in the BNST neurons themselves. Then, depending on the projection target and the neurotransmitter packaged for release, this change in activity will be translated into increased or decreased likelihood of reinstatement of drug-seeking or related behaviors. Differentiating cell-specific mechanisms of plasticity in the BNST will be especially important due to the known heterogeneity of and complex inter-relationships among cells within the BNST (Gungor and Pare, 2016; Lebow and Chen, 2016).

Within the rat BNST, neurons positive for the neuropeptide corticotropin releasing factor (CRF) undergo high frequency stimulation (HFS)-induced long term potentiation (LTP) that is further potentiated by repeated restraint stress specifically in Type III CRF neurons that are defined by their electrophysiological response to positive and negative current injection (Dabrowska et al., 2013a). This process was determined to be dependent on a lack of expression of striatal-enriched tyrosine phosphatase (STEP), an enzyme that shows downregulation with repeated restraint stress. LTP in CRF neurons would thus be expected to increase CRF release either in the BNST from interneurons or in projection targets. As CRF signaling is critical for cocaine-induced enhancement of short term potentiation (Kash et al., 2008b), stressful stimuli that engage LTP of this population may exacerbate changes in excitatory transmission within the region as a result of extended drug exposure and have long term effects on BNST plasticity. Extrahypothalamic CRF is critical for stress-induced reinstatement of drug-seeking behavior, as CRF itself can act as a stimulus for reinstatement and CRFR1 antagonists reduce stress-induced reinstatement when injected systemically or directly to the BNST (Wang et al., 2006; Zislis et al., 2007). The role of CRF is independent of the drug of abuse, the type of stressor, or the experimental procedure used (Shalev et al., 2010). CRF levels in the BNST are elevated during withdrawal from alcohol and normalize after re-exposure (Olive et al., 2002), a process that will lead to increased engagement of a BNST-VTA projection population via enhancement of excitatory transmission (Silberman et al., 2013). Thus, LTP of BNST CRF neurons and enhancement of this process by chronic stressors may drive reinstatement behaviors. Both the connection between CRF and LTP, as well as the role of other neuropeptides and genetic markers expressed in the BNST including but not limited to neuropeptide Y (NPY), somatostatin

(SST), and protein kinase Cδ (PKCδ) remain to be further explored (for a review of neuropeptide signaling in the BNST, see Kash et al 2015, and Daniel and Rainnie 2016).

In addition to defining neuronal populations by their expression pattern of genetic markers, BNST neurons can also be defined based on their projection target. Although not directly applied to plasticity changes in the BNST or with abstinence and reinstatement, this approach allowed for distinction of projection-specific functions that contribute to the various phenotypes associated with anxiety-like behavior in rodent models. Specifically, optogenetic excitation of BNST afferents in the lateral hypothalamus (LH) elicits reduced risk avoidance in the elevated plus maze, while those in the PBN elicits reduced respiratory rate and those in the VTA elicits increased positive valence (Kim et al., 2013). Although these responses have not been fully translated into the behaviors seen with reinstatement of drug-seeking, nor have the behaviors seen with reinstatement of drug-seeking been elegantly dissected in this manner, one could imagine parallels of these effects in the rodent undergoing protracted abstinence from drugs of abuse.

Finally, the data presented thus far suggests that experience-dependent or stimulation-induced LTP in either CRF+ neurons or anxiogenesis-inducing projections from the BNST to the VTA, LH and PBN would likely increase the probability of reinstatement. This begs the question of whether the LTD observed through a variety of mechanisms described above could represent a therapeutic end-goal for reducing the ability of stress or other factors to re-engage the circuitry necessary for reinitiating drug-seeking behaviors. However, G_q-mediated LTD initiated by the hM3Dq DREADD in VGAT+ BNST neurons elicited anxiety-like behaviors and lead to increased engagement of downstream neuronal activity in the VTA, the PBN, and the locus coeruleus (LC), suggesting that either LTD occurs in interneurons in the BNST and leads to

disinhibition of BNST projection neurons, or that decreased firing of BNST neurons leads to disinhibition of downstream target neurons in the VTA and other regions of interest. New genetic tools like INTRSECT (Intronic Recombinase Sites Enabling Combinatorial Targeting) will allow for populations like interneurons to be isolated with or without the use of a genetic marker and studied to answer questions such as these (Marcinkiewcz et al., 2016).

Modulation of plasticity: catecholamine receptor modulation

As more information is gained on the mechanism and specificity of LTP and LTD, molecular targets for modulation of these processes are likely to emerge. Currently, much focus has been placed on NMDAR antagonists like Ro25-6981, as they have been shown to attenuate *ex vivo* and *in vivo* LTP in the BNST (Wills et al., 2012; Glangetas et al., 2015, 2017). This work has promising applications related to the clinical use of ketamine and other similar drugs, but may be limited due to off-target as well as undesired on-target effects. Due to the complex and bidirectional actions on BNST synaptic plasticity and neurotransmission in general, targeting of the receptors for the catecholamines dopamine and norepinephrine represents a potential therapeutic modality for these synaptic changes as well as their resultant behavioral outcomes. Dopamine and norepinephrine input to the BNST spans the dorsoventral extent of the nucleus, with a patterned distribution where dopamine input is more prominent in the dorsal aspect and norepinephrine in the ventral (Figure 1) (Miles et al., 2002).

Dopamine

Release of dopamine in the BNST through stimulant action or exogenous drug actions at dopamine receptors is permissive and enhancing of the molecular changes that underlie STP and LTP in the region. Many drugs of abuse, including morphine, nicotine, cocaine and alcohol, lead to increased extracellular levels of dopamine in the BNST as they do in the nucleus accumbens

(Carboni et al., 2000). Palatable substances like sucrose also increase dopamine while aversive stimuli such as quinine reduce these levels, a profile opposite that of norepinephrine (Park et al., 2012). Once released, dopamine initiates excitatory actions in the BNST, enhancing glutamatergic transmission via signaling at D1 and D2 receptors in an activity- and CRFR1-dependent manner in the mouse (Kash et al., 2008b) and inhibiting GABAergic transmission via D2Rs in the rat oval subnucleus (Krawczyk et al., 2011a). Potentiating these excitatory actions, dopamine enhances the short-term component of high frequency stimulation-induced LTP in the mouse BNST (Kash et al., 2008b). Upon contingent drug exposure paradigms, however, these excitatory actions become inhibitory, with upregulation of the D1R leading to enhancement and LTP of $GABA_A$ inhibitory postsynaptic currents (IPSCs) not seen in control, sucrose self-administering, cocaine self-administration acquiring, and cocaine-yoked rats (Krawczyk et al., 2011b). This $GABA_A$ LTP involves c-Srk tyrosine kinase and neurotensin receptor signaling pathways, and is independent of canonical G-protein and other tyrosine kinase signaling pathways. Further, the magnitude $GABA_A$ LTP is proportional to the break-point on the progressive ratio schedule of cocaine reinforcement, a measure that defines motivation for reward-seeking behaviors. Inhibitory actions of dopamine can also be seen on NMDAR currents in *ex vivo* brain slices from cocaine self-administering rats via D1Rs and D2Rs via activation of PLC and protein phosphatases (Krawczyk et al., 2014), as well as on LTP of excitatory transmission in the rat jcBNST in a D1-dependent manner (Francesconi et al., 2009a). Regardless of the directionality of effects on neurotransmission in the region, blockade of dopamine signaling at D1Rs in the BNST alters drug-seeking behaviors as evidenced by decreased alcohol-motivated responding (Eiler et al., 2003) and decreased cocaine reinforcement (Epping-Jordan et al., 1998), suggesting that targeting dopamine-mediated transmission and its

downstream effects on plasticity represents a therapeutic modality for drug- and alcohol-seeking behaviors.

Norepinephrine

Norepinephrine receptor modulators are specifically known to modulate stress-induced reinstatement of drug-seeking behavior and to affect BNST plasticity. Specifically, disruption of the norepinephrine input to the BNST as well as inhibition of β- and α_1-adrenergic receptor signaling and agonism of α_2-adrenergic receptors inhibits stress-induced reinstatement of drug-seeking behaviors (Erb et al., 1998; Shaham et al., 2000b; Shalev et al., 2001). In *ex vivo* brain slices, 20 but not 10 minute application of norepinephrine (100 uM) initiates LTD mimicking α_1-AR-LTD (McElligott and Winder, 2008), and α_1-AR-LTD is disrupted as a result of aberrant norepinephrine signaling in the norepinephrine transporter (NET) and α_{2A}-AR knockout mouse model (McElligott and Winder, 2008). In the BLA, norepinephrine is known to gate LTP via decreased inhibitory tone on pyramidal projection neurons likely via actions on local inhibitory interneurons, enabling the plastic changes that occur with fear conditioning paradigms (Tully et al., 2007). If norepinephrine-mediated α_1-AR-LTD were to occur in BNST inhibitory interneurons and decrease their inhibition of BNST-VTA projection neurons, for example, a similar process may control BNST-dependent reinstatement behaviors.

Modulation of norepinephrine action and potential effects of norepinephrine on abstinence-induced changes in plasticity represents a promising therapeutic strategy for addiction. These effects could be due to direct inhibition of norepinephrine release via autoreceptor α_2-ARs or via blockade of norepinephrine actions at α_1-ARs, β-ARs or heteroceptor α_2-ARs. Direct administration of β_1- and β_2-AR antagonists or α_2-AR agonists to the BNST blocks stress induced reinstatement of cocaine- and morphine-seeking behaviors (Wang et al.,

2001; Leri et al., 2002; Mantsch et al., 2010; Vranjkovic et al., 2014), highlighting a role for these receptors in the process that we hypothesize is connected to abstinence-induced changes in plasticity. Similarly, direct administration of α_1-, β_1-, and β_2-AR antagonists to the BNST elicits anxiolysis (Khoshbouei et al., 2002). With respect to changes in activity, briefly, β-ARs broadly enhance BNST neuronal activity via a postsynaptic mechanism while α_1-ARs elicit LTD and α_2-ARs inhibit both norepinephrine and glutamate release (for a more detailed review see Flavin and Winder 2013). β-AR activity specifically enhances BNST activity through a microcircuit involving CRF signaling while BNST α_{2A}-ARs inhibit glutamate release in an input-specific manner at PBN but not BLA terminals (Nobis et al., 2011; Flavin et al., 2014), highlighting the potential for actions that can be targeted to specific BNST inputs and outputs as more information is gleaned from work on the specificity of changes in plasticity as described above. In addition, G_q-coupled LTD-mediated activation of downstream components of addiction-related neurocircuitry (Rinker et al., 2017) and potential excitatory actions of α_{2A}-ARs within the BNST (Savchenko and Boughter, 2011; Flavin et al., 2014) highlight the possibility that activation of inhibitory signaling cascades and their effects on neuronal activity, and thus neuronal plasticity, are not always direct and thus may inform future work in the area of plasticity.

Summary of synaptic plasticity in the BNST and contributions to behavior

Stress increases the risk of neuropsychiatric disease in general and addiction in particular. Chronic exposure to drugs and stress lead to changes in neurotransmission and synaptic plasticity in the bed nucleus of the stria terminalis (BNST), a component of the extended amygdala critical for reinstatement of drug- and alcohol-seeking behaviors. We hypothesize that long-term changes in activity in this region prime those with substance use disorders for relapse during

protracted abstinence. Here, we discuss the mechanisms underlying long term potentiation (LTP) and depression (LTD) in the region, and highlight how these changes interact with a history of stress and drug exposure in rodent models. In addition, we highlight important future directions including input- and cell-specific bidirectional changes in activity. A better understanding of the molecular correlates and mechanisms underlying synaptic plasticity will lead to more effective treatment strategies that have the ultimate goal of decreasing the emergence of reinstatement and relapse behaviors during abstinence. Here we discuss the role of catecholamine receptor modulators in the process, as inhibition of both dopamine and norepinephrine receptors affect reinstatement behaviors while activation enhances or initiates LTP and LTD, respectively. We hope that the insights gained from studying the specific changes that underlie synaptic plasticity in the BNST during protracted abstinence from alcohol and other drugs of abuse will provide insight into the biology underlying relapse behavior in people with substance use disorders and alcoholics and inform future treatment modalities for this complex biological problem.

The α_{2A} adrenergic receptor as a molecular target to reverse allostatic changes in plasticity

In the remainder of this thesis, we will explore the physiology and pharmacology of α_{2A}-ARs within the BNST as a potential drug target for abstinence-induced changes in neuronal activity. Although the connection between α_{2A}-ARs and synaptic plasticity has been relatively unexplored in the BNST, this receptor is an intriguing target to counteract the effects of chronic drug use and cycles of abstinence on neurotransmission within the extended amygdala. Further, α_{2A}-AR agonists are FDA-approved and clinically well-tolerated (Strawn et al., 2017), and have minimal on-target adverse effects at peripheral α_{2A}-ARs although correct dosing is imperative (Walton et al., 2014). Agonism at the α_{2A}-AR inhibits presynaptic release of norepinephrine, glutamate, and GABA in the BNST and thus has short-term effects on neurotransmission in the

BNST (Palij and Stamford, 1993; Egli et al., 2005; Shields et al., 2009; Krawczyk et al., 2011a; Herr et al., 2012). Based on the concept of Hebbian plasticity, decreased neurotransmission at these synapses that are hypothesized to be activated by chronic drug use and stressful stimuli would decrease connectivity to counteract the effects of long term strengthening as seen in LTP (Fox and Stryker, 2017). Similarly, decreasing presynaptic norepinephrine release through autoreceptor actions would decrease norepinephrine-induced long-term depression, which is known to be anxiogenic and likely contributes to withdrawal-induced negative affect and relapse susceptibility (McElligott and Winder, 2008; McElligott et al., 2010; Mazzone et al., 2018). We hypothesize that these actions would counteract the molecular changes that occur in protracted abstinence from drugs of abuse and that the behavioral effects of acute injection would translate in this context as well. Before testing this hypothesis, though, a full understanding of receptor actions and relationships among differentially localized α_{2A}-ARs is required (Flavin et al., 2014). Here we dissect actions of postsynaptic α_{2A}-ARs within the BNST and their contributions to neuronal activity within the region and anxiety-like behaviors. Overall, the work in this dissertation will address:

Hypothesis: Activation of postsynaptic α_{2A}-ARs enhances excitatory responses in a population of BNST neurons through inhibition of HCN channels.

Specific Aim 1: To identify the α_{2A}-AR subpopulation responsible for guanfacine activation of BNST neurons.

Specific Aim 2: To determine the mechanisms underlying guanfacine activation of BNST neurons.

Specific Aim 3: To determine the behavioral and physiological relevance of postsynaptic α_{2A}-AR signaling in vivo.

Chapter 2

Dorsal BNST α_{2A}-adrenergic receptors produce HCN-dependent excitatory actions that initiate anxiogenic behaviors

Introduction

Stress contributes to the development of many neuropsychiatric disorders (Larzelere and Jones, 2008). Chronic stress exposure perpetuates maladaptive behaviors and leads to long-term physiological changes and autonomic dysregulation (Goeders, 2003; McEwen, 2004; Lampert et al., 2016; Sharma et al., 2016). Anxiety disorders can result from adverse life events and involve stress response generalization (Stein and Sareen, 2015; Miloyan et al., 2018). Anxiety disorder prevalence is as high as 22.8% (Kessler et al., 2005a) and treatments are only partially effective with significant adverse effects (Griebel and Holmes, 2013). Further, anxiety and negative affect can occur during withdrawal and abstinence from drugs of abuse and alcohol (Sinha et al., 1999, 2011; Kassel et al., 2003; Heilig et al., 2010; Blaine et al., 2016). Thus, anxiolytics may also be a viable treatment modality for addiction (Heilig and Egli, 2006; Bruijnzeel, 2017).

Agonists at the α_2-adrenergic receptor (α_2-AR) inhibit norepinephrine signaling to induce anxiolysis and decrease the stress response, among other actions (Buffalari et al., 2012; Ji et al., 2014; Strawn et al., 2017). For example, the α_{2A}-AR agonist guanfacine elicits antidepressant-like effects in the forced swim test (Mineur et al., 2015), and α_{2A}-AR knockout mice show elevated baseline anxiety- and depressive-like behaviors (Schramm et al., 2001; Lahdesmaki et al., 2002). Further, in rodent models of addiction, α_2-AR agonists block stress-induced

reinstatement of drug-seeking behaviors (Erb et al., 1998; Shaham et al., 2000b; Highfield et al., 2001; Mantsch et al., 2010).

Direct administration of α_2-AR agonists to the bed nucleus of the stria terminalis (BNST) inhibits both stress-induced anxiety-like (Schweimer et al., 2005) and drug-seeking behaviors (Delfs et al., 2000; Wang et al., 2001). As part of the extended amygdala, the BNST functions in stress-reward integration and has been implicated in both anxiety disorders (Adhikari, 2014) and reinstatement of drug-seeking behaviors (Koob, 2009). Noradrenergic input to the BNST via the ventral noradrenergic bundle (VNAB) is critical for stress-induced reinstatement of drug-seeking behavior (Shalev et al., 2001; Wang et al., 2001). Presynaptic α_{2A}-ARs inhibit norepinephrine release in the BNST and may inhibit stress effects in this manner (Park et al., 2009). However, heteroceptor α_{2A}-ARs regulate glutamatergic transmission in the BNST in an input-specific manner, inhibiting parabrachial nucleus (PBN) but not basolateral amygdala (BLA) afferents (Shields et al., 2009; Flavin et al., 2014). By immunoelectron microscopy, BNST α_{2A}-ARs are expressed in both presynaptic (i.e. asymmetric/symmetric axon terminals) and postsynaptic specializations (dendrites, spines, soma) (Flavin et al., 2014). The relationship among α_{2A}-AR populations and their contributions to behavior remain unknown.

α_{2A}-ARs are G_i-coupled GPCRs and are thus classically thought to impair neuronal signaling. However, stimulatory effects on neuronal activity have been reported for this and other G_i-GPCRs (Federman et al., 1992; Andrade, 1993; Winder and Conn, 1993). Guanfacine upregulates expression of the immediate early gene cfos, an indirect marker of neuronal activity, in the BNST and other regions (Savchenko and Boughter, 2011). In the prefrontal cortex, α_{2A}-AR activation has been shown to decrease the open probability of hyperpolarization-activated and cyclic nucleotide-gated cation (HCN) channels localized to the dendritic neck separating the

dendritic spine from the dendrite and the soma to increase fidelity of synaptic current transmission and pyramidal neuron network activity (Wang et al., 2007).

Here, we show that guanfacine-induced excitatory actions within the dBNST occur via activation of postsynaptic α_{2A}-ARs using convergent techniques including transgenic mouse models targeting the α_{2A}-AR, RNA *in situ* hybridization, *ex vivo* incubation, and chemogenetics. The mechanism underlying this effect is shown to involve pacemaker channels containing HCN2-subunits, which are anatomically and functionally co-localized in dBNST neurons expressing α_{2A}-ARs and are both necessary and sufficient for guanfacine-induced excitatory actions. Finally, at the behavioral level, postsynaptic α_{2A}-AR activity within the BNST is shown to compete with the overall anxiolytic actions of systemic guanfacine application, as introduction and expression of an unrelated inhibitory chemogenetic receptor, hM4Di, elicited activity-enhancing effects and lead to anxiety-like behavior in transduced mice.

Methods

Animals – Male and female mice of at least 8 weeks of age were used throughout this study. Male C57/Bl6J mice (RRID: IMSR_JAX:000664; Jackson Laboratories; Bar Harbor, ME) were delivered at 7 weeks of age and acclimated for one week before use. Multiple lines of α_{2A}-AR transgenic mice were bred in-house from homozygote (TG- WT-/- x TG+ WT-/- where TG=*Dbh-Adra2a* and WT= *Adra2a*) or heterozygote breeders (TG- WT+/- x TG+ WT+/-) and genotyped as previously described (Gilsbach et al., 2009). Wild-type controls were negative for *Dbh-Adra2a* and homozygous positive for WT *Adra2a*. *cfos-eGFP* mice (RRID: IMSR_JAX:014135; Jackson Laboratories) were bred in-house and genotyped as previously described (Barth et al., 2004). Thy1-COP4 mice (line 9) were bred in-house on a homozygote

background (RRID: IMSR_JAX:007615; Jackson Laboratory strain 007615) (Arenkiel et al., 2007). For *Adra2a* KO, *Dbh-Adra2a*, *Adra2a* WT, *cfos-eGFP*, and Thy1-COP4 mouse lines, mice of both sexes were utilized to minimize the total number of animals. No sex differences were apparent, so each group is compiled into a single value representative of both sexes. Each mouse line was maintained on a C57/Bl6J background and back-crossed as needed. All mice were group housed 2-5 animals per cage and maintained on 12 h light/dark cycle (lights on at 0600 hours) under controlled temperature (20–25 °C) and humidity (30–50%) levels. Mice were given access to food and water *ad libitum.* All treatments and interventions were approved by the Vanderbilt Animal Care and Use Committee.

Reagents: All *in vivo* injections were done with sterile saline as vehicle (0.9% sodium chloride; Hospira, Lake Forest, IL). Guanfacine hydrochloride (#1030, >99%) and atipamezole hydrochloride (#2937, >99%) were obtained from Fisher Scientific (Hampton, NH) and diluted in sterile saline (guanfacine: 1 mg/10 mL=0.35 mM) or deionized (di)H_2O as stock solution (both: 10 mM). ZD7288 was obtained from R&D systems (#1000, >99%; Minneapolis, MN) and diluted in diH_2O as stock solution (10 mM). Clonidine (#0690, >99%) and UK-14,304 (#2466, >99%) were obtained from Tocris Biosciences (Bristol, United Kingdom) and diluted in diH_2O as stock solution (10 mM). Clozapine-N-oxide (CNO) was obtained from Sigma Aldrich (#C0832, >98%; St. Louis, MO) and diluted in sterile saline (3 mg/10 mL=0.88 mM). Metacam was obtained from Patterson Veterinary (#07-845-6986; Greeley, CO) and diluted in sterile saline (2.5 mg/10 mL). Primary antibodies were used at 1:1000 dilution and included rabbit anti-cfos (Millipore, Darmstadt, Germany; abe457; RRID:AB_2631318), mouse anti-NeuN (Millipore mab377 clone A60; RRID:AB_2298772), and chicken anti-GFP (Abcam, Cambridge,

United Kingdom; ab13970; RRID:AB_300798). Secondary antibodies (Jackson ImmunoResearch, West Grove, PA) including Cy2 donkey anti-rabbit (711-225-152; RRID:AB_2340612), Cy3 donkey anti-mouse (715-165-150; RRID:AB_2340813), Cy2 donkey anti-chicken (703-225-155; RRID:AB_2340370) and Cy5 donkey anti-rabbit (711-175-152; RRID:AB_2340607) were diluted in equal volumes sterile H_2O and glycerol and were used at a final dilution of 1:400. Adeno-associated viral (AAV) vectors were used as received and included AAV5-CaMKIIα-hM4Di:mCherry (AAV5-hM4Di; UNC Viral Vector Core), AAV5-CaMKIIα-mCherry (AAV5-mCherry; UNC Viral Vector Core), AAV9-CMV-eGFP (AAV9-GFP; UNC Viral Vector Core), and AAV5-hSyn-GCaMP6f (AAV5-GCaMP6f; Addgene, Cambridge, MA). AAV5-GCaMP6f and AAV5-hM4Di or AAV5-mCherry were mixed in equal volumes immediately prior to injection. In addition, AAV9-hU6-shHCN1-shHCN2-CaMKIIα-eGFP (AAV9-shHCN1/2) was produced by standard protocol, purified with an iodixanol density gradient, and filtered and concentrated in PBS using centrifugal filter cartridges. Final titers were determined by qPCR, and specificity and efficiency were tested by qPCR and Western Blot in cell culture and hippocampal tissue (data not shown).

Fast-scan cyclic voltammetry - Slice preparation (Wills et al., 2012; Flavin et al., 2014) and voltammetry were performed as described previously (Melchior et al., 2015; Melchior and Jones, 2017). Briefly, mice were anesthetized with isoflurane, decapitated, and coronal slices (300 um thick) containing BNST were prepared in ice-cold, oxygenated artificial cerebrospinal fluid (ACSF) consisting of (in mM) NaCl (126), KCl (2.5), NaH_2PO_4 (1.2), $CaCl_2$ (2.4), $MgCl_2$ (1.2), $NaHCO_3$ (25), glucose (11), L-ascorbic acid (0.4) and pH adjusted to 7.4. Slices were allowed to recover in oxygenated ACSF at room temperature for 1 hour, then transferred to a recording

chamber through which 32°C oxygenated ACSF was perfused at a rate of 2 mL/min. A carbon fiber electrode (150 μm length) was placed into the ventral BNST approximately 200 μm ventral to the anterior commissure. Extracellular catecholamine signals were monitored at the carbon fiber electrode every 100 ms using fast scan cyclic voltammetry (Wightman et al., 1988) with an applied waveform ranging from -0.4 to 1.2 V vs Ag/AgCl reference, at a rate of 400 volts per second. A bipolar stimulating electrode was placed on the surface of the slice approximately 150 μM from the carbon fiber recording electrode. Catecholamine release was evoked by an electrical pulse (550 μA, 4 ms duration) applied as a 20-pulse stimulation train (20 Hz) once every 10 min. Baseline recordings were obtained until the catecholamine release amplitude was stable (< 10% variation across 3 recordings). Subsequently, Guanfacine Hydrochloride (10 μM) was applied to the slice buffer and recordings continued for 60 min. For each slice, a single baseline release value was determined by averaging the final two baseline recordings, and the drug effect was determined by averaging the final two recordings in drug and presented as the percent change from the baseline value.

Fluorescent Immunohistochemistry – Mice were handled for five days as described previously (Olsen and Winder, 2010). After removal from the colony, mice recovered for at least one hour in a Med Associates sound-attenuating chamber and were injected intraperitoneally with guanfacine (1 mg/kg), clozapine-N-oxide (CNO, 3 mg/kg), guanfacine and CNO, or saline 90 minutes prior to perfusion. Under isoflurane anesthesia, mice were transcardially perfused with 10 mL ice-cold phosphate buffered saline (PBS) followed by 20 mL 4% paraformaldehyde (PFA) in PBS. Extracted brains were submerged in 4% PFA for 24 hours at 4°C and cryoprotected in 30% sucrose in PBS for a minimum of two days. Coronal sections were cut on a

cryostat (Leica, CM3050S) in Optimal Cutting Temperature (OCT) solution (VWR, Radnor, PA) at a thickness of 40 µm and stored in PBS at 4°C until immunological staining.

For cfos staining, coronal sections were washed with PBS (4x10 min), permeabilized with 0.5% Triton X-100 in PBS (1 hour), and blocked with 5% Normal Donkey Serum (NDS) and 0.5% Bovine Serum Albumin (BSA) for 1 hour at room temperature (RT). Primary antibodies were applied in blocking solution and slices were incubated in primary antibody (rabbit anti-cfos, mouse anti-NeuN, chicken anti-GFP) for 24 hours at RT, washed in PBS (4x10 min), and incubated in combinations of secondary antibodies (Cy2 donkey anti-rabbit, Cy2 donkey anti-chicken, Cy3 donkey anti-mouse, Cy5 donkey anti-rabbit) in 0.1% Triton X-100 in PBS for 24 hours at 4°C. Slices were stained with DAPI (1:10,000, Life Technologies, Carlsbad, CA; D3571), washed in PBS (4x10 min), mounted on Fisher plus slides (Fisher Scientific), and coverslipped with PolyAquamount (Polysciences, Warrington, PA) when dry. Slight modifications were used to visualize cfos-eGFP transgene expression. In this case, a modified blocking solution (10% NDS and 0.1% Triton X-1000 in PBS), a shorter time of permeabilization (30 minutes), and longer primary antibody incubation (48 hours at 4°C) were used.

All images were obtained with a Zeiss 880 scanning confocal microscope using either a 20X/0.80 N.A. Plan-Apochromat, 40X/1.30 N.A. C Plan-Apochromat Oil, or 63X/1.40 N.A. Plan-Apochromat Oil objective lens. Excitation/emission wavelengths (nm) for each fluorophore were 405.0/461.5 (DAPI), 448/521.5 (Cy2, GFP), 561.0/610.8 (Cy3, mCherry) and 633.0/701.8 (Cy5). The same acquisition parameters and alterations to brightness and contrast in ImageJ were used across all images within an experiment. Cells were manually counted using ImageJ by a blinded reviewer. No overt differences were observed between sub-nuclei of the dorsal BNST so

all numbers are reported as a single averaged value for each dBNST and then averaged for each animal.

RNA in situ hybridization – A variant of fluorescence *in situ* hybridization (FISH) known as RNAScope (ACD; Advanced Cell Diagnostics; Hayward, CA) was used to visualize RNA transcripts in fresh-frozen BNST coronal sections. The procedure was performed as described previously (Ghamari-Langroudi et al., 2015). RNAScope cDNA probes and detection kits were purchased from ACD and used according to the company's online protocols. All probes were generated against *Mus musculus*-specific transcripts and included *Adra2a* (#425341, channel C1, target region 2345-3381, accession number NM_007417.4), *Fos* (#316921-C2, C2, 407-1427, NM_010234.2), *Hcn1* (#423651-C2, C2, 2158-3777, NM_010408.3), *Hcn2* (#427008-C2, C2, 687-1878, NM_008226.2), *Prkcd* (#441791-C3, C3, 334-1237, NM_011103.3), *Penk* (#318761-C2, C2, 106-1332, NM_0001002927.2), *Calb2* (#313641-C2, C2, 147-1265, NM_007586.1), *Crf* (#316091-C2, C2, 20-1262, NM_205769.2), and *Npy* (#313321-C3, C3, 28-548, NM_023456.2).

Mice used to monitor *Fos* transcript co-localization were handled and injected as described above. For expression analysis of HCN subunits, mice were equivalently handled but never injected. Brains were extracted under isoflurane anesthesia, submerged in oxygenated (5% CO_2/95% O_2) ice-cold artificial cerebrospinal fluid (ACSF; in mM: 124 NaCl, 4.4 KCl, 2.5 $CaCl_2$, 1.3 $MgSO_4$, 1 NaH_2PO_4, 10 glucose, 26 $NaHCO_3$), and frozen in OCT using Super Friendly Freeze-It Spray (Fisher Scientific). Embedded brains were stored in dry ice and then at -80°C until further use. 16 µm sections were cut on a cryostat (Leica CM3000) and transferred to Fisher plus slides (Fisher Scientific) chilled with dry ice and stored at -80°C. Samples were fixed in 4% PFA at 4°C for 15 minutes, dehydrated in an ethanol dilution series (50%, 70%, 100% x2

for 5 minutes each) and air-dried for 5 minutes. A hydrophobic barrier was drawn around each slice with a PAP barrier pen prior to incubation with ACD's pretreatment 4 solution (30 minutes at 40°C), then RNAScope probes (2 hours at 40°C), then Amp 1-FL solution (30 minutes at 40°C), Amp 2-FL solution (15 minutes at 40°C), Amp 3-FL solution (30 minutes at 40°C), and Amp 4-FL ALT B solution (15 minutes at 40°C) with two minutes of washing in Wash Buffer (2x) in between each step. Slides were counterstained with 1:10,000 DAPI for 30 seconds at RT before coverslipping with Aqua PolyMount. A minimum of two slices (one slice per slide) were used from each animal: one experimental group and one negative control (3 probe sets for bacterial DapB mRNA in channels 1-3, ACD). Slices from each mouse were examined with different probes.

Sections were imaged with a Zeiss 880 scanning confocal microscope using either a Plan-Apochromat 20X/0.80 N.A or 63X/1.40 oil lens. Z stacks were done on all high magnification images such that the depth of the tissue was covered in 8 images (1 image per 2 um). The BNST was visualized at 10X magnification (10X/0.50 N.A. lens) and then three 63X images were obtained to cover the dorsal, medial, and lateral components of the dorsal BNST. Each image was quantified individually, but since no differences observed between the three subregions, the counts were compiled into a single average value for each dorsal BNST, then averaged for each animal. Z stacks were transformed into single layer images using ImageJ Z-project (maximum intensity). Transcripts were readily identified as small, round, and distinct dots over and surrounding DAPI-labelled nuclei (see Figures 2C and 6A for example images). Negative control images were used to determine brightness and contrast parameters that minimized observation of the bacterial transcripts and autofluorescence, which were then used for experimental images. Dots per cell were manually counted across all images by a blinded reviewer. To determine the

threshold for transcript positivity in experimental slices, the number of dots per cell were counted in negative control images, and the threshold for positivity was calculated as the mean number of dots per cell plus three standard deviations such that 99.7% of negative control cells were below this threshold.

Ex vivo preincubation – Brain slices were obtained as described above. *cfos-eGFP* mice were handled and injected as described above. After preparation, slices were sequentially transferred to one of four holding chambers in oxygenated ACSF at 28°C and allowed to recover for one hour. In the first preincubation experiment, guanfacine (1 µM), atipamezole (1 µM), both guanfacine and atipamezole, or vehicle were added to the holding chamber from stock solutions. In the second preincubation experiment, guanfacine (1 µM), clonidine (10 µM), UK-14,304 (10 µM), or vehicle were equivalently added. After 60 minutes of incubation, slices were fixed in 4% PFA for 30 minutes at RT before being transferred to 4°C for 24 hours. Slices were then transferred to PBS and maintained at 4°C until further use.

The Brain Blocking of Lipids and Aldehyde Quenching (BLAQ) procedure was used as previously described (Kupferschmidt et al., 2015). Sections were washed for 1 hour in PBST (0.2% Triton X-100 in PBS), rinsed twice for one minute in diH_2O, quenched in freshly prepared sodium borohydride ($NaBH_4$; 5 mg/mL=132 mM in diH_2O; Sigma, #213462, 99%), rinsed again in diH_2O (2x for 1 minute), incubated twice for 15 minutes in Sudan Black B solution (0.2% in 70% ethanol), washed twice for 30 minutes in PBS, and incubated for 4 hours in 5% normal donkey serum in PBST. Slices were incubated in primary antibody (chicken anti-GFP, mouse anti-NeuN) for 72 hours at 4°C, washed four times in PBST for a total of 24 hours at 4°C, and then incubated in secondary antibody (Cy2 donkey anti-chicken, Cy3 donkey-anti mouse) for 48

hours at 4°C. Finally, slices were washed four times in PBST for a total of 24 hours at 4°C, washed in PBS for 1 hour at RT, and mounted on Fisher plus slides and coverslipped with Poly AquaMount when dry. Images were obtained with a Zeiss 880 scanning confocal microscope using a 63X/1.40 N.A. Plan-Apochromat Oil objective lens and processed as described above for fluorescent immunohistochemistry.

Microinjection Surgeries: Mice were anesthetized with isoflurane (initial dose = 3%; maintenance dose = 1.5%) and injected intracranially with recombinant AAV constructs. A targeted microinjection of the viruses (200-300 nL) was made into the BNST (AP: 0.14, ML: +/- 0.88, DV: -4.24) (Paxinos and Franklin, 2004) at a 15.03° angle. All injections were bilateral except for the dual AAV5-GCaMP6f and AAV5-hM4Di or AAV5-mCherry injections, which were unilateral on the right side. Mice were treated with 5 mg/kg injections of ketoprofen or metacam for 48 hours following surgery. All mice except for the GCaMP6f-injected animals were killed 3 weeks after surgery for anatomical analysis. GCaMP6f-injected animals underwent implantation of optical fibers at least three weeks after viral injection followed by subsequent behavioral analysis.

Electrophysiology Recordings – Current Clamp Recordings Whole-cell current-clamp recordings were performed as previously reported (Kash and Winder, 2006; Silberman et al., 2013; Flavin et al., 2014). For current-clamp recordings, electrodes (3.0-5.0 MΩ) were filled with (in mM): 135 K^+-gluconate, 5 NaCl, 10 Hepes, 0.6 EGTA, 4 Na_2GTP (pH 7.2-7.4, osmolarity 290-295).

cfos-eGFP mice were handled and injected, and brain slices were prepared as described above. After one hour of recovery in heated (28°C) oxygenated ACSF, slices were transferred to

a second heated holding chamber with either unaltered ACSF or ACSF containing 10 µM ZD7288 for one hour prior to recording. In the recording chamber slices were continuously perfused with oxygenated and heated (28°C) ACSF at a rate of 1-2 mL/min. Picrotoxin (25 µM) was used to isolate excitatory transmission. cfos-eGFP+ cells were identified using a mercury lamp light source, EN-GFP filter cube, and infrared video microscopy (all Olympus) for patching.

After achieving whole-cell configuration, cells were equilibrated for 2-5 minutes prior to recording. Postsynaptic parameters were monitored continuously during the experiments and cells were excluded if the access resistance (R_a) changed by >20% in either direction. Current clamp profiles, defined here as the whole-cell membrane potential changes that occur in response to positive and negative current injections, were obtained at resting membrane potential and consisted of current injections ranging from -200 pA to +200 pA with a step of 20 pA per injection. Once a current clamp profile was obtained, spontaneous excitatory postsynaptic potentials were recorded for five minutes. After one hour of recording, slices were transferred to 4% PFA and processed for Brain BLAQ as described above. Current clamp recordings from shRNA-injected C57/Bl6J mice were similarly performed, except that these mice were never injected, and slices were not incubated with ZD7288.

All whole cell data were recorded with Clampex 10.2 and analyzed with pClamp 10.2 (Molecular Devices, San Jose, CA). Resting membrane potential was calculated prior to current injection. Hyperpolarization sag was calculated as the difference between the initial maximal negative membrane potential and the steady state current after negative current injection. The time constant of I_h activation (τ) was calculated as the time to reach 1-1/e (63.2%) of steady state potential from maximal negative potential. Spontaneous EPSP measurements were analyzed with

pClamp 10.2 using the "Event Detection" template created for each trace individually to obtain amplitude and frequency of sEPSP events.

Electrophysiology Recordings – Field Potentials Thy1-COP4 mice were used for optical field potential recordings. Slices were prepared as described above. Picrotoxin (25 µM) was used to isolate excitatory transmission. Light stimulation was driven from a T-Cube LED Driver (LEDD1B; Thorlabs, Newton, NJ) passed through an EN-GFP filter cube (Olympus) to produce blue wavelength light. Light stimuli were approximately 2 ms in duration and occurred every 10 seconds. Optically-evoked field potentials were observed as negative deflections with dual N1 (oN1) and N2 (oN2) components. The oN2 component was kynurenic acid-sensitive while the oN1 component was kynurenic acid-insensitive (data not shown), and are thus analogous to the fiber volley potential N1 and the synaptic potential N2 recorded as part of electrically evoked field potentials within the BNST (Weitlauf et al., 2004; Egli et al., 2005; Conrad et al., 2012). Data was excluded if the oN1 changed by >20% during the experiment. All field potential data was collected using Clampex 10.2 (Molecular Devices) and analyzed via Clampfit 10.2 (Molecular Devices) as previously described (Shields et al 2009; Flavin et al 2014). Plotted time courses are represented as one-minute averages relative to baseline (0-5 minutes for guanfacine, 0-10 minutes for ZD7288).

Stereotaxic Chronic Optical Fiber Implantation – Three weeks after injection of AAV5-GCaMP6f and AAV5-hM4Di or AAV5-mCherry, mice were anesthetized with isoflurane and underwent stereotaxic surgery for optical fiber implantation. The optical fiber implant was constructed from a 0.22 NA 300 µm core multimode fiber (Thorlabs) placed inside a mounting

ferrule with Epo-Tek general room temperature cure epoxy (Fiber Optic Center, New Bedford, MA) and cured at 45°C overnight. The fiber was cut on one end with an Ideal DualScribe Wedge Tip Carbide Scribe (Fiber Optic Center) and polished using a Ferrule Polishing Disc (Thorlabs) on progressively fine aluminum oxide lapping sheets (5 um, 3 um, 1 um, 0.1 um). Both sides were visually inspected for aberrations and were not used if deemed unsatisfactory. Briefly, after exposure of the skull, gel etchant was used to clean the skull, a screw was placed rostral to the craniotomy hole, the implant was slowly lowered through the previously made craniotomy hole into the BNST at a 15.03° angle, Optibond FL Primer was applied around the implant, Optibond FL Adhesive was applied and cured, and Herculite Unidose Enamel was applied and cured. After surgery, mice were given Diet Gel as well as subcutaneous injections of ketoprofen or metacam and 1 mL saline for 72 hours. A minimum of two weeks of recovery was used before mice underwent behavioral and fiber photometric testing.

In vivo fiber photometry apparatus –The fiber photometry measurements in this study were carried out by the ChiSquare 2-202 dual-probe system (ChiSquare Biomaging, Brookline, MA). Briefly, blue light from a 473-nm picosecond-pulsed laser (at 50 MHz; pulse width ~80 ps FWHM) was delivered to the sample through a single mode fiber. Fluorescence emission from the tissue was collected by a multimode fiber. The single mode and multimode fibers were arranged side by side (Cui et al., 2013) in a ferrule that is connected to a detachable multimode fiber implant. The emitted photons collected through the multimode fiber pass through a bandpass filter (FF01-550/88, Semrock) to a single-photon detector. Photons were recorded by the time-correlated single photon counting (TCSPC) module (SPC-130EM, Becker and Hickl GmbH, Berlin, Germany) in the ChiSquare 2-202 dual-probe system. A fluorescence intensity

trace was obtained by plotting the number of photons recorded in 20 ms intervals against time. Fluorescence decay kinetics were used to confirm *in vivo* GcaMP6f expression.

Elevated Plus Maze Behavior and Fiber Photometric Recordings – All behavior experiments were performed during the light phase. Mice were handled and injected as described above prior to and during behavioral experiments. In addition, the last two days of handling involved transport to the laboratory and habituation to fiber photometry manipulations including cleaning of implants with ethanol and lens paper, and recording fiber photometry signal via a 200 µm core 0.5 N.A. FC/PC to 1.25 mm ferrule patch cable (Thorlabs) connected to the implant. Before behavioral testing, mice were injected with CNO or saline two hours prior to recording a baseline for two minutes. This baseline recording occurred in the home cage after acclimation to connection with the patch cord for five minutes. Then mice were transferred to the elevated plus maze (EPM) for five minutes. This apparatus is elevated 55 cm above the floor and consists of four arms (30.5x6.5 cm), two open and two closed (16cm wall height) with a 5x5 cm open center zone. Lighting was set to approximately 60-70 lux in the open arm and 10-20 lux in the closed arm. Mice were visualized, recorded, and tracked by a camera using AnyMaze software (Stoelting Co, Wood Dale, IL). Fiber photometry recordings began upon receipt of a TTL (Transistor-Transistor Logic) pulse from AnyMaze; therefore, the behavior and fiber photometry signal were precisely time-locked. Raw photon count was converted to $\Delta F/F_0$ using a segmented normalization procedure with a bin of 4 seconds. Ca^{2+} transients were identified using a Savitsky-Golay filter and empirically determined kinetic parameters using the mLspike algorithm (Deneux et al., 2016). The frequency of Ca^{2+} transients was calculated for both

recordings. In addition, the transients were temporally aligned with mouse location to yield open and closed arm frequencies.

Experimental Design and Statistical Analysis

The number of animals to be used in each experiment were pre-determined based on analyses of similar experiments in the literature and supplemented as needed based on observed effect sizes (Savchenko and Boughter, 2011; Silberman et al., 2013; Flavin et al., 2014; Ghamari-Langroudi et al., 2015; Kupferschmidt et al., 2015, 2017; Holleran et al., 2016). For experiments involving male and female mice, a minimum of three mice of both sexes was used in order to allow for sex difference statistical comparisons to be performed. All data are represented as mean±SEM. All statistics were run using Prism 7 (Graphpad, La Jolla, CA). Differences between groups were assessed using t-tests, one-way ANOVAs, and two-way ANOVAs, with significance set at α=0.05. When significant main effects were obtained using ANOVA tests, appropriate post-hoc comparisons between groups were performed. Robust regression and Outlier removal (ROUT) tests were performed on each data set but no data were excluded as a result.

Results

Guanfacine induces cfos expression in the dBNST dependent on the expression of α_{2A}-ARs in non-noradrenergic neurons

To determine what populations of α_{2A}-ARs contribute to guanfacine-induced cfos expression in the dBNST, we compared effects in wildtype mice and two transgenic mouse strains targeting the *Adra2a* gene. The transgenic genotypes were (1) a complete α_{2A}-AR knockout (*Adra2a*-/-) and (2) a transgenic rescue reintroducing the *Adra2a* gene under the

control of the dopamine β-hydroxylase promoter into an *Adra2a*-/- background (Gilsbach et al., 2009). The rescue results in the expression of α_{2A}-AR exclusively in adrenergic neurons. These lines allow for the differentiation of autoreceptor and heteroceptor mechanisms of α_{2A}-AR physiology and pharmacology (Figure 1A-B). We validated the functional autoreceptor expression pattern of α_{2A}-ARs within these mouse lines using fast scan cyclic voltammetry. To do this, we measured extracellular catecholamine levels in the ventral BNST after local electrical stimulation and determined autoreceptor α_{2A}-AR function by measuring the effects of guanfacine (10 μM) on catecholamine levels (Figure 1C). In wild-type mice, guanfacine decreased stimulus-evoked catecholamine transients to 69.2±3.9% of baseline levels (baseline: 10-30 minutes; guanfacine: 70-90 minutes; paired t-test, $p=0.002$; Figure 1D, blue). This effect was absent in full *Adra2a*-/- mice (109.1±3.1%; $p=0.12$; Figure 1D, red) but rescued in heteroceptor-specific *Adra2a-/-* mice (76.5±5.1%; $p=0.01$; Figure 1D, green). A repeated measures two-way ANOVA revealed a significant effect of time ($F(9,126)=8.01$, $p<0.0001$), genotype ($F(2,14)=19.99$, $p<0.0001$), and subject ($F(14,126)=2.93$, $p=0.0007$), as well as an interaction between time and genotype ($F(18,126)=4.81$, $p<0.0001$) on measured extracellular catecholamine levels. Holm-Sidak's multiple comparison test was performed *post hoc* between the genotypes at all time points. Extracellular catecholamine levels were lower in wild-type than full *Adra2a-/-* mice at all time points after 50 minutes (0 minutes, $p=0.47$; 10 min, $p=0.84$; 20 min, $p=0.92$; 30 min, $p=0.92$; 40 min, $p=0.07$; 50 min, $p=0.004$; 60 min, $p<0.0001$; 70 min, $p<0.0001$; 80 min, $p<0.0001$; 90 min, $p<0.0001$) and in heteroceptor-specific relative to full *Adra2a-/-* mice after 60 minutes (0 min, $p=0.90$; 10 min, $p=0.84$; 20 min, $p=0.92$; 30 min, $p=0.92$; 40 min, $p=0.36$; 50 min, $p=0.57$; 60 min, $p=0.03$; 70 min, $p=0.01$; 80 min, $p<0.0001$; 90 min, $p<0.0001$). Between 50 and 70 minutes, heteroceptor-specific *Adra2a-/-* mice were

significantly higher than wild-type littermates (0 min, p=0.47; 10 min, p=0.998; 20 min, p=0.92; 30 min, p=0.92; 40 min, p=0.36; 50 min, p=0.02; 60 min, p=0.004; 70 min, p=0.02; 80 min, p=0.31; 90 min, p=0.23). To determine overall guanfacine effect, a one-way ANOVA was performed at the final time points (70-90 minutes) and revealed significant differences among the three genotypes ($F(2,12)=27.94$, $p<0.0001$; Figure 1E). Holm-Sidak's multiple comparison test was performed *post hoc* between all genotypes and showed there to be significant differences between wildtype and full ($p<0.0001$) but not heteroceptor-specific ($p=0.38$) *Adra2a-/-* mice. Further, there was a significant difference between full and heteroceptor-specific ($p<0.0001$) knockout mice.

We next evaluated neuronal cfos expression 90 minutes after saline or guanfacine (1 mg/kg) injections (Figure 1F-G). A two-way ANOVA revealed a significant interaction between treatment and genotype ($F(2,105)=11.62$, $p<0.0001$) alongside no significant effect of genotype alone ($F(2,105)=0.88$, $p=0.42$) and a significant effect of treatment alone ($F(1,105)=5.24$, $p=0.02$) (Figure 1H). A Holm-Sidak multiple comparisons test was performed *post hoc* between all groups. Guanfacine-injected animals showed increased cfos levels in wild-type animals (WT saline: 4.4±0.9%; WT guanfacine: 14.2±1.4%; $p=0.0004$) but not in full α_{2A}-AR knockout (KO saline: 13.5±1.3%; KO guanfacine: 9.0±0.6%; $p=0.19$) or heteroceptor-specific α_{2A}-AR knockout animals (KO+TG saline: 8.8±1.6%; KO+TG guanfacine: 11.7±1.4%; $p=0.58$).When injected with saline, α_{2A}-AR knockout mice show increased cfos expression relative to wild-type controls ($p=0.0004$), while there was no difference between heteroceptor-specific α_{2A}-AR knockout mice and wild-type controls ($p=0.33$) or full α_{2A}-AR knockout mice ($p=0.07$). Together, these data show that guanfacine-induced cfos expression is only observed in wild-type animals and an elevated cfos response to saline occurs in α_{2A}-AR knockout mice.

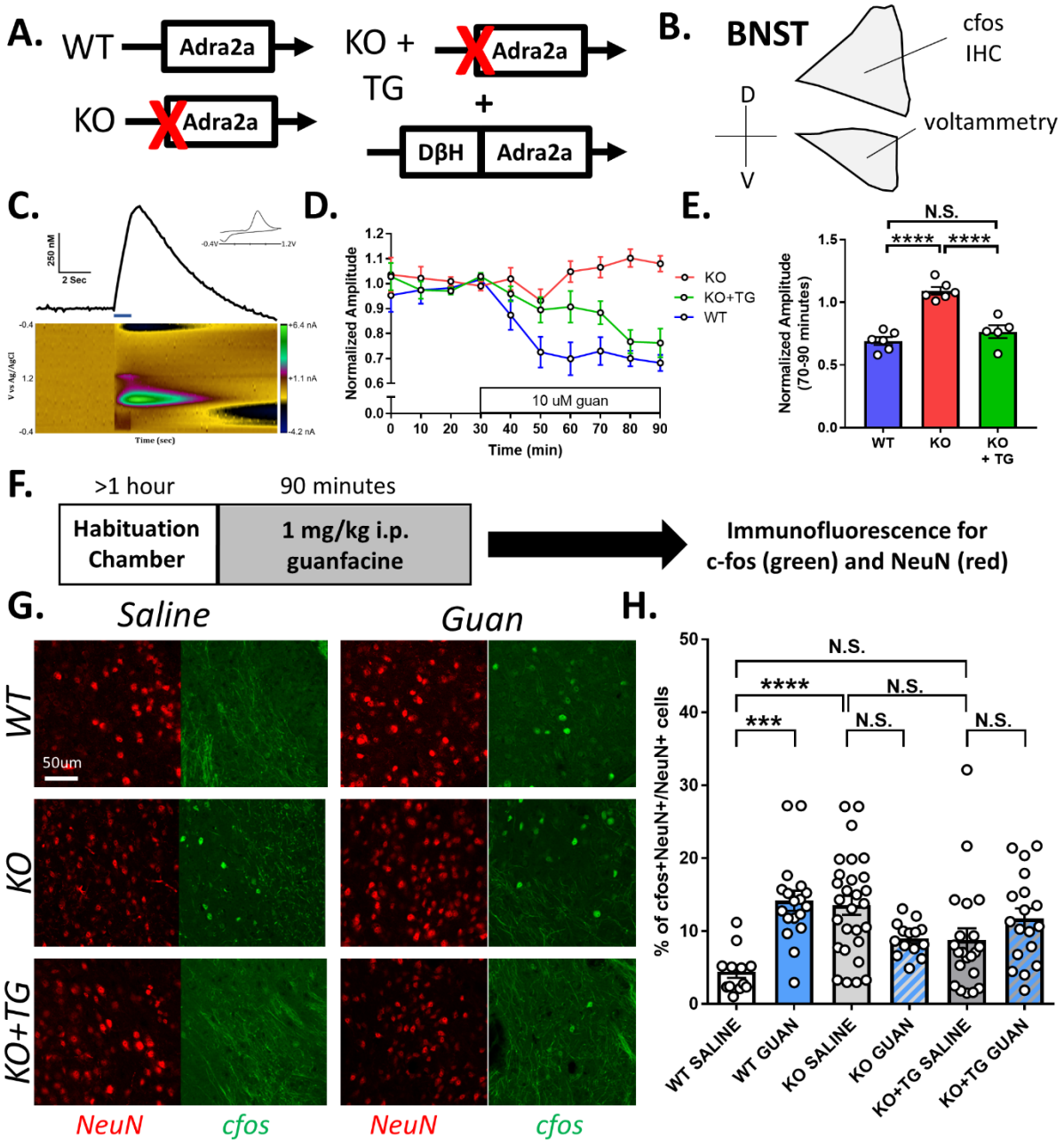

Figure 2 – Guanfacine-induced cfos expression in the dBNST is dependent on the expression of α2A-ARs in non-noradrenergic neurons. (A) Schematic showing genetic differences between the three different *Adra2a* mouse lines. (B) Anatomical diagram showing location of immunohistochemistry and voltammetry experiments within the BNST (C) Representative fast scan cyclic voltammetry trace showing catecholamine measurement after electrical stimulation in ventral BNST. (D) Time course of guanfacine (10 uM) application on amplitude of extracellular catecholamine in the ventral BNST. Wild-type and heteroceptor-specific *Adra2a-/-* mice show a decrease after guanfacine (70-90 minutes) application relative to baseline (10-30 minutes; WT:

69.2±3.9%, p=0.002; KO+TG: 76.5±5.1%, p=0.01) while full *Adra2a-/-* do not (109.1±3.1%, p=0.12). Two-way ANOVA: time effect F(9,126)=8.01, p<0.0001, genotype effect F(2,14)=19.99, p<0.0001, subject F(14,126)=2.93, p=0.0007, interaction F(18,126)=4.81, p<0.0001. P-values were determined by *post hoc* Holm-Sidak multiple comparison's test (E) Relative to wild-type littermates, full *Adra2a-/-* mice show a loss of guanfacine activity at autoreceptor α_{2A}-ARs, a deficit rescued in the heteroceptor-specific *Adra2a-/-* mice (F(2,12)=27.94, p<0.0001). N=5-6 slices from 3 animals per group (F) Schematic showing timeline of animal habituation, injection, and immunofluorescence. (G) Representative images of NeuN (red) and cfos (green) expression after saline and guanfacine injections in wild-type (WT, B), full *Adra2a-/-* (KO, C), and heteroceptor-specific *Adra2a-/-* (KO+TG, D) mice. (H) Guanfacine induced cfos expression in NeuN+ cells was higher after guanfacine injection than after saline injection only in wild-type mice, but not in full or heteroceptor-specific *Adra2a-/-* littermates. Elevated saline-induced cfos expression was observed in full but not heteroceptor-specific *Adra2a-/-* mice relative to wild-type littermates. N=12-26 animals per group. Two-way ANOVA: treatment effect F(1:105)=5.24, p=0.02, genotype effect F(2,105)=0.88, p=0.42, interaction F(2:105)=11.62, p<0.0001. P-values were determined by *post hoc* Holm-Sidak multiple comparison's test. All data represented as mean±SEM. *P<0.05, **P<0.01, N.S. P>0.05.

Guanfacine-induced cfos responses occur in dBNST^{Adra2a} neurons.

Next, we aimed to determine the population of dBNST neurons that express cfos after guanfacine administration. Due to lack of antibody specificity for the α_{2A}-AR, we utilized *Adra2a* transcript expression as a means of identification (Figure 2A-B). The *Adra2a* probe was anatomically validated by observation within the dBNST (Figure 2B, top) alongside a lack of detectable expression of the negative control bacterial probe *DapB* in the dBNST (Figure 2B, middle) and in the α_{2A}-AR-lacking dorsal striatum within the same coronal section (Figure 2B, bottom) (Nicholas et al., 1993). On average, the density of *Adra2a*+ cells in the dorsal BNST was 282±45 cells/mm^2 in saline-injected animals and 269±56 in guanfacine-injected animals representing 31.8±3.9% and 28.6±5.9% of DAPI+ cells, respectively. The difference between either of these values was not statistically significant (unpaired t tests, p=0.85 and p=0.64). We monitored *Fos* transcript expression within *Adra2a*+ cells 90 minutes after saline or guanfacine injections (Figure 2C). Treatment with guanfacine significantly increased the percentage of

Adra2a+ cells that were also *Fos*+ (14.5±4.1% saline versus 66.3±5.1% guanfacine, unpaired t-test, $p<0.0001$; Figure 2D). In addition, treatment with guanfacine led to a small but significant increase in the percentage of *Adra2a*- cells that were *Fos*+ (7.3±2.1% saline versus 24.0±6.0% guanfacine, unpaired t-test, $p=0.02$; Figure 2E). Thus, guanfacine injection leads to upregulation of *Fos* within *Adra2a*+ and *Adra2a*- cells within the dBNST.

In an effort to better classify *Adra2a*+ dBNST cells, we aimed to co-localize *Adra2a* transcript expression with a number of genetic markers known to be expressed in sub-populations of dBNST neurons. *Adra2a* co-localization was modest with the transcripts *Prkcd* (29.8±3.1%), *Penk* (35.5±6.3%), *Calb2* (29.7±8.5%), *Crh* (24.1±8.1%), and *Npy* (9.2±0.3%), suggesting that the *Adra2a*+ population is a heterogeneous one.

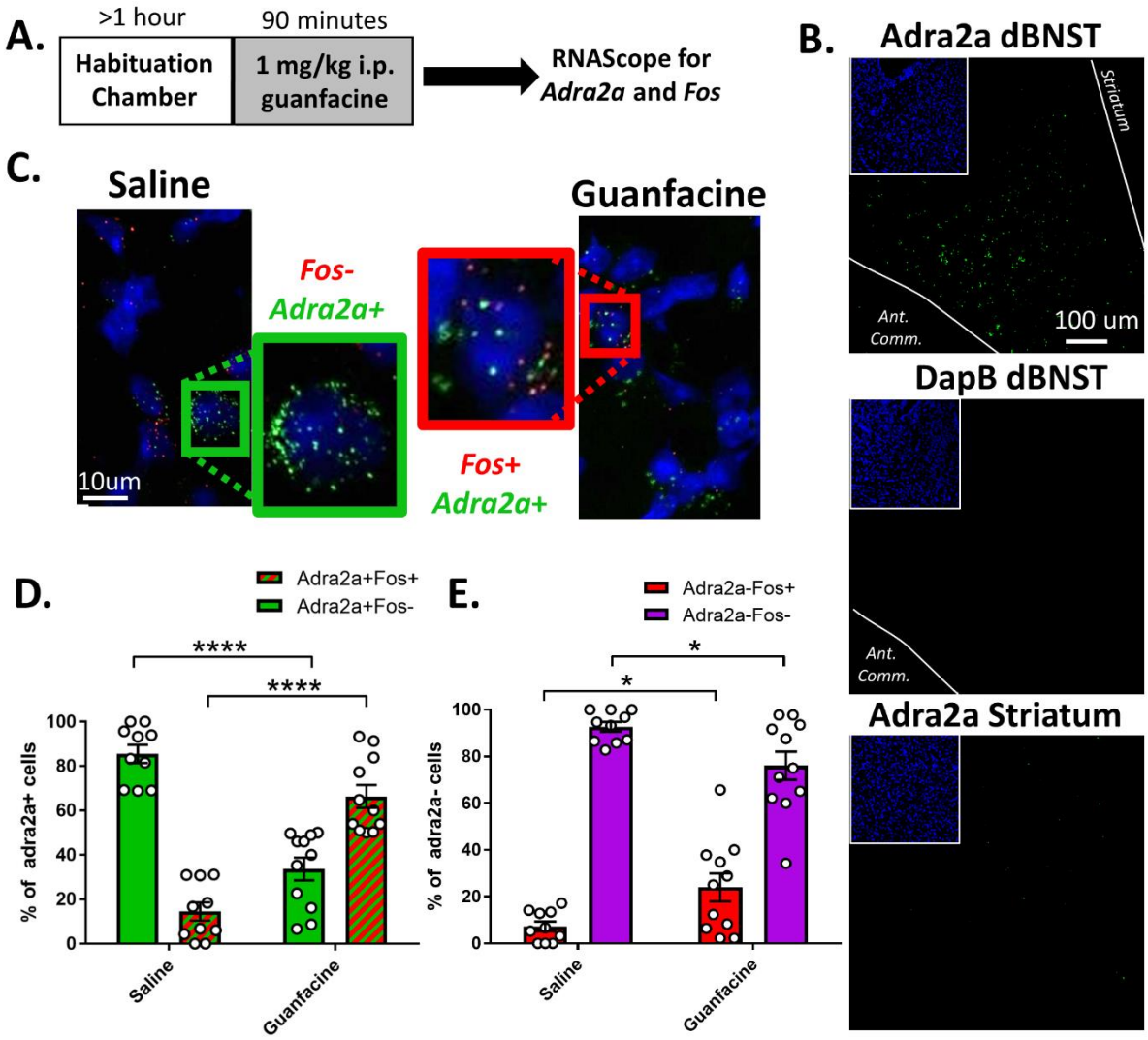

Figure 3 – Guanfacine induces cfos expression in dBNSTAdra2a neurons. (A) Schematic showing timeline of animal habituation, injection, and RNA Scope. (B) Anatomical validation of *Adra2a* probe specificity shows significant expression in dBNST (top) alongside lack of negative control bacterial probe *DapB* in dBNST (middle) and lack of *Adra2a* expression in α_{2C}-AR-expressing dorsal striatum (C) Representative images of DAPI+ nuclei (blue) as well as the transcripts *Adra2a* (green) and *Fos* (red) after saline and guanfacine injections. (Inset) Higher magnification visualization of a representative *Adra2a+Fos-* (B) and *Adra2a+Fos+* (C) cell after saline- and guanfacine-injections, respectively. (D) *Adra2a+* cells are largely *Fos-* (85.5±4.1%) after saline-injection but up-regulate *Fos* after guanfacine injection (66.3±5.1% *Fos+*). All data are represented as mean±SEM. P-values determined by unpaired t-test. ****P<0.0001. N=10-11 animals per group.

Guanfacine-induced cfos expression is dBNST autonomous.

Upregulation of cfos/*Fos* can be achieved through several mechanisms, some due to direct pharmacological action and others by indirect effects on circuitry. To gain insight into whether guanfacine-induced cfos expression in the dBNST resulted from interactions with other brain regions in an experience-dependent manner, we combined the use of a *cfos-eGFP* transgenic mouse strain which expresses a GFP-labeled cfos fusion protein (Barth et al., 2004) with thick slice immunohistochemistry (Kupferschmidt et al., 2015) to determine if guanfacine-induced cfos expression could be mimicked in an *ex vivo* brain slice. Coronal sections (300 µm thick) containing the dBNST were exposed to artificial cerebrospinal fluid (ACSF), the α_{2A}-AR agonist guanfacine (1 µM) (pEC_{50}=7.1-7.3) (MacLennan et al., 1997; Jasper et al., 1998), the α_2-AR antagonist atipamezole (1 µM) (pK_i=8.4-9.5) (Blaxall et al., 1991; Vacher et al., 2010; Vucicevic et al., 2016), as well as a combination of guanfacine and atipamezole for one hour at 28°C. Slices were fixed and stained for NeuN to identify neurons and GFP to quantify cfos-eGFP expression (Figure 3A). cfos-eGFP+ cells were readily identified with minimal background activity and quantified as a proportion of neuronal cells (Figure 3B-C). A two-way ANOVA showed a significant effect of guanfacine ($F(1,44)=12.39$, $p=0.001$) and atipamezole ($F(1,44)=12.04$, $p=0.001$), as well as a significant interaction between the two ($F(1,44)=18.22$, $p=0.0001$). A Holm-Sidak multiple comparisons test showed significant upregulation of cfos in guanfacine-incubated slices relative to ACSF-incubated controls (control: 10.9±1.8%, guanfacine: 28.3±3.0%, $p<0.0001$) and no effect of atipamezole relative to ACSF-incubated controls (atipamezole: 12.7±2.0%, $p=0.92$). Incubation of slices in guanfacine and atipamezole did not alter cfos expression relative to ACSF-incubated controls (guanfacine and atipamezole: 11.0±2.1%, $p=0.97$) or atipamezole-incubated samples ($p=0.92$), but did block guanfacine-

induced cfos expression ($p<0.0001$). Thus, guanfacine is capable of inducing cfos expression in *ex vivo* dBNST slices, and this expression can be blocked by co-incubation with the α_2-AR antagonist atipamezole.

Ex vivo incubation in clonidine and UK-14,304 induces cfos expression in dBNST neurons

To determine the specificity of guanfacine-induced cfos expression, *ex vivo* dBNST slices were incubated with other α_2-AR agonists. We incubated slices in 10 µM clonidine, a α_2-AR partial agonist, and 10 µM UK-14,304, a α_2-AR full agonist, alongside 1 µM guanfacine as a positive control and ACSF as a negative control (Figure 3D-E). A one-way ANOVA showed a significant effect of drug incubation on *ex vivo* cfos-eGFP expression ($F(3,32)=4.63$, $p=0.009$). A Holm-Sidak multiple comparison's test showed that, relative to ACSF-incubated controls (214±68 cells/mm^2), cfos-eGFP expression was upregulated after exposure to guanfacine (826±174 cells/mm^2; $p=0.02$), clonidine (878±161 cells/mm^2; $p=0.02$) and UK-14,304 (854±167 cells/mm^2; $p=0.02$). There were no significant differences between slices incubated in the different α_2-AR agonists (guanfacine vs clonidine, $p=0.99$; guanfacine vs UK-14,304, $p=0.99$, clonidine vs UK-14,304, $p=0.99$). Thus, all three of these α_2-AR agonists can induce cfos-eGFP expression *ex vivo* in dBNST sections.

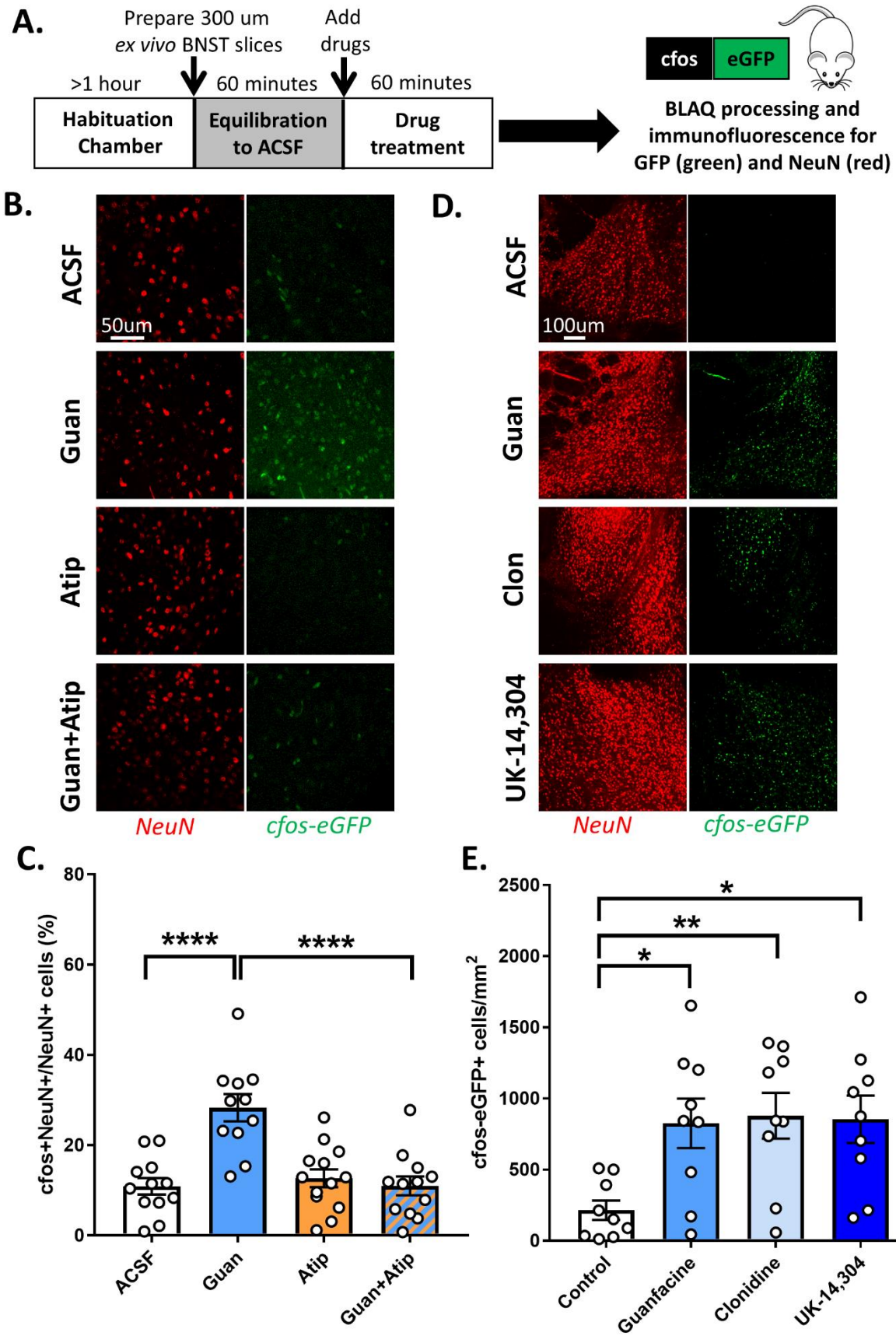
A.
Prepare 300 um
ex vivo BNST slices
Add
drugs
>1 hour
60 minutes
60 minutes
Habituation Chamber
Equilibration to ACSF
Drug treatment
cfos
eGFP
BLAQ processing and immunofluorescence for GFP (green) and NeuN (red)
B.
ACSF
Guan
Atip
Guan+Atip
50um
NeuN
cfos-eGFP
D.
ACSF
Guan
Clon
UK-14,304
100um
NeuN
cfos-eGFP
C.
cfos+NeuN+/NeuN+ cells (%)
****
****
ACSF
Guan
Atip
Guan+Atip
E.
cfos-eGFP+ cells/mm2
*
**
*
Control
Guanfacine
Clonidine
UK-14,304

Figure 4 – Incubation of ex vivo dBNST slices with guanfacine is sufficient to induce cfos expression and can be blocked by atipamezole. (A) Schematic showing timeline of animal habituation, slice preparation, drug application, and immunostaining. (B) Representative images of NeuN (red) and *cfos-eGFP* expression (green) after incubation in ACSF, guanfacine (1 uM), atipamezole (1 uM), or simultaneous application of guanfacine and atipamezole (1 µM each). Two-way ANOVA: guanfacine effect $F(1,44)=12.39$, $p=0.001$, atipamezole effect $F(1,44)=12.04$, $p=0.001$, interaction $F(1,44)=18.22$, $p=0.0001$. (C) Guanfacine incubation induces cfos-eGFP expression in comparison to ACSF-incubated controls. Atipamezole incubation does not alter dBNST cfos-eGFP expression but does block guanfacine-induced cfos induction to almost control levels. (D) Representative images of NeuN (red) and cfos-eGFP expression (green) after incubation in ACSF, guanfacine (1 uM), clonidine (10 uM), or UK-14,304 (10 uM). (E) Guanfacine, clonidine, and UK-14,304 significantly upregulate cfos-eGFP expression in comparison to ACSF-incubated control slices. All data are presented as mean±SEM. One-way ANOVA: drug effect $F(3,32)=4.63$, $p=0.009$. P-values obtained from *post hoc* Holm-Sidak multiple comparisons test. *P<0.05, **P<0.01, ****P<0.0001. N=9-13 animals represented across all groups.

Activation of hM4Di in dBNST neurons by clozapine-N-oxide mimics guanfacine-induced cfos induction.

To determine whether guanfacine-induced cfos expression is translatable to other G_i-coupled GPCRs, we virally introduced the chemogenetic receptor hM4Di:mCherry or mCherry-encoding control constructs under the control of the CaMKIIα promoter in dBNST neurons and evaluated expression of cfos-eGFP after intraperitoneal injections of guanfacine (1 mg/kg) and clozapine-N-oxide (CNO; 3 mg/kg) alone or in combination (Figure 4A-B). In hM4Di-injected mice, a two-way ANOVA showed a significant effect of both CNO ($F(1,31)=5.23$, $p=0.03$) and guanfacine ($F(1,31)=9.68$, $p=0.004$), as well as a significant interaction ($F(1,31)=21.18$, $p<0.0001$) on the number of cfos-eGFP+ cells (Figure 4C). A Holm-Sidak multiple comparisons test determined significant increases relative to saline-injected controls (60±11 cells/mm^2) for guanfacine (213±17 cells/mm^2, $p<0.0001$), CNO (196±28 cells/mm^2, $p=0.0002$), and guanfacine and CNO (167±18 cells/mm^2, $p=0.0028$). There were no differences among animals injected with guanfacine and CNO alone or in combination (guanfacine vs CNO, $p=0.56$; guanfacine vs

guanfacine & CNO, p=0.29; CNO vs guanfacine & CNO, p=0.50). A similar distribution was obtained when the number of cfos-eGFP+ cells were quantified as a proportion of hM4Di:mCherry+ cells (Figure 4D). A two-way ANOVA showed a significant effect of guanfacine ($F(1,28)=5.36$, $p=0.03$) and a significant interaction between guanfacine and CNO ($F(1,28)=5.36$, $p=0.03$), but no effect of CNO alone ($F(1,28)=1.244$, $p=0.27$). A Holm-Sidak multiple comparison's test showed significant upregulation of cfos-eGFP relative to saline injected controls (7.5±1.5% of hM4Di:mCherry+ cells) in animals injected with guanfacine (26.2±5.7%; $p=0.003$), CNO (21.6±5.8%; $p=0.01$), and guanfacine and CNO (21.3±2.4%; $p=0.02$). There were no statistically significant differences among animals injected with guanfacine, CNO, or guanfacine and CNO (guanfacine vs CNO, $p=0.72$; guanfacine vs guanfacine & CNO, $p=0.38$; CNO vs guanfacine & CNO, $p=0.66$). Thus, CNO activation of hM4Di induces a cfos response in BNST neurons that is equivalently sized and blocks further guanfacine-induced cfos expression.

In mCherry-injected controls (Figure 4B, bottom), a two-way ANOVA shows a significant effect of guanfacine ($F(1,8)=116.3$, $p<0.0001$) and CNO ($F(1,8)=6.57$, $p=0.04$), but no significant interaction ($F(1,8)=0.008$, $p=0.93$) (Figure 4E). A Holm-Sidak multiple comparisons test shows significant increases in cfos-eGFP numbers relative to saline-injected controls (64±12 cells/mm^2) for animals injected with guanfacine (239±22 cells/mm^2, $p=0.0003$) and guanfacine and CNO (198±18 cells, $p=0.001$), but a trend towards decreased cfos expression in CNO-injected animals (21±11 cells, $p=0.19$) rather than the increase seen in hM4Di-injected animals. Significant upregulation was also observed relative to CNO-injected animals in guanfacine- and dual guanfacine- and CNO-injected animals (CNO vs guanfacine, $p<0.0001$; CNO vs guanfacine & CNO, $p=0.0003$). There was no difference between guanfacine-injected

animals and those injected with both guanfacine and CNO ($p=0.19$). Here we show that CNO does not induce cfos expression without the presence of hM4Di and does not compete with guanfacine-induced cfos expression.

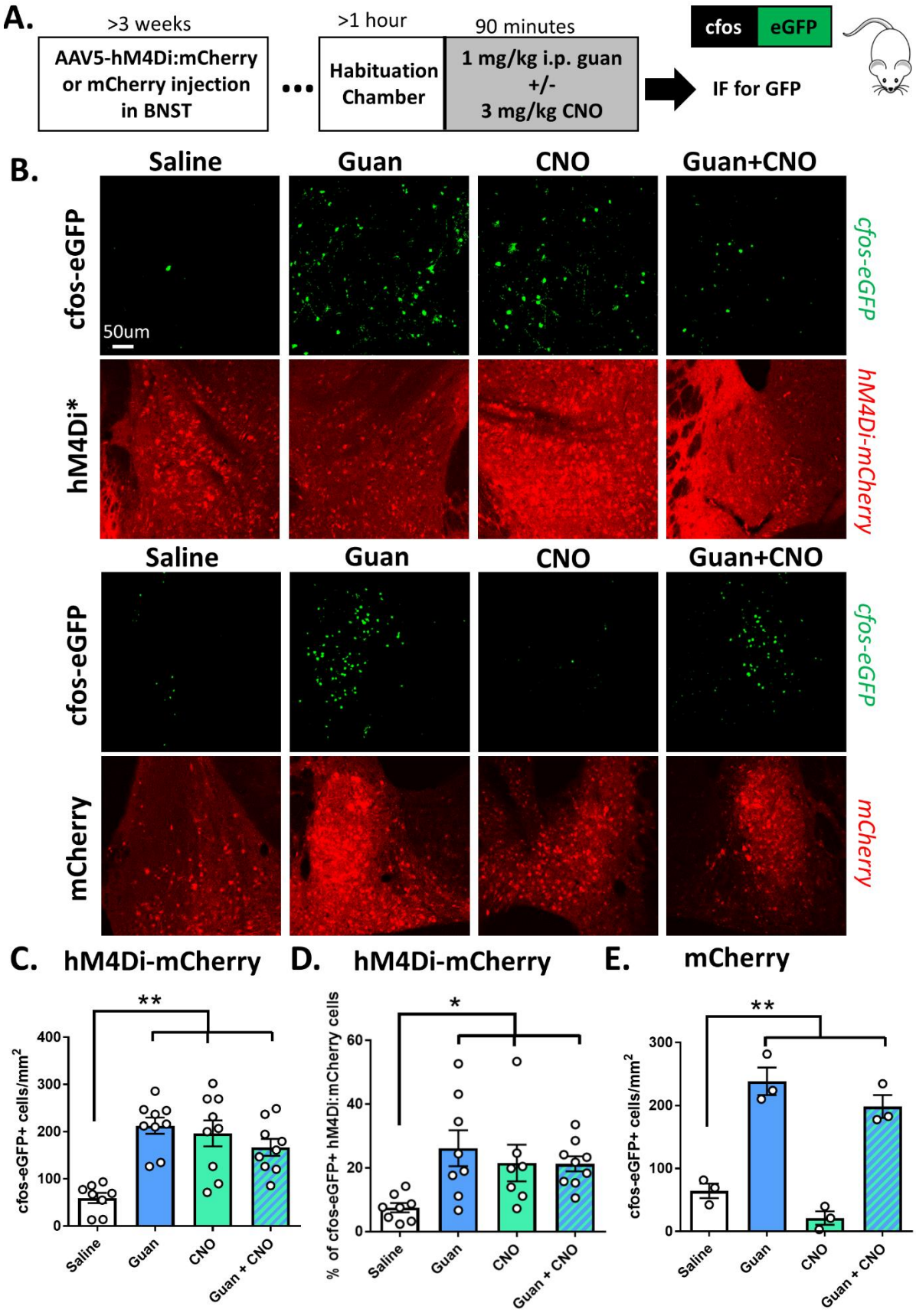
A.
>3 weeks
AAV5-hM4Di:mCherry or mCherry injection in BNST
>1 hour
Habituation Chamber
90 minutes
1 mg/kg i.p. guan +/- 3 mg/kg CNO
cfos
eGFP
IF for GFP
B.
Saline
Guan
CNO
Guan+CNO
cfos-eGFP
50um
hM4Di*
hM4Di-mCherry
mCherry
C. hM4Di-mCherry
cfos-eGFP+ cells/mm2
D. hM4Di-mCherry
% of cfos-eGFP+ hM4Di:mCherry cells
E. mCherry
Saline
Guan
CNO
Guan + CNO

Figure 5 – Activation of hM4Di in dBNST neurons by clozapine-N-oxide mimics guanfacine-induced cfos expression in vivo. (A) Schematic showing timeline of animal habituation, adeno-associated viral vector injection, drug injection, and immunofluorescence. (B) Representative images of cfos-eGFP (green) and hM4Di:mCherry (red, top) or mCherry (red, bottom) expression in the dBNST; animals were injected with saline, guanfacine (1 mg/kg), clozapine-N-oxide (CNO; 3 mg/kg), or guanfacine and CNO. (C) Injections of guanfacine and CNO alone or in combination lead to increased cfos-eGFP expression relative to saline-injected controls in mice expressing hM4Di in the dBNST. There are no differences in cfos-eGFP levels among hM4Di-expressing animals injected with guanfacine or CNO alone or in combination. Two-way ANOVA: CNO effect $F(1,31)=5.229$, $p=0.029$, guanfacine effect $F(1,31),=9.68$, $p=0.004$, interaction $F(1,31)=21.18$, $p<0.0001$. (D) Injections of guanfacine (1 mg/kg) and CNO (3 mg/kg) alone or in combination lead to increased dBNST cfos-eGFP expression in hM4Di:mCherry+ cells relative to saline-injected controls in hM4Di-expressing mice. There are no differences in cfos-eGFP levels among hM4Di-expressing animals injected with guanfacine or CNO alone or in combination. Two-way ANOVA: CNO effect $F(1,28)=1.244$, $p=0.27$, guanfacine effect $F(1,28),=5.36$, $p=0.03$, interaction $F(1,28)=5.36$, $p=0.03$.. (E) Injections of guanfacine (1 mg/kg) with or without CNO (3 mg/kg) leads to increased cfos-eGFP expression relative to saline- and CNO-injected mCherry-expressing controls. Addition of CNO did not significantly affect either saline- or guanfacine-induced cfos expression levels. Two-way ANOVA: CNO effect: $F(1,8)=6.57$, $p=0.04$, guanfacine effect $F(1,8)=116.3$, $p<0.0001$, interaction $F(1,8)=0.01$, $p=0.93$. All P-values were determined by *post hoc* Holm-Sidak multiple comparisons test. N=3-9 mice per group. *P<0.05, **P<0.01. All data are presented as mean±SEM.

Guanfacine-activated Adra2a+ dBNST neurons express functional HCN subunits.

To allow for the study of putative guanfacine-activated neurons more precisely, *cfos-eGFP* mice were intraperitoneally injected with guanfacine (1 mg/kg) 90 minutes prior to brain slice preparation and electrophysiological recording (Figure 5A). This strategy allowed for identification of cfos-eGFP-expressing cells that were examined by whole cell electrophysiology and confirmed by *post hoc* immunohistochemistry (Figure 5B). Current clamp profiles, defined here as membrane potential responses to positive and negative current injections, were obtained and showed that 8/11 cells had a hyperpolarization sag on negative current injection (average amplitude=1.9±0.5 mV, Figure 5C). This characteristic response to negative current injection of an initial hyperpolarization followed by a slower depolarization is generally suggestive of underlying HCN channel activity (Wahl-Schott and Biel, 2009). A one-hour incubation of the

slices with the HCN channel inhibitor ZD7288 (10 μM) abolished this sag in 10/11 cells recorded (0.09±0.09 mV; Figure 5D). The difference between untreated and ZD7288-treated slices was significant (unpaired t-test, p=0.001; Figure 5E). Kinetic analyses were performed on the hyperpolarization sag aiming to uncover which of the four mammalian HCN channel subunits (HCN1-HCN4) may constitute the pacemaker current in dBNST neurons. The average τ of activation calculated from the point of maximal hyperpolarization to the steady-state potential was 149.2±12.9 ms (range 97.4-223 ms; Figure 5F), suggesting involvement of HCN1 or HCN2 subunits which display similar values either in homomeric or heteromeric channels (Ulens and Tytgat, 2001).

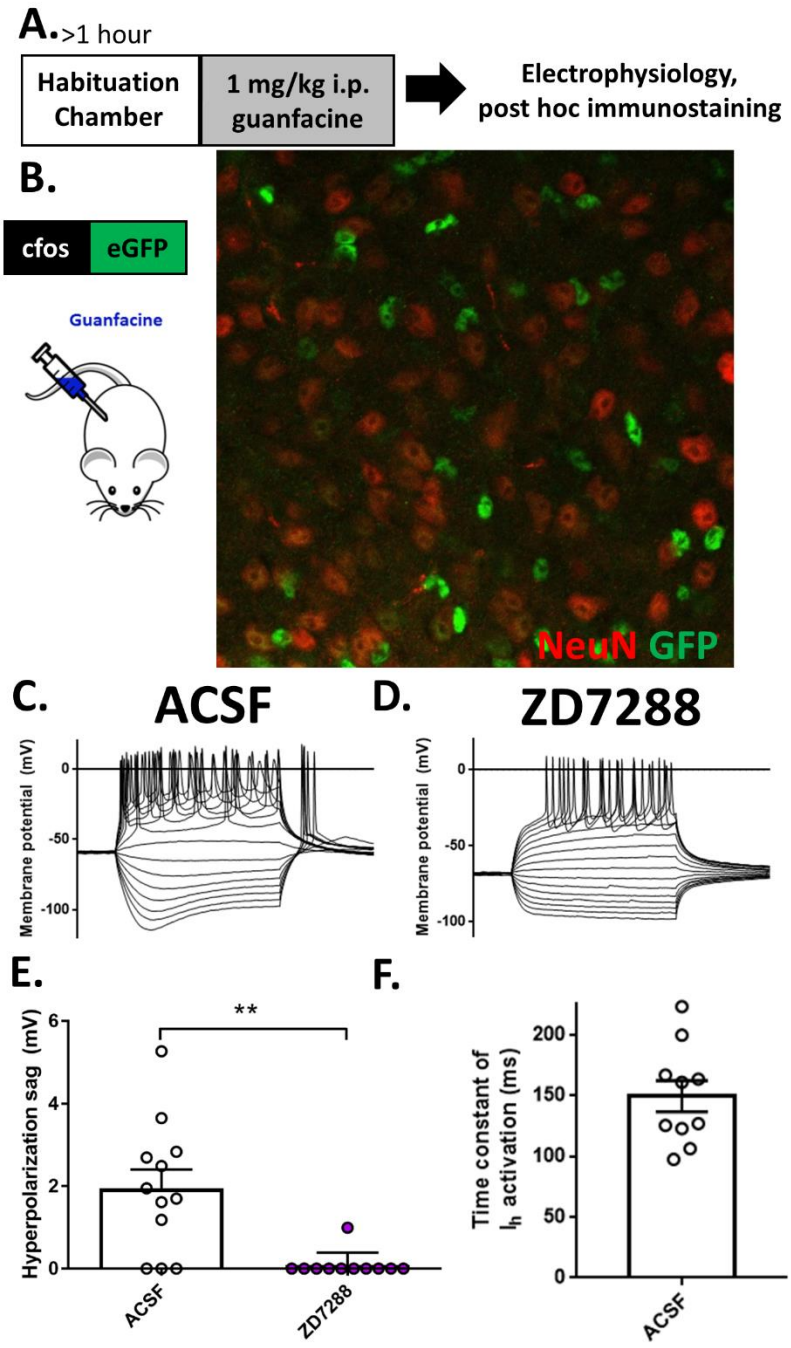

Figure 6 – dBNST neurons that express cfos after systemic guanfacine administration show a high prevalence of HCN activity. (A) Schematic showing timeline for *cfos-eGFP* animal habituation, guanfacine injection, and slice preparation for electrophysiology and immunostaining. (B) Representative image showing the expression of *cfos-eGFP* (green) and NeuN+ neurons (red) in the dBNST in a *post hoc* fixed 300 µm thick slice that was stained after electrophysiological recording. (C-E) Current clamp profiles of cfos-eGFP+ dBNST neurons. The characteristic hyperpolarization sag indicating HCN channel activity was seen in control recordings (ACSF incubation) (C) but not after incubation in 10 µM ZD7288 (D). P-values were

calculated from an unpaired t-test. **P<0.01. N=11-12 cells from 4-5 mice. (F) Kinetic analyses of the hyperpolarization sag show an average time constant of I_h activation of 149.2±12.9 ms, suggesting HCN1 or HCN2 expression. All data are presented as mean±SEM.

A fluorescent *in situ* hybridization approach was used to confirm HCN transcript expression in *Adra2a*+ dBNST neurons (Figure 6A). On average, the density of transcript-positive cells within the dBNST was 301±37 cells/mm^2 for *Adra2a*+ cells (representing 34.5±3.3% of DAPI+ cells), 127±24 for *Hcn1*+ cells (15.3±4.7% of DAPI+ cells), and 550±85 for *Hcn2*+ cells (62.1±6.4% of DAPI+ cells). While a majority of *Adra2a*+ cells were negative for *Hcn1* transcripts (78.6±5.4%), a large fraction was positive for *Hcn2* transcripts (71.4±7.3%; Figure 6B). Unpaired t-tests on the number of cells observed (Figure 6C) confirm that *Adra2a*+ cells are more likely to be *Hcn1*-negative than to express *Hcn1* transcripts (*Adra2a*+*Hcn1*+: 76±13 cells/mm^2; *Adra2a*+*Hcn1*-: 292±62 cells/mm^2; p=0.04), and more likely to be *Hcn2*-positive than not express *Hcn2* transcripts (*Adra2a*+*Hcn2*+: 208±53 cells/mm^2; *Adra2a*+*Hcn2*-: 62±11 cells/mm^2; p=0.04). Together, in addition to expressing cfos transcripts after guanfacine injection, a majority of *Adra2a*+ cells also co-express *Hcn2* transcripts.

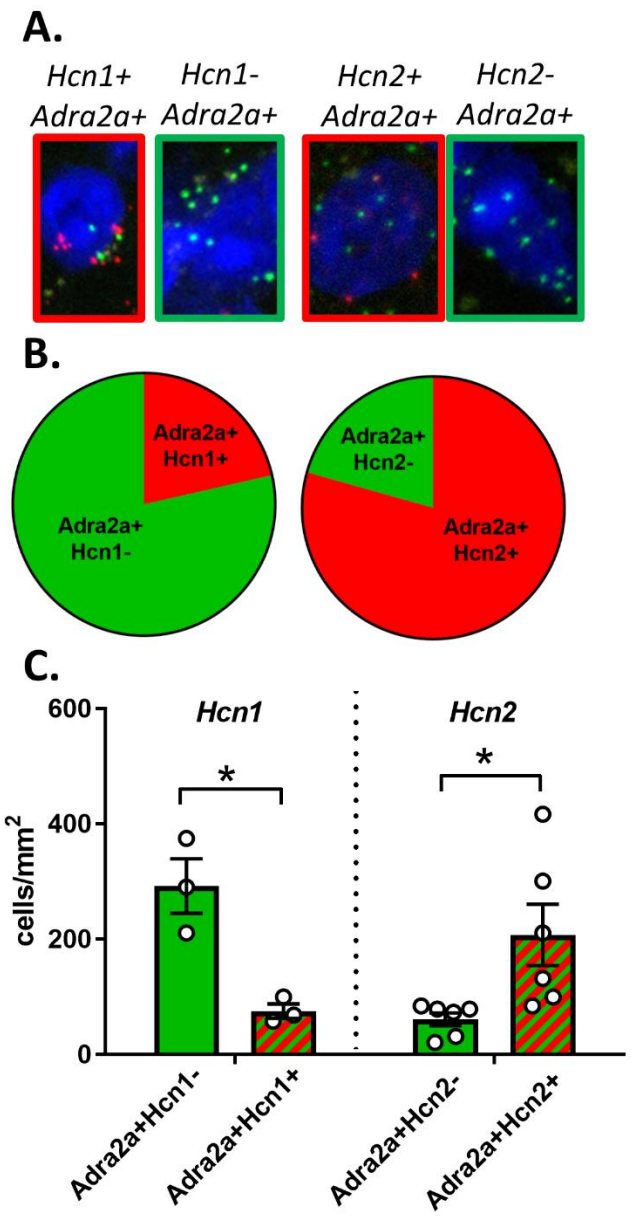

Figure 7 – A majority of Adra2a+ dBNST neurons co-express Hcn2 while a minority co-express Hcn1. (A) Representative images of DAPI+ nuclei (blue) in dBNST which express *Adra2a* transcripts (green) with or without either *Hcn1* transcripts (red, left) or *Hcn2* transcripts (red, right). (B) As a proportion of *Adra2a+* cells, 21.5±5.4% co-express *Adra2a* and *Hcn1* transcripts while 71.4±7.3% co-express *Adra2a* and *Hcn2 transcripts*. (C) The number of *Adra2a+Hcn1-* cells is greater than the number of *Adra2a+Hcn1+* cells, while the number of *Adra2a+Hcn2+* cells is greater than the number of *Adra2a+Hcn2-* cells. P-values were determined by unpaired t-test. *P<0.05. All data are represented as mean±SEM.

HCN channel inhibition is sufficient for excitatory actions on glutamatergic transmission in the dBNST

Co-localization of *Adra2a* and *Hcn2* transcripts suggests that receptor-dependent signaling might have an impact on HCN channel activity. In prefrontal cortex, postsynaptic α_{2A}-ARs enhance glutamatergic transmission by inhibition of HCN channels through a process whereby decreased postsynaptic cAMP decreases the HCN channel open probability and diminishes HCN-dependent filtering of synaptic currents passing through the dendritic neck (Wang et al., 2007). We tested the effects of the HCN channel inhibitor ZD7288 on optically evoked excitatory transmission in a Thy1-COP4 transgenic mouse line (line 9). This mouse line expresses a transgene encoding channelrhodopsin-2 (ChR2) under the control of the thymus cell antigen 1 (Thy1) promoter randomly inserted into the genome, which as a result leads to expression within subsets of projection neurons across the brain, including neurons from the cortex, hippocampus, thalamus, midbrain, brainstem, cerebellar mossy fibers, and retinal ganglion cells (Arenkiel et al., 2007). Importantly, this mouse line has been shown to minimally express ChR2 in dBNST neurons and shows little to no co-localization of ChR2 with calcitonin gene-related peptide (CGRP), a high fidelity marker of the guanfacine-inhibited parabrachial nucleus afferents within the dBNST (Flavin et al., 2014). Use of this mouse line thus allows for enrichment of light-induced presynaptic release of glutamate from non-parabrachial nucleus afferents within the dBNST. The pattern of activity elicited by *ex vivo* optical stimulation within the dBNST in this mouse strain was previously shown to unmask excitatory actions of guanfacine, presumably due to the lack of presynaptic inhibition of glutamate release by α_{2A}-AR activity at parabrachial nucleus terminals (Flavin et al., 2014). In this experiment, optically evoked field potentials were observed as two negative deflections defined here as oN1 and oN2,

analogous to the fiber volley potential N1 and synaptic potential N2 observed in electrically evoked field potential recordings in the dBNST (Figure 7A).We first replicated previous findings that bath application of guanfacine (1 µM) for ten minutes significantly increases the amplitude of oN2 by 15.9±6.0% (range: -17.3 to +67.7%; paired t-test, p=0.03; Figure 7B). Then, in a separate cohort of animals, we bath applied ZD7288 (10 µM) for 40 minutes, which increased the oN2 amplitude by 18.7±7.6% (range: -14.1 to +53.4%; paired t-test, p=0.04; Figure 7C).

To gain insight into potential cell-type specific effects of ZD7288, we recorded from cfos-eGFP+ cells 90 minutes after guanfacine injection (Figure 7D). To maximize potential activation of endogenous HCN channels by avoiding voltage-clamp mediated inhibition and minimize loss of HCN current observation and modulation due to long-term cell dialysis, spontaneous excitatory postsynaptic potentials (sEPSPs) were recorded in cfos-eGFP+ cells after one-hour incubation in ZD7288 or vehicle (10 µM; Figure 7D). ZD7288 incubation did not significantly affect resting membrane potential (control: -60.6±1.8 mV; ZD7288: -63.9±2.2 mV; unpaired t-test, p=0.26; Figure 7E). The treatment had no effect on average sEPSP amplitude (control: 1.1±0.1 mV; ZD7288: 1.0±0.1 mV; unpaired t-test, p=0.40; Figure 7F), but did significantly increase sEPSP frequency (control: 2.0±0.3 Hz; ZD7288: 3.6±0.4 Hz; unpaired t-test, p=0.002; Figure 7G). An increase in sEPSP frequency is classically interpreted as resulting from modulation of presynaptic glutamate release. However, an increase in sEPSP frequency could also result from release of dendritic filtering on synapses distant from the location of somatic recording with resulting low amplitude spontaneous events (Larkum et al., 1998; Williams and Mitchell, 2008; Gantz et al., 2013). To differentiate between these possibilities, we evaluated the distribution of events across amplitudes in ACSF and ZD7288-preincubated slices (Figures 7H-7J). When comparing the frequency distribution of sEPSP amplitudes with or

without ZD7288 preincubation, a two-way ANOVA shows a significant interaction between drug treatment and amplitude ($F(9,190)=2.35$, $p=0.02$) but no effect of drug ($F(1,190)=2x10^{-14}$, $p>0.9999$) or amplitude ($F(9,190)=0.48$, $p=0.89$) alone. Fisher's LSD analysis shows significant differences between the treatments at the lowest amplitude bin (<0.7 mV, ACSF=7.2±1.5%, ZD7288=14.2±3.2%, $p=0.01$) and two highest amplitude bins (2.2 to 3.1 mV, ACSF=12.2±2.4%, ZD7288=5.6±1.5%, $p=0.02$; >3.1 mV, ACSF=10.9±3.6%, ZD7288=4.9±2.3%, $p=0.03$), with ZD7288 preincubation increasing the frequency of low amplitude events and decreasing the frequency of high amplitude events as a proportion of all events. To determine whether this change in frequency distribution is due to increased numbers of low amplitude events or decreased high amplitude events, we compared the number of events with amplitudes greater than or less than 1.52 mV, the point of intersection for the frequency distributions across drug treatments. Here, by repeated measures two-way ANOVA, we observed a significant effect of amplitude ($F(1,19)=6.89$, $p=0.02$) and a significant interaction between amplitude and drug treatment ($F(1,19)=4.75$, $p=0.04$) but no effect of treatment alone ($F(1,19)=3.44$, $p=0.08$). A Holm-Sidak multiple comparisons test showed that ZD7288 preincubation increased the number of low amplitude events (ACSF=72.3±12.0 events, ZD7288=134.4±18.2 events, $p=0.01$) with no difference in high amplitude events (ACSF=65.6±14.8 events, ZD7288=62.1±16.1 events, $p=0.98$). Finally, in comparing the cumulative frequency distribution between the treatments and fitting a nonlinear line of best fit to the data (Figure 7J), we observed a left shift after ZD7288 preincubation and a difference in the line of best fit when constraining the maximum (100%) and minimum (0%) curve parameters and varying the Hill coefficient (ACSF=0.94±0.09, ZD7288=1.12±0.10) and IC50 (ACSF=1.37±0.04 mV, ZD7288=1.124±0.03 mV). Using different parameters for each of the data sets resulted in a better fit of the data ($F(2,206)=16.27$,

p<0.0001) than using the same parameters for both, confirming that the shape and the amplitude distribution are statistically different. In sum, ZD7288 enhanced spontaneous glutamatergic transmission in cfos-eGFP+ cells after guanfacine injection likely via decreased dendritic filtering of low amplitude spontaneous EPSPs.

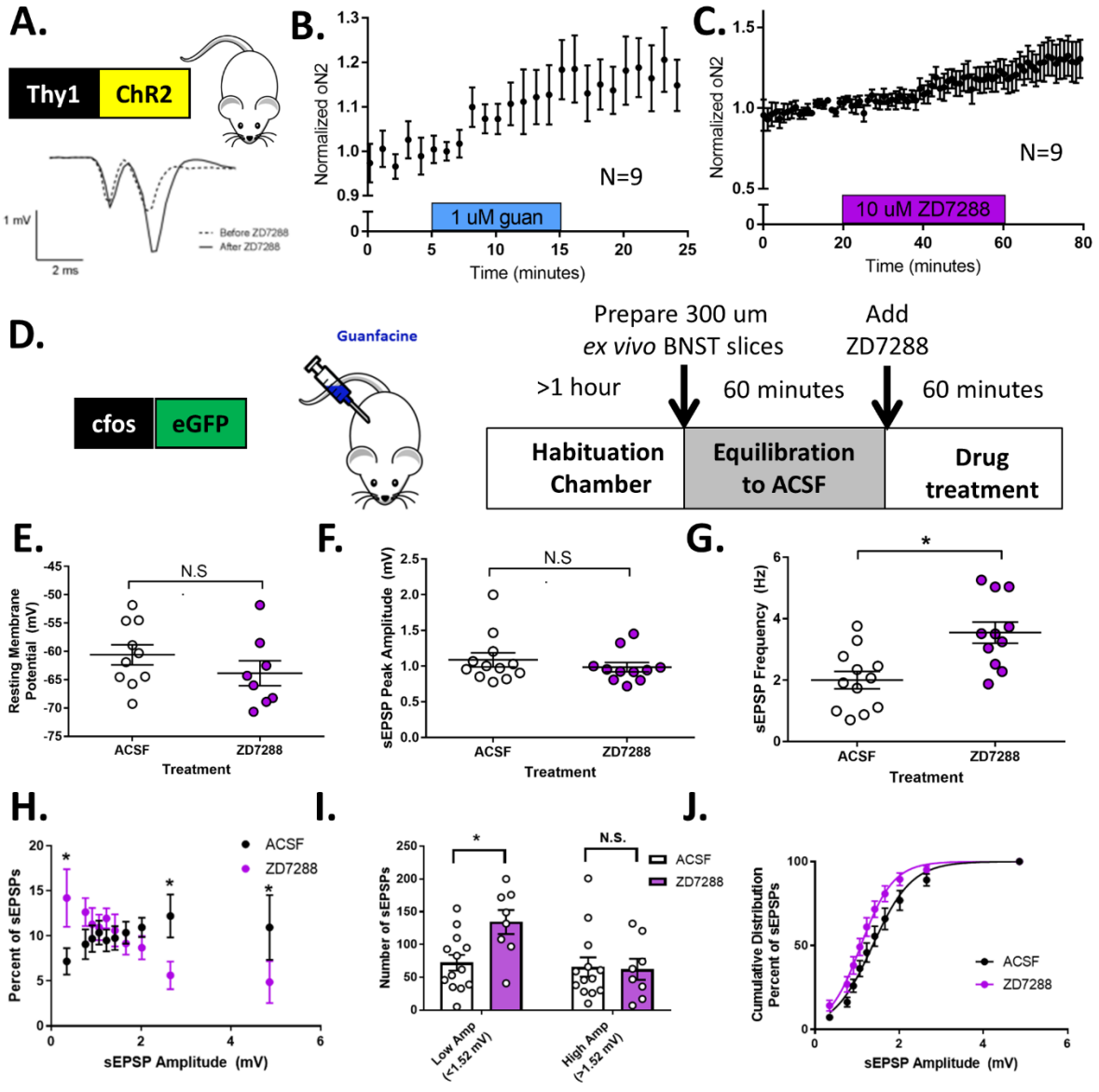

Figure 8 – HCN channel inhibition by ZD7288 is sufficient for excitatory actions on glutamatergic transmission within the dBNST. (A) Representative trace of an optically-evoked field potential in the dBNST of Thy1-COP4 mice showing an oN1 and oN2 component

analogous to electrically-evoked field potentials in the region. (B) Guanfacine application (1 µM for 10 minutes) enhances oN2 amplitude by 15.9±6.0% in the dBNST of Thy1-COP4 mice. N=9 slices from 4 mice. (C) ZD7288 application (10 µM for 40 minutes) also enhances oN2 amplitude by 18.7±7.6% in the dBNST of Thy1-COP4 mice. N=9 slices from 5 mice. (D) Schematic showing the timeline of *cfos-eGFP* animal habituation, slice preparation, ZD7288 (10 uM) incubation and electrophysiology recording. (E-G) ZD7288 incubation did not affect resting membrane potential and had no effect on spontaneous excitatory postsynaptic potential amplitude in cfos-eGFP+ dBNST neurons but did increase sEPSP frequency. (H-J) ZD7288 preincubation increases the proportion of low amplitude sEPSPs and decreases the proportion of high amplitude sEPSPs among all sEPSPs, increases only the number of low amplitude sEPSPs (<1.52 mV), and causes a leftward shift in the cumulative frequency distribution of sEPSP amplitudes relative to ACSF preincubated controls. Two-way ANOVA on sEPSP amplitude proportion: drug effect ($F(1,190)=2x10^{-14}$,$p>0.9999$), amplitude effect ($F(9,190)=0.48$, $p=0.89$), interaction ($F(9,190)=2.35$, $p=0.02$. Two-way ANOVA on sEPSP amplitude number: drug effect ($F(1,19)=3.44$, $p=0.08$, amplitude effect ($F(1,19)=6.89$, $p=0.02$), interaction ($F(1,19)=4.75$, $p=0.04$). Nonlinear regression line of best fit comparison: ($F(2,206)=16.27$, $p<0.0001$. P-values were determined by unpaired t-tests (E, F, G), Fisher's LSD analysis (H) or Holm-Sidak (I) multiple comparisons test. N.S. $P>0.05$, $*P<0.05$. All data are represented as mean±SEM.

shRNA knockdown of HCN1 and HCN2 occludes guanfacine-induced cfos expression

Having demonstrated that HCN channel inhibition causes excitatory actions within the dBNST, we addressed the question of whether HCN channels are a downstream target of guanfacine actions. To do this, we used AAVs encoding small hairpin RNAs (shRNAs) directed against both the HCN1 and HCN2 channel subunits (AAV9-shHCN1/2; Figure 8A). Current clamp responses to positive and negative current injections were obtained from injected animals and sham controls (Figures 8B-8C). Hyperpolarization sag amplitude was determined from these responses as the difference in membrane potential between the initial maximal negative potential and steady state potential upon negative current injection. After dual subunit knockdown, the amplitude of the hyperpolarization sag was decreased by 43.8% (sham: 3.0±0.5 mV; shHCN1/2: 1.3±0.4 mV; unpaired t-test, p=0.008; Figure 8D), validating a functional loss of HCN channel activity. Of note, dual subunit knockdown did not affect resting membrane potential (sham: -80.3±1.6 mV; shHCN1/2: -82.8±2.3 mV; unpaired t-test, p=0.40), sEPSP frequency (sham:

1.8±0.2 Hz; shHCN1/2: 1.8±0.2 Hz; unpaired t-test, p=0.92), or sEPSP amplitude (sham: 1.4±0.1 mV; shHCN1/2: 1.7±0.2 mV; unpaired t-test, p=0.35) in AAV9-shHCN1/2+ BNST neurons, suggesting either that identification of guanfacine-activated neurons is necessary for observation of excitatory effects or that viral knockdown does not mimic acute pharmacological inhibition of HCN channel activity in this regard.

We used the same strategy to test for an interaction between HCN channel activity and guanfacine-induced cfos responses alongside controls injected with a recombinant control virus expressing only GFP (AAV9-GFP; Figure 8E). A two-way ANOVA revealed a significant effect of shRNA injection on cfos+ cells ($F(1,16)=7.86$, $p=0.01$), no effect of guanfacine exposure ($F(1,16)=2.40$, $p=0.14$), and a trend towards a significant interaction ($F(1,16)=3.14$, $p=0.10$) (Figure 8F). A Holm-Sidak multiple comparisons test showed upregulation of cfos relative to saline-injected AAV9-GFP controls (71±9 cfos+ cells/mm^2) in guanfacine-injected AAV9-GFP controls (102±6 cfos+ cells/mm^2, $p=0.03$), saline-injected AAV9-shHCN1/2 animals (113±9 cfos+ cells/mm^2, $p=0.02$), and guanfacine-injected AAV9-shHCN1/2 animals (110±11 cfos+ cells/mm^2, $p=0.02$). No differences were observed between AAV9-shHCN1/2 animals injected with saline and guanfacine ($p=0.88$). To begin to assess the behavioral relevance of this difference, the elevated plus maze was used to determine anxiety-like behavior in a separate cohort of mice. No baseline differences were observed between AAV9-GFP and AAV9-shHCN1/2 animals in open arm time (GFP: 164.7±14.2 seconds; shHCN1/2: 163.6±20.2 seconds; unpaired t-test, $p=0.96$), closed arm time (GFP: 91.7±11.1 seconds; shHCN1/2: 100.1±17.8 seconds; unpaired t-test, $p=0.69$), center zone time (GFP: 105.3±13.2 seconds; shHCN1/2: 87.4±12.8 seconds; unpaired t-test, $p=0.34$), or total distance traveled (GFP: 7.9±0.6 meters; shHCN1/2: 9.3±0.6 meters; unpaired t-test, $p=0.13$).

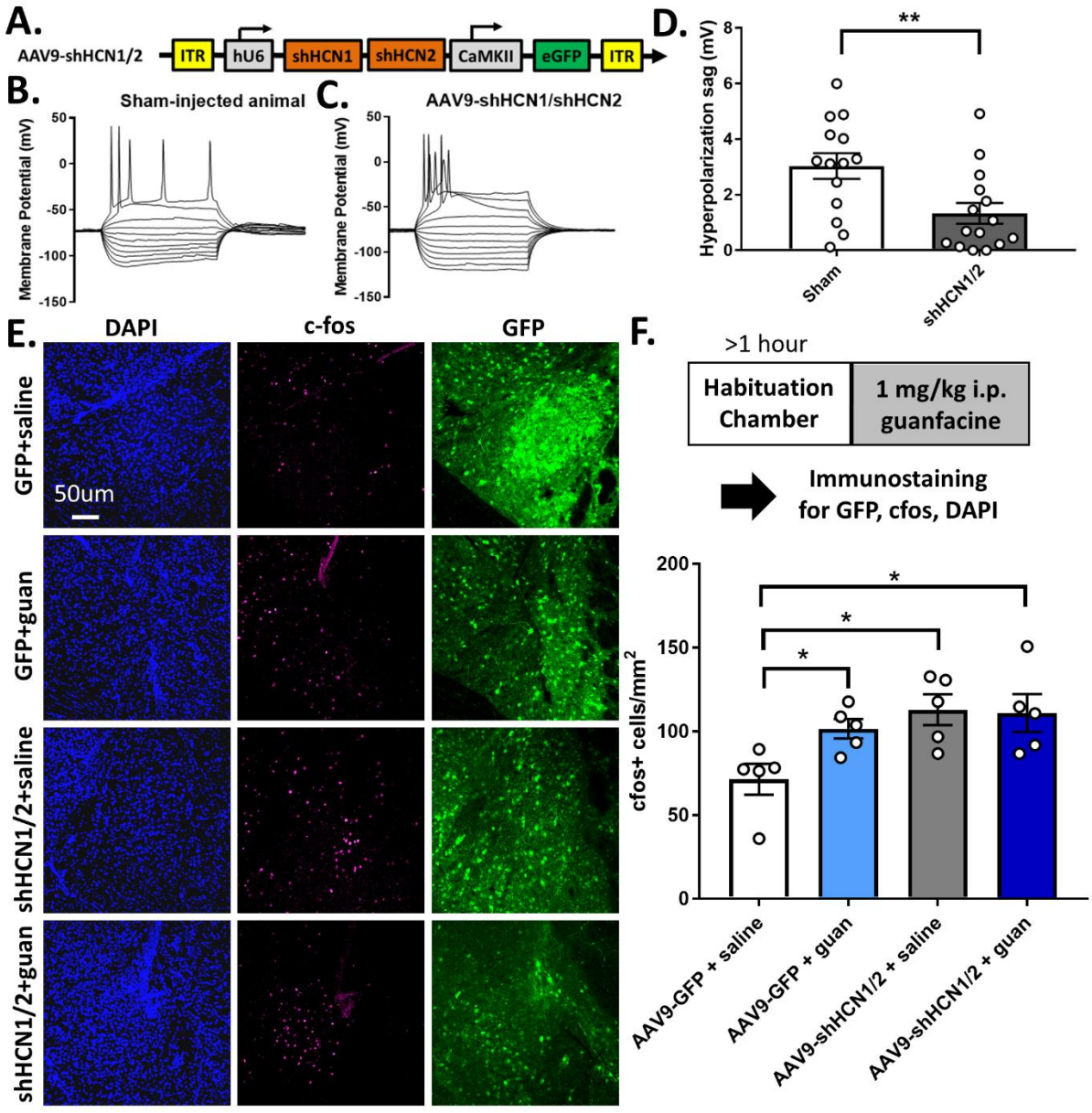

Figure 9 – Delivery of shRNAs directed against HCN channel subunits to the dBNST occludes guanfacine-induced cfos expression. (A) Schematic of AAV9-shHCN1/2 virus; inverted terminal repeat (ITR), human U6 (hU6) promoter driving expression of *Hcn1* and *Hcn2*-specific shRNAs, *CaMKII* promoter used for neural expression of *eGFP*. (B-C) Current clamp profiles of sham-injected (B) and AAV9-shHCN1/2 animals (C) show the presence and absence of a hyperpolarization sag, respectively. (D) Injection of shHCN1/2-encoding virions reduces the average amplitude of hyperpolarization sag in dBNST neurons. (E) Representative images of DAPI+ (blue), cfos (magenta) and virally-expressed eGFP (green) in dBNST after saline or guanfacine treatment. (F) Guanfacine increases cfos expression in AAV9-eGFP control mice but not in mice that were injected with AAV9-shHCN1/2. Expression of cfos in AAV9-shHCN1/2

animals was similar to values obtained in controls injected with guanfacine, a result reminiscent of cfos expression in *Adra2a*-/- transgenic mice (KO, see Figure 2). Two-way ANOVA: shRNA effect: ($F(1,16)=7.86$, $p=0.01$), guanfacine effect ($F(1,16)=2.40$, $p=0.14$), interaction ($F(1,16)=3.14$, $p=0.10$. P-values were determined by unpaired t-test (D) or *post hoc* Holm-Sidak multiple comparisons test. *P<0.05, **P<0.01. All data are represented as mean±SEM.

Activation of hM4Di in dBNST neurons elicits anxiogenic behavior and activity increases in the elevated plus maze.

Finally, we aimed to determine the behavioral and physiological relevance of this non-canonical aspect of α_{2A}-AR signaling using clozapine-N-oxide (CNO) activation of the chemogenetic G_i-coupled DREADD receptor, hM4Di, expressed in dBNST neurons. We recorded dBNST-based Ca^{2+} transients during the elevated plus maze from implanted animals tethered to the fiber photometry system by a flexible patch cord. Animals stereotaxically injected with AAV5-GCaMP6f and AAV5-hM4Di or AAV5-mCherry were given an intraperitoneal (i.p.) injection of either saline or CNO (3 mg/kg) 120 minutes prior to behavioral testing. In comparison to saline-injected AAV5-hM4Di controls, CNO-injected animals showed increased anxiety-like behavior as manifested in increased closed arm time (saline: 156.6±15.5 s; CNO: 205.8±12.0 s; unpaired t-test, $p=0.02$; Figure 9A) and decreased open arm time (saline: 93.4±15.1 s; CNO: 52.6±10.8 s; unpaired t-test, $p=0.03$; Figure 9B). There were no effects on the time spent in the center zone (saline: 22.9±3.0 s; CNO: 34.5±6.0 s; unpaired t-test, $p=0.10$; Figure 9C) or locomotion (total distance traveled; saline: 4.9±0.5 m; CNO: 4.6±0.6 m; unpaired t-test, $p=0.6790$; Figure 9D). In AAV5-mCherry controls, there were no differences between saline- and CNO-injected animals in the time spent in the closed arm (saline: 150.4±15.3 s; CNO: 146.4±14.0 s; unpaired t-test, $p=0.85$; Figure 9E), open arm (saline: 105.5±10.6 s; CNO: 111.3±11.5 s; unpaired t-test, $p=0.71$; Figure 9F), center zone (saline: 43.7±8.3 s; CNO: 38.87±8.1 s; unpaired t-test, $p=0.68$; Figure 9G), or total distance traveled (saline: 7.7±0.9 m;

CNO: 7.1±1.4 m; unpaired t-test, p=0.69; Figure 9H). Thus, activation of hM4Di in dBNST neurons elicits anxiogenic behavior in the elevated plus maze in addition to mimicking guanfacine-induced cfos expression.

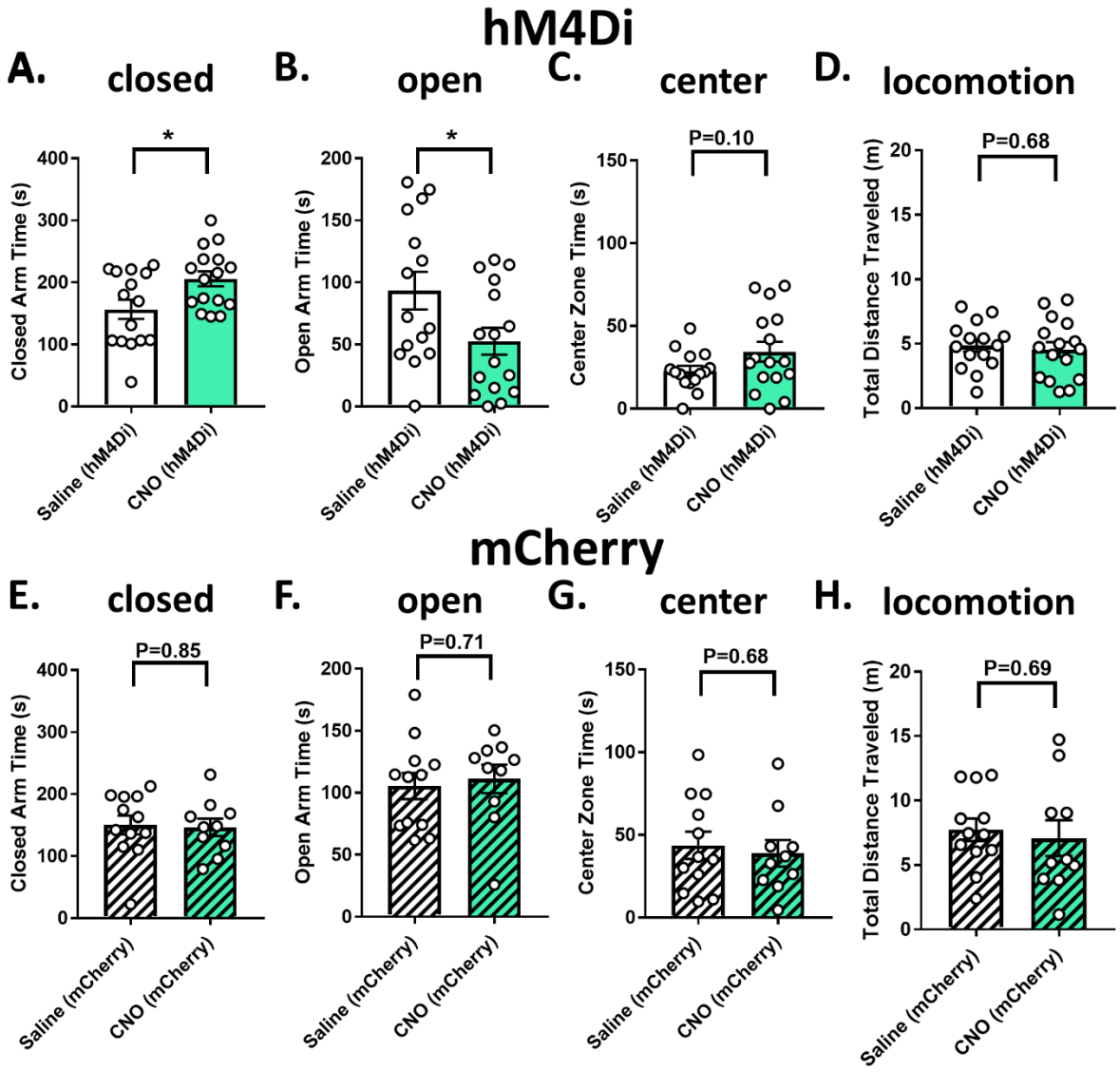

Figure 10 – Activation of hM4Di receptors expressed in dBNST neurons elicits anxiety-like behavior in the elevated plus maze. (A-D) Behavioral data from the elevated plus maze show increased anxiety-like behavior in CNO-injected mice expressing the hM4Di receptor compared to saline-injected control animals. CNO led animals to spend more time in the closed arm (A) and, subsequently, less time in the open arm (B) with no change in time spent in the center zone (C) or total distance traveled (D). (E-H) No effect was observed after CNO injection in AAV5-mCherry animals during the elevated plus maze: no change in time spent in the closed arm (E),

open arm (F), center zone (G) and total distance traveled (H). P-values were calculated by unpaired t-test. *P<0.05. N=10-16 animals per group. All data are presented as mean±SEM.

dBNST activity was monitored via fiber photometry during and prior to the elevated plus maze test (Figure 10A-B). GCaMP6f fluorescence signals were normalized to $\Delta F/F_0$ values using segmented normalization and frequencies of Ca^{2+} transients were extracted using the mLspike algorithm (Deneux et al., 2016). To validate the fidelity of Ca^{2+} transient observation by this algorithm, a subset of mice was anesthetized with isoflurane during fiber photometric recordings (Figure 10C). Isoflurane anesthesia decreased dBNST GCaMP6f imputed Ca^{2+} transients from 0.82±0.21 Hz at baseline to 0.06±0.03 Hz (paired t-test, p=0.03). Having thus validated Ca^{2+} transient quantification, fiber photometric recordings were obtained during a two-minute baseline prior to the behavioral task and during the five minute elevated plus maze test (Figure 10D). The magnitude of the change in Ca^{2+} transient frequency between the baseline measurements and elevated plus maze measurements were calculated (Figures 10E-F). In AAV5-hM4Di animals, CNO injection resulted in more Ca^{2+} transients compared to the baseline measurements in the same animal as well as to saline-injected animals (saline: 2.1±0.6-fold increase; CNO: 6.1±1.6-fold increase; unpaired t-test, p=0.03; Figure 10D). In AAV5-mCherry controls, CNO injection did not affect this measure (saline: 3.1±0.8-fold increase; CNO: 2.7±0.9-fold increase; unpaired t-test, p=0.75; Figure 10F). We also assessed dBNST Ca^{2+} transient frequency in relation to mouse location in the maze (Figure 10G). Specifically, a two-way ANOVA showed a significant effect of EPM arm on Ca^{2+} transient frequency ($F(1,21)=6.32$, $p=0.02$) but no effect of CNO ($F(1,21)=0.20$, $p=0.66$) or an interaction between the two ($F(1,21)=1.78$, $p=0.20$). A Holm-Sidak multiple comparisons test showed that saline-injected animals had increased open arm activity relative to closed arm activity (closed arm: 0.6±0.2 Hz;

open arm: 1.6±0.4 Hz; p=0.03), but CNO-injected animals did not (closed arm: 1.1±0.3 Hz; open arm: 1.4±0.4 Hz; p=0.40). In AAV5-mCherry controls, a two-way ANOVA also showed a significant effect of EPM arm on Ca^{2+} transient frequency ($F(1,17)=20.44$, $p=0.0003$) but no effect of CNO ($F(1,17)=0.0009$, $p=0.98$) or an interaction between the two ($F(1,17)=0.19$, $p=0.67$). A Holm-Sidak multiple comparisons test showed that both saline- and CNO-injected animals had increased open arm activity relative to closed arm activity (saline closed arm: 2.2±0.3 Hz, saline open arm: 2.4±0.3 Hz, p=0.004; CNO closed arm: 2.7±0.3 Hz, CNO open arm: 2.9±0.4 Hz, p=0.01; Figure 10H). Of note, AAV5-mCherry controls show higher values of arm-specific BNST Ca^{2+} transient frequency than AAV5-hM4Di experimental animals. However, interpretation of this effect is complicated by potential cohort differences related to signal variability (i.e. viral expression, fiber fidelity), supporting the use of a within-subject experimental design and analysis. Thus, CNO activation of the hM4Di receptor increases overall Ca^{2+}-signaled activity in the EPM and eliminates the difference of behaving mice between closed and open arm activities.

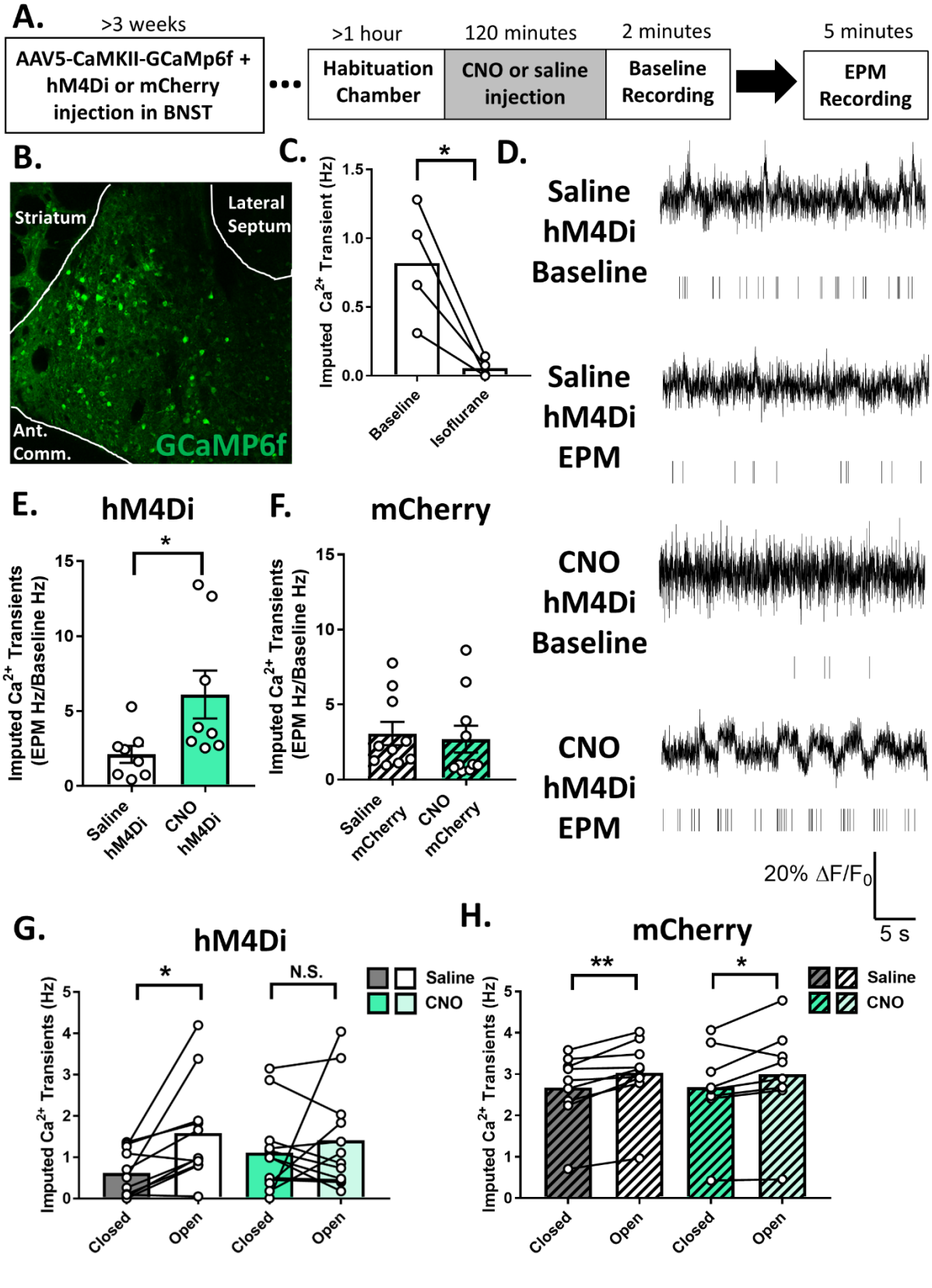
A.
>3 weeks
AAV5-CaMKII-GCaMp6f + hM4Di or mCherry injection in BNST
>1 hour
Habituation Chamber
120 minutes
CNO or saline injection
2 minutes
Baseline Recording
5 minutes
EPM Recording
B.
Striatum
Lateral Septum
Ant. Comm.
GCaMP6f
C.
Imputed Ca2+ Transient (Hz)
Baseline
Isoflurane
D.
Saline hM4Di Baseline
Saline hM4Di EPM
CNO hM4Di Baseline
CNO hM4Di EPM
20% ΔF/F0
5 s
E.
hM4Di
Imputed Ca2+ Transients (EPM Hz/Baseline Hz)
Saline hM4Di
CNO hM4Di
F.
mCherry
Saline mCherry
CNO mCherry
G.
hM4Di
N.S.
Saline
CNO
Closed
Open
H.
mCherry

Figure 11 – Activation of hM4Di receptors expressed in dBNST neurons elicits GCaMP6f activity increases relative to saline-injected controls. (A) Schematic showing the timeline of adeno-associated viral vector injection, animal habituation, drug injection, baseline fiber photometry recording and elevated plus maze testing. (B) Representative image of GCaMP6f expression within the dBNST. (C) Imputed Ca^{2+} transients within the dBNST were significantly reduced under isoflurane anesthesia. (D) Representative fiber photometry traces showing changes in $\Delta F/F_0$ as a function of time for two minutes after either saline or CNO injection in AAV5-hM4Di animals during baseline recordings or recordings obtained in the elevated plus maze. (E) Both saline and CNO injections in mice expressing the hM4Di receptor led to an increase in Ca^{2+} transient frequency in the elevated plus maze relative to baseline values. The CNO-induced enhancement of activity was greater than that observed in saline-injected animals. (F) No differences in the ratio of activity in the EPM relative to baseline were observed between saline- and CNO-injected AAV5-mCherry control animals. (G) In saline-injected mice expressing the hM4Di receptor, open arm activity was consistently greater than closed arm activity as measured in imputed Ca^{2+} transient frequency. In CNO-injected mice expressing the hM4Di receptor, there was no significant difference between the two arms. Repeated measures two-way ANOVA: EPM arm effect $F(1,21)=6.32$, $p=0.02$, CNO effect $F(1,21)=0.20$, $p=0.66$, interaction $F(1,21)=1.78$, $p=0.20$. (H) In both saline- and CNO-injected AAV5-mCherry control mice, open arm activity was greater than closed arm activity. Repeated measures two-way ANOVA: EPM arm effect $F(1,17)=20.44$, $p=0.0003$, CNO effect $F(1,17)=0.0009$, $p=0.98$, interaction $F(1,17)=0.19$, $p=0.67$. P-values were calculated by unpaired t-test (C, E, F) or *post hoc* Holm-Sidak multiple comparisons test (G, H). N.S. $P>0.05$, *$P<0.05$, **$P<0.01$. N=4-9 animals per group

Discussion

Here we show that postsynaptic α_{2A}-ARs excite dBNST neurons via HCN channel inhibition, in contrast to presynaptic inhibition. Further, we show that CNO activation of the chemogenetic receptor hM4Di in dBNST neurons mimics aspects of α_{2A}-AR signaling, induces anxiogenesis and increases *in vivo* neuronal activity. Together, this data informs our understanding of α_{2A}-AR subpopulation interactions and relevance to anxiety and addiction treatments. Moreover, our hM4Di receptor data emphasizes that great care must be taken in the interpretation of DREADD-based approaches.

Postsynaptic α_{2A}-ARs mediate guanfacine-induced cfos expression.

α_{2A}-ARs are expressed in both presynaptic and postsynaptic compartments throughout BNST neuronal populations, in addition to glia (Flavin et al., 2014). The functions of these receptor subpopulations are incompletely understood. Within the BNST, α_2-AR agonists inhibit the release of norepinephrine, glutamate and GABA via presynaptic mechanisms (Palij and Stamford, 1993; Egli et al., 2005; Shields et al., 2009; Krawczyk et al., 2011a; Herr et al., 2012). Specificity of presynaptic actions have been shown, as guanfacine inhibits afferent-specific stimulation of parabrachial nucleus (PBN) but not basolateral amygdala (BLA) afferents (Flavin et al., 2014). Interestingly, though, in a Thy1-COP4 transgenic mouse line that minimally co-expresses channelrhodopsin-2 (ChR2) with the PBN-marking neuropeptide calcitonin gene-related peptide (CGRP), guanfacine enhances ChR2-initiated excitatory transmission (Flavin et al., 2014). This suggests that inhibitory actions at presynaptic α_{2A}-ARs may mask excitatory actions from other receptor subpopulations.

To identify the α_{2A}-AR locus for excitatory actions, we first used voltammetry-validated full- and heteroceptor-specific *Adra2a-/-* mouse lines to differentiate between autoreceptor actions within norepinephrine neurons and heteroceptor actions elsewhere (Gilsbach et al., 2009). Guanfacine-induced cfos responses were absent in full- and heteroceptor-specific *Adra2a-/-* mice, suggesting this is a heteroceptor-mediated action although a ceiling effect could occlude guanfacine actions. Interestingly, full *Adra2a-/-* mice show greater saline injection-induced cfos than wild-type littermates with intermediate levels in heteroceptor-specific *Adra2a-/-*. *Adra2a-/-* mice show baseline anxiety-like behaviors (Schramm et al., 2001; Lähdesmäki et al., 2004) and increased basal immediate early gene expression in stress-sensitive brain regions (Davies et al.,

2003). Thus, we speculate that saline-induced cfos in *Adra2a-/-* mice is stress-induced and distinct from guanfacine-induced cfos.

Heteroceptor α_{2A}-ARs are expressed in many cells and locations. We investigated dBNST-expressed α_{2A}-ARs through RNA *in situ* hybridization for the transcript *Adra2a*. *Adra2a+* cells upregulate *Fos* expression after guanfacine relative to saline injection. Like CGRP receptor-expressing neurons in the CeA, *Adra2a+* cells heterogeneously expressed several genetic markers (*Prkcd, Penk, Calb2, Crf, Npy*), suggesting that responsivity to catecholamines in *Adra2a+* cells and PBN input in CGRPR+ cells define these populations (Han et al., 2015). This shared organization pattern suggests cell-specific informational and functional divergence as a theme of GPCR signaling in the brain. In addition to upregulating *Fos* expression in *Adra2a+* dBNST cells, guanfacine increased the proportion of *Fos+ Adra2a-* cells, suggesting additional mechanisms underlying guanfacine-induced cfos/*Fos* expression. Disinhibition and/or excitation downstream of *Adra2a+* neurons or network activity outside of the BNST could engage *Adra2a-* dBNST neurons. Alternatively, *Adra2a-* BNST neurons could express the *Adra2a* transcript below the detection limit of this technique and thus be activated by guanfacine via an intracellular process, or could express alternative targets for guanfacine such as the α_{2C} adrenergic receptor encoded by the *Adra2c* transcript.

Guanfacine initiates cfos expression across the brain (Savchenko and Boughter, 2011). To exclude dBNST neuron activation by network activity, we assessed cfos induction in *ex vivo* brain slices from cfos-eGFP transgenic mice (Barth et al., 2004). Guanfacine incubation recruited cfos-eGFP expression, suggesting sufficiency of α_{2A}-ARs within this simplified system to initiate dBNST cfos expression. Interestingly, *ex vivo* guanfacine-induced cfos expression was

larger (4.6-fold increase relative to controls) than *in vivo* (2.8-fold increase), suggesting diminishment by inhibitory circuit activity outside the dBNST.

Multiple α_{2A}-AR agonists induced cfos expression, and we also introduced the inhibitory chemogenetic receptor hM4Di into dBNST neurons and observed CNO-induced cfos that mimicked and occluded further guanfacine-induced effects, suggesting translatability among postsynaptic G_i-GPCRs. Of note, no cfos activation was observed in controls, confirming hM4Di-specific actions and not off-target effects of CNO or clozapine (Gomez et al., 2017). Although consistent with an intracellular signaling pathway reminiscent of guanfacine-induced cfos expression, the possibility remains that CNO-induced excitatory actions may occur through alternative mechanisms that should be explored in future studies.

Together, this set of convergent data provides strong evidence in support of postsynaptic α_{2A}-ARs inducing cfos expression in a subset of dBNST neurons through a cell-autonomous experience-independent mechanism.

HCN channel involvement in guanfacine-induced activity enhancement.

G_i-coupled GPCRs can have excitatory actions through many mechanisms including alternative adenylyl cyclase recruitment (Federman et al., 1992), augmentation of G_s-coupled GPCR signaling (Andrade, 1993; Winder and Conn, 1993), GPCR-induced channel modulation (Wang et al., 2007), and MAPK/ERK pathway activation. We tested the hypothesis that α_{2A}-AR-mediated excitation occurs via inhibition of cyclic nucleotide-sensitive HCN channels as occurs in the PFC (Wang et al., 2007). This was based on a high prevalence of HCN-mediated I_h in guanfacine-induced cfos-eGFP+ cells and high *Adra2a* co-localization with *Hcn2*, the HCN subunit with fast kinetics and cAMP sensitivity (Ulens and Tytgat, 2001). Consistent with the

proposed mechanism, we show excitatory actions of both α_{2A}-AR agonism and HCN channel inhibition in the Thy1-COP4 mouse line that segregates ChR2 and CGRP expression, although with varying kinetics due to pharmacological differences (Shin et al., 2001).

Further, we assessed HCN inhibition effects on spontaneous excitatory transmission in guanfacine-induced cfos-eGFP+ cells. ZD7288 preincubation increased sEPSP frequency but not amplitude, suggesting an inhibitory role of HCN channels on spontaneous neurotransmission. While this effect could occur via presynaptic HCN channels, as observed in entorhinal cortex (Huang et al., 2011), we hypothesize that release of filtering at the dendritic spine may uncover previously undetectable synaptic potentials due to small amplitudes and space clamp error (Larkum et al., 1998; Williams and Mitchell, 2008). Consistent with an HCN channel interaction occurring in dendritic spines, we observed expression of the α_{2A}-AR within this compartment (Flavin et al., 2014). Further, having shown sufficiency of HCN inhibition for excitatory actions, we tested necessity via shRNA-mediated knockdown. Similar to *Adra2a-/-* mice, shHCN1/2-injected animals show no guanfacine-induced cfos expression but have elevated basal expression, suggesting that reducing HCN-dependent filtering at the dendritic neck releases the inhibitory tone on guanfacine-activated neurons and thus occludes further guanfacine-induced cfos expression. However, shHCN1/2 and GFP expressing mice did not differ in spontaneous BNST neurotransmission or baseline anxiety-like behaviors. Although one potential explanation of these results is that HCN channel knockdown is sufficient for cfos expression but is insufficient for these effects, confounds related to circuit effects resulting from nonspecific shRNA expression limit interpretability.

Potential anxiogenic actions of G_i-coupled signaling in dBNST neurons.

To assess the behavioral relevance of guanfacine-induced activation of dBNST neurons, we investigated CNO effects at dBNST-expressed hM4Di receptors in the elevated plus maze (EPM). CNO induced anxiogenic behavior (increased closed arm time, decreased open arm time), contrasting with anxiolytic actions of BNST lesions/silencing (Walker et al., 2003). Stress and anxiogenic drug exposure upregulates cfos in the BNST (Cullinan et al., 1995; Singewald et al., 2003), supporting a connection between BNST activation and anxiogenesis. Guanfacine has anxiolytic/antidepressant actions, but with very narrow effective concentrations (Mineur et al., 2015). Our data suggest the locus of guanfacine anxiolytic/antidepressant actions may be presynaptic. An alternative explanation of CNO-induced anxiogenesis that involves inhibitory actions on neuronal activity remains plausible and is dependent on cell- and subnucleus-specific expression of hM4Di. Although no overt differences were noted between groups in this regards, the balance between inhibition (or excitation) of anxiogenic *Drd1a*+ BNST neurons localized to the oval subnucleus and anxiolytic neurons in the anterodorsal BNST downstream of input from the basolateral amygdala could impact overall behavioral phenotype in the EPM. Future studies should aim to more rigorously test the effects of cell-, subnucleus-, and circuit-specific effects of hM4Di activation.

CNO activation of dBNST-expressed hM4Di receptors enhances neuronal activity in the EPM as measured by GCaMP6f fiber photometry. The profile of activity is treatment-dependent, as saline-injected animals show higher open arm activity than closed arm and CNO-injected animals do not, with saline- or CNO-injected AAV5-mCherry controls resembling saline-injected AAV5-hM4Di animals. Thus, G_i-coupled GPCR activation in dBNST neurons can be both anxiogenic and activity-enhancing within the elevated plus maze.

Relevance of hM4Di excitatory actions to the use of DREADDs.

In addition to detailing guanfacine effects on dBNST activity, we show that CNO activation of dBNST-expressed hM4Di is activity-enhancing and anxiogenic in the elevated plus maze. Neither CNO effect was recapitulated in control animals, highlighting effect specificity. These data question the assumption that hM4Di activation is universally inhibitory, like the assumption that agonism at hM3Dq is universally excitatory that has been confirmed as incomplete (Mazzone et al., 2018). Instead, these data suggest that hM4Di-mediated actions elicit G_i-coupled GPCR signaling cascades that may lead to unexpected cellular responses depending on downstream effectors. This, however, is not surprising given the extant literature on excitatory actions of G_i-GPCRs (Federman et al., 1992; Andrade, 1993; Winder and Conn, 1993; Wang et al., 2007; Kawaura et al., 2014). This highlights the importance of hM4Di effect interpretation as resulting from invoked G_i-GPCR signaling pathways and not necessarily neuronal inhibition.

Limitations and Future Directions

Clinical studies with guanfacine have begun to uncover potential sex differences (Fox et al., 2014; Milivojevic et al., 2017). For example, guanfacine decreased stress and cue imagery-induced drug craving, anxiety, and negative emotion in cocaine-dependent females but not males (Fox et al., 2014). Similarly, in rodents, guanfacine shows sex differences in cfos expression patterns (Mineur et al., 2015). In this study, males and females were combined due to lack of apparent sex differences. However, future studies should aim to rigorously test such differences to maximize clinical utility.

Conclusion

Extended amygdala α_{2A}-ARs are targets for anxiety disorders and stress-induced addictive behaviors. Here we show that postsynaptic α_{2A}-ARs in the dBNST mediated guanfacine-induced cfos expression via an HCN-dependent process. Interestingly, while presynaptic α_{2A}-ARs are hypothesized to be anxiolytic, these postsynaptic effects appear to be anxiogenic. Thus, competition among presynaptic inhibition and postsynaptic excitation may complicate the effects of guanfacine. The interplay among effects at different α_{2A}-AR subpopulation needs to be further explored to support preclinical and clinical approaches to anxiety and addictive disorders.

Chapter 3

Discussion and Future Directions

Contributions of auto- and heteroceptor α_{2A}-adrenergic receptors to physiology, pharmacology and behavior

The classes of α_2-adrenergic receptors in general and the α_{2A}-adrenergic receptor in particular are expressed widely throughout the brain. Tritiated para-amino-clonidine has been shown to bind to norepinephrine centers in the nucleus of the solitary tract (NTS) and the locus coeruleus (LC) and downstream norepinephrine target regions (Unnerstall et al., 1994). This is similar but not identical to the distribution of the *Adra2a* (α_{2A}-AR) transcript (McCune et al., 1993; Nicholas et al., 1993; Rosin et al., 1996; Wang et al., 1996). The functional consequence of this organization system is that there are regions of the brain that express different combinations of autoreceptor and heteroceptor α_{2A}-ARs. Differentiating actions at these subpopulations will inform our understanding of the physiology of α_{2A}-ARs and the pharmacology of α_{2A}-AR agonists.

Autoreceptor α_2-AR function within norepinephrine neurons in the locus coeruleus (LC) has been well-defined as inhibitory and via canonical mechanisms (Aghajanian and Vandermaelen, 1982). Specifically, clonidine hyperpolarizes LC neurons and decreases input resistance to inhibit cell firing and, thus, norepinephrine release (Aghajanian and Vandermaelen, 1982). This occurs via inhibition of adenylate cyclase, followed by subsequent decreased cAMP and increased potassium conductances (Aghajanian et al., 1985; Williams et al., 1985; Aghajanian and Wang, 1986, 1987). Because of these actions at autoreceptor α_2-ARs, norepinephrine actions are inhibited throughout the neuraxis, including those at heteroceptor α_2-ARs. Similarly, α_2-AR antagonists block this negative feedback loop and effectively increase

norepinephrine signaling across the brain, including at heteroceptor α_{2A}-ARs. For this reason, auto- and heteroceptor α_2-AR functions are not easily untangled and thus the effects of α_2-AR agonists were historically interpreted as solely being the result of autoreceptor signaling pathways.

Knockout models targeting the α_{2A}-AR gene *Adra2a* show decreased autoreceptor function that results in increased extracellular norepinephrine levels (Lakhlani et al., 1997; Lahdesmaki et al., 2002; Davies et al., 2003). As a result, these mice show impaired autonomic stability in addition to a number of neuropsychiatric phenotypes including increased depression- and anxiety-like behaviors in the forced swim test, light-dark box, elevated plus maze, marble burying test, open field test and discrete cue memory test (Schramm et al., 2001; Lahdesmaki et al., 2002; Davies et al., 2003). Further, the responsivity of these mice to α_2-AR agonist-induced sedation, anesthetic sparing, analgesia, anti-depression, and anxiolysis is blocked or inhibited (Lakhlani et al., 1997; Schramm et al., 2001; Lähdesmäki et al., 2004). As above, these actions were attributed to loss of autoreceptor function until the development of a transgenic rescue mouse model where the *Adra2a* gene is re-expressed in norepinephrine-expressing neurons under the control of the dopamine β-hydroxylase (DβH) promoter on a *Adra2a*-/- and *Adra2c*-/- background (Gilsbach et al., 2009). It was quickly recognized that α_2-AR agonist functions absent in the full *Adra2a*-/- mouse previously attributed to the autoreceptor were not rescued in the heteroceptor-specific *Adra2a*-/- mouse and are thus likely heteroceptor-mediated actions. These include agonist-induced analgesia, hypothermia, sedation, anesthesia-sparing, bradycardia, and hypotension. Autoreceptor α_{2A}-AR function was confirmed in norepinephrine feedback inhibition, spontaneous locomotion, and cardiac remodeling by rescue in the heteroceptor-specific *Adra2a*-/- mouse (Gilsbach et al., 2009, 2010; Gilsbach and Hein, 2012). The

application of this schema to neuropsychiatric phenotypes of interest and related agonist actions remains to be fully explored.

In the bed nucleus of the stria terminalis (BNST), α_{2A}-ARs are widely expressed and show a pattern of immunoreactivity to a hemagglutinin tag (HA-α_{2A}-AR) that suggests the presence of both auto- and heteroceptors based on incomplete overlap with DβH expression (Shields et al., 2009). An immunoelectron microscopic map after clonidine injection to induce internalization confirmed and extended this observation by showing expression in dendritic spines, dendrites, soma, axons, axon terminals (both symmetric and asymmetric), and glial cells (Flavin et al., 2014). Due to this extensive expression pattern and the well-delineated inhibitory functions of presynaptic α_{2A}-ARs on norepinephrine, glutamate and GABA terminal release (Palij and Stamford, 1993; Egli et al., 2005; Shields et al., 2009; Krawczyk et al., 2011a; Herr et al., 2012), we aimed to differentiate auto- and heteroceptor α_{2A}-AR functions and further subclassify heteroceptors based on subcellular compartment expression pattern in this region. Here we observed that guanfacine-induced cfos expression was absent in both full- and heteroceptor-specific *Adra2a*-/- mice, suggesting a heteroceptor locus of origin. However, elevated baseline cfos expression in full *Adra2a*-/- mice and an intermediate phenotype in heteroceptor-specific *Adra2a*-/- mice complicates this interpretation due to a potentially confounding ceiling effect. These results prompt further exploration of BNST α_{2A}-AR function in these mouse models directed at delineating the mechanism underlying elevated baseline cfos in *Adra2a*-/- mice, extending BNST-dependent phenotypic characterization of this mouse, and further validating the postsynaptic mechanism hypothesized to be underlying guanfacine-induced excitatory actions using these mouse lines. These will be delineated in detail below.

Elevated baseline expression of immediate early genes in the full *Adra2a*-/- mouse has been shown to previously occur as increased Zif268 and Arc mRNA in the frontal cortex and the hippocampus of saline-injected mice (Sanders, 2016). An explanation of this phenomenon that contrasts with the current hypothesis of excitatory postsynaptic α_{2A}-ARs in the prefrontal cortex and BNST states that this elevated baseline cfos expression results from loss of inhibitory tone from this receptor. Alternatively, this elevation may be distinct from guanfacine-induced cfos expression and thus occur in different populations of BNST neurons. Due to the baseline anxiety-like phenotype of the *Adra2a*-/- described above and its exaggerated response to injection stress (Schramm et al., 2001), it is possible that the elevated baseline cfos expression is in a stress-sensitive population of neurons distinct from the *Adra2a*+ and guanfacine-induced cfos+ populations. BNST neurons are known to induce cfos expression after exposure to a variety of stressors including injection stress (Sharp et al., 1991) but also restraint (Figueiredo et al., 2003), forced swim (Gaszner et al., 2012), social defeat (Martinez et al., 1998), predator odor (Day et al., 2004) and auditory stressors (Campeau and Watson, 1997). We hypothesize that the neurons activated by injection stress in full *Adra2a*-/- mice are BNST neurons expressing the neuropeptide corticotropin releasing factor (CRF). Importantly, we note that the transcript for CRF (*Crf*) is minimally expressed in *Adra2a*+ BNST cells. CRF-producing neurons are present throughout the BNST and are known to upregulate CRF and cfos expression after exposure to a variety of stressors (Cummings et al., 1983; Ju et al., 1989; Makino et al., 1994; Day et al., 1999; Funk et al., 2006; Dabrowska et al., 2013b). Further, these neurons are inhibited by guanfacine (T. Fetterly, unpublished data). This hypothesis can be tested by RNA *in situ* hybridization for the *Fos* and *Crf* transcripts, or through cfos immunofluorescence in either full- or heteroceptor-specific *Adra2a-/-* mice also expressing tdTomato in CRF+ neurons as done previously

(Silberman et al., 2013, 2015) through genetic introduction of CRF-ires-Cre (Taniguchi et al., 2011) alongside a Rosa-tomato reporter line (Madisen et al., 2015). If elevated, means of reversal or blockade could then be investigated, including exposure to non-adrenergic anxiolytics or evaluating cfos in the absence of any injection.

If the intermediate cfos expression level seen in heteroceptor-specific *Adra2a-/-* mice is like that of full *Adra2a-/-* and driven by baseline stress and anxiety, we would hypothesize that neuropsychiatric phenotypes exhibited by the full *Adra2a-/-* mouse may also be affected in this line. As stated above, the full *Adra2a-/-* mouse shows anxiety- and depressive-like behaviors in a number of behavioral assays including the forced swim test, light-dark box, elevated plus maze, marble burying test, open field test and discrete cue memory test (Schramm et al., 2001; Lahdesmaki et al., 2002; Davies et al., 2003). A rescue of baseline phenotypes in the heteroceptor-specific *Adra2a-/-* mouse would suggest anxiolytic actions of the autoreceptor α_{2A}-AR at baseline or in the presence of an agonist. In addition to anxiolytic actions of α_{2A}-AR agonism in these mouse lines, the effects on stress-induced reinstatement of drug-seeking behaviors merits attention. Agonists at the α_2-ARs robustly uncouple stress from drug-seeking behaviors in rodent models (Erb et al., 1998; Shaham et al., 2000b; Highfield et al., 2001; Le et al., 2005; Mantsch et al., 2010) and these actions are mimicked by direct injection to the BNST (Delfs et al., 2000; Wang et al., 2001). However, it is unclear if these effects are due to autoreceptor-induced inhibition of norepinephrine release or heteroceptor actions. To test this, full- and heteroceptor-specific *Adra2a-/-* mice alongside wildtype littermates would undergo conditioned place preference to cocaine injection as previously described (Conrad et al., 2013), followed by extinction of this preference. Stress-induced reinstatement will then be assessed with forced swim stress in the presence or absence of α_2-AR agonists (Vranjkovic et al., 2012). After

this procedure, we will be able to compare conditioning, extinction, stress-induced reinstatement, and α_2-AR agonism-induced inhibition of reinstatement across genotypes to distinguish auto- and heteroceptor contributions to addictive-like behaviors in this rodent model.

In addition to molecular and behavioral characterization of auto- and heteroceptor contributions of α_{2A}-AR and associated ligands, these two mouse lines can be used as a tool to test our hypotheses about specific actions of receptor subpopulations. Namely, the heteroceptor locus, mechanism and consequences of postsynaptic α_{2A}-AR excitatory actions within the BNST can be tested in these mice. Specifically, these mice could be used for analyses of cfos expression after CNO activation of hM4Di, cfos expression after *ex vivo* guanfacine incubation, cfos expression after shHCN1/2 expression, spontaneous excitatory postsynaptic potential parameters after ZD7288 incubation, and fiber photometry-recorded Ca^{2+} transients during anxiety-like behavioral tests. The interpretation of some of these results, such as CNO activation of hM4Di, may be confounded by increased baseline activity. This issue could be averted by observing the effects of multiplex G_i-DREADD activation of the kappa opioid receptor DREADD (KORD) in CRF+ cells to silence these putative stress-activated cells and hM4Di expression in CaMKII+ cells to determine the extent of postsynaptic G_i-GPCR mediated cellular activation, for example (Vardy et al., 2015). Alternatively, development of a mouse line with *Adra2a*-driven Cre recombinase would allow for targeting of G_i-DREADD expression to these guanfacine-activated BNST neurons and selective activation of hM4Di within this population of cells (Roth, 2016). Together, each of these experiments would provide insight into the complicated biology of postsynaptic α_{2A}-ARs in the BNST and their effects on physiology and behavior. Further, this work would provide a framework for the careful use of knockout mouse models, which are largely used for drug validation and broad directionality of effects but could

also be used to parse out subtleties in drug action and resultant changes on circuit activity and behavioral outcomes.

Further defining the guanfacine-activated BNST neuron and contributions to physiology

One of the defining features of the bed nucleus of the stria terminalis is the heterogeneity of cell types in the region. Whether defined by electrophysiological parameters (Hammack et al., 2007), expression of genetic markers (Lebow and Chen, 2016), or responsivity to specific inputs or ligands (Flavin et al., 2014), BNST neurons are diverse. Here we identify and characterize two overlapping populations of neurons, one positive for the transcript *Adra2a* that encodes the α_{2A}-adrenergic receptor (α_{2A}-AR) and the other expressing cfos after guanfacine injection. Further defining these populations of cells and their contribution to BNST physiology will provide insights into the biology of this complex brain region and contributions to the pathophysiology and treatment of neuropsychiatric disorders.

The *Adra2a*+ population of BNST cells was shown to express the *Fos* transcript after guanfacine injection, co-express the *Hcn2* but not *Hcn1* transcript, and minimally express any of five genetic markers tested (*Crf, Npy, Prkcd, Penk, Calb2*). The function of these cells could be further delineated with causative experiments upon development of the transgenic mouse line described above that expresses Cre recombinase under the control of the *Adra2a* promoter. This could allow for the expression of Cre-dependent genetic tools to study these cells either under naturalistic conditions (tdTomato for *ex vivo* electrophysiology and immunofluorescence, GCaMP6f for *in vivo* calcium transient recordings), excitation (channelrhodopsin-2), inhibition/deletion (halorhodopsin, diphtheria toxin receptor), or direct pharmacological manipulation (shHCN1/2, hM3Dq, hM4Di), for example.

Identifying this population of cells by *Adra2a* expression allowed for in-depth study and characterization of responsivity to guanfacine. However, this population itself is heterogeneous and includes BNST neurons that express the postsynaptic α_{2A}-AR but also BNST neurons that express presynaptic α_{2A}-ARs within the BNST as interneurons or elsewhere in the brain as projection neurons and non-neuronal cells that include glial populations known to also express the receptor. For example, BNST neurons positive for the neuropeptide corticotropin releasing factor (CRF) are inhibited by guanfacine and do not express cfos after guanfacine injection (T. Fetterly, unpublished data), but express significant amounts of the *Adra2a* transcript themselves while being a minority of *Adra2a*+ cells (see Appendix XII). This data suggests that BNST CRF neurons are *Adra2a*+ but are not guanfacine-activated, complicating identification of guanfacine-activated neurons by this expression pattern. Further complicating this issue, GPCR expression is transient and *Adra2a* transcripts throughout the central nervous system have been shown to vary with stimuli including stress exposure (Flügge et al., 2003), chronic drug exposure (Tamagaki et al., 2010; Smith et al., 2016), electroconvulsive therapy (Lillethorup et al., 2015), and nerve injury (Ali et al., 1999; Birder and Perl, 1999; Stone et al., 1999).

In attempting to classify guanfacine-activated BNST neurons, we also show that this population includes not only *Adra2a*+ neurons but also *Adra2a*- neurons likely activated by an alternative mechanism. This means that any characterization of *Adra2a*+ neurons as described above would not include analysis of guanfacine-activated *Adra2a*- neurons. Guanfacine-induced *Fos* expression in *Adra2a*- cells could result from direct effects at the α_{2C}-AR, through indirect activation or disinhibition via network activity within or outside of the BNST downstream of *Adra2a*+ cellular activation, or through a different mechanism entirely. The first of these can be tested by RNA *in situ* hybridization and co-localization of the *Adra2c* transcript with *Fos* and

Adra2a. Due to the specificity of guanfacine at the α_{2A}-AR over the α_{2C}-AR, we hypothesize that this is not the mechanism of guanfacine-induced cfos in *Adra2a*- BNST cells. Instead, we hypothesize that activation of *Adra2a*+ neurons leads to *Fos* expression in *Adra2a*- cells through activation via release of an activity-enhancing neuropeptide or disinhibition through a microcircuit mechanism involving an intermediary inhibitory interneuron or projection neuron. As above, introduction of Cre recombinase under the control of the *Adra2a* promoter would allow for characterization of the downstream effects of *Adra2a*+ neuronal activation by channelrhodopsin-2 or the designer receptor hM4Di. Alternatively, inhibition by halorhodopsin or deletion by genetically-expressed diphtheria toxin could be used to block downstream effects of activation. The overall effects of these perturbations on *Adra2a*- guanfacine-activated neurons could be determined by introduction of a fluorescent reporter (tdTomato) in *Adra2a*+ cells in the cfos-eGFP mouse line so that *Adra2a*-/cfos+ neurons could be studied in isolation. Although complicated in nature, these experiments would directly test and provide evidence for the mechanism underlying guanfacine-induced cfos expression in *Adra2a*- BNST cells.

The complexity of this system could be simplified upon identification of alternative ways to define these populations of guanfacine-activated neurons beyond positivity for *Adra2a* and/or *Fos* transcripts after guanfacine injection. A low throughput way in which BNST neurons could be classified using RNA *in situ* hybridization to look at genetic markers in combination with *Adra2a* and *Fos* after guanfacine injection to identify markers for each of the following classes of cells: *Adra2a+Fos+*, *Adra2a-Fos+*, *Adra2a+Fos-*, and *Adra2a-Fos-* BNST cells. We observed minimal overlap between *Adra2a* and each of *Crf, Prkcd, Penk, Calb2,* and *Npy* but have only looked at *Prkcd, Calb2,* and *Penk* with both *Adra2a* and *Fos* and see that it is not enriched in any of these populations (see Appendix XII). Other transcripts that could be tested for overlap with

Adra2a include *Drd1* due to the D1 receptor's role in inhibiting α_{2A}-AR+ prefrontal cortex neurons (Gamo et al., 2015), *Calcrl* due to the presumed connectivity with CGRP+ parabrachial nucleus afferents (Flavin, 2014), *Avp* due to the ability of α_2-AR agonists to reduce vasopressin levels (Waeber et al., 1984), *Pdyn* due to the known role of dynorphin and kappa opioid receptors in stress-induced reinstatement (Le et al., 2018), or *Drd2* due to the shared organizational pattern seen with G_q-GPCRs in the BNST that may be translatable to the D2 receptor and other G_i-GPCRs (Mazzone et al., 2018). However, this is a low-throughput approach that yielded limited results in prior analyses.

Instead, a hypothesis-generating approach could be used to isolate guanfacine-activated neurons using a cell-sorting technique followed by characterization. This technique has been successfully utilized to determine transcriptional changes in dorsal striatal neurons during incubation of methamphetamine craving (Li et al., 2015). Following guanfacine injection, cfos+ or cfos-eGFP+ BNST neurons could be sorted and analyzed by RNA Sequencing (RNASeq) to semi-quantitatively define the transcriptional profile of these cells. Raw transcript values within this population would be informative to identify sensitive genetic markers that could be used to manipulate these neurons. In addition to simplifying interpretation of these findings, specific markers could be identified by comparison to other cell populations within the BNST. First, transcript comparisons with cfos- BNST neurons would help to identify differentiating factors. However, due to the heterogeneity of this population of cells that includes both guanfacine-inhibited cells and those not affected by guanfacine, a more homogeneously inhibited population such as CRF+ BNST neurons would allow for more interpretable conclusions. This could be obtained by crossing the cfos-eGFP mouse line with the CRF-tdTomato mouse line described above and separating cells based on both cfos-eGFP and CRF-tdTomato positivity, for example.

Similarly, this technique could be used to determine the mechanism of cfos expression in *Adra2a*- cells in an *Adra2a*-tdTomato mouse line by identifying transcriptional differences between *Adra2a*+cfos+ and *Adra2a*-cfos+ sorted cells. Finally, if a sensitive and specific genetic marker was found for guanfacine-activated neurons, cell sorting techniques and transcriptional profiling would allow for the identification of pathways upregulated after guanfacine exposure and changes that occur within this population with extended drug use, such as those pathways mediating changes in synaptic plasticity. This analysis would allow for specific and impactful work to be done in the study of guanfacine-activated BNST neurons.

A potential outcome of these analyses, though, is that guanfacine-activated neurons are best defined by positivity for the transcript *Adra2a*+ and that the downstream effects are mediated by activation of these cells. In a similar attempt to subclassify neurons in the central nucleus of the amygdala based on responsivity to parabrachial nucleus (PBN) neurons positive for the neuropeptide calcitonin gene related peptide (CGRP), it was found that the marker with highest sensitivity and specificity was the CGRP receptor *Calcrl* (Han et al., 2015). This pattern implies that, in both cases, the cell population is defined by responsivity to specific input and not other features. The study of these cells would thus be facilitated with the use of an *Adra2a*-Cre line as described above. However, this observation raises the question of the origin and nature of the endogenous catecholamine input that is defining this cell population, a question not yet answered due to the intricacies of signaling at subpopulations of adrenergic receptors. The assumption is that norepinephrine from the nucleus of the solitary tract activates postsynaptic α_{2A}-ARs due to the strong input from these cells in the BNST. However, dopamine affinity to the α_{2A}-AR is comparable to norepinephrine (Cornil and Ball, 2008) and dopamine innervation is more prominent than norepinephrine in the dorsal component of the BNST (Phelix et al., 1992).

To identify catecholamine input to these cells, simultaneous light-activated control of presynaptic neurotransmitter release could be obtained by injecting Cre-dependent channelrhodopsin into the ventral tegmental area (VTA) of mice with Cre expression in tyrosine hydroxylase neurons (TH-Cre) or into the nucleus of the solitary tract (NTS) of mice with dopamine β-hydroxylase-driven Cre (DβH-Cre) simultaneous to recording of effect in guanfacine-activated BNST neurons. The latter could be done with observing effects of optical stimulation on electrophysiological recordings from cfos-eGFP+ BNST neurons, on Ca^{2+} transients (GCaMP6f) or voltage sensors (Piatkevich et al., 2018) from targeted cell populations (i.e. *Adra2a*-Cre) using *ex vivo* two-photon microscopy, or on direct measurements of catecholamine levels with newly developed genetic sensors (Patriarchi et al., 2018), also from targeted cell populations. The latter two would be benefited by not disrupting the intracellular milieu and blockade of HCN-dependent processes. Regardless of means of observation, the dependency of these effects on α_{2A}-AR agonism could be validated by preincubation of the slices in antagonists to the other adrenergic (α_1-AR, β-AR) and dopaminergic (D1-like, D2-like) receptors or to the α_{2A}-AR itself. HCN dependency of excitatory effects could also be validated in this experimental design. The dopaminergic or catecholaminergic origin of postsynaptic α_{2A}-AR agonism and cellular activation would inform our understanding of the actions of these neurotransmitters in the BNST and their effects on synaptic plasticity and extended drug use-mediated changes therein as described above.

Pharmacology of *ex vivo* guanfacine-induced cfos expression

A complication of evaluating psychotropic drug actions *in vivo* is the potentially limitless confounding variables of network activity and cell-specific changes in activity that occur as a result of drug exposure. By reducing this system to only the afferent terminals and cellular

populations present within a 300 micron-thick *ex vivo* brain slice containing the BNST, we were able to evaluate *ex vivo* cfos induction and rule out network activity influences on the activity-enhancing effects of guanfacine. Importantly, GABAergic and other interneurons within the BNST and microcircuit effects of their activation or inhibition cannot be ruled out using this technique. Due to the known inhibitory effect of guanfacine on electrically evoked inhibitory postsynaptic currents, these microcircuit effects remain a possibility and should be explored in future studies (Shields et al., 2009). In addition to testing whether or not this effect is BNST autonomous, in using the α_2-AR antagonist atipamezole we showed that this effect is mediated by this population of receptors and in using the α_2-AR agonists clonidine and UK-14,304 we showed that this effect occurs with an alternative partial agonist as well as a full agonist of the receptor, respectively. In showing translatability among α_2-AR agonists in both the presence and extent of cfos induction, this data supports the hypothesis that this effect is mediated by canonical drug actions at the receptor, such as inhibition of adenylyl cyclase and reduction of intracellular cAMP levels, and not guanfacine-specific conformational changes, for example. Specifically, discrepancies between α_2-AR ligand recruitment of β-arrestin recruitment (clonidine > guanfacine) (Lu et al., 2009) and alternative coupling to G_q and G_s G-proteins (guanfacine > clonidine) (Jasper et al., 1998) would be expected to lead to differential amounts of recruitment that were not observed in this reduced system . This highlights the utility of this method for basic pharmacological studies done in a medium-throughput manner. Other facile applications that can be applied to guanfacine and other cfos-inducing ligands include determining dose response curves, receptor specificity of agonist and antagonist effects, mechanism underlying excitatory actions, interactions with behavioral history (i.e. chronic

stress), cell-specific signaling with a genetically-encoded fluorescent reporter, and effects on activity of novel ligands.

HCN channel inhibition: effects on BNST physiology and relevant behaviors

Our model of excitatory actions initiated by guanfacine agonism at α_{2A}-ARs involves depletion of intracellular cAMP within the dendritic spine that decreases the open probability of hyperpolarization-activated cyclic nucleotide-gated nonspecific cation (HCN) channels localized to the dendritic neck, thus releasing inhibitory filtering of currents at this locus and increasing activity of the postsynaptic neuron. This mechanism has been shown to occur in prefrontal cortex pyramidal neurons and underlies beneficial effects of norepinephrine and guanfacine on working memory (Wang et al., 2007; Thuault et al., 2013). This hypothesis is supported by data showing high prevalence of the hyperpolarization-activated current (I_h) in guanfacine-activated neurons, the presence of *Hcn2* transcript within these cells, and the necessity and sufficiency of HCN channel inhibition for excitatory actions within the BNST. Prior to this work, the extent of investigation into BNST HCN channels was limited to anatomy of expression (Monteggia et al., 2000; Notomi and Shigemoto, 2004) and as a means of cell-specific subtyping (Hammack et al., 2007; Hazra et al., 2011; Daniel et al., 2017). All four HCN channels subunits (HCN1-4) are expressed within the BNST, and cell-type specificity is shown among the three types of BNST neurons defined by their electrophysiological current clamp profiles (Type I: HCN2, HCN4; Type II: HCN1, HCN2, HCN3, HCN4; Type III: HCN4). Although useful as a tool to help classify BNST neurons into functionally distinct subpopulations (Szücs et al., 2010; Hazra et al., 2012; Dabrowska et al., 2013a; Rainnie et al., 2014; Nagano et al., 2015; Smithers et al., 2017), the functional consequences of HCN channel modulation on physiology or behavior have been minimally investigated in this region.

By RNA *in situ* hybridization, we show that *Adra2a* transcripts co-localize with *Hcn2* but minimally do so with *Hcn1*. The *Adra2a+Hcn2+* cells, though, are only a minority of all cells expressing the *Hcn2* transcript (see Appendix XII). Only a minority of *Hcn1+* or *Hcn2+* BNST cells co-express the *Adra2a* transcript, suggesting alternative functions of HCN channels in BNST neurons. HCN channel function largely depends on subcellular expression pattern, with somatically-expressed channels enhancing neuronal activity by resting membrane depolarization and dendritically-expressed channels inhibiting synaptic activity through filtering mechanisms (McCormick and Pape, 1990; Cardenas et al., 1999; Day et al., 2005; Park and Lee, 2007; Wanat et al., 2008; George et al., 2009; Okamoto et al., 2018). In the hippocampus, for example, HCN channel density increases with distance from the soma in order to constrain integration of synaptic events and filter these events to normalize somatic output independent of location within the dendritic tree (Magee, 1998; Lörincz et al., 2002; Tsay et al., 2007). An immunoelectron microscopic map of HCN channel expression in the BNST would inform the distribution and potential function of BNST HCN channels.

Nonspecific HCN channel inhibition by ZD7288 or HCN channel knockdown by an shRNA construct targeting both HCN1 and HCN2 channels both had excitatory actions in the BNST. This effect could be driven by excitatory actions in *Adra2a+* BNST neurons but could also be indicative of other excitatory contributions. ZD7288 enhances the frequency of spontaneous excitatory postsynaptic potentials in guanfacine-activated BNST neurons specifically, but also enhanced optically evoked field potentials elicited by stimulation of channelrhodopsin-2 (ChR2) expressed in the Thy1COP4 transgenic mouse line. Based on the segregation of ChR2 with the parabrachial nucleus-marking neuropeptide calcitonin gene related peptide (CGRP), this stimulation protocol minimizes recruitment of this guanfacine-inhibited

afferent population and enriches for inputs whose postsynaptic response is putatively enhanced by α_{2A}-AR agonism. Although the effects of ZD7288 support overall activity-enhancing effects of HCN inhibition within the BNST, this stimulation protocol-induced enrichment of specific synapses could mask alternative inhibitory mechanisms of somatically-expressed HCN channels. However, upon expression of shHCN1/2 non-specifically in BNST neurons (hU6 promoter), we see no change in resting membrane potential or sEPSP frequency or amplitude (see Appendix III). This negative result could be due to competition between excitatory and inhibitory actions, or due to confounding variables such as molecular compensation and synaptic reorganization in the three weeks between shRNA injection and recording. Identification and isolation of guanfacine-activated neurons would allow for the focused study of HCN channel inhibition or knockdown on both *Adra2a*+ and *Adra2a*- neurons.

Excitatory actions of HCN channel inhibition within *Adra2a*+ BNST neurons suggests that this modulation would result in increased anxiety-like behaviors, mimicking CNO-induced activation of these cells via hM4Di agonism. However, non-selective HCN1/2 knockdown by shRNA showed no effect in the elevated plus maze, suggesting a lack of BNST HCN channel involvement in anxiety-like behaviors (see Appendix IV). Broadly, HCN channel inhibition or knockdown has been shown to both upregulate (Park et al., 2011; Zhong et al., 2018) and downregulate (Kim et al., 2012, 2017; Shah, 2012; Koga et al., 2015) anxiety- and depressive-like behaviors in a variety of brain regions. Therefore, competing actions within different cell populations may alter the balance of excitatory and inhibitory or anxiogenic and anxiolytic actions when these channels are knocked down in the heterogeneous BNST. More specific expression of the shRNA directed against HCN1/2 would allow for more conclusive interpretations to be drawn. Further, due to possible compensation effects during the three weeks

of viral incubation, *in vivo* micro-injections of ZD7288 to the BNST would test for time-course dependent effects on behavior and physiology. This would overcome pharmacological issues with systemic HCN channel inhibition due to the role of these channels in the rhythmic firing of cardiac pacemaker cells. An alternative strategy involves targeting the interaction between HCN channels and the TRIP8b (tetratricopeptide repeat-containing Rab8b-interacting protein) protein, which has been shown to be an auxiliary subunit of HCN channels critical for subcellular expression patterning (Lewis et al., 2009; Santoro et al., 2009; Han et al., 2011; Lyman et al., 2017). Disrupting this interaction has been shown to induce antidepressant behavior in mice (Lewis et al., 2011; Han et al., 2017). This may become a useful tool for dissecting systemic actions of HCN channel modulation and localizing some of those effects to the BNST.

Postsynaptic G_i-DREADD activation effects within the BNST and the rest of the brain

Activation of the designer receptor hM4Di expressed in CaMKIIα+ BNST neurons elicits signaling cascades that culminate in cfos expression in a subset of infected neurons. Overlap in this population and guanfacine-activated neurons is suggested by nonadditive expression of cfos when both guanfacine and clozapine-N-oxide (CNO) are injected simultaneously. Although a majority of hM4Di+ BNST neurons are likely inhibited by CNO, this data suggests that cell-specific effects are not necessarily uniform and inhibitory. As a result, all DREADD effects should require validation (Andero et al., 2014; Pina and Cunningham, 2017; Xia et al., 2017; Adekunbi et al., 2018). This is commonly done by electrophysiological recordings, with the G_q-coupled DREADD hM3Dq generally showing depolarization (Krashes et al., 2011; Li et al., 2016; Douglass et al., 2017), increased neuronal spiking (Vazey and Aston-Jones, 2014; Shen et al., 2015; Hausen et al., 2016; Camille et al., 2018) or neurotransmitter release (Calipari et al., 2016), and the G_i-coupled DREADD hM4Di showing hyperpolarization (Krashes et al., 2011;

Toda et al., 2016; Mu et al., 2017) or decreased neuronal spiking (Garner et al., 2012; Mahler et al., 2014; Zhang et al., 2017). In addition, CNO-induced cfos expression is commonly used to validate hM3Dq cellular activation (Krashes et al., 2011; Garner et al., 2012; Yiu et al., 2014; Douglass et al., 2017) or hM4Di reversal of stimulus-driven cfos expression (Kerstetter et al., 2016; Ognjanovski et al., 2017) but not to evaluate cfos activation by hM4Di activation alone. Due to the transient nature of HCN channel function after cell dialysis and the observed increase in cfos expression, we used fiber photometric recordings of GCaMP6f fluorescence to evaluate the physiological effects of hM4Di activation. This has previously been used to validate hM4Di-mediated inhibition of D1R- and D2R-expressing neurons in the nucleus accumbens (Calipari et al., 2016). Validating excitatory effects of hM4Di activation in CaMKII+ BNST neurons, we see increased BNST activity during the elevated plus maze normalized to baseline activity in CNO-injected animals relative to saline-injected controls. Prior to this work, BNST DREADD manipulations have been validated using the same methods as above, with hM3Dq activation having been shown to depolarize VGAT+ neurons (Mazzone et al., 2018), depolarize CRF+ neurons (Marcinkiewcz et al., 2016), and induce cfos expressing in GAD67+ neurons (Kodani et al., 2017). In addition, hM4Di activation has been shown to hyperpolarize both VGAT+ (Mazzone et al., 2018) and CRF+ neurons (Pleil et al., 2015b; Marcinkiewcz et al., 2016), and reduce stimulus-driven cfos expression in hSyn+ neurons (Pina et al., 2015). Future studies should aim to characterize DREADD responsivity in more neuronal populations and utilize convergent approaches, especially those that do not disrupt the intracellular milieu such as perforated patch recordings and *in vivo/ex vivo* fluorescent indicator measurements (Kumar et al., 2017).

In addition to determining the physiological outcome of hM4Di activation in CaMKII+ BNST neurons, we aimed to determine the behavioral relevance of this signaling pathway in anxiety-like behavior as assessed in the elevated plus maze (EPM). In the EPM, CNO application in hM4Di animals increased closed arm time and decreased open arm time, with no effect on center zone time and locomotor activity as within-animal controls, suggesting an anxiogenic effect of the drug. These effects were not seen after CNO in mCherry-injected controls or naïve animals, highlighting specific actions at the hM4Di receptor. Activity of BNST neurons has been shown to be capable of bidirectional modulation of behavior in the elevated plus maze (Kim et al., 2013), suggesting subsets of anxiogenic and anxiolytic neurons that elicit these outcomes after increased activity. The anxiogenic effects of hM4Di activation could thus be a result of increased activity of putative anxiogenic neurons and/or decreased activity of anxiolytic neurons. CaMKII+ BNST neurons have not been extensively characterized, so both options are a possibility. Previously, hM4Di activation of VGAT+ neurons has been shown to have no effect on behavior within the EPM while hM3Dq activation of those same neurons both induces long term depression and anxiety-like behaviors (Mazzone et al., 2018). Similarly, BNST CRF neurons have been shown to be inhibited by cell-specific expression of hM4Di and block fluoxetine-induced anxiety in the EPM, suggesting anxiolytic effects of CNO in this context. Generally, CaMKII expression within the BNST is complementary to GAD67, suggesting increased expression within non-GABAergic neurons that do not express VGAT+ (Benson et al., 1992). However, future studies should utilize high resolution techniques that allow for cell-specific levels of overlap such as the RNA *in situ* hybridization approach used here to rigorously assess expression patterns. Overlap of CaMKII with CRF has not been established. More extensive characterization of this population of neurons as well as the role of CaMKII signaling

within these cells, which has been shown to be necessary for CRF-mediated effects within the region (Myers and Meerveld, 2010) and is reduced during abstinence from chronic alcohol exposure (Kash et al., 2009), is needed.

Although historical data specifically connecting CaMKII+ BNST neuronal activity to anxiety-like behavior is lacking, we hypothesize that activating these neurons by hM4Di-mediated mechanisms underlies the anxiogenic behavioral outcome for two reasons. First, CNO activation of CaMKII-expressed hM4Di induces cfos expression in the BNST. Although nonspecific, cfos expression within the BNST has been shown to occur after exposure to stressors known to elicit anxiety-like behaviors (Arnold et al., 1992; Martinez et al., 1998; Figueiredo et al., 2003; Singewald et al., 2003; Day et al., 2004; Funk et al., 2006; Gaszner et al., 2012). Second, BNST inhibition has been shown to decrease anxiety-like behaviors after a number of different manipulations and behavioral measurements (Walker and Davis, 1997; Walker et al., 2003; Resstel et al., 2008; Duvarci et al., 2009), suggesting that anxiolysis would be observed if hM4Di activation non-specifically inhibited BNST neurons. In order to answer the question about whether CNO-induced activation of a subset of CaMKII+ hM4Di-expressing cells is sufficient to drive anxiogenic behavior, a means of accessing these cells is required. This would be benefited by the cell-specific strategies described above assuming guanfacine- and CNO-activated neurons are overlapping populations. However, this could also be extended to include the recently developed tools that allow for genetic access to activated populations of neurons. These tools are commonly driven by immediate early gene promoters (Guenthner et al., 2013; Sørensen et al., 2016; Wang et al., 2017) and invoke introduction of tools used to measure or alter neuronal activity (Garner et al., 2012; *Fos*que et al., 2015). Identifying and isolating

guanfacine- or CNO-activated neurons in this manner would allow for clarifying the role of this functionally-defined population of cells in BNST physiology and behavior.

In vivo BNST activity measurements and contributions to behavior

In addition to observing CNO-induced increases in BNST activity during the elevated plus maze, we also observed a difference in the pattern of activity observed during the test. Specifically, saline-injected hM4Di-expressing animals and all mCherry-expressing controls show increased activity when the mouse is in the open arm relative to the closed arm. CNO-injected animals, on the other hand, show no such difference. This suggests that BNST neurons are activated by the anxiogenic stimuli of being in the open arm, which has been shown previously to be sufficient for expression of cfos in BNST neurons (Nguyen et al., 2006). In ventral hippocampus, anxiety-sensing neurons were recently shown to be similarly activated by anxiogenic stimuli (Jimenez et al., 2018). Inhibition of ventral hippocampal neurons in the open arm reduced the anxiogenic phenotype while activation of lateral hypothalamus-projecting ventral hippocampal neurons increased anxiogenic behavior in the open field test, suggesting that disruption of responsivity to increased threat in the open arm by CNO activation of BNST-expressed hM4Di may underlie the observed anxiogenic phenotype. To test this hypothesis, bidirectional optogenetic control of BNST activity time-locked to EPM location could be used to assay the connection between location-specific neuronal activity and behavioral phenotype in this and related assays.

The interpretation of BNST activity correlating with perceived threat in this simple rodent behavioral test is mirrored by recent human functional imaging data investigating the responsivity of this region to various stimuli. This work was aided by the development of a high resolution mask (Avery et al., 2014) and follow-up structural studies on the BNST and its

connectivity patterns (Krüger et al., 2015; Torrisi et al., 2015; Tillman et al., 2018). Broadly, these studies have attributed to the BNST a role in evaluating the valence of threats in the environment (Mobbs et al., 2010; Somerville et al., 2010), and anticipation of aversion as a result of exposure to those threats (Grupe et al., 2013; Klumpers et al., 2017). BNST activation is especially noted when the perceived threats are either sustained (Somerville et al., 2013) or unpredictable (Alvarez et al., 2011), consistent with the rodent literature that shows that BNST activity is critical for anxiety-like responses to chronic and unpredictable stressful, while the amygdala encodes the fear response engaged acute and predictable stimuli (Walker et al., 2003). Interestingly, heightened BNST responses to threat and conditions of uncertainty have been observed in patients with generalized anxiety disorder or those at risk for developing an anxiety disorder (Yassa et al., 2012; Shackman et al., 2017). Although causality cannot be inferred from this data, increased BNST activity in response to stressful stimuli in anxious individuals mirrors the CNO-dependent phenotype in mice expressing hM4Di in BNST neurons where activation of this designer receptor induces an anxiety-like phenotype and increased BNST activity as measured in calcium transients during the elevated plus maze behavioral test. Continuing to dissect out BNST activity patterns in response to a variety of stimuli that mirrors human functional data will prove to be informative in validating mouse models of anxiety-like behavior and the conclusions we draw from them. This can be accomplished by non-specific activity monitoring during other tests of anxiety-like behavior based on threat perception such as the open field test or contextual fear conditioning. In addition, BNST activity patterns in tests that force competition between appetitive and aversive stimuli such as the novelty suppressed feeding and novelty-induced hypophagia tests (Louderback et al., 2013), as well as models of depression-like behavior and learned helplessness such as the forced swim (Crestani et al., 2010) or tail

suspension tests (Hiraoka et al., 2017), will allow for testable hypotheses about the role of the human BNST in these processes that have been previously shown to invoke BNST activity within mouse models of these disease processes.

The molecular biology of guanfacine-induced cfos expression

In addition to marking guanfacine-induced upregulation of neuronal activity within *Adra2a*+ BNST neurons, upregulation of cfos has its own biological consequences as a part of the AP-1 transcription factor complex with the Jun family of proteins (Chiu et al., 1988; Halazonetis et al., 1988; Nakabeppu et al., 1988; Rauscher et al., 1988; O'Shea et al., 1989; Turner and Tjian, 1989). The transcriptional profile initiated by cfos depends on its binding partners in the AP-1 complex (Hess, 2004) as well as the time course of activation (Nestler, 2001). Therefore, a detailed analysis of genes upregulated by α_{2A}-AR agonism in putative guanfacine-activated neurons that includes both immediate early gene transcription factors and their downstream targets would greatly inform our understanding of this complex system. This could be accomplished by RNA Sequencing after isolation of these neurons from the heterogeneous collection of cells within the BNST through any of the methods described above.

The results of an analysis of the transcriptional profile generated from guanfacine activation of these neurons would be correlational and hypothesis-generating about the molecules implicated in the effects of guanfacine on BNST physiology and behavior. An alternative approach to test whether cfos activation is specifically required for activity enhancement of guanfacine-activated neurons and the anxiogenic effect observed after CNO activation of hM4Di-expressing BNST neurons would be to utilize either acute cfos knockdown or the cfos knockout mouse line. Antisense oligonucleotides directed against cfos have been utilized to show that this molecule is involved in the processes underlying synaptic plasticity and

memory formation within the hippocampus (Guzowski, 2002; Kemp et al., 2013), perirhinal cortex (Seoane et al., 2012), retrosplenial cortex (Katche and Medina, 2017), and parabrachial nucleus (Yasoshima et al., 2006), among others. Similar results have been obtained after life-long cfos deficiency in the knockout mouse model (Fleischmann et al., 2003). The effects of cfos knockdown or knockout on synaptic plasticity within the BNST have not been evaluated, but the contributions and interactions of plasticity within this region with chronic drug use suggest that the study of cfos expression and upregulation could be informative beyond marking activated neurons.

The implications of competition between pre- and postsynaptic α_{2A}-ARs

Potential competition between pre- and postsynaptic α_{2A}-ARs in terms of effects on BNST activity and anxiety-like behaviors may hinder the current clinical utility of agonists but could be harnessed to increase more effective use or the development of new targets. Data on the effects of different α_2-AR agonists in rodent models of anxiety-like behavior suggests that the observed behavioral effect can vary depending on the baseline stress level and environmental influences at the time of testing. In the presence of a stressor, dexmedetomidine consistently acts as an anxiolytic by reversing stress-induced contextual freezing, hyperlocomotion, cognitive impairment, and anxiety-like behaviors in the open field test and elevated plus maze (Ji et al., 2014). However, when undergoing the elevated plus maze task in the absence of a stressor, the effects of agonists are mixed, with some studies showing no effect (Cole et al., 1995) and others showing increased anxiety-like behaviors (Johnston et al., 1988; Uzsoki et al., 2011). As the negative valence of the behavioral test is increased, the effects of α_2-AR agonists tend towards anxiolytic and antidepressant actions. Clonidine and dexmedetomidine both disrupt the expression of fear-related memories after fear conditioning paradigms (Davies et al., 2004;

Gamache et al., 2012) and clonidine inhibits the expression of learned helplessness in the forced swim test (Malikowska et al., 2017), suggesting an adaptability to stressful environments in the behavioral response to these ligands. One potential cause of these discrepant outcomes may be differential affinities of norepinephrine and other α_2-AR ligands at pre- and postsynaptic α_{2A}-ARs. Guanfacine has been shown to have a very narrow effective dose range for antidepressant effects in the forced swim test. Decreased immobility time is observed after acute injection of 0.15 mg/kg guanfacine, while no effect is seen after injections of 0.05, 0.10, or 0.3 mg/kg (Mineur et al., 2015). Obtaining dose response curves for guanfacine inhibition of catecholamine release using fast scan cyclic voltammetry, inhibition of glutamate release using whole cell recordings of electrically evoked excitatory postsynaptic currents (Shields et al., 2009), enhancement of glutamate effect in optically evoked field potential responses in the Thy1COP4 mouse line (Flavin et al., 2014), and induction of cfos expression after *ex vivo* preincubation would all inform the question of differential receptor affinities dependent on subcellular compartment of expression. Alternatively, as more is learned about the mechanisms underlying the effects of agonism at pre- and postsynaptic α_{2A}-ARs, combinatorial drug treatments could be used to enhance or inhibit specific pathways. For example, blocking postsynaptic excitability enhancement via downstream HCN channel modulation as described above would limit the ability of postsynaptic α_{2A}-ARs to compete with presynaptic populations of the receptor.

Overall Conclusions

The bed nucleus of the stria terminalis and long-term changes in neuronal activity therein is hypothesized to underlie the maladaptive effects of long-term drug use and the propensity of stress to engage relapse behaviors in patients with substance use disorders. Norepinephrine receptor modulators in general and α_{2A}-AR agonists in particular are being investigated as a

means to counteract these changes and block their behavioral effects. In this thesis, our work on the postsynaptic α_{2A}-AR expressed within BNST neurons and its interactions with other α_{2A}-ARs in the region informs our understanding of this system and provides new tools to test contributions of this system to BNST physiology and resultant effects on relevant behavioral outcomes. Specifically, we show that postsynaptic α_{2A}-ARs enhance neuronal activity in the BNST through an HCN channel-dependent mechanism, and that this effect is mimicked by activation of the designer receptor hM4Di by clozapine-N-oxide, which itself induces anxiety-like behaviors. This suggests competing influences of pre- and postsynaptically-expressed α_{2A}-ARs that may explain preclinical effects in anxiety models as well as clinical effects in the treatment of addiction. A deeper understanding of signaling at these receptors will allow for more specific hypothesis-testing on contributions to synaptic plasticity in the BNST and stress-induced reinstatement behaviors in the future, with the long-term goal of providing new insight into the effective treatment of patients with substance use disorders and blockade of relapse behaviors.

Appendix I

Presynaptic mechanisms of guanfacine inhibition of glutamate release in the BNST

Understanding the mechanisms that differentiate presynaptic and postsynaptic effects of α_{2A}-adrenergic receptor (α_{2A}-AR) agonism may allow for specific targeting of actions for therapeutic purposes. Presynaptic G_i-coupled GPCRs can inhibit neurotransmitter release through a variety of mechanisms (Miller, 1998). Three such mechanisms include inhibition of voltage-gated calcium channels (Takahashi et al., 1996; Dolphin, 1998; Tedford and Zamponi, 2006), activation of G protein-coupled inwardly rectifying potassium (GIRK) channels, or direct inhibition of the vesicle release machinery (Silinsky, 1984; Blackmer, 2001; Glitsch, 2006; Yoon et al., 2007, 2008; Gerachshenko et al., 2009; Iremonger and Bains, 2009; Zhang et al., 2011; Wells et al., 2012; Van Hook et al., 2017). Norepinephrine signaling at presynaptic α_{2A}-ARs has specifically been shown to inhibit exocytosis via Gβγ interactions with release machinery, in addition to Gαi1/2-mediated inhibition of refilling of the readily releasable granule pool (Delaney et al., 2007; Zhao et al., 2010). We hypothesize that this occurs via direct inhibition of SNAP25 by the Gβγ subunit.

During neurotransmitter release from presynaptic membranes, soluble NSF-attachment protein receptors (SNAREs) are critical components necessary and sufficient for fusion of vesicular and plasma membranes and, thus, exocytosis (Weber et al., 1998; Criado et al., 1999; Sørensen et al., 2003). Vesicular (v-SNARE) and target (t-SNARE) SNAREs are core components of vesicle machinery and can be modulated by calcium levels and a number of interacting proteins including Gβγ. Specifically, Gβγ binds to residues on the extreme C terminus of SNAP25 after activation of $G_{i/o}$-coupled GPCRs, a component that is cleaved off by

botulinum toxin A to mediate its effects (Zurawski et al., 2016). This interaction competes with synaptotagmin and thus inhibits vesicle fusion and eventual exocytosis.

To determine the physiological and behavioral relevance of this mechanism connecting G_i-coupled GPCR agonism and inhibition of release machinery, a transgenic mouse line was developed within which the nucleotides encoding the proximal three amino acid residues of the SNAP25 gene were deleted (SNAP25Δ3). This mutation was previously shown to partially reduce Gβ1γ2 binding while minimally affecting other functions of the protein (Zurawski et al., 2016). These mice are developmentally normal but display impaired gait and supraspinal nociception. Autonomic dysfunction is suggested by elevated stress-induced hyperthermia in the SNAP25Δ3 mouse relative to wild-type littermates. This test is commonly used as a proxy for anxiolytic pharmacological effects. For this reason, we hypothesized that presynaptic α_{2A}-AR function may be disrupted with this mutation and aimed to test its effects on guanfacine-induced inhibition of glutamate release from presynaptic axon terminals within the BNST. To evaluate specificity, we recorded effects in the BNST, central nucleus of the amygdala (CeA), and hippocampus, and compare guanfacine actions to those of baclofen, a $GABA_B$ agonist. GABA signaling at presynaptic $GABA_B$ receptors is thought to mediate its inhibitory effects on transmission via Ca^{2+} channel inhibition (Dolphin and Scott, 1987; Hamid et al., 2014). We hypothesize that the inhibitory effects of guanfacine and baclofen thus occur via different mechanisms.

To evaluate α_{2A}-AR function, coronal slices were obtained as described above (see Chapter II). Field potentials were recorded with pipettes filled with ACSF while stimuli were evoked by electrical stimulation of a nichrome wire placed in the stria terminalis. All BNST and CeA experiments were done in the presence of 25 uM picrotoxin to isolate fast excitatory

transmission. Picrotoxin was not added to hippocampal recordings in order to avoid excitotoxic signaling. The fiber volley potential (N1) was monitored continuously throughout the duration of the experiment. Experiments in which N1 changed by 20% in either direction were not included in subsequent analysis. Experiments were analyzed by measuring peak amplitudes of the N1 and N2 (synaptic potential) relative to the amplitude with no stimulation. This measure was then normalized to the last ten minutes of the baseline period (10-20 minutes). Welch's t-test was used to compare the average amplitude over the last 20 minutes of the experiment relative to baseline across the two genotypes.

Excitatory field potentials were recorded extracellularly as two negative deflections, the tetrodotoxin-sensitive fiber volley potential N1 and the AMPAR antagonist CNQX-sensitive synaptic potential N2. As expected, bath application of guanfacine (1 μM) reduced the amplitude of the N2 in both wild-type (76.2±1.2% of baseline) and SNAP25Δ3 animals (91.4±2.7%) (Figure 12A). When compared directly, the reduction in N2 observed in SNAP25Δ3 mice was significantly reduced relative to the change in WT animals (unpaired t-test, p=0.0005) (Figure 12B). Bath application of baclofen (10 μM) also reduced N2 amplitude in both wild-type (78.3±4.0%) and SNAP25Δ3 (80.6±5.8%) (Figure 12C). The difference between these values, though, was not statistically significant (unpaired t-test, p=0.77; Figure 12D), suggesting that the mechanisms underlying guanfacine- and baclofen-induced inhibition of electrically evoked field potential responses occur via distinct mechanisms. The loss of guanfacine-induced inhibition in the SNAP25Δ3 mouse suggests that this mechanism occurs via Gβγ-mediated inhibition of exocytosis machinery, while the maintenance of baclofen-induced inhibition in this mouse suggests that this mechanism occurs via alternative mechanisms such as calcium channel inhibition.

In an effort to expose any baseline differences between the SNAP25Δ3 mice and wild-type littermates in terms of neurotransmission, we performed an input-output analysis on BNST response to electrical stimulation. To do this, we increased the stimulus strength applied to the nichrome wire and recorded subsequent changes in N2 as a function of the size of N1. Since the fiber volley potential N1 is indicative of recruited axons during stimulation and the synaptic potential N2 is indicative of the postsynaptic response, any changes in N2 as a function of N1 can be interpreted as a change in synaptic strength (Figure 12E). We calculated lines of best fit for the average input-output trace for each genotype and both WT and MUT lines of best fit did not deviate from linearity (runs test; WT: $p=0.88$; MUT: $p=0.98$). Both wild-type and SNAP25Δ3 showed increasing N2 as a function of increased stimulus intensity and N1 (Figure 12F). This is confirmed by a positive slope for both lines that is significantly non-zero (WT: 0.30±0.02 mV N2/mV N1; MUT: 0.14±0.01 mV N2/mV N1). When directly compared, these slopes are statistically different ($F(1,16)=39.56$, $p<0.0001$). Because of observation of different slopes, it is not possible to test whether the intercepts of the lines of best fit are significantly different as well. In the calculation of the line of best fit for each genotype, though, the y-intercept for wild-type mice is -0.17±0.02 mV and SNAP25Δ3 mice is -0.37±0.01 mV, suggesting a higher baseline N2 in these mice. We hypothesize that the smaller slope of N2 as a function of N1 and higher baseline N2 value are both due to a lack of tonic inhibitory tone on presynaptic terminals from α_{2A}-ARs and other G_i-coupled GPCRs. This would result in a hyperactive terminal and a more readily available readily releasable pool of neurotransmitter-containing vesicles.

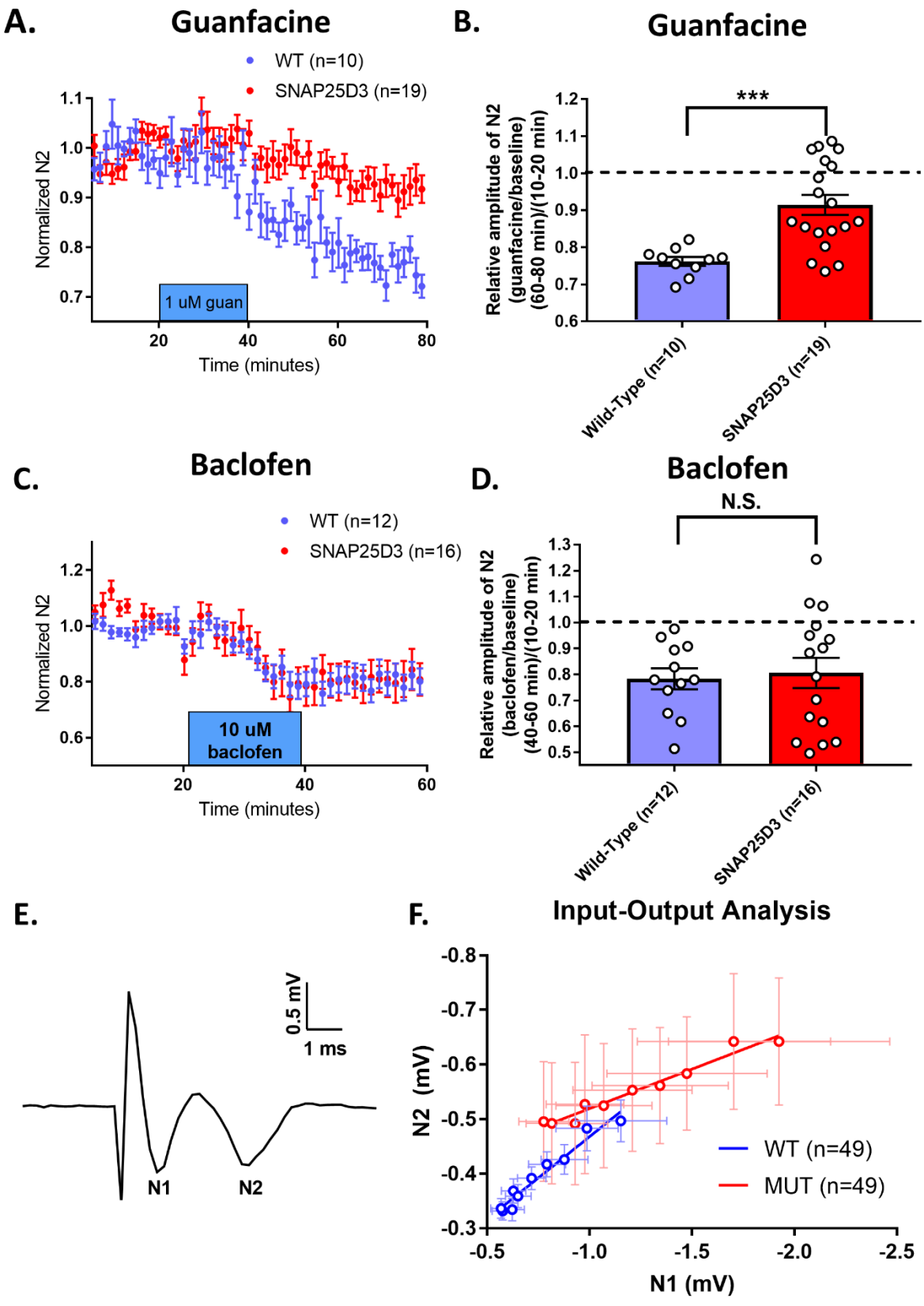
A.
Guanfacine
WT (n=10)
SNAP25D3 (n=19)
Normalized N2
1 uM guan
Time (minutes)
B.
Guanfacine
***
Relative amplitude of N2
(guanfacine/baseline)
(60-80 min)/(10-20 min)
Wild-Type (n=10)
SNAP25D3 (n=19)
C.
Baclofen
WT (n=12)
SNAP25D3 (n=16)
Normalized N2
10 uM
baclofen
Time (minutes)
D.
Baclofen
N.S.
Relative amplitude of N2
(baclofen/baseline)
(40-60 min)/(10-20 min)
Wild-Type (n=12)
SNAP25D3 (n=16)
E.
0.5 mV
1 ms
N1
N2
F.
Input-Output Analysis
N2 (mV)
N1 (mV)
WT (n=49)
MUT (n=49)

Figure 12: SNAP25Δ3 mutation affects excitatory transmission in the BNST and its inhibition by α2A-ARs but not GABABRs. (A) Guanfacine inhibits the synaptic field potential N2 in wild-type and SNAP25Δ3 mice (WT: 76.2±1.2% of baseline; MUT: 91.4±2.7%). (B) Guanfacine-induced inhibition is, however, reduced in SNAP25Δ3 mice. (C) Baclofen inhibits N2 in both wild-type and SNAP25Δ3 mice (WT: 78.3±4.0%; MUT: 80.6±5.8%). (D) SNAP25Δ3 mutation does not affect baclofen inhibition relative to wild-type littermates. (E) Example field potential trace showing the fiber volley potential N1 and the synaptic potential N2. (F) Input-output analysis shows a line of best fit for SNAP25Δ3 mice and wild-type littermates. The slopes of the two lines of best fit differ, with SNAP25Δ3 mice showing a reduced N2 as a function of N1 (WT: -0.17±0.02 mV, MUT: -0.37±0.01 mV). This may be due to elevated baseline N2 in SNAP25Δ3 mice relative to wild-type littermates.

We next investigated α_{2A}-AR effects in the central nucleus of the amygdala (CeA) and the hippocampus to determine whether the effects observed within the BNST were specific to signaling within this region. Field potentials were evoked dorsally to the recording pipette throughout the extent of the region. Guanfacine inhibited electrically evoked excitatory field potentials in the CeA of wild-type mice (82.3±0.2% of baseline; paired t-test, p=0.0006) and trended towards an effect in SNAP25Δ3 mice (90.0±0.5%; paired t-test, p=0.059) (Figure 13A). The difference between these effects was not statistically significant (p=0.26), suggesting that the effects in the BNST are specific to presynaptic α_{2A}-ARs or that this study is underpowered to observe a statistically significant difference between the groups (Figure 13B). We hypothesize that the latter is the case due to the similar trend in the data as observed in the BNST recordings.

In the hippocampus, recordings were made in the CA1 (Cornu Ammonis 1) subregion with stimulation upstream in the CA3 subregion. The field potential amplitude was quantified as the amplitude of the population spike that occurs after hippocampal stimulation (we refer to it here as N2 for the sake of simplicity). This population spike is roughly representative of the number of CA1 neurons firing action potentials as a result of recruitment by upstream axon terminal neurotransmitter release. Interestingly, guanfacine did not affect N2 amplitude in wild-type animals (91.4±7%; paired t-test, p=0.35) but did significantly reduce it in SNAP25Δ3

animals (75.6±0.5%; paired t-test, p=0.02) (Figure 13C). The difference between these two was not statistically significant but was trending (unpaired t-test, p=0.10) (Figure 13D). This result will need replication, but an unmasking of inhibitory effects of guanfacine within the hippocampus of SNAP25Δ3 mice could occur via a number of interesting mechanisms. These include observation being an artifact of higher initial amplitude, differential importance of SNAP25Δ3 interaction with Gβγ in GABAergic interneurons and glutamatergic projection neurons, or interactions with other neurotransmitter systems within the hippocampal slices.

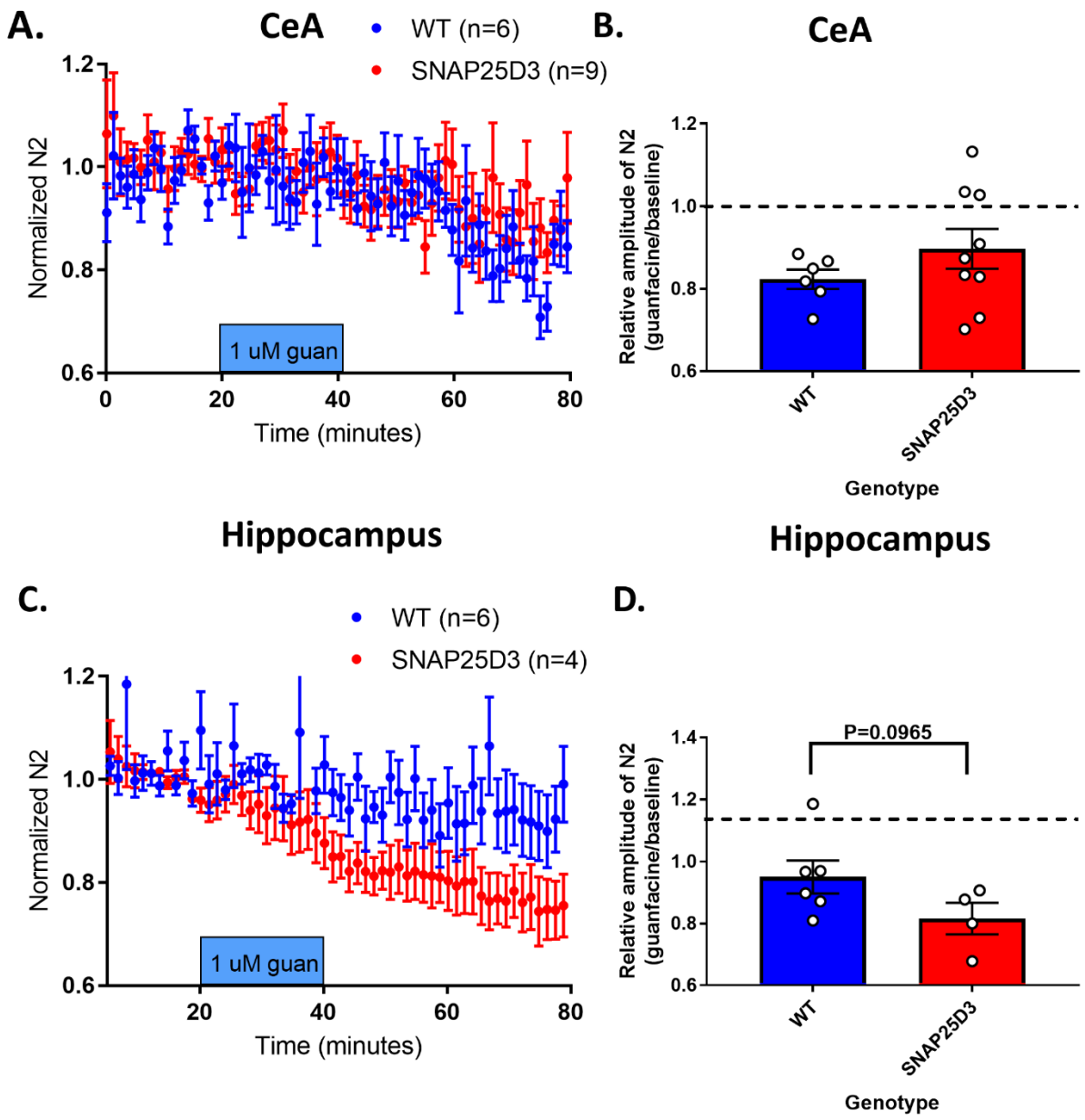

Figure 13: Preliminary data on guanfacine effects on neurotransmission in the central nucleus of the amygdala and hippocampus suggest regional differences. (A) Guanfacine inhibits electrically evoked excitatory field potentials in wild-type mice (WT: 82.3±0.2% of baseline, paired t-test, p=0.0006) and trended towards an effect in SNAP25Δ3 mice (90.0±0.5%; paired t-test, p=0.059). (B) Inhibition did not differ between the genotypes (upnaired t-test, p=0.26). (C) Guanfacine did not affect N2 amplitude in wild-type mice (91.4±7%; paired t-test, p=0.35) but did significantly reduce it in SNAP25Δ3 animals (75.6±0.5%; paired t-test, p=0.02), suggesting an unmasking effect. (D) This difference, though, was not statistically significant (unpaired t-test, p=0.10)

We also investigated the effects of SNAP25Δ3 mutation on $GABA_BR$ receptor signaling within the hippocampus. Baclofen significantly reduced the N2 amplitude in both wild-type (41.7±8.4% of baseline; paired t-test, p=0.006) and SNAP25Δ3 (20.2±11.1%; paired t-test, p<0.0001) (Figure 14A). The difference between the level of inhibition was statistically significant between the groups (unpaired t-test, p=0.002) (Figure 14B). Due to the potential confound of differences in initial amplitude, we also compared baclofen effects in terms of raw value for N2 amplitude. Here we see a trend towards a statistically significant decrease in wild-type animals (baseline: -1.60±0.49 mV; baclofen: -0.58±0.08 mV; paired t-test, p=0.10) while SNAP25Δ3 showed a significant decrease (baseline: -2.71±0.69 mV; baclofen: -0.35±0.12 mV; paired t-test, p=0.009) Figure 14C). The difference between these groups was not statistically significant (unpaired t-test, p=0.23), suggesting that the differences between the groups observed with relative amplitude may be an artifact of altered baseline values (Figure 14D). To confirm this difference, we evaluated the effects of increasing stimulus voltage on N1 and N2 amplitude (Figure 14E-F). Here, we observed that wild-type and SNAP25Δ3 mice increased N1 as a function of stimulus intensity in a similar manner (two-way ANOVA; voltage effect: $F(9,108)=7.77$, $p<0.0001$; genotype effect: $F(1,12)=0.01$, $p=0.91$; interaction: $F(9,108)=0.43$, $p=0.92$; subjects matching: $F(12,108)=12.82$, $p<0.0001$), but the effects on N2 were substantially larger for SNAP25Δ3 mutants than wild-type counterparts (two-way ANOVA; voltage effect: $F(9,108)=4.27$, $p<0.0001$; genotype effect: $F(1,12)=2.45$, $p=0.14$; interaction: $F(9,108)=1.52$, $p=0.15$; subjects matching: $F(12,108)=12.82$, $p<0.0001$). These differences should be further evaluated in future studies.

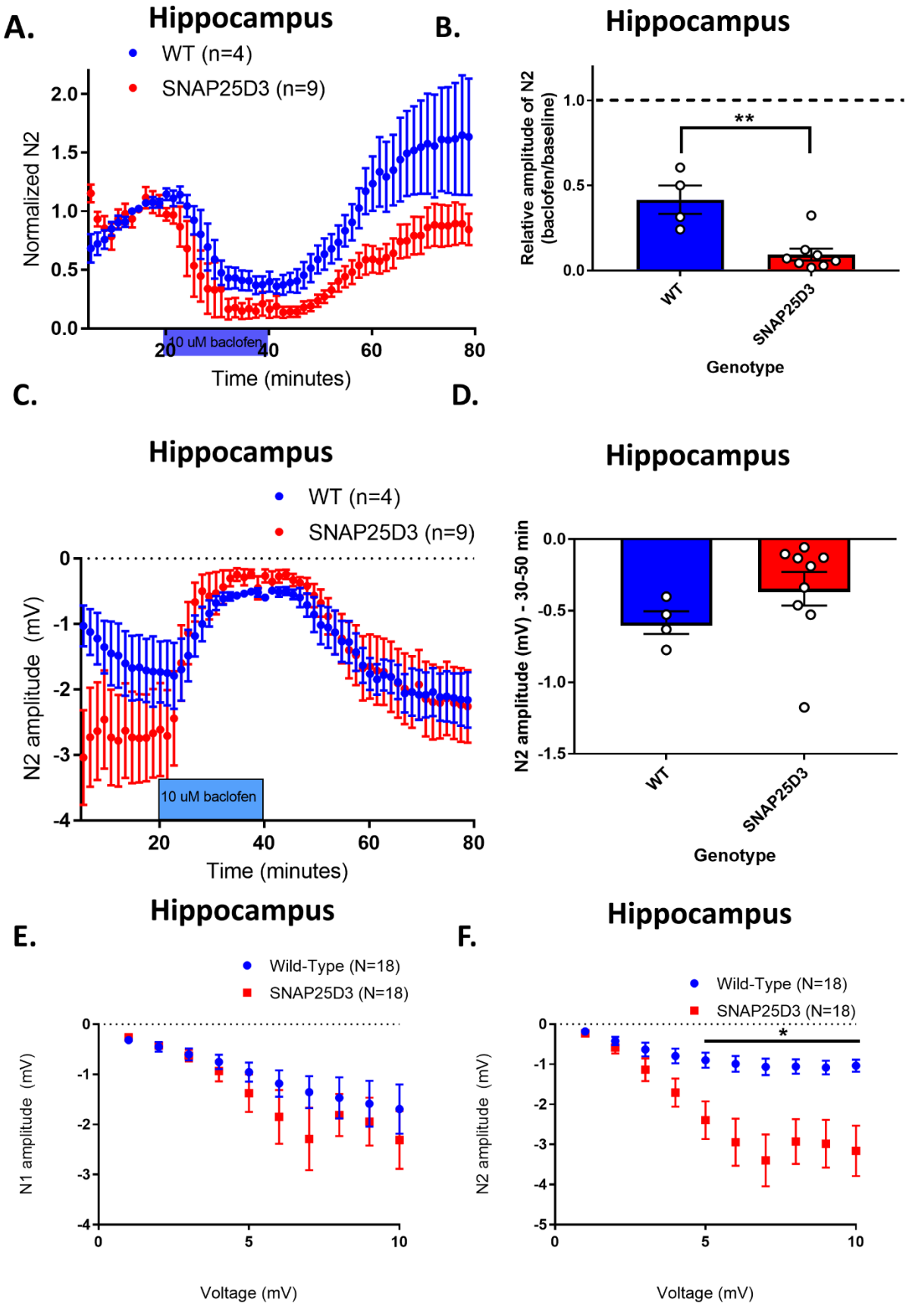
A.
Hippocampus
WT (n=4)
SNAP25D3 (n=9)
Normalized N2
Time (minutes)
10 uM baclofen
B.
Hippocampus
Relative amplitude of N2 (baclofen/baseline)
**
WT
SNAP25D3
Genotype
C.
Hippocampus
WT (n=4)
SNAP25D3 (n=9)
N2 amplitude (mV)
Time (minutes)
10 uM baclofen
D.
Hippocampus
N2 amplitude (mV) - 30-50 min
WT
SNAP25D3
Genotype
E.
Hippocampus
Wild-Type (N=18)
SNAP25D3 (N=18)
N1 amplitude (mV)
Voltage (mV)
F.
Hippocampus
Wild-Type (N=18)
SNAP25D3 (N=18)
*
N2 amplitude (mV)
Voltage (mV)

Figure 14: Preliminary data on baclofen effects within the hippocampus of SNAP25Δ3 mice and wild-type littermates. (A) Baclofen reduces N2 amplitude in both wild-type (41.7±8.4% of baseline; paired t-test, p=0.006) and SNAP25Δ3 (20.2±11.1%; paired t-test, p<0.0001) mice. (B) Baclofen inhibition is amplified in SNAP25Δ3 mutants relative to wild-type littermates (unpaired t-test, p=0.002). (C) When displayed as a function of amplitude, baclofen only trends towards a decreased amplitude in wild-type animals (baseline: -1.60±0.49 mV; baclofen: -0.58±0.08 mV; paired t-test, p=0.10) while SNAP25Δ3 showed a significant decrease (baseline: -2.71±0.69 mV; baclofen: -0.35±0.12 mV; paired t-test, p=0.009). (D) The difference between these groups was not statistically significant (unpaired t-test, p=0.23). (E) N1 amplitude as a function of stimulus intensity did not differ between genotypes (two-way ANOVA; voltage effect: $F(9,108)=7.77$, $p<0.0001$; genotype effect: $F(1,12)=0.01$, $p=0.91$; interaction: $F(9,108)=0.43$, $p=0.92$; subjects matching: $F(12,108)=12.82$, $p<0.0001$). (F) N2 amplitude as a function of stimulus intensity was larger for SNAP25Δ3 mutants relative to wild-type counterparts (two-way ANOVA; voltage effect: $F(9,108)=4.27$, $p<0.0001$; genotype effect: $F(1,12)=2.45$, $p=0.14$; interaction: $F(9,108)=1.52$, $p=0.15$; subjects matching: $F(12,108)=12.82$, $p<0.0001$).

In summary, guanfacine inhibition of excitatory transmission in the BNST is reduced in SNAP25Δ3 mutants, suggesting that Gβγ inhibition of exocytosis machinery is part of the mechanism whereby heteroceptor α_{2A}-ARs presynaptically inhibit neurotransmission. This differs from $GABA_BR$-mediated inhibition, which was not affected by SNAP25Δ3 mutation. This difference could be physiologically and behaviorally relevant given the stress-induced hyperthermia phenotype in this mouse and the known role of presynaptic α_{2A}-ARs within the BNST in stress and addiction phenotypes. This mouse could be further utilized to dissect out guanfacine and other G_i-GPCR agonist actions within the BNST and the specific contributions of α_{2A}-ARs localized in different subcellular compartments. First, autoreceptor α_{2A}-AR function should be tested in this mouse by fast scan cyclic voltammetry. Second, postsynaptic α_{2A}-AR function should be tested by evaluating guanfacine-induced cfos expression and enhancement of optical field potentials in the Thy1-COP4 transgenic mouse, in addition to evaluating HCN contributions to these phenotypes. Third, presynaptic and postsynaptic G_i-DREADD hM4Di functions could be tested by evaluating CNO-induced cfos expression, anxiogenesis, and BNST Ca^{2+} transients during the elevated plus maze. Fourth and finally, these mice could be tested for

stress-induced reinstatement behaviors and the ability of guanfacine to inhibit this clinically relevant behavioral phenotype. In addition, the differences in signaling mechanisms observed between the CeA and the hippocampus in both guanfacine and baclofen-induced effects should be further dissected.

Appendix II

Electrophysiological characterization of guanfacine-activated cfos-eGFP+ BNST neurons after incubation in guanfacine or ZD7288

Guanfacine agonism at postsynaptic α_{2A}-ARs initiates signaling cascades that result in cfos expression and excitatory activity. Typically masked by inhibitory presynaptic actions of the drug, guanfacine-induced enhancement of optically-evoked field potentials was observed in the Thy1-COP4 transgenic mouse line that minimally recruits the guanfacine-inhibited parabrachial nucleus afferents with BNST stimulation (Flavin et al., 2014). This effect, though, is representative of integrated activity of a number of neurons and does not allow for conclusions to be drawn at activity on a cell-specific basis, which is important given the extent of cellular heterogeneity within the BNST (Lebow and Chen, 2016) as well as the diverse expression profile of α2A-ARs (Flavin et al., 2014).

Resolution of single-cell effects among putative guanfacine-activated neurons have been obtained after intraperitoneal injections of guanfacine in the cfos-eGFP transgenic mouse line (Barth et al., 2004) and whole cell recordings of cfos-eGFP+ BNST neurons. Using this method, we have seen that cfos-eGFP+ cells have a high prevalence of the hyperpolarization-activated current Ih, suggesting expression of HCN channels. This was confirmed and extended by RNA in situ hybridization experiments that showed overlap of the transcript *Adra2a* (α2A-AR) with *Fos* (c-fos) and *Hcn2* (HCN2). Interestingly, guanfacine has been shown to inhibit electrically-

evoked excitatory postsynaptic currents (eEPSCs) in cfos-eGFP+ cells (Flavin, 2014), suggesting inhibitory actions. Even though this population of cells has been shown to express the α_{2A}-AR, the locus of the specific α_{2A}-AR receptors underlying this inhibitory action remains unclear from this experiment. We hypothesize that the electrical stimulation required for eEPSC observation enriches for observation of glutamate effect downstream from release from parabrachial nucleus axon terminals, and that any effect of postsynaptic α_{2A}-ARs is masked by inhibition of glutamate release by presynaptic α_{2A}-ARs from these axon terminals. Parabrachial nucleus axon terminals form axosomatic synapses with BNST neurons (Shimada et al., 1989; Dobolyi et al., 2005) that likely express α_{2A}-ARs (Flavin et al., 2014). Due to the close proximity of these synapses to the somatic site of recording and associated lack of space clamp error (Larkum et al., 1998; Williams and Mitchell, 2008), in addition to the instructive nature of these synapses (Flavin et al., 2014), electrical stimulation likely biases recordings of postsynaptic effects towards those elicited at these synapses. It is not clear whether this bias exists in recordings of spontaneous transmission, so we aimed to evaluate postsynaptic effects of modulating postsynaptic α_{2A}-AR and associated signaling pathways in this experimental set-up. Due to the additional confounds of cell dialysis disrupting HCN channel function and voltage clamp limiting the extent of hyperpolarization-mediated activation of HCN channels, we specifically recorded effects on spontaneous excitatory postsynaptic potentials (sEPSPs) after one-hour preincubation in guanfacine or ZD7288.

Whole-cell current-clamp recordings were performed as described above. Briefly, *cfos-eGFP* mice were handled for five days prior and to brain slice preparation. Guanfacine injection (1 mg/kg) was performed 90 minutes prior to preparation of 300 um coronal sections. Slices were allowed to recover for one hour in ACSF prior to one hour incubation in either guanfacine (1 uM) or ZD7288 (10 uM). Recordings were done in the presence of picrotoxin (25 uM) to

isolate excitatory transmission. After achieving whole-cell configuration, cells were equilibrated for 2-5 minutes prior to recording. Current clamp profiles and sEPSPs were then recorded and analyzed.

Recordings of postsynaptic parameters and spontaneous neurotransmission within guanfacine-activated cfos-eGFP+ cells showed minimal effects of guanfacine on a number of measures. Specifically, guanfacine preincubation did not affect resting membrane potential (ACSF: -64.4±1.7 mV; Guan: -63.5±0.9 mV; unpaired t-test, $p=0.66$; Figure 15A), membrane potential response to current injection (two-way ANOVA; current injection effect: $F(19,456)=100.9$, $p<0.0001$; treatment effect: $F(1,24)=0.4$, $p=0.52$; interaction: $F(19,456)=0.1$, $p>0.9999$, subjects matching: $F(24,456)=3.9$, $p<0.0001$; Figure 15B), number of action potentials fired during current injection (two-way ANOVA; current injection effect: $F(19,456)=113.0$, $p<0.0001$; treatment effect: $F(1,24)=0.2$, $p=0.67$; interaction: $F(19,456)=1.1$, $p=0.32$, subjects matching: $F(24,456)=18.2$, $p<0.0001$; Figure 15C), access resistance (ACSF: 23.0±1.0 MΩ; Guan: 20.2±1.6 MΩ; unpaired t-test, $p=0.16$; Figure 15D), membrane resistance (ACSF: 278.8±32.8 MΩ; Guan: 362.5±54.6 MΩ; unpaired t-test, $p=0.20$; Figure 15E), or membrane capacitance (ACSF: 25.8±3.1 pF Guan: 25.5±1.6 pF; unpaired t-test, $p=0.92$; Figure 15F). In the analysis of sEPSPs, guanfacine preincubation did not affect sEPSP amplitude (ACSF: 1.7±0.2 mV; Guan: 1.7±0.1 mV; unpaired t-test, $p=0.87$; Figure 15G), frequency (ACSF: 1.2±0.1 Hz; Guan: 1.2±0.2 Hz; unpaired t-test, $p=0.93$; Figure 15H), frequency distribution (two-way ANOVA; amplitude effect: $F(9,216)=0.2$, $p=0.99$; treatment effect: $F(1,24)=0.8$, $p=0.37$; interaction: $F(9,216)=0.5$, $p=0.84$; subjects matching: $F(24,216)=8*10^{-14}$, $p>0.9999$; Figure 15I), maximum rise slope (ACSF: 6.0±0.2 mV/ms; Guan: 6.0±0.2 mV/ms; unpaired t-test, $p=0.94$;

Figure 15J), or maximum decay slope (ACSF: -4.6±0.2 mV/ms ; Guan: -4.7±0.2 mV/ms; unpaired t-test, p=0.66; Figure 15K).

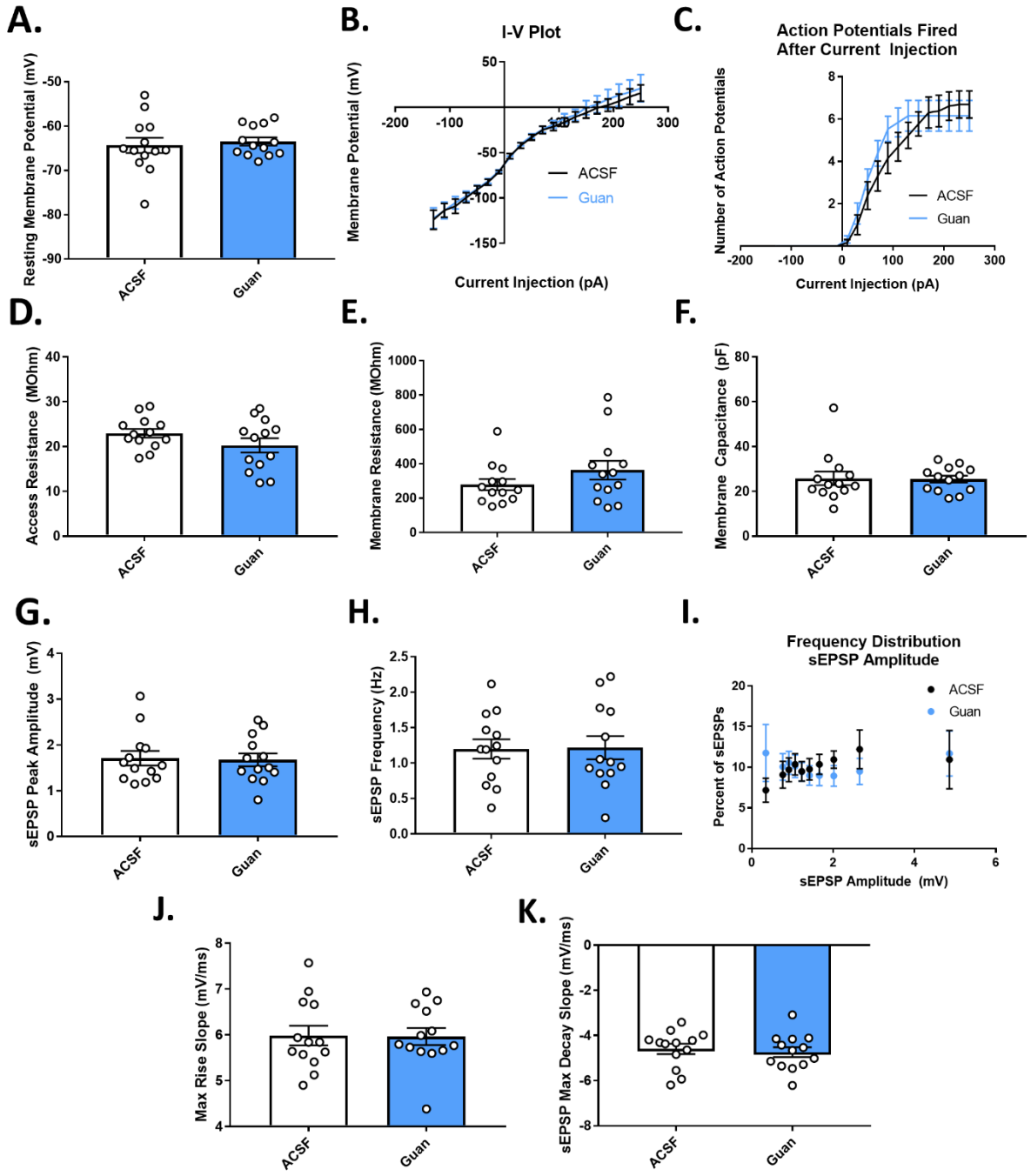

Figure 15: Guanfacine preincubation does not affect electrophysiological characteristics of cfos-eGFP+ BNST neurons after intraperitoneal guanfacine injection. Guanfacine preincubation did not affect resting membrane potential (A), membrane potential response to current injection (B), number of action potentials fired during current injection (C), access resistance (D), membrane

resistance (E), or membrane capacitance (F), sEPSP amplitude (G), sEPSP frequency (H), sEPSP frequency distribution (I), maximum rise slope (J), or maximum decay slope (K).

This paradoxical panel of negative data suggests lack of effect of α_{2A}-AR agonism in guanfacine-activated cfos-eGFP+ cells. However, RNA *in situ* hybridization contradicts that assertion. We hypothesize that this lack of effect occurred as a result of either competing effects from inhibitory presynaptic and excitatory postsynaptic α_{2A}-ARs, or agonist-induced internalization of the postsynaptic receptor. This hypothesis could be tested by evaluating the effects of guanfacine after acute bath application in an experimental set-up that maintains intracellular integrity, such as *ex vivo* two photon microscopy of GCaMP6f fluorescence or perforated patch recording techniques. These experiments would inform our understanding of guanfacine action at this particular subset of BNST neurons.

The effects of ZD7288 preincubation on the activity of guanfacine-activated cfos-eGFP+ BNST neurons, on the other hand, were not precluded by this experimental technique. This is presumably due to the different mechanisms of action of each ligand at their respective protein target. ZD7288 preincubation abolished hyperpolarization sag and enhanced sEPSP frequency in guanfacine-activated cfos-eGFP+ BNST neurons without affecting sEPSP amplitude (Figure 5). In addition to these parameters, we also analyzed other effects of ZD7288 on the activity of these neurons. ZD7288 preincubation did not affect resting membrane potential (ACSF: -64.4±1.7 mV; ZD7288: -64.3±1.5 mV, unpaired t-test, $p=0.97$; Figure 16A), membrane potential response to current injection (two-way ANOVA; current effect: $F(19,361)=91.2$, $p<0.0001$; treatment effect $F(1,19)=0.1$, $p=0.74$; interaction: $F(19,361)=0.1$, $p>0.9999$; subjects matching: $F(19,361)=4.88$, $p<0.0001$; Figure 16B), or number of action potentials fired after current injection (two-way ANOVA: current effect: $F(19,361)=51.9$, $p<0.0001$; treatment effect:

F(1,19)=0.2, p=0.65; interaction: F(19,361)=0.3, p=0.998; subjects matching: F(19,361)=14.6, p<0.0001; Figure 16C) suggesting lack of somatic modulation of postsynaptic excitability. Further, no differences were observed between ACSF- and ZD7288-preincubated slices with respect to access resistance (ACSF: 23.0±1.0 MΩ; ZD7288: 21.0±2.1 MΩ, unpaired t-test, p=0.33; Figure 16D), membrane resistance (ACSF: 278.8±32.8 MΩ; ZD7288: 212.4±25.1 MΩ, unpaired t-test, p=0.15; Figure 16E), or membrane capacitance (ACSF: 25.8±3.1 pF; ZD7288: 31.2±4.7 pF, unpaired t-test, p=0.32; Figure 16F). ZD7288 preincubation did decrease maximum rise slope (ACSF: 6.2±0.2 mV/ms; ZD7288: 5.5±0.1 mV/ms, unpaired t-test, p=0.05; Figure 16G) without significantly affecting maximum decay slope (ACSF: -7.3±0.4 mV/ms; ZD7288: -6.7±0.1 mV/ms; unpaired t-test, p=0.21; Figure 16H), suggesting a change in sEPSP kinetics. A lack of robust effect of ZD7288 on markers of postsynaptic excitability suggests that the observed changes in sEPSP frequency occur via modulation of synaptic transmission. A presynaptic locus of effect cannot be excluded from this data and should be investigated further. Future studies should aim to determine the mechanism underlying the effects of ZD7288 preincubation as well as their specificity.

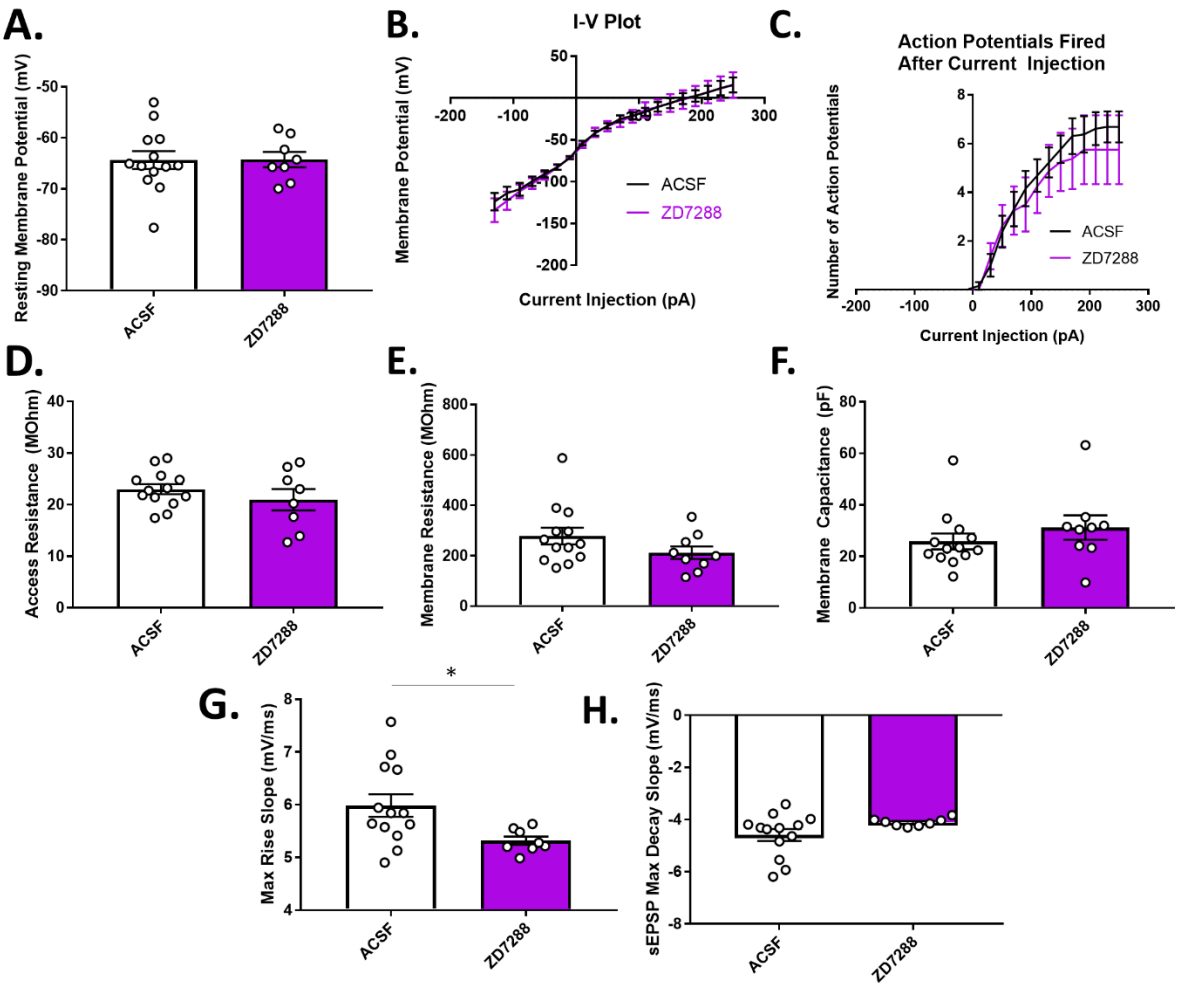

Figure 16: ZD7288 preincubation minimally affects postsynaptic electrophysiological parameters of cfos-eGFP+ cells after intraperitoneal guanfacine injection but does affect kinetics of spontaneous transmission. ZD7288 preincubation did not affect resting membrane potential (A), membrane potential response to current injection (B), the number of action potentials fired as a function of current injection (C), access resistance (D), membrane resistance (E), or membrane capacitance (F). Interestingly, ZD7288 preincubation did decrease maximum rise slope (G) but not maximum decay slope (H), suggesting effects on spontaneous neurotransmission beyond increased frequency of sEPSPs.

Appendix III

Electrophysiological effects of shRNA-mediated knockdown of BNST HCN channel subunits

Guanfacine agonism at postsynaptic α_{2A}-ARs is hypothesized to elicit synapse-specific excitatory actions via release of filtering at the dendritic neck by inhibition of HCN channels. To test for necessity of HCN channel inhibition in guanfacine-induced cfos expression, we utilized an shRNA-mediated knockdown strategy to reduce expression of HCN1 and HCN2 channels within BNST neurons. Knockdown led to a significant reduction in hyperpolarization sag and elevated baseline cfos expression that occluded further increases by guanfacine. This suggests that HCN channels are necessary for guanfacine-induced cfos expression. Because of the elevated baseline cfos expression, we hypothesized that knockdown of HCN1 and HCN2 channels in BNST would have excitatory effects on cellular activity. To test this hypothesis, we performed whole cell recordings after stereotaxic injection of AAV9-hU6-shHCN1-shHCN2-GFP (shHCN1/2) or sham injection from BNST neurons.

Viral injections and electrophysiological recordings were performed as described above. Briefly, mice were injected intracranially with shHCN1/2 (200 µL) in one BNST and were subjected to a sham injection into the other BNST (AP: 0.14, ML: +/-0.88, DV: -4.24) (Paxinos and Franklin, 2004), both at a 15.03° angle. Three weeks after surgery, coronal BNST sections were prepared for electrophysiological recordings. Recordings were done in the presence of picrotoxin (25 µM) to isolate excitatory transmission. After achieving whole-cell configuration, cells were equilibrated for 2-5 minutes prior to recording. Current clamp profiles and sEPSPs were then recorded and analyzed.

Knockdown of HCN1 and HCN2 channels by injection of shHCN1/2 had minimal effects on electrophysiological parameters and spontaneous neurotransmission in BNST neurons. Specifically, relative to sham injection, BNST neurons expressing shHCN1/2 show no difference in resting membrane potential (Sham: -80.3±1.6 mV; shHCN1/2: -82.8±2.3 mV; unpaired t-test, $p=0.40$; Figure 17A), membrane potential response to current injection (two-way ANOVA; current effect: $F(19,570)=334.5$, $p<0.0001$; treatment effect: $F(1,30)=3.3$, $p=0.08$; interaction: $F(19,570)=0.1$, $p>0.9999$; subjects matching: $F(30,570)=6.7$, $p<0.0001$; Figure 17B), number of action potentials fired in response to current injection (two-way ANOVA; current effect: $F(19,570)=159.6$, $p<0.0001$; treatment effect: $F(1,30)=0.8$, $p=0.37$; interaction: $F(19,570)=1.1$, $p=0.35$; subjects matching: $F(30,570)=14.6$, $p<0.0001$; Figure 17C), access resistance (Sham: 17.0±1.6 MΩ; shHCN1/2: 20.2±1.4 MΩ; unpaired t-test, $p=0.14$; Figure 17D), membrane resistance (Sham: 373.3±30.3 MΩ; shHCN1/2: 400.2±65.7 MΩ; unpaired t-test, $p=0.72$; Figure 17E), or membrane capacitance (Sham: 26.6±2.6 pF; shHCN1/2: 26.9±3.2 pF; unpaired t-test, $p=0.94$; Figure 17F). In terms of effects on spontaneous neurotransmission, shHCN1/2 had no effect on peak amplitude (Sham: 1.4±0.1 mV; shHCN1/2: 1.7±0.2 mV; unpaired t-test, $p=0.35$; Figure 17G) or frequency (Sham: 1.8±0.2 Hz; shHCN1/2: 1.8±0.2 Hz; unpaired t-test, $p=0.92$; Figure 17H), and did not consistently affect the frequency distribution of peak amplitude (two-way ANOVA; amplitude effect: $F(9,243)=0.002$, $p>0.9999$; treatment effect: $F(1,27)=0.04$, $p=0.84$; interaction: $F(9,243)=1.715$, $p=0.09$; subjects matching: $F(27,243)=5.259$, $p=<0.0001$; Figure 17I). Intriguingly, shHCN1/2 appeared to slow sEPSP kinetics specifically during sEPSP decay, as no difference was observed with maximum rise slope (Sham: 5.6±0.1 mV/ms; shHCN1/2: 5.5±0.2 mV/ms; unpaired t-test, $p=0.61$; Figure 17J) but there was a statistically

significant difference between groups with respect to maximum decay slope (Sham: -4.1±0.1 mV/ms; shHCN1/2: -3.8±0.1; unpaired t-test, p=0.02; Figure 17K).

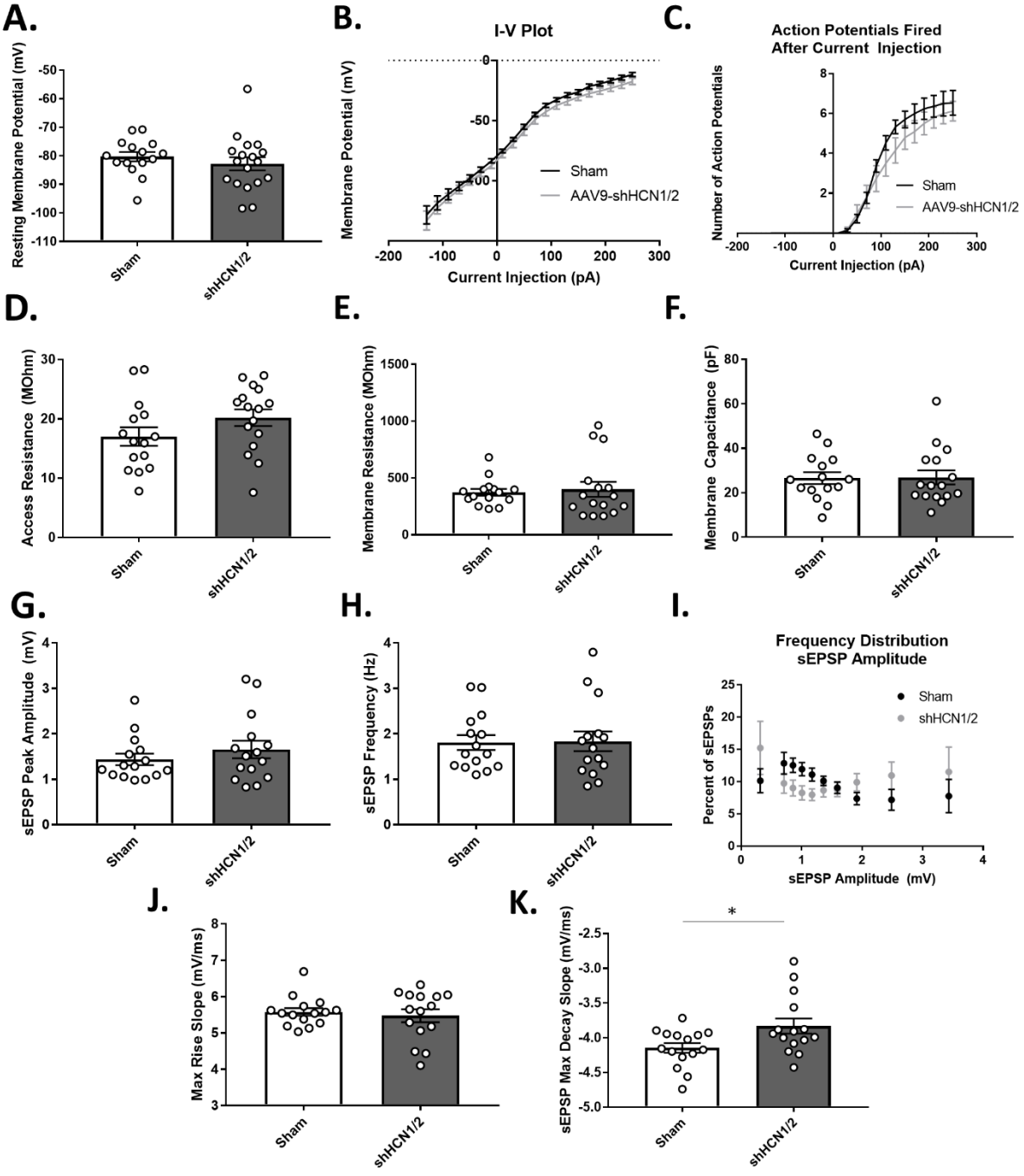

Figure 17: Expression of shHCN1/2 minimally affects postsynaptic electrophysiological parameters of BNST neurons and spontaneous neurotransmission therein but does specifically affect decay kinetics of spontaneous transmission. Expression of shHCN1/2 did not affect resting membrane potential (A), membrane potential response to current injection (B), the number of

action potentials fired as a function of current injection (C), access resistance (D), membrane resistance (E), or membrane capacitance (F). Interestingly, ZD7288 preincubation did not affect maximum rise slope (G) but did significant slow the maximum decay slope (H), suggesting effects on spontaneous neurotransmission.

Interpretation of the effects of HCN1 and HCN2 knockdown on BNST neuronal activity is limited due to the heterogeneity observed within the BNST and the potential differential effects of HCN channel activity on activity of specific neuronal populations. Due to the GFP tag on the shRNA utilized in this experiment, isolation of putative guanfacine-activated neurons such as was done previously in the cfos-eGFP transgenic mouse line was not possible. Interestingly, there is significant heterogeneity in many of the parameters recorded here, suggesting that shHCN1/2-mediated knockdown did impact neuronal activity but in a variable fashion. Further, decreased HCN1 and HCN2 expression appears to have slowed sEPSP decay, suggesting a loss of dendritic filtering and increased prevalence of synaptic events distal from the somatic site of recording. However, this hypothesis requires further testing. Isolating guanfacine-activated BNST neurons and modulating HCN channels therein will be an important future direction as we learn more about postsynaptic α_{2A}-ARs within this region of the brain.

Appendix IV

Effects of HCN1 and HCN2 knockdown in BNST neurons on anxiety-like behavior as assessed by the elevated plus maze.

Activation of the chemogenetic receptor hM4Di expressed in BNST neurons by clozapine-N-oxide mimicked guanfacine activation of postsynaptic α_{2A}-ARs and induced equivalent cfos expression while occluding further guanfacine-induced expression. Thus, CNO activation of BNST-expressed hM4Di allows for the testing of hypotheses about contributions of postsynaptic G_i-coupled GPCRs to BNST physiology and behavior in the absence of actions at presynaptic receptor subpopulations. We tested *in vivo* relevance of these signaling pathways by

recording GCaMP6f fluorescence during anxiety-like behavioral testing in the elevated plus maze (EPM) and observed both CNO-induced BNST activity enhancement during the EPM and increased anxiety-like behaviors. This suggests that postsynaptic G_i-coupled GPCR activation of BNST neurons elicits anxiety-like behavior. Due to the role of HCN channel inhibition in guanfacine-induced cfos expression, then, we hypothesized that shRNA-mediated knockdown of HCN1 and HCN2 in BNST neurons would also induce anxiogenic behavior in the EPM. To test this hypothesis, we injected AAV9-hU6-shHCN1/2 (shHCN1/2) or AAV9-CMV-GFP (GFP) into the BNST and evaluated effects on baseline anxiety-like behavior in the EPM.

Viral injections and behavioral testing were performed as described above. Briefly, mice were bilaterally injected intracranially with either shHCN1/2 or GFP (200 µL) into each BNST (AP: 0.14, ML: +/-0.88, DV: -4.24) (Paxinos and Franklin, 2004), both at a 15.03° angle. Three weeks after surgery, behavioral experiments were performed. Mice were handled for five days prior to testing. On test day, the mice were transferred to the elevated plus maze (EPM) for five minutes. As above, lighting was set to approximately 60-70 lux in the open arm and 10-20 lux in the closed arm. Mice were visualized, recorded, and tracked by a camera using AnyMaze software.

Knockdown of BNST-expressed HCN1 and HCN2 channels by shRNA injection appeared to have minimal effect on anxiety-like behavior in the elevated plus maze. No difference was observed between the groups with respect to closed arm time (GFP: 91.7±11.1 seconds; shHCN1/2: 100.1±17.8 seconds; unpaired t-test, p=0.69; Figure 18A), open arm time (GFP: 164.7±14.2 seconds; shHCN1/2: 163.6±20.2 seconds; unpaired t-test, p=0.96; Figure 18B), center zone time (GFP: 105.3±13.2 seconds; shHCN1/2: 87.4±12.8 seconds; unpaired t-

test, p=0.34; Figure 18C), or total distance traveled (GFP: 7.9±0.6 meters; shHCN1/2: 9.3±0.7 meters; Figure 18D).

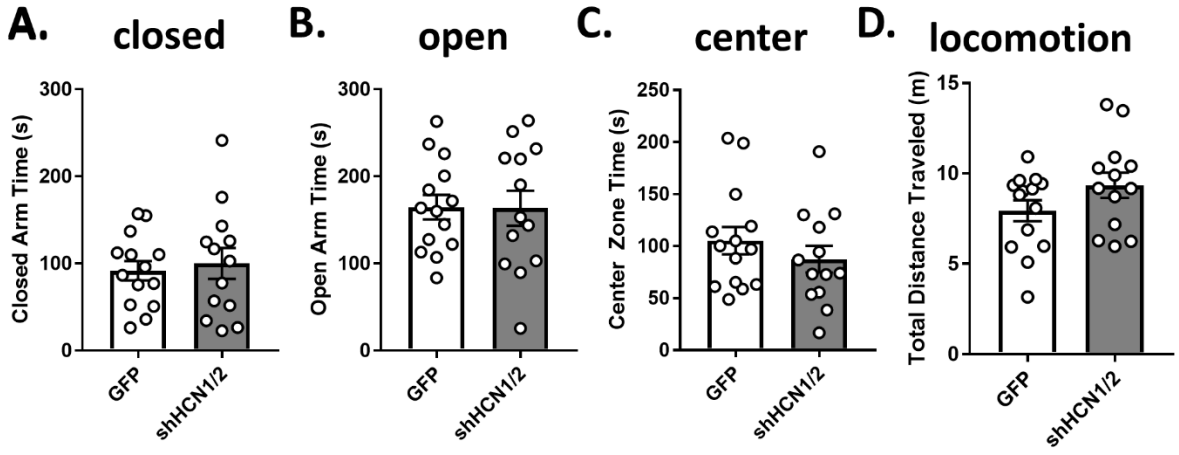

Figure 18: BNST expression of shHCN1/2 does not affect anxiety-like behavior in the elevated plus maze. No difference was observed between the groups with respect to closed arm time (A), open arm time (B), center zone time (C), or total distance traveled (D).

This lack of apparent difference could be due to experimental differences between behavioral cohorts, but the values obtained in this data set are generally in agreement with those from the experiment assessing behavioral effects of CNO-mediated activation of BNST-expressed hM4Di (Figure 10), suggesting that this is not the case. Instead, we hypothesize that a lack of apparent difference between the groups is a result of heterogeneous biological effects of shRNA-mediated knockdown of HCN1 and HCN2 within BNST neurons. Specifically, although both elicited increases in baseline cfos expression within the BNST, hM4Di was expressed within CaMKIIα-expressing BNST neurons while shHCN1/2 was expressed ubiquitously in hU6-expressing cells. As a result, the ratio of excitatory to inhibitory actions may differ between the groups and result in different behavioral phenotypes. This hypothesis could be tested with cell-specific expression of hM4Di or shHCN1/2 in guanfacine-activated neurons, for example. Alternatively, the lack of apparent differences between the groups could result from HCN-

independent mechanisms of hM4Di-mediated anxiogenesis, compensation after shRNA-mediated knockdown that does not occur with acute drug application, or other unaccounted for experimental differences such as laterality of injection, presence of implant, or other factors. These hypotheses can and should be tested in future experiments.

Appendix V

Expression of a cAMP-insensitive HCN2 channel does not affect guanfacine-induced cfos expression

Guanfacine activation of postsynaptic α_{2A}-ARs is hypothesized to initiate a signaling cascade that inhibits HCN channels localized to the dendritic neck to cease filtering at this location. HCN channels are cyclic nucleotide-gated, with cAMP binding to the CNB (cyclic nucleotide binding) domain leading to increased open probability of the channel at more depolarized and thus physiological membrane potentials (Kaupp and Seifert, 2001). Canonical G_i-coupled GPCR signaling mechanisms could thus mediate the interaction between α_{2A}-AR agonism and HCN channel inhibition. Specifically, $G\alpha_i$-mediated inhibition of adenylate cyclase would lead to decreased production of cAMP within the dendritic spine and thus decreased open probability of the synaptic current-filtering HCN channels. This is the mechanism that was tested and validated as a model underlying the activity-enhancing effects of guanfacine and norepinephrine at postsynaptic α_{2A}-ARs within the prefrontal cortex (Wang et al., 2007).

The cAMP sensitivity of HCN2 channels has been localized to a single amino acid within the N-terminal intracellular domain. Mutation of the arginine at residue 591 into glutamic acid (R591E) abolishes cAMP sensitivity of the channel in isolated systems (Chen et al., 2001; Wang et al., 2002; Magee et al., 2015). In the absence of cAMP-mediated gating, this mutated form of the HCN2 channel is constitutively autoinhibited but still shows hyperpolarization-activated

voltage dependency albeit at more hyperpolarized potentials than the non-autoinhibited forms of the channel. This mutation was recently introduced into a mouse line. We hypothesized that R591E mutant mice would show decreased guanfacine-induced cfos expression relative to wild-type littermates due to the hypothesized role of cAMP-mediated gating of HCN2 channels in excitatory actions of the drug. To test this, we evaluated cfos expression ninety minutes after guanfacine injection as done previously.

Fluorescence immunohistochemistry was performed as described above. Briefly, mice were handled for five days and then injected with either saline or guanfacine ninety minutes prior to perfusion with 10 mL PBS and 20 mL 4% PFA followed by brain extraction. Brains were then fixed in PFA, cryoprotected in 30% sucrose in PBS, and cut on a cryostat into 40 µm coronal sections. These sections were then stained for cfos and NeuN, imaged on a confocal microscope, and counted by a blinded reviewer.

The results from this experiment show a robust effect of guanfacine on cfos expression, as expected, but a minimal effect of genotype (two-way ANOVA; treatment effect: $F(1,8)=21.3$, $p=0.002$; genotype effect: $F(1,8)=1.9$, $p=0.21$; interaction: $F(1,8)=0.2$, $p=0.70$; Figure 19). A Holm-Sidak multiple comparisons test showed that both HCN2 wild-type (Saline: 106±12 cfos+ cells; Guan: 156±9 cells; $p=0.02$) and R591E mutant (Saline: 117±18 cells; Guan: 177±5 cells; $p=0.02$) mice showed significant upregulation of cfos after guanfacine injection.

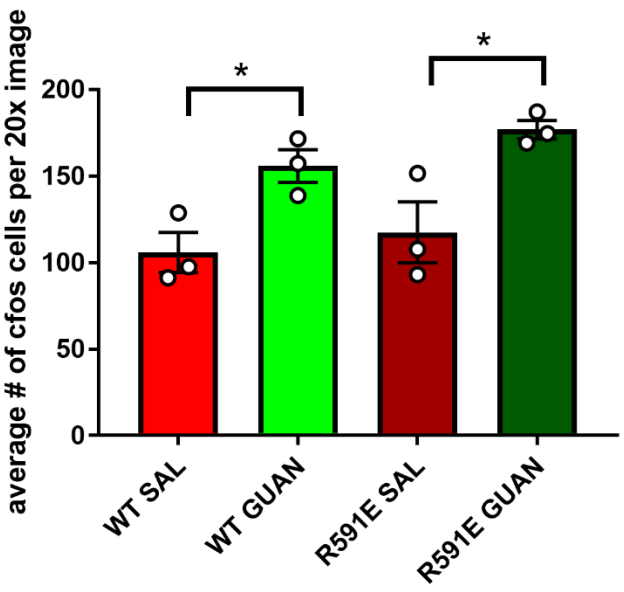

Figure 19: HCN2 mutant mice that do not show cAMP sensitivity (R591E) maintain guanfacine-induced cfos expression. Both HCN2 wild-type and R591E mutant mice show equivalent levels of upregulation of cfos expression after guanfacine injection.

Presence of guanfacine-induced cfos expression in both wild-type and cAMP-insensitive HCN2 R591E mutants suggests a minimal role of cAMP in the signaling cascade connecting α_{2A}-AR agonism to cfos expression. A possible explanation for this observation would be that cAMP-independent signaling mechanisms downstream of activation of this G_i-coupled GPCR mediates HCN channel inhibition, such as inositol production pathways (Pian et al., 2006). Alternatively, observation of blockade of a cAMP-dependent effect of guanfacine could be precluded by compensatory expression patterns in this transgenic mouse line or formation of heteromer HCN channels that maintain cAMP sensitivity despite single subunit loss thereof. Future studies should aim to investigate expression patterns of HCN channel subunits within the BNST of R591E mutant mice, including subcellular trafficking and heteromer formation patterns.

Appendix VI

CNO activation of presynaptic hM4Di expressed in Calca+ parabrachial nucleus afferent terminals inhibits excitatory neurotransmission within the BNST

The parabrachial nucleus (PBN) is a hindbrain nucleus known to be involved in interoceptive processing and other physiological processes such as pain, thirst, fear, and feeding (Campos et al., 2018; Palmiter, 2018). The PBN is one of only a few regions of the brain that express the neuropeptide calcitonin gene-related peptide (CGRP). Like the PBN in general, CGRP has specifically been implicated in a number of core physiological processes like pain (Shinohara et al., 2017), but also in the pathophysiology of anxiety and other stress-dependent phenotypes (Sink et al., 2011). CGRP+ positive neurons from the PBN project to the extended amygdala and form axosomatic synapses that are hypothesized to be analogous to the detonator synapses between climbing fibers and Purkinje neurons in the cerebellum (Shimada et al., 1989; Dobolyi et al., 2005). The projection from the PBN to the central nucleus of the amygdala (CeA) has been heavily characterized as critically involved in the process of encoding threat memory (Han et al., 2015). The projection to the BNST is hypothesized to be anxiety-inducing, as CGRP injection into the BNST elicits anxiogenesis (Sink et al., 2011, 2013a) and CGRP receptor antagonists block these effects (Sink et al., 2013b).

Optical stimulation of glutamatergic afferents from the PBN in *ex vivo* BNST slices can activate or inhibit BNST neurons either via a monosynaptic excitation or feedforward inhibition (Flavin et al., 2014). This has also been shown to occur in the CeA (Sugimura et al., 2016). In addition to expressing CGRP, PBN neurons also express the α_{2A}-AR (Rosin et al., 1996) and agonism of this receptor by guanfacine inhibits optically evoked excitatory postsynaptic currents (oEPSCs) from PBN projection neurons in the BNST (Flavin et al., 2014). The effect on the

feedforward inhibitory effects of PBN stimulation, on the other hand, are more variable. Guanfacine inhibition of oEPSCs mimics inhibition of nonspecific electrically-evoked excitatory postsynaptic currents (eEPSCs) in the BNST (Shields et al., 2009). We hypothesize that guanfacine inhibition of eEPSCs is driven by presynaptic inhibition of PBN afferents due to the axosomatic morphology of these synapses and the resultant proximity-induced minimization of space clamp error (Larkum et al., 1998; Williams and Mitchell, 2008) at the somatic recording site. To test this hypothesis, we introduced the designer receptor hM4Di into CGRP+ neurons in the PBN to mimic the actions of endogenous α_{2A}-ARs within this projection neuron population and recorded the effects of CNO-induced activation of this receptor on eEPSCs recorded from BNST neurons.

Viral injections and electrophysiological recordings were performed as described above. Briefly, Calca-Cre mice were unilaterally injected intracranially with AAV5-DIO-hM4Di:mCherry into one parabrachial nucleus and sham injected into the other parabrachial nucleus (AP: -5.34 mm, ML: +/-1.31 mm, DV: -3.37 mm) (Paxinos and Franklin, 2004), both at a 15.03° angle. After a minimum of six weeks after surgery, coronal BNST sections were prepared for electrophysiological recordings. Intracellular recording pipettes (3-5 MΩ) were filled with potassium gluconate internal solution and stimuli were evoked through a nichrome wire placed in the stria terminalis. Recordings were done in the presence of picrotoxin (25 uM) to isolate excitatory transmission. After achieving whole-cell configuration, cells were equilibrated for 2-5 minutes prior to recording. After achievement of a stable eEPSC baseline for five minutes, CNO (500 nM) was bath applied for ten minutes and then washed out for fifteen minutes.

CNO-mediated activation of hM4Di expressed in CGRP+ PBN neurons reduced the amplitude eEPSCs in BNST neurons with minimal effect in sham-injected control animals (two-way ANOVA; time effect: $F(149,750)=2.3$, $p<0.0001$; virus effect: $F(1,750)=297.9$, $p<0.0001$; interaction: $F(149,750)=1.4$, $p=0.002$). Relative to baseline levels (0-5 minutes), eEPSC amplitude was reduced to a value of 53.3±7.7% by CNO in hM4Di+ slices (paired t-test, $p=0.008$) but to 93.2±11.6% in hM4Di- slices (paired t-test, $p=0.40$), highlighting specificity for signaling at this designer receptor.

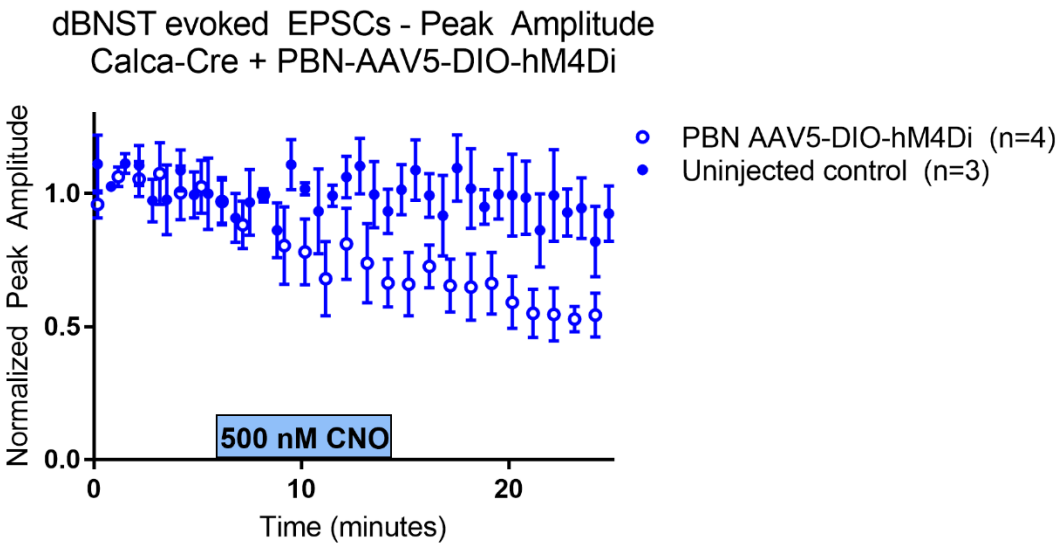

Figure 20: CNO activation of hM4Di expressed in PBN Calca+ neurons inhibits electrically evoked EPSCs in BNST neurons. Bath application of CNO inhibited eEPSCs in BNST neurons with hM4Di expression but not sham injection

Activation of hM4Di by CNO in CGRP+ PBN terminals within BNST slices thus inhibited eEPSCs in BNST neurons. This result supports the hypothesis that electrical stimulation of excitatory synaptic activity enriches for activation of axon terminals from projection neurons originating in the PBN. Interestingly, the magnitude of this effect is similar to that effect by guanfacine in eEPSCs (42.2±6.8% inhibition at the saturating dose of 5 µM)

suggesting commonality (Shields et al., 2009). Further, the low concentration of CNO here as well as the lack of effect in hM4Di- slices highlights the specificity of CNO effects at hM4Di (Gomez et al., 2017). Finally, with validation of inhibitory actions mimicking those of endogenously expressed G_i-coupled GPCRs in PBN terminals within the BNST, we can now confidently use this approach to determine the effects of modulating PBN-BNST synapse on relevant physiology and behavior.

Appendix VII

Preliminary data from mechanistic studies on *ex vivo* guanfacine-induced cfos expression

Guanfacine upregulates cfos expression in a subset of BNST both *in vivo* after intraperitoneal injection or *ex vivo* after slice incubation. Through convergent experimental techniques, we show that *in vivo* cfos expression occurs after agonism of α_{2A}-ARs and downstream HCN channel inhibition, which itself is necessary and sufficient for excitatory actions within the BNST. This mechanism has previously been shown to underlie the excitatory effects of guanfacine in the prefrontal cortex that enhance working memory (Wang et al., 2007). Our model posits that HCN channels localized to the dendritic neck filter synaptic currents under normal levels of cAMP but decrease this filtering to enhance excitatory transmission upon α_{2A}-AR activation by guanfacine. We hypothesize that *ex vivo*-mediated cfos expression occurs through this same mechanism. To test this hypothesis, we used the *ex vivo* preincubation model to mechanistically study guanfacine-induced cfos expression by co-incubation with ZD7288 to inhibit HCN channels, CNQX to inhibit AMPA receptors, and picrotoxin to inhibit $GABA_A$ receptors.

Evaluation of *ex vivo* cfos induction after drug preincubation was performed as described above. Briefly, brain slices were prepared from *cfos-eGFP* mice after handling and allowed to

recover for one hour prior to preincubation. Drugs were then added from stock solutions for one hour prior to slice fixing in 4% PFA at RT for 30 minutes and then 4ºC for 24 hours. The Brain BLAQ protocol was then followed (Kupferschmidt et al., 2015). Once completed, slices were imaged using a confocal microscope and counted by a blinded reviewer.

HCN channel inhibition by ZD7288 was previously shown to elicit excitatory actions in electrophysiological recordings of optically evoked field potential responses in the Thy1COP4 mouse line and spontaneous excitatory postsynaptic potentials, respectively mimicking and extending the excitatory effects of guanfacine. We aimed to determine whether ZD7288 would mimic *ex vivo* guanfacine-induced cfos expression by incubating for one hour in either ACSF, guanfacine (1 µM), ZD7288 (10 µM), or guanfacine and ZD7288 together. A repeated-measures two-way ANOVA showed no significant effect of guanfacine or ZD7288 (guanfacine effect: $F(1,4)=0.8$, $p=0.42$; ZD7288 effect: $F(1,4)=0.1$, $p=0.79$; interaction: $F(1,4)=4.4$, $p=0.11$; Figure 21A). Lack of statistical power is suggested by the insignificance of the positive control guanfacine effect apparent increases that fail to reach statistical significance after guanfacine incubation with or without ZD7288 but no effect of ZD7288 alone (ACSF: 14.1±3.1%; guanfacine: 23.9±5.2%; ZD7288: 15.6±0.9%; guanfacine and ZD7288: 20.0±3.7%). Lack of ZD7288 effect suggests that HCN inhibition does not mimic guanfacine effect in this experimental design. However, we alternatively hypothesize that a lack of effect of HCN inhibition may occur due to insufficient incubation exposure time rooted in the difference of pharmacokinetics observed in the electrophysiological recordings of guanfacine and ZD7288 on optically-evoked field potentials in the Thy1-COP4 mouse line. To test this hypothesis, future studies should evaluate ZD7288 effects on *ex vivo* cfos induction over a variable and longer time course.

Guanfacine agonism at α_{2A}-ARs in the dendritic spine are hypothesized to increase the somatic integration of glutamate-evoked currents after release of dendritic filtering by HCN channel inhibition. Thus, glutamate signaling is hypothesized to be necessary for guanfacine-induced cfos expression. We tested this hypothesis by incubating BNST slices in either ACSF, guanfacine (1 µM), CNQX (10 µM), or guanfacine and CNQX together. Here, a two-way ANOVA showed no significant effect of either guanfacine or CNQX on *ex vivo* cfos induction (guanfacine effect: $F(1,10)=2.5$, $p=0.15$; CNQX effect: $F(1,10)=2.9$, $p=0.12$; interaction: $F(1,10)=3.3$, $p=0.10$; Figure 21B). Again, a lack of statistical power is suggested by the insignificance of guanfacine effect as a positive control and an apparent increase that did not reach statistical significance for guanfacine alone but not CNQX alone or with guanfacine (ACSF: 17.5±5.2% cfos+ neurons; guanfacine: 44.7±9.1%; CNQX: 18.5±8.0%; guanfacine and CNQX: 16.5±6.9%). If future experiments show this trend of CNQX-mediated blockade of guanfacine-induced cfos expression to be significant, this would suggest that glutamate signaling is necessary for guanfacine-induced *ex vivo* cfos induction, consistent with our model of excitatory actions occurring as a result of α_{2A}-AR agonism.

An intracellular pathway connecting α_{2A}-AR agonism to increased cellular activity only accounts for a portion of excitatory actions of guanfacine within the BNST, as expression was observed in both *Adra2a+* and *Adra2a-* BNST cells. We hypothesize that activation of *Adra2a+* BNST neurons leads to disinhibition of *Adra2a-* neurons through $GABA_A$-mediated inhibition of an inhibitory interneuron. To test this microcircuit hypothesis, we incubated slices in ACSF, guanfacine (1 µM), picrotoxin (25 µM), or guanfacine and picrotoxin together. A two-way ANOVA again showed no significant effect of either treatment (guanfacine effect: $F(1,2)=4.5$, $p=0.17$; picrotoxin effect: $F(1,2)=0.8$, $p=0.47$; interaction: $F(1,2)=1.6$, $p=0.34$; Figure 21C). Lack

of statistical power is again suggested by insignificant effects of guanfacine and an apparent increase that did not reach statistical significance after incubation in guanfacine alone or in combination with picrotoxin but not with picrotoxin alone (ACSF: 7.4±1.8%; guanfacine: 26.0±6.8%; picrotoxin: 8.1±4.5%; guanfacine and picrotoxin: 20.1±3.1%). If experiments with more statistical power would corroborate these trends, this would suggest that $GABA_A$-mediated transmission is not necessary for guanfacine-induced cfos expression.

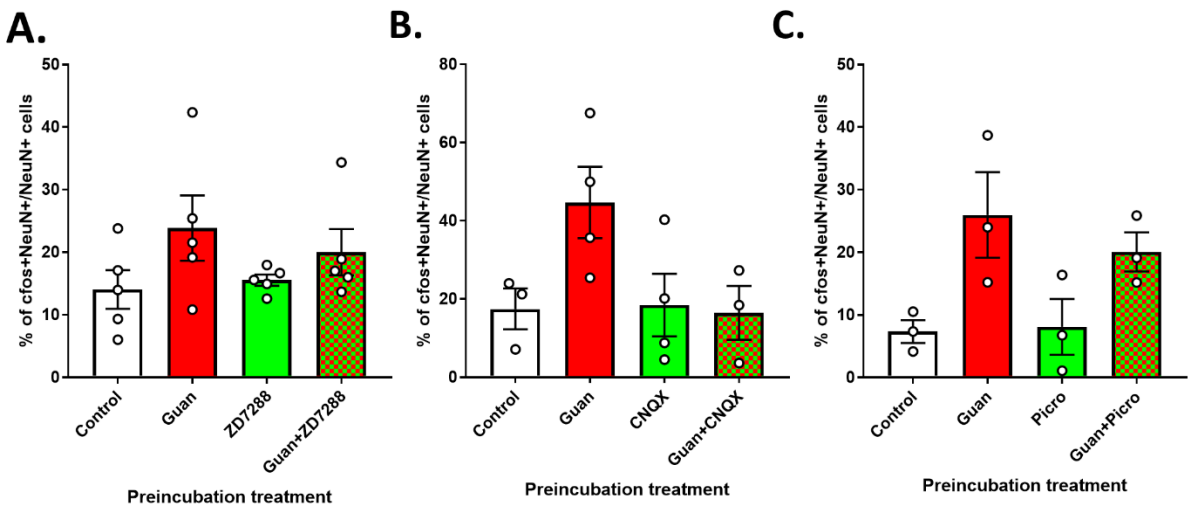

Figure 21: Preliminary data from experiments attempting to either mimic or block guanfacine-induced cfos-eGFP expression in ex vivo BNST brain slices. (A) BNST slices were incubated for 60 minutes in either ACSF, guanfacine (1 uM), ZD7288 (10 uM), or guanfacine and ZD7288 together. No significant effect of guanfacine or ZD7288 on cfos-eGFP expression was observed, suggesting lack of statistical power. (B) BNST slices were incubated for 60 minutes in either ACSF, guanfacine (1 uM), CNQX (10 uM), or guanfacine and CNQX together. Again, no significant effect of guanfacine or CNQX was observed. (C) BNST slices were incubated for 60 minutes in either ACSF, guanfacine (1 uM), picrotoxin (25 uM), or guanfacine and picrotoxin together. Again, no significant effect of guanfacine or picrotoxin was observed.

Appendix VIII

Guanfacine minimally affects anxiety-like behavior in the elevated plus maze but may alter BNST activity therein

The ability of α_2-AR agonists to dampen noradrenergic tone suggests that ligands of this class would counteract the anxiogenic effects of norepinephrine and induce anxiolysis instead. However, the effects of α_2-AR agonists in general and α_{2A}-AR agonists in particular in rodent models of anxiety-like behavior is variable where drug responses can be anxiolytic (Ji et al., 2014), anxiogenic (Johnston et al., 1988; Uzsoki et al., 2011), or have no effect (Cole et al., 1995). The behavioral effect of guanfacine and other α_2-AR agonists in these and related tests appears to depend on the negative valence associated with either an experimental manipulation that precedes the test or the test itself (Davies et al., 2004; Gamache et al., 2012; Malikowska et al., 2017). We aimed to determine the effects of guanfacine on anxiety-like behavior as assessed by the elevated plus maze. In addition, we hypothesize that BNST activity will correlate with anxiety-like behavior and test this hypothesis by performing fiber photometric recordings of GCaMP6f fluorescence *in vivo* while animals are in the elevated plus maze.

Viral injections, fiber optic implantation, and behavioral testing were performed as described above. Briefly, mice were bilaterally injected intracranially with AAV5-hSyn-GCaMP6f (300 uL) into the right BNST (AP: 0.14, ML: +/-0.88, DV: -4.24) (Paxinos and Franklin, 2004) at a 15.03° angle. Three weeks after surgery, a second surgery was performed whereby an optical fiber implant was placed into the BNST at 15.03º angle and adhered to the skull. After at least one week of recovery, behavioral experiments were performed. Mice were handled for five days prior to testing. Two hours prior to behavioral testing, baseline BNST activity was recorded in the home cage and mice were injected with 1 mg/kg guanfacine or

saline. After the two hours, mice were transferred to the elevated plus maze (EPM) for five minutes. As above, lighting was set to approximately 60-70 lux in the open arm and 10-20 lux in the closed arm. Mice were visualized, recorded, and tracked by a camera using AnyMaze software. Fiber photometry recordings were simultaneously recorded and used to calculate BNST Ca^{2+} transient frequency through the use of the mLspike algorithm.

Relative to saline-injected controls, guanfacine did not have an effect on anxiety-like behavior as assessed by the elevated plus maze. Specifically, no difference was observed between animals treated with saline or guanfacine with respect to closed arm time (saline: 152.2±23.3 seconds; guanfacine: 194.4±32.4 seconds; unpaired t-test, p=0.34) or open arm time (saline: 72.9±28.2 seconds; guanfacine: 37.42±11.0 seconds; unpaired t-test, p=0.24). However, guanfacine did decrease center zone time (saline: 65.8±11.7 seconds; guanfacine: 23.2±7.9 seconds; unpaired t-test, p=0.01), although the interpretation of this effect is uncertain. Importantly, there was no difference between the groups with respect to total distance traveled (saline: 5.8±1.0 meters; guanfacine: 4.3±1.1 meters; unpaired t-test, p=0.34), decreasing likelihood of this potential confound and confirming lack of sedation at the 1 mg/kg dose.

Simultaneous recordings of BNST activity suggested guanfacine inhibition of BNST activity despite lack of behavioral effect. Specifically, fiber photometric recordings of GCaMP6f fluorescence and *post hoc* imputation of calcium transients show a trend towards decreased total frequency in the EPM (saline: 2.2±0.7 Hz; guanfacine: 0.7±0.4 Hz; unpaired t-test, p=0.08). When these transients were localized to EPM compartment, though, statistically significant decreases were seen in both the open arm (saline: 2.7±0.6 Hz; guanfacine: 0.5±0.2 Hz; unpaired t-test, p=0.01) and closed arm (saline: 2.1±0.4 Hz; guanfacine: 0.6±0.4 Hz; unpaired t-test,

p=0.04) but only a trend in the center zone (saline: 2.3±0.5 Hz; guanfacine: 0.8±0.4 Hz; unpaired t-test, p=0.07). Thus, guanfacine inhibits BNST activity during the EPM test.

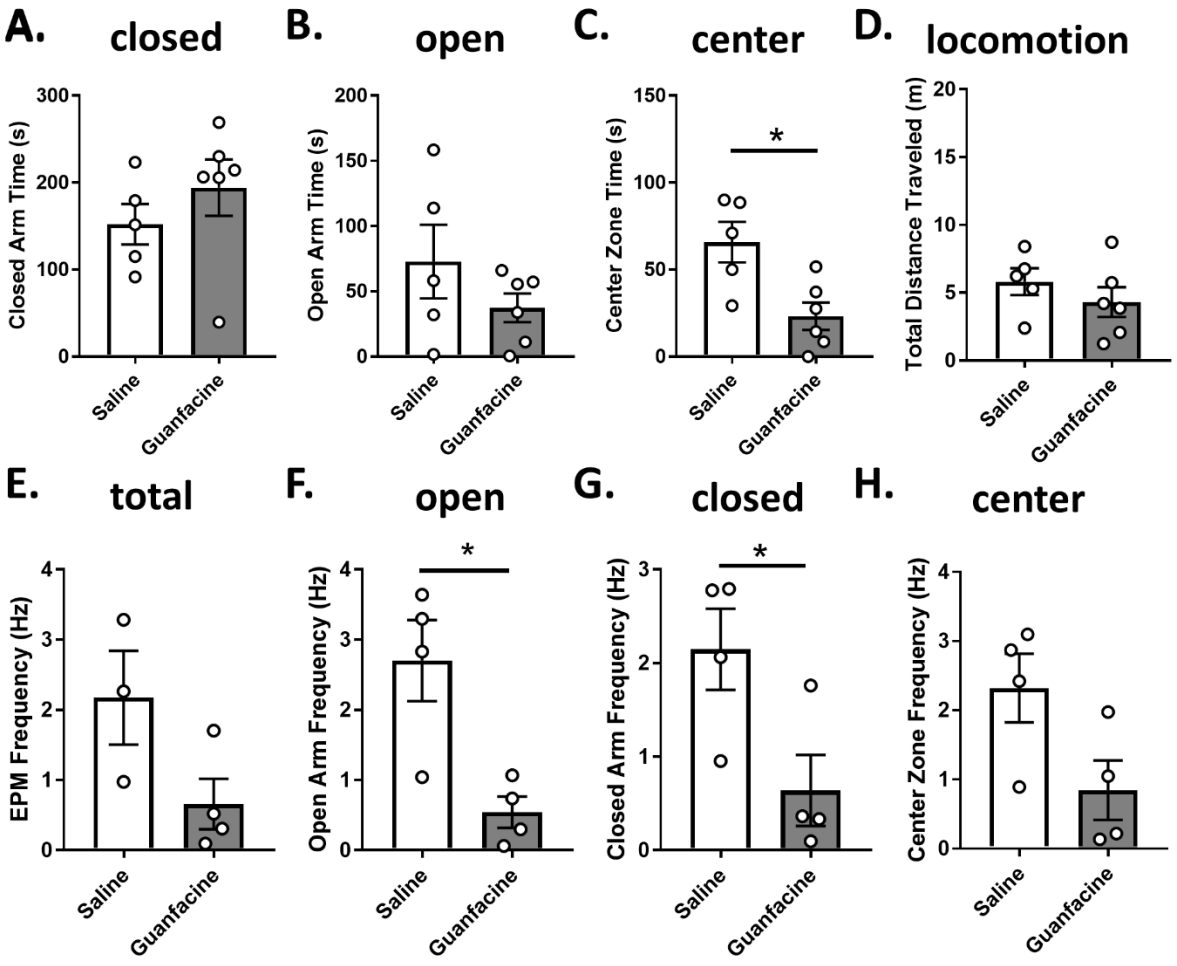

Figure 22: Guanfacine does not affect behavior in the elevated plus maze but does inhibit BNST Ca2+ transients. Mice underwent anxiety-like behavioral testing in the elevated plus maze 120 minutes after saline or guanfacine injection and showed no difference in the behaviorally-relevant measures of closed arm time (A) or open arm time (B). Guanfacine injection did reduce center zone time (C) but did not affect locomotion (D). In simultaneous fiber photometry recordings of BNST GCaMP6f fluorescence, imputed Ca^{2+} transients trended towards a decrease in the EPM test as a whole (E), but showed statistically significant decreases in BNST activity specifically when in the open (F) or closed (G) arms but not the center zone (H) of the apparatus.

In addition to evaluating the global effects of guanfacine on BNST activity, *in vivo* fiber photometry recordings also allow for time-locked analyses of activity during specific behavioral actions observed during the test. In the EPM, for example, the effects of guanfacine on BNST

activity before, during, and after transition to a new compartment of the maze can be determined. Changes in activity can be seen in the GCaMP6f signal before and after transitions into the open (Figure 23A, Figure 23G) and closed (Figure 23B, Figure 23H) arms of the maze, with minimal activity around entrances to the center zone (Figure 23C). These peaks are also present but appear to be less consistent in the guanfacine-injected animals (Figures 23D-F, Figures 23I-J). No statistical differences were observed between animals treated with saline or guanfacine when comparing activity during transitions into the open arm (saline prior: 7.1±0.5%; guanfacine prior: 8.5±0.5%; Fisher's LSD, $p=0.08$; saline post: 7.4±0.5%; guanfacine post: 8.2±0.6%; Fisher's LSD, $p=0.29$; repeated measures two-way ANOVA; time effect: $F(1,69)=0.0001$, $p=0.99$; treatment effect: $F(1,60)=2.2$, $p=0.14$; interaction: $F(1,69)=1.4$, $p=0.25$; subjects matching: $F(69,69)$, $p<0.0001$), closed arm (saline prior: 7.8±0.4% dF/F; guanfacine prior : 7.3±0.5% dF/F; Fisher's LSD, $p=0.53$; saline post: 8.3±0.5% dF/F; guanfacine post: 7.3±0.6 dF/F; Fisher's LSD, $p=0.19$; repeated measures two-way ANOVA; time effect: $F(1,82)=1.3$, $p=0.26$; treatment effect: $F(1,82)=1.1$, $p=0.31$; interaction: $F(1,82)=1.1$, $p=0.30$, subjects matching: $F(82,82)=8.1$, $p<0.0001$), or center zone (saline prior: 7.4±0.4%; guanfacine prior: 7.2±0.4%; Fisher's LSD, $p=0.70$; saline post: 7.5±0.3%; guanfacine post: 7.2±0.4%; Fisher's LSD, $p=0.60$; repeated measures two-way ANOVA; time effect: $F(1,141)=0.005$, $p=0.94$; treatment effect: $F(1,141)=0.2$, $p=0.63$; interaction: $F(1,141)=0.05$, $p=0.83$; subjects matching: $F(141,141)=8.3$, $p<0.0001$). Due to the small effect size between treatments and the lack of statistical effects within these comparisons, the interpretation of these results is unclear.

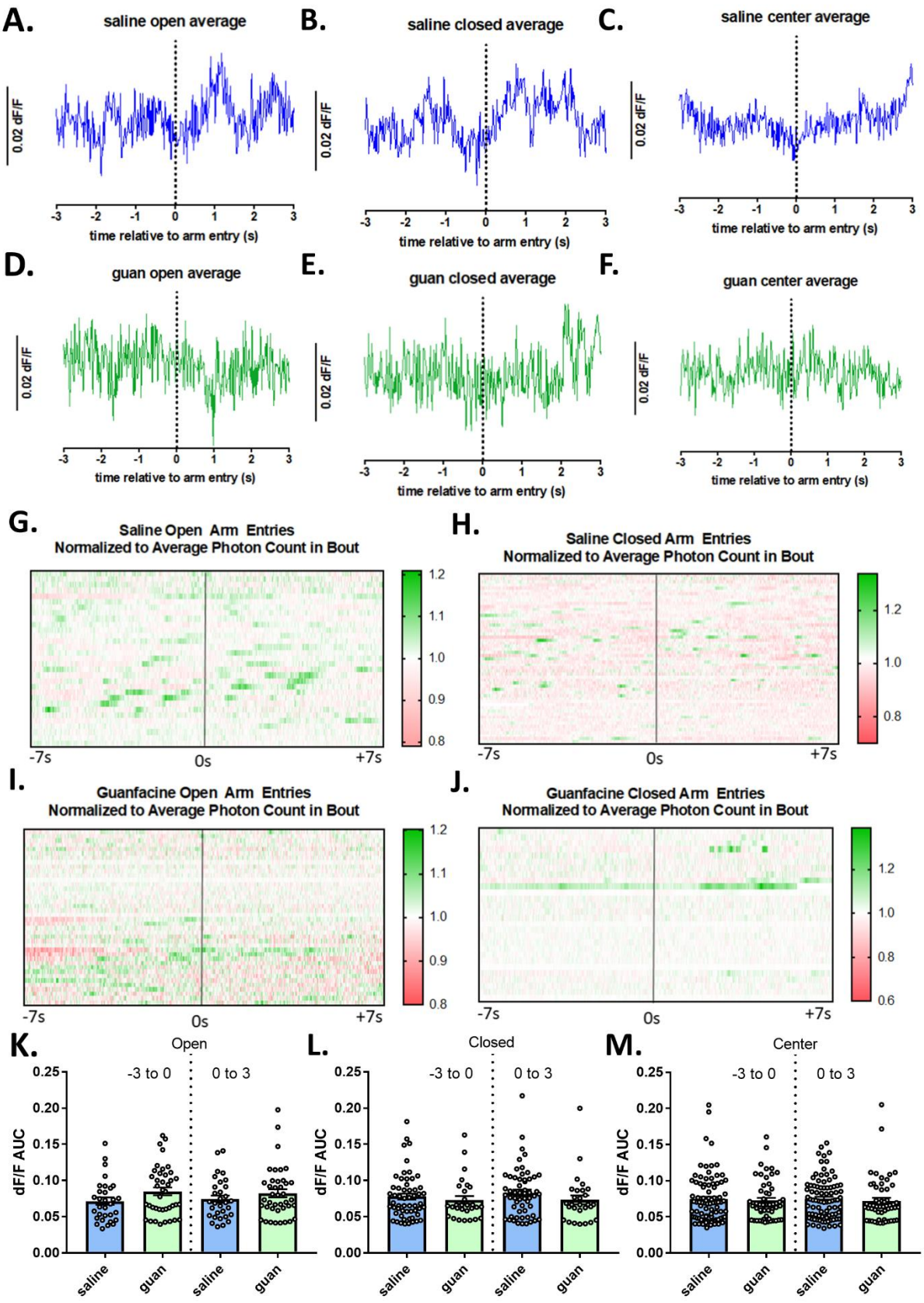
A.
saline open average
0.02 dF/F
time relative to arm entry (s)
B.
saline closed average
0.02 dF/F
time relative to arm entry (s)
C.
saline center average
0.02 dF/F
time relative to arm entry (s)
D.
guan open average
0.02 dF/F
time relative to arm entry (s)
E.
guan closed average
0.02 dF/F
time relative to arm entry (s)
F.
guan center average
0.02 dF/F
time relative to arm entry (s)
G.
Saline Open Arm Entries
Normalized to Average Photon Count in Bout
-7s
0s
+7s
H.
Saline Closed Arm Entries
Normalized to Average Photon Count in Bout
-7s
0s
+7s
I.
Guanfacine Open Arm Entries
Normalized to Average Photon Count in Bout
-7s
0s
+7s
J.
Guanfacine Closed Arm Entries
Normalized to Average Photon Count in Bout
-7s
0s
+7s
K.
Open
-3 to 0
0 to 3
dF/F AUC
saline
guan
saline
guan
L.
Closed
-3 to 0
0 to 3
dF/F AUC
saline
guan
saline
guan
M.
Center
-3 to 0
0 to 3
dF/F AUC
saline
guan
saline
guan

Figure 23: Preliminary data suggests minimal effects of guanfacine injections on transitions during the elevated plus maze relative to saline-injected control animals. (A-C) Saline-injected animals show transients both before and after entering the open (A) or closed (B) arms of the elevated plus maze but minimal changes when entering the center zone (C). (D-F) Guanfacine-injected animals show less characteristic peak shapes in when entering either the open arm (D), closed arm (E) or center zone (F). (G-J) Heat maps of closed and open arm transitions after injection with saline or guanfacine are shown to show individual differences between specific entrances. (K-M) Guanfacine injection had no statistically significant effect on area under the curve analyses for these transitions, but trends towards increased activity during open arm transitions and decreased for closed arm transitions while minimally affecting center zone transitions.

The signal-to-noise ratio of the raw photometry signal even after normalization to $\Delta F/F$ is low and may preclude observation of guanfacine effects. Calcium transient peak assignment using the mLspike algorithm increases this signal-to-noise ratio and allows for simple quantification of the fiber photometric recording. Therefore, we utilized this algorithm to identify calcium transients that occurred during the same transitions as above in the elevated plus maze (Figures 24A-D). Comparisons of activity three seconds prior to and after entering each compartment of the maze were performed between animals treated with saline or guanfacine. In transitions into the open arm (repeated measures two-way ANOVA; treatment effect: $F(1,96)=3.1$, $p=0.08$; time effect: $F(1,96)=0.5$, $p=0.50$; interaction: $F(1,96)=4.3$, $p=0.04$; subjects matching: $F(96,96)=6.5$, $p<0.0001$), guanfacine decreased the frequency of calcium transients after (saline: 2.5±0.2 Hz; guanfacine: 1.8±0.3 Hz; Holm-Sidak, $p=0.04$) but not before (saline: 2.2±0.2 Hz; guanfacine: 1.9±0.3 Hz; Holm-Sidak, $p=0.38$) entering the arm. In transitions into the closed arm (repeated measures two-way ANOVA; treatment effect: $F(1,102)=9,3$ $p=0.003$; time effect: $F(1,102)=1.0$, $p=0.33$; interaction: $F(1,102)=0.1$, $p=0.70$; subjects matching: $F(102,102)=3.2$, $p<0.0001$), guanfacine decreased calcium transient frequency both prior to (saline: 2.0±0.1 Hz; guanfacine: 1.2±0.3 Hz; Holm-Sidak, $p=0.009$) and after (saline: 2.1±0.1 Hz; guanfacine: 1.3±0.3 Hz; Holm-Sidak, $p=0.01$) entering the arm. This same effect occurred

during transitions into the center zone (repeated measures two-way ANOVA; treatment effect: $F(1,196)=9.4$, $p=0.003$; time effect: $F(1,196)=3.7$, $p=0.06$; interaction: $F(1,196)=1.1$, $p=0.29$; subjects matching: $F(196,196)=4.0$, $p<0.0001$), with guanfacine also decreasing calcium transient frequency both prior to (saline: 2.0±0.1 Hz; guanfacine: 1.5±0.2 Hz; Holm-Sidak, $p=0.02$) and after (saline: 2.3±0.1 Hz; guanfacine: 1.6±0.2 Hz; Holm-Sidak, $p=0.003$) entering the zone, suggesting lack of specificity for the other transitions. Of note, these effects are not statistically significant across animals (data not shown), suggesting there may be nested effects within the data set. Rigorously testing this hypothesis will require additional statistical power. Again, the biological significance of this data remains unclear, although we hypothesize that inhibitory actions at presynaptic α_{2A}-ARs underlie this effect.

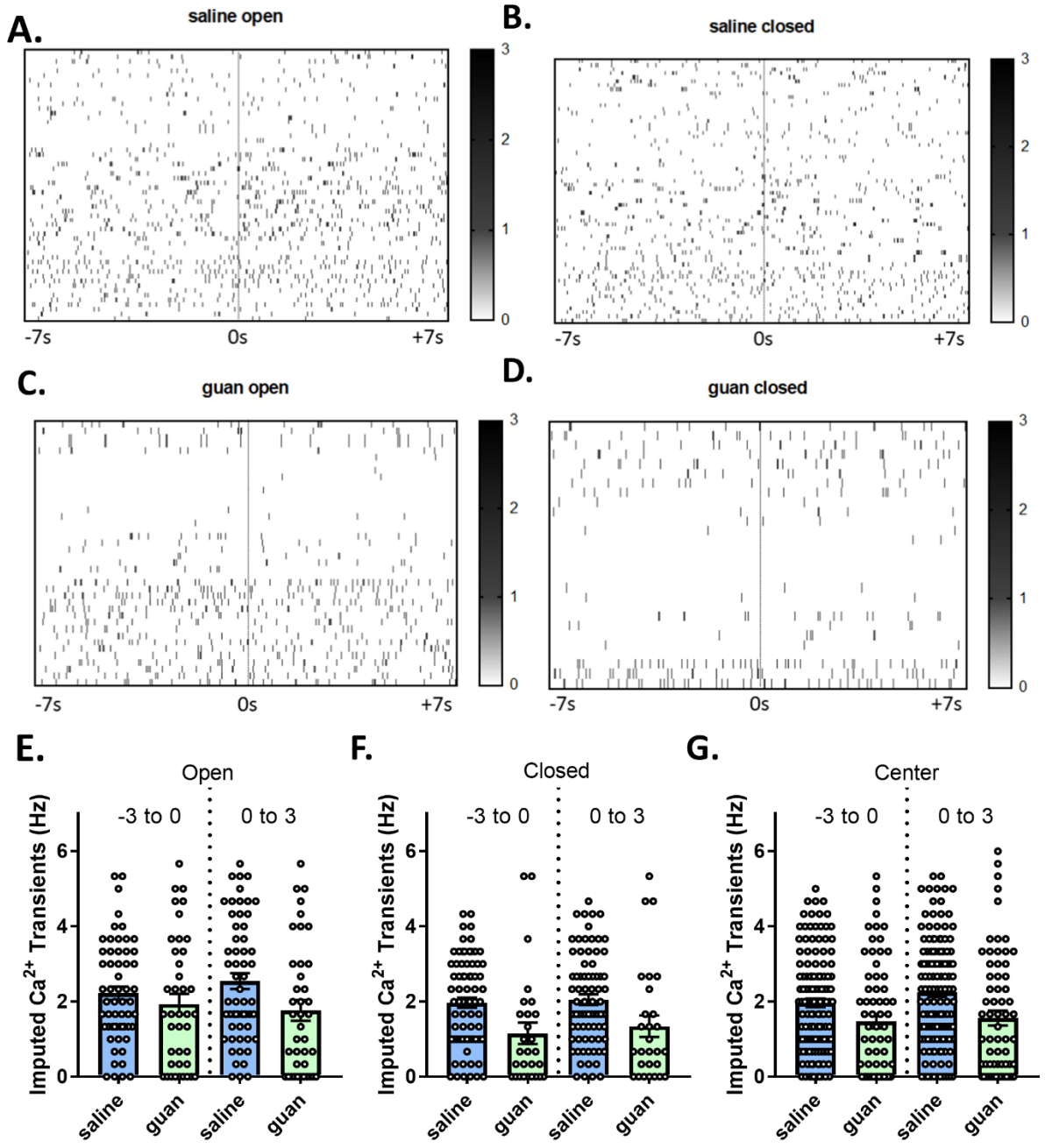

Figure 24: Guanfacine appears to have inhibitory effects on BNST during transitions into the various compartments of the elevated plus maze when quantified as imputed calcium transients. (A-D) Imputed calcium transients were calculated prior to and after entering the various compartments of the elevated plus maze. (E-F) When compared across treatments, guanfacine appeared to have an inhibitory effect on activity after entering the open arm, and both prior to and after entering the closed arm or the center zone of the elevated plus maze.

In addition, we performed the same analysis on a subset of the mice expressing both GCaMP6f and hM4Di in the BNST after treatment with the designer drug clozapine-N-oxide (CNO). Again, we analyzed fiber photometric recordings of GCaMP6f fluorescence prior to and after entering the different compartments of the elevated plus maze (Figure 25A-E), as well as the mLspike-calculated imputed calcium transients that occurred during these same transitions (Figures 25F-G). As with guanfacine, no significant effects were seen for transitions to the open arm (repeated measures two-way ANOVA; treatment effect: $F(1,42)=0.03$, $p=0.87$; time effect: $F(1,42)=0.6$, $p=0.44$; interaction: $F(1,42)=2.4$, $p=0.13$; subjects matching: $F(42,42)=4.3$, $p<0.0001$; CNO prior: 7.6±0.4% dF/F; CNO post: 6.7±0.2%; Holm-Sidak prior, $p=0.65$; Holm-Sidak post, $p=0.65$), closed arm (repeated measures two-way ANOVA; treatment effect: $F(1,84)=1.5$, $p=0.23$; time effect: $F(1,84)=3.1$, $p=0.08$; interaction: $F(1,84)=0.2$, $p=0.70$; subjects matching: $F(84,84)=5.4$, $p<0.0001$; CNO prior: 7.2±0.2% dF/F; CNO post: 7.5±0.3%; Holm-Sidak prior, $p=0.37$; Holm-Sidak post, $p=0.37$), or center zone (repeated measures two-way ANOVA; treatment effect: $F(1,125)=0.1$, $p=0.73$; time effect: $F(1,125)=1.3$, $p=0.26$; interaction: $F(1,125)=1.9$ $p=0.17$; subjects matching: $F(125,125)=5.6$, $p<0.0001$; CNO prior: 7.6±0.3% dF/F; CNO post: 7.0±0.1%; Holm-Sidak prior, $p=0.82$; Holm-Sidak post, $p=0.63$). However, effects of CNO on imputed calcium transients did show inhibitory effects for transitions to the open arm (repeated measures two-way ANOVA; treatment effect: $F(1,69)=19.8$, $p<0.0001$; time effect: $F(1,69)=0.6$, $p=0.44$; interaction: $F(1,69)=0.8$, $p=0.37$; subjects matching: $F(69,69)=3.6$, $p<0.0001$; CNO prior: 0.7±0.2 Hz; CNO post: 0.7±0.1 Hz; Holm-Sidak prior, $p=0.0006$; Holm-Sidak post, $p<0.0001$), closed arm (repeated measures two-way ANOVA; treatment effect: $F(1,106)=36.7$, $p<0.0001$; time effect: $F(1,106)=1.0$, $p=0.33$; interaction: $F(1,106)=0.1$, $p=0.73$; subjects matching: $F(106,106)=2.1$, $p=0.0001$; CNO prior: 0.8±0.1 Hz; CNO post: 0.9±0.2 Hz;

Holm-Sidak prior, $p<0.0001$; Holm-Sidak post, $p<0.0001$), and center zone (repeated measures two-way ANOVA; treatment effect: $F(1,177)=60.4$, $p<0.0001$; time effect: $F(1,177)=0.6$, $p=0.46$; interaction: $F(1,177)=3.0$, $p=0.08$; subjects matching: $F(177,177)=2.2$, $p<0.0001$; CNO prior: 0.8±0.1 Hz; CNO post: 0.7±0.1 Hz; Holm-Sidak prior, $p<0.0001$; Holm-Sidak post, $p<0.0001$). Future studies should aim to replicate these effects and to determine the underlying mechanism and biological significance.

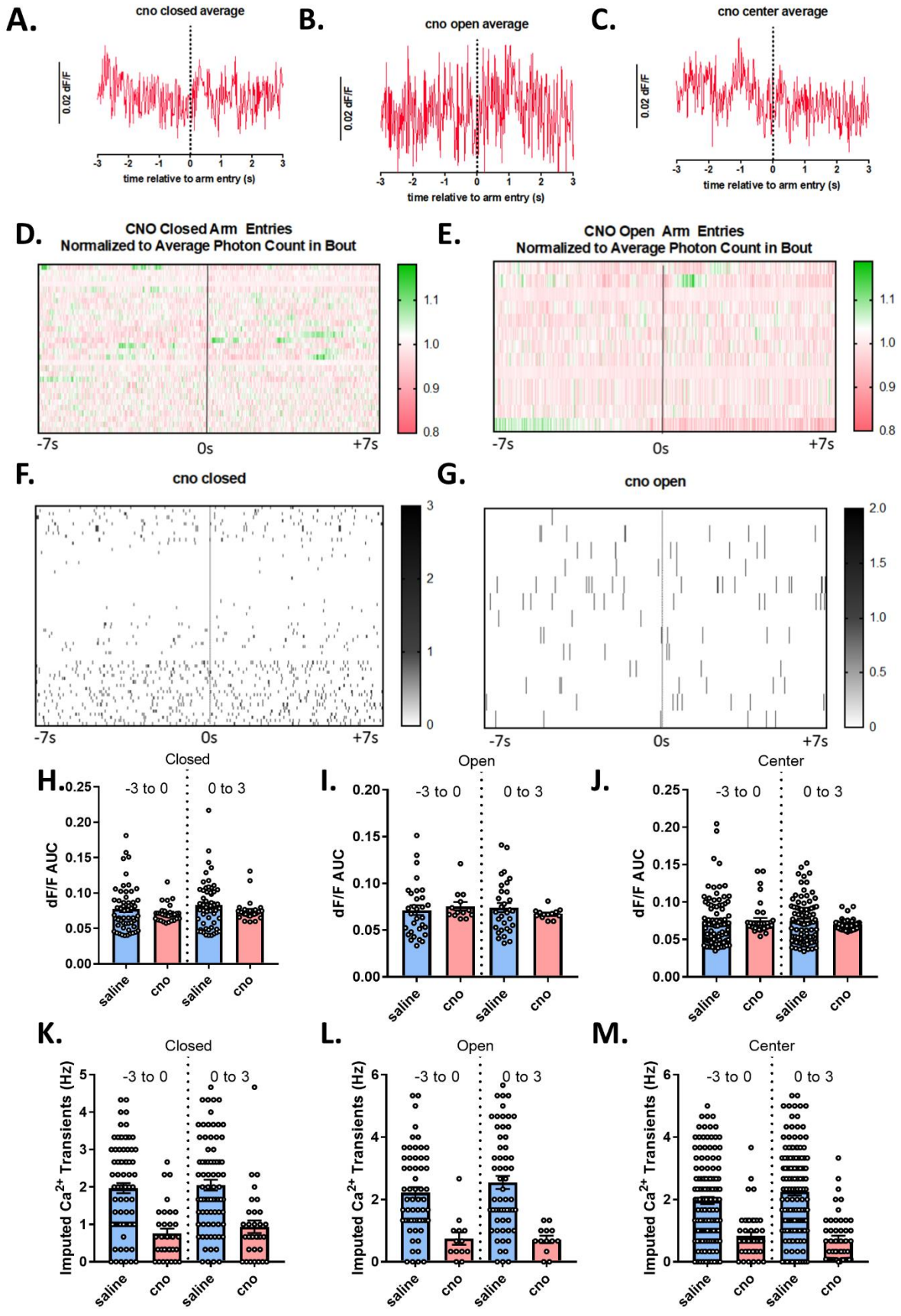
A.
cno closed average
0.02 dF/F
time relative to arm entry (s)
B.
cno open average
0.02 dF/F
time relative to arm entry (s)
C.
cno center average
0.02 dF/F
time relative to arm entry (s)
D.
CNO Closed Arm Entries
Normalized to Average Photon Count in Bout
-7s
0s
+7s
E.
CNO Open Arm Entries
Normalized to Average Photon Count in Bout
-7s
0s
+7s
F.
cno closed
-7s
0s
+7s
G.
cno open
-7s
0s
+7s
H.
Closed
-3 to 0
0 to 3
dF/F AUC
saline
cno
saline
cno
I.
Open
-3 to 0
0 to 3
dF/F AUC
saline
cno
saline
cno
J.
Center
-3 to 0
0 to 3
dF/F AUC
saline
cno
saline
cno
K.
Closed
-3 to 0
0 to 3
Imputed Ca2+ Transients (Hz)
saline
cno
saline
cno
L.
Open
-3 to 0
0 to 3
Imputed Ca2+ Transients (Hz)
saline
cno
saline
cno
M.
Center
-3 to 0
0 to 3
Imputed Ca2+ Transients (Hz)
saline
cno
saline
cno

Figure 25: Inhibitory effects of hM4Di on BNST activity during transitions in the elevated plus maze is evident from imputed calcium transients but not photometry signal normalized to photon count. (A-C) dF/F signal from hM4Di-expressing and CNO-injected animals. (D-E) Heat map showing individual bouts and BNST activity therein. (F-G) Imputed calcium transients during those bouts. (H-J) Minimal effects of CNO on BNST activity are present when analyzing area under the curve three seconds prior to and after transitions in the elevated plus maze. (K-M) Inhibitory effects are unmasked when this signal is translated into imputed calcium transients by the mLspike algorithm.

A lack of behavioral effect of guanfacine in the elevated plus maze is not unexpected given the extant literature on the subject (Johnston et al., 1988; Cole et al., 1995; Uzsoki et al., 2011; Ji et al., 2014). Future studies should aim to determine whether anxiolytic actions of guanfacine can be unmasked by increasing the presence of anxiety-inducing stimuli either during the test itself through increased light intensity, for example, or through pretreatments such as restraint stress or anxiogenic pharmacological injections. Although no behavioral effect of guanfacine was observed, inhibitory effects on BNST activity were observed, mimicking guanfacine actions in *ex vivo* BNST slices (Shields et al., 2009). This data suggests that inhibition of BNST activity is insufficient for anxiolysis. We hypothesize that competing inhibitory and excitatory actions contribute to this finding. Future studies should aim to manipulate subpopulations of α_{2A}-ARs *in vivo* to determine effects on both BNST activity and anxiety-like behavior. In addition, the replicability and behavioral relevance of changes in BNST activity observed during transitions between compartments in the BNST after treatment with guanfacine or CNO relative to saline controls should be an additional area of future study.

Appendix IX

ZD7288 does not affect electrically evoked excitatory field potentials in the BNST

The physiological effect of hyperpolarization-activated cyclic nucleotide-gated nonspecific cation (HCN) channels on neuronal activity is variable and depends on what subcellular compartment the channel is targeted to for expression (McCormick and Pape, 1990;

Cardenas et al., 1999; Day et al., 2005; Park and Lee, 2007; Wanat et al., 2008; George et al., 2009; Okamoto et al., 2018). Subcellular compartmentalization patterns for HCN channels within the BNST have not been ascertained nor has effect on neuronal activity been substantially investigated. Here we show that nonspecific HCN channel inhibition by ZD7288 enhances optical field potentials elicited upon light-evoked stimulation from afferent populations that show segregated expression of channelrhodopsin-2 (ChR2) and calcitonin gene-related peptide (CGRP), a high fidelity marker of the guanfacine-inhibited parabrachial nucleus afferent terminals within the BNST (Flavin et al., 2014). Further, putative guanfacine-activated neurons as defined by cfos-eGFP positivity after guanfacine injection show enhanced frequency of spontaneous excitatory postsynaptic potentials (sEPSPs). These data support the hypothesis that HCN channels are inhibitory at baseline and their inhibition by ZD7288 or signaling pathways downstream of α_{2A}-AR agonism enhances neuronal activity in cells that express both the channel and the receptor. We hypothesize that these actions are driven by HCN2 channels based on kinetic analyses and transcript co-localization between *Hcn2* and *Adra2a*.

HCN channels are expressed throughout the BNST, though, suggesting that actions downstream of the α_{2A}-AR are only one of the modulatory actions of the class of channels (Hazra et al., 2011). This is confirmed in our transcript profile analysis of BNST neurons where we see significant expression of *Hcn2* in both *Adra2a*+ and *Adra2a*- neurons, as well as significant expression of *Hcn1* and *Hcn4* transcripts within this region. The functions of these channels is unknown. We observed that shRNA-mediated knockdown of HCN1 and HCN2 channels did not affect sEPSP amplitude or frequency of infected neurons, one interpretation of which is that HCN channel inhibition differentially affects *Adra2a*+ and *Adra2a*- BNST neurons and that competition between these effects precludes observations of group effects in recordings from

unidentified neurons. We aimed to determine the effects of HCN inhibition by ZD7288 on electrically-evoked field potentials to ascertain contribution of these channels to excitatory transmission within the BNST.

Slice preparation and field potential recordings were performed as described above. Briefly, slices were prepared from C57/Bl6J mice and allowed to recover for one hour before recording. Field potentials were recorded with pipettes filled with ACSF while stimuli were evoked by electrical stimulation of a nichrome wire placed in the stria terminalis. All experiments were done in the presence of 25 μM picrotoxin to isolate fast excitatory transmission. The fiber volley potential (N1) was monitored continuously throughout the duration of the experiment. Experiments in which N1 changed by 20% in either direction were not included in subsequent analysis.

HCN inhibition by ZD7288 minimally affected electrically-evoked excitatory field potential responses recorded in the BNST (Figure 26A). Forty minutes of ZD7288 application led to a 1.9% decrease in the synaptic potential N2 (baseline: 99.0±2.4%; ZD7288: 97.1±11.2%; unpaired t-test, p=0.88; range -18.1% to +20.4%). Lack of effect here suggests that HCN channel inhibition does not have population-wide effects on excitatory transmission within the BNST. However, given that ZD7288 enhances optically-evoked field potentials in the Thy1-COP4 mouse line, a lack of effect on electrically-evoked field potentials suggests competing excitatory and inhibitory actions precluding observation of either. This outcome is possible if both somatic and dendritic HCN channels are present within BNST neurons and have excitatory and inhibitory influences on neuronal activity, respectively. More statistical power and convergent experimental techniques such as immunoelectron microscopy will be required to rigorously test this hypothesis.

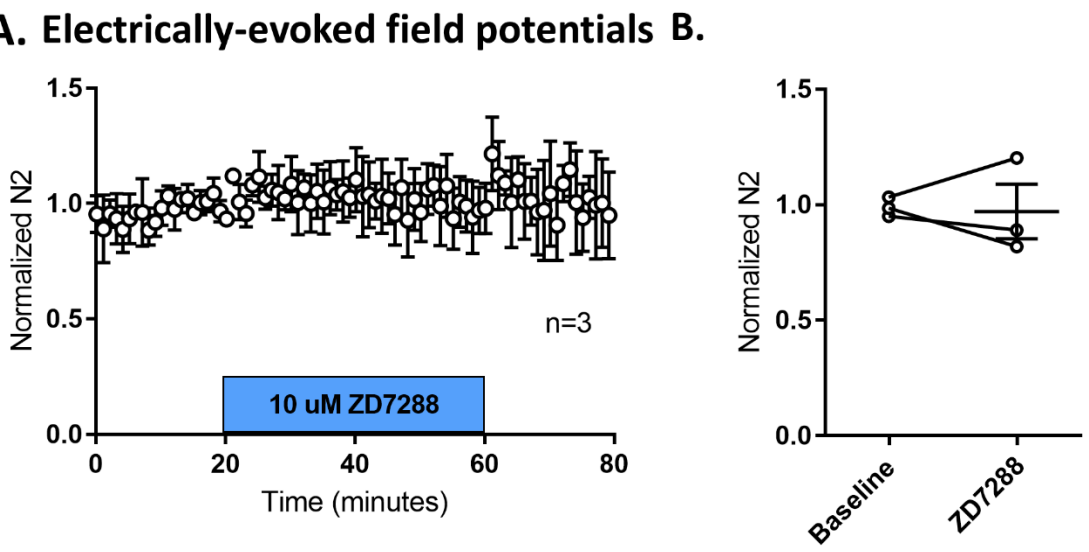

Figure 26: Preliminary data suggests that HCN inhibition by ZD7288 minimally affects electrically-evoked excitatory field potential responses recorded in the BNST. (A). Forty minutes of ZD7288 application led to a 1.9% decrease in the synaptic potential N2 (baseline: 99.0±2.4%; ZD7288: 97.1±11.2%). (B) This effect was not statistically significant (paired t-test, p=0.88; range -18.1% to +20.4%).

Appendix X

Guanfacine enhances the amplitude of spontaneous inhibitory postsynaptic potentials in CRF+ BNST neurons

Corticotropin releasing factor (CRF) is a neuropeptide and hormone that initiates the hypothalamic-pituitary-adrenal (HPA) axis response to stressors (Dedic et al., 2018b). Extra-hypothalamic CRF is additionally known to play a key role in stress- and addiction-related behaviors such as stress-induced reinstatement and binge alcohol drinking (Lowery et al., 2010; Henckens et al., 2016). In general, the CRF system has been heavily implicated as a key mediator of stress-related behaviors in rodents and humans (Le et al., 2000; Marinelli et al., 2007; Pomrenze et al., 2017). The extended amygdala is a key nexus for these actions and CRF therein has been shown to be critical for stress-induced reinstatement of drug-seeking (Erb and Stewart, 1999; Erb et al., 2001) and involved in withdrawal-induced negative affect (Olive et al.,

2002), among other behaviors of interest (Silberman and Winder, 2013; Micioni Di Bonaventura et al., 2014; Albrechet-Souza et al., 2017; Dedic et al., 2018a). Norepinephrine and CRF have been shown to interact in the expression of stress-induced reinstatement (Brown et al., 2009) with norepinephrine signaling hypothesized to engage CRF signaling pathways potentially through modulation of excitatory drive. Recent work has begun to unravel the effects of norepinephrine and other receptor modulators on excitatory drive to BNST CRF neurons (Kash et al., 2008b; Nobis et al., 2011; T. Fetterly, unpublished data), but GABAergic regulation of these neurons has not been as extensively studied (Pleil et al., 2015b; Partridge et al., 2016). Here we aimed to determine the effects of α_{2A}-AR agonism on inhibition of BNST CRF neurons. We hypothesize that guanfacine will enhance inhibition of CRF+ cells, suggesting a role for this population of neurons as the inhibitory interneuron mediating disinhibition of *Adra2a*- BNST cells downstream of *Adra2a*+ BNST neuronal activation.

Whole-cell current-clamp recordings were performed as described above. CRF-tdTomato were bred by crossing CRF-ires-Cre mice with Ai9:Rosa-tdTomato mice as done previously (Silberman and Winder, 2013). Slices were prepared as described above and allowed to recover for one hour prior to recordings. tdTomato+ neurons were readily identified using a mercury lamp light source, RFP filter cube, and infrared video microscopy for patching. All experiments were done in the presence of kynurenic acid to isolate inhibitory transmission. After achieving whole-cell configuration, cells were equilibrated for 2-5 minutes prior to recording. Postsynaptic parameters were monitored continuously during the experiments and cells were excluded if the access resistance (R_a) changed by >20% in either direction. Spontaneous inhibitory postsynaptic potentials were recorded for five minutes prior to guanfacine (1 µM) application. After ten minutes of drug application, guanfacine was washed out.

Guanfacine application enhances inhibition of CRF+ BNST neurons, suggesting a role for α_{2A}-ARs in the regulation of activity of this neuronal population. Specifically, guanfacine application heterogeneously affected sIPSP frequency to yield no group effect (baseline: 2.1±0.3 Hz; guanfacine: 2.3±0.3 Hz, p=0.47; Figure 27A), but consistently increased sIPSP amplitude (baseline: 1.0±0.1 mV; guanfacine: 1.2±0.1 mV; paired t-test, p=0.008; Figure 27B).

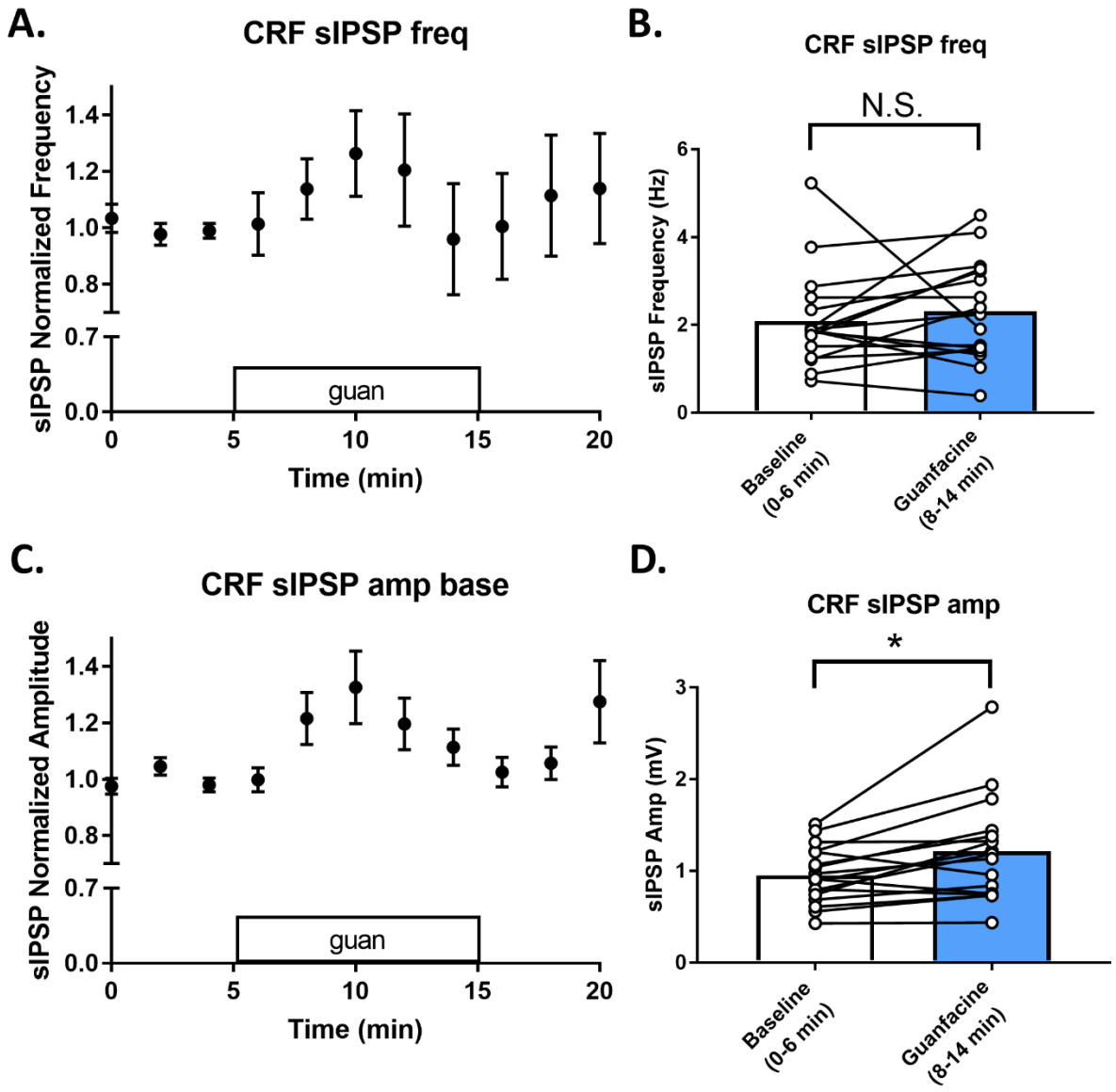

Figure 27: Guanfacine enhances inhibitory tone in CRF+ BNST neurons. (A) The frequency of spontaneous inhibitory postsynaptic potentials were recorded from CRF-tdTomato+ BNST neurons before and after guanfacine application. (B) Guanfacine heterogeneously affected

frequency of sIPSPs in these neurons. (C) The amplitude of sIPSPs was also measured during before, during and after guanfacine application. (D) Guanfacine enhanced sIPSP amplitude in CRF+ BNST neurons.

Enhancement of inhibitory transmission in CRF+ BNST neurons supports the hypothesis that guanfacine activation of *Adra2a+* BNST neurons inhibits CRF+ BNST neurons to disinhibit *Adra2a-Fos+* neurons downstream in the BNST microcircuit. However, the expected result in this model would be increased frequency of sIPSPs and not amplitude, as the former is generally indicative of presynaptic alterations while the latter is generally postsynaptic. The time course of sIPSP frequency suggests an enhancement of sIPSP frequency after guanfacine application but the heterogeneity of effect within CRF+ BNST neurons appears to minimize the impact of this minor enhancement. One possible cause of this is that different populations of BNST CRF+ neurons respond differently to guanfacine. This could be based on neuronal identity, as BNST CRF neurons can be both projection neurons and interneurons, or based on expression of the α_{2A}-AR itself, as approximately half of *Crf+* BNST cells express the *Adra2a* transcript. Future studies could utilize the INTRSECT approach to enrich the CRF+ BNST population for interneurons specifically, as has been done previously (Marcinkiewcz et al., 2016). Independent of mechanism, though, guanfacine robustly and consistently enhances sIPSP amplitude in CRF neurons. The postsynaptic locus of enhancement of inhibitory transmission in BNST CRF cells should first be confirmed by the recording of miniature IPSPs in the presence of tetrodotoxin (TTX), then the mechanism of this effect should be uncovered. Both presynaptic and postsynaptic enhancement of inhibitory transmission could occur through a variety of mechanisms, such as receptor insertion, subunit exchange, and phosphorylation of effector molecules (Farrant and Nusser, 2005). These should be a focus of future studies on inhibitory transmission enhancement by guanfacine in BNST CRF cells. Interestingly, guanfacine has

previously been shown to inhibit electrically-evoked inhibitory postsynaptic currents (eIPSCs) in BNST neurons, suggesting differential effects of α_{2A}-AR agonism on BNST CRF cells specifically (Shields et al., 2009). This highlights the important role of this receptor population in modulating and controlling aspects of BNST neuronal signaling in general and CRF signaling in particular.

Appendix XI

Full- and heteroceptor-specific α_{2A}-AR knockout mice show atypical stress-induced cfos responses relative to wildtype littermates

Stress activates BNST neurons (Sharp et al., 1991; Campeau and Watson, 1997; Martinez et al., 1998; Figueiredo et al., 2003; Day et al., 2004; Sterrenburg et al., 2012) and induces release of norepinephrine into the region (Pacak et al., 1995). As a result, norepinephrine mediates its effects through α_1-ARs, α_2-ARs, and β-ARs, each of which initiates signaling cascades within neurons or terminals within the region (Flavin and Winder, 2013). After release, norepinephrine binding to autoreceptor α_{2A}-ARs directly inhibits norepinephrine release into the BNST and indirectly inhibits heteroceptors adrenergic receptor actions as a result of this inhibition. The α_{2A}-AR knockout mouse thus shows elevated baseline norepinephrine levels and potentially desensitized adrenergic receptors as a result (Lakhlani et al., 1997; Lahdesmaki et al., 2002; Davies et al., 2003; McElligott and Winder, 2008; Flavin, 2014). The α_{2A}-AR knockout mouse additionally displays a number stress-related phenotypes in anxiety- and depression-like behavioral tests (Lakhlani et al., 1997; Schramm et al., 2001; Lahdesmaki et al., 2002; Davies et al., 2003). Rescue of α_{2A}-AR autoreceptors by reintroduction of the *Adra2a* gene downstream of the dopamine-β-hydroxylase promoter (DβH) has been shown to rescue a number of phenotypes

including agonist-induced analgesia, hypothermia, sedation, anesthesia-sparing, bradycardia, and hypotension (Gilsbach et al., 2009). However, the stress-related neuropsychiatric phenotypes and associated changes in BNST physiology have been minimally explored in the autoreceptor rescue mouse. Here, we aim to determine whether stress-induced activation of BNST neurons is affected by full- and heteroceptors-specific knockout of the α_{2A}-AR by continuing our analysis of cfos expression in these mice. Further, we evaluate guanfacine effect on recruitment of stress signaling pathways by pretreating mice prior to restraint stress.

Fluorescence immunohistochemistry was performed as described above. Briefly, mice were handled for five days to minimize handling stress. Mice were injected with either saline guanfacine at time zero. If in a stress group, at thirty minutes mice were placed in a 30 mL conical tube with air holes for thirty minutes before placement back in the home cage for thirty more minutes. At this point, mice were perfused with 10 mL PBS and 20 mL 4% PFA followed by brain extraction. Brains were then fixed in PFA, cryoprotected in 30% sucrose in PBS, and cut on a cryostat into 40 um coronal sections. These sections were then stained for cfos and NeuN, imaged on a confocal microscope, and counted by a blinded reviewer.

Effects of treatment and genotype on cfos expression after stress or guanfacine were assessed (Figure 28). A two-way ANOVA showed significant effects of genotype ($F(2,147)=3.5$, $p=0.03$), treatment ($F(3,147)=10.2$, $p<0.0001$), and an interaction between the two ($F(6,147)=4.2$, $p=0.0007$). For the sake of clarity, we will separate comparisons between those within genotypes and those across genotypes. In wild-type animals, all conditions led to an upregulation of cfos relative to saline injection (Holm-Sidak; saline: 4.4±0.9% cfos+ NeuN cells; guanfacine: 14.2±1.4%, $p=0.02$; stress: 27.3±6.2%, $p<0.0001$; guanfacine + stress: 24.0±6.7%, $p=0.0001$). Interestingly, guanfacine-induced cfos expression was less than that invoked by stress

alone (p=0.001) or stress and guanfacine together (p=0.04). Stress-induced cfos was not different with either saline or guanfacine injection (p=0.47). In knockout animals, on the other hand, there was not significant upregulation of cfos in any of the groups (Holm-Sidak; saline: 13.5±1.3%; guanfacine: 9.0±0.6%, p=0.37; stress: 19.6±5.6%, p=0.41; guanfacine + stress: 20.2±5.4%, p=0.33), nor any difference between guanfacine- and stress-induced cfos regardless of whether they were both given alone (p=0.23) or in combination relative to guanfacine alone (p=0.07) or stress alone (p=0.91). Similarly, in heteroceptor-specific knockout animals, there was no effect on cfos expression relative to saline in any treatment (Holm-Sidak; saline: 8.8±1.6%; guanfacine: 11.7±1.4%, p=0.75; stress: 10.2±2.1%, p=0.88; guanfacine + stress: 17.2±1.1%, p=0.48), or between the guanfacine and stress conditions (guanfacine v stress, p=0.23; guanfacine v guanfacine + stress, p=0.75; stress v guanfacine + stress, p=0.67).

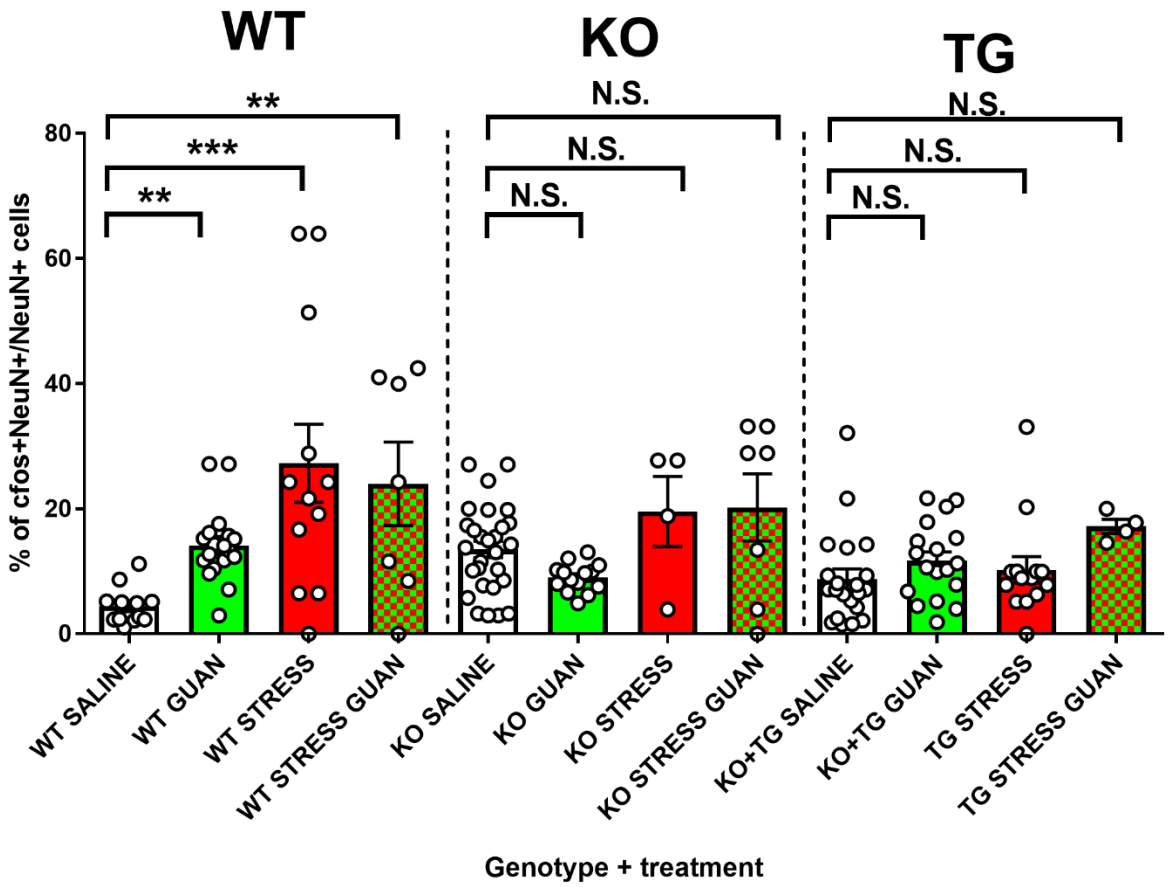

Figure 28: Responsivity to guanfacine and stress are dysfunctional in full- and heteroceptor-specific α_{2A}-AR knockout mice. Full- and heteroceptor-specific α_{2A}-AR knockout mice were either injected with saline or guanfacine and either restrained for thirty minutes or were kept in their home cage. Upregulation of cfos in all conditions was seen in wild-type littermates relative to saline injection, while no difference was observed between any groups in knockout or transgenic animals, suggesting norepinephrine signaling dysfunction.

This panel of data suggests that stress responsivity is absent in the full *Adra2a*-/- animal and is not rescued by reintroduction of autoreceptor α_{2A}-ARs, although more animals are required to ensure statistical power is sufficient in each of the groups. The repercussions of this for anxiety-like behaviors and stress-induced reinstatement should be investigated further through neuropsychiatric behavioral phenotyping of these mice. Further, a lack of guanfacine

inhibition of stress recruitment in any group suggests lack of anxiolytic activity in this context, although postsynaptic α_{2A}-ARs and guanfacine-induced cfos expression at this locus likely confounds this interpretation in wild-type animals. Guanfacine responsivity of behavioral phenotypes should be assessed, in addition to modulation by both adrenergic and non-adrenergic anxiolytics such as β-AR antagonists and benzodiazepines, for example. As we learn more about the pharmacology and physiology of auto and heteroceptor α_{2A}-ARs within the BNST and beyond, it will be important to consider baseline differences such as these when evaluating phenotypes of interest.

Appendix XII

A cell type-specific analysis of transcript profiles within subpopulations of BNST neurons

The bed nucleus of the stria terminalis is a heterogeneous region of the brain composed of many different cell types (Lebow and Chen, 2016; Nguyen et al., 2016). As cell-specific recording modalities and means of manipulation have increased, our understanding of the physiological significance of this heterogeneity has increased. Here we aim to use RNA *in situ* hybridization to sub-classify BNST neurons based on transcript expression and analyze co-expressed transcripts to gain insight into physiology and function. We have successfully utilized this tool to identify a new subpopulation of BNST neurons that express the *Adra2a* transcript and observed that a majority of *Adra2a*+ BNST cells co-express *Hcn2* transcripts but not *Hcn1, Crf, Prkcd, Npy, Calb2,* and *Penk*. Further, *Adra2a*+ BNST cells co-express *Fos* after guanfacine injection, suggesting activity enhancement. For further discussion of *Adra2a*+ cells, see Chapter II. Here we will describe transcript expression for each of these transcripts in addition to *Hcn4* and *Arc*, as well as their patterns of co-localization. The rationale for analysis of each of these transcripts is described for each transcript individually below.

RNA *in situ* hybridization procedures were performed as described above. Briefly, mice were handled for five days prior to brain extraction and flash freezing. For all experiments, mice were allowed to acclimate after transport from the vivarium for one hour to reduce the effects of transport stress on transcript expression within the BNST. For experiments involving co-localization of the *Fos* transcript, animals were injected with saline or guanfacine 90 minutes prior to brain extraction. BNST sections (16 µm thick) were cut on a cryostat and underwent the RNAScope staining procedure. Both experimental and negative control slices were processed, and the latter was used to determine threshold positivity for the former. Slices were imaged on a confocal microscope and transcripts per cell were counted by a blinded reviewer. We present data here as a sum of the three images taken at high magnification of the oval, dorsolateral, and dorsomedial subnuclei of the BNST due to the lack of substantial differences in expression patterns throughout these regions.

We first determined the size of the different BNST transcript-expressing cell populations (Figure 29A). The newly identified *Adra2a*+ population represents 27.1±3.6% of DAPI+ cells, while the other genetic markers range from 8.0±1.1% (*Npy*) to 51.6±11.2% (*Hcn2*) (*Prkcd*: 28.3±4.8%; *Crf*: 15.0±6.8%; *Hcn4*: 36.3±4.0%; *Hcn1*: 15.3±4.7%). In addition, we looked at whether guanfacine treatment affected the number of cells within transcript-expressing cell populations (Figure 29B). Of these, only the *Fos*+ population of cells increased in size after guanfacine treatment (*Fos,* saline: 11.6±3.3%, guanfacine: 23.2%, p=0.04; *Adra2a,* saline: 30.3±3.6% DAPI+ cells, guanfacine: 27.4±3.2%, p=0.21; *Prkcd,* saline: 17.3±2.8%, guanfacine: 22.0±7.0%, p=0.50; *Penk,* saline: 30.3±2.6, guanfacine: 41.9±4.0, p=0.07; *Calb2,* saline:24.6±9.1, guanfacine: 18.0±4.7%, p=0.10; *Arc,* saline: 14.0±3.1%, guanfacine: 38.0±13.4%, p=0.11), although some trended towards an increase (*Prkcd, Penk, Arc*) and others

a decrease (*Calb2, Adra2a*). Future studies should aim to corroborate and extend these findings with more statistical power.

Next, we evaluated the extent of co-localization between pairs of transcripts. We will classify extent of co-localization into thirds and label the extent as low (0-33.3%), intermediate (33.4-66.6%), or high (66.7-100%) based on the mean proportion of positive cells. We first evaluated co-localization in BNST neurons expressing transcripts for the pacemaker channel subunits *Hcn1, Hcn2,* and *Hcn4*. Each of these subunits is known to be expressed within the BNST (Monteggia et al., 2000; Notomi and Shigemoto, 2004) and to show cell-specific expression patterns based on electrophysiological subtyping (Hammack et al., 2007; Hazra et al., 2011; Daniel et al., 2017). Cell-type specific expression patterns were determined by current clamp analyses of electrophysiological response to positive and negative current injection and single cell PCR. Specifically, this showed that Type I BNST neurons are characterized by hyperpolarization sag and a regular firing pattern alongside expression of *Hcn2* and *Hcn4* subunits, Type II neurons are characterized by hyperpolarization sag but a burst firing pattern alongside expression of all four HCN channel subunits, and Type III neurons are characterized by a lack of hyperpolarization sag and fast inward rectification alongside express of *Hcn4* only. Here we show that *Hcn1*+ BNST cells express intermediate-to-high levels of *Adra2a* (62.2±6.3% co-expression) alongside low levels of *Prkcd* (24.3±7.3% co-expression) (Figure 29D). High expression of *Adra2a* is unexpected given that *Hcn1*+ are only a minority of *Adra2a*+ cells. We have shown *Prkcd* to be a marker of oval subnucleus specificity, so minimal overlap with this transcript suggests that *Hcn1* transcripts are less likely to be expressed in this region. In both *Hcn2*+ and *Hcn4*+ BNST cells, extent of co-localization with *Adra2a* was low-to-intermediate (*Hcn2*: 32.4±4.2%; *Hcn4*: 30.2±21.0) while co-localization was lower with *Prkcd* (*Hcn2*:

27.5±6.5%; *Hcn4*: 12.2±6.7%). This level of *Adra2a* expression in *Hcn2*+ BNST cells contrasts with high levels of *Hcn2* expression in *Adra2a*+ BNST cells, suggesting the potential for differential actions in neuronal subpopulations. An immunoelectron microscopic map of HCN2 expression within the BNST in addition to functional studies on a cell-specific basis would inform our understanding of channel function. Lack of overlap between both *Hcn2* and *Hcn4* with *Prkcd* similarly suggests non-oval expression patterns. Finally, *Hcn4* expression is low in *Adra2a*+ BNST cells, although with significant variability (Figure 29F; 27.2±20.4%). Intermediate-to-low levels of *Adra2a* in *Hcn4*+ BNST cells and low levels of *Hcn4* in *Adra2a*+ cells suggests a lack of interaction between these proteins. The function of BNST-expressed HCN4 channels either alone or in heteromers with other subunits remains unclear.

We additionally investigated transcript expression within subsets of BNST neurons positive for a number of genetic markers that could be used for cell-specific targeting with the Cre-Lox system. Specifically, we evaluated transcripts within BNST cells positive for *Prkcd*, *Calb2*, *Penk*, *Crf*, and *Npy* (Figures 28G-K). *Prkcd* is the transcript that encodes protein kinase Cδ (PKCδ). This gene was identified during a microarray analysis for amygdala-enriched genes and was determined to be expressed in 50% of neurons in the lateral subdivision of the central nucleus of the amygdala (CeAL) (Zirlinger et al., 2001; Zirlinger and Anderson, 2003). In the CeA, *Prkcd*+ neurons are inhibited by conditioned stimuli in a fear conditioned paradigm and thus counteract the effects of CRF neurons therein (Haubensak et al., 2010). Additionally, *Prkc*+ CeA neurons are implicated in feeding and anxiety-like behaviors (Cai et al., 2014; Botta et al., 2015). In the BNST, *Prkcd*+ neurons are localized to the oval subnucleus and we hypothesized that their actions would similarly complement the anxiogenic effects of the guanfacine-inhibited CRF+ BNST neurons. Lack of expression in *Adra2a*+ cells suggests otherwise. In co-localizing

Prkcd with other transcripts, though, we see intermediate expression levels of *Adra2a* (41.0±4.4%), low levels of *Hcn1* (15.7±7.4%), and intermediate levels of *Hcn2* (53.9±11.6%). Lack of co-expression with *Hcn1* with intermediate levels of *Hcn2* suggests that *Prkcd*+ BNST neurons may be Type I neurons and not Type II neurons, the physiological significance of which is unclear. Intermediate co-expression with *Adra2a* and *Hcn2* suggests that some but not all *Prkcd*+ neurons may be guanfacine-activated, consistent with the observation that *Prkcd*+*Adra2a*+ neurons and *Prkcd*-*Adra2a*+ neurons are both approximately equally activated by guanfacine exposure (data not shown).

Finally, we looked at the expression levels of *Adra2a* in a number of genetically-defined subpopulations of BNST neurons, each of which was shown to only make up a minority of *Adra2a*+ cells. Interestingly, intermediate levels of *Adra2a* are present in *Calb2*+ (38.9±11.8%), *Penk*+ (38.3±7.3%), *Crf*+ (51.7±7.6%), and *Npy*+ (34.4±4.7%), suggesting that α_{2A}-AR agonism or antagonism would not be a specific way to directly modulate the activity of these cells, although indirect actions remain viable. *Calb2* encodes for calbindin-2, a calcium-binding protein that has been shown to be critically involved in synaptic plasticity (Schmidt, 2012) and responsive to either chronic stress (Iacopino and Christakos, 1990; Krugers et al., 1996; Nowak et al., 2010) or drug exposure (Tirumalai and Howells, 1994; Garcia et al., 1996; Yin et al., 2010). Stress responsivity of expression has specifically been shown to occur within the BNST (Gos et al., 2014) and loss of calbindin-2 increases anxiety-like behaviors (Harris et al., 2016; Li et al., 2017). However, lack of robust *Adra2a* expression in *Calb2*+ cells and lack of *Calb2* expression in *Adra2a*+ cells suggests that modulation of anxiety-like behavior via α_{2A}-AR agonism does not occur directly through modulation of *Calb2*+ BNST cells. Similarly, the *Penk* transcript encodes for proenkephalin, an endogenous opioid peptide agonist for the δ and μ

opioid receptors involved in analgesia and stress resilience (Inturrisi et al., 1980; Henry et al., 2017, 2018). This peptide is expressed in BNST neurons as well as in afferent populations (Gros et al., 1978). Enkephalin and related peptides generally inhibit BNST neurons (Westheimer, 1981; Dalsass and Siegel, 1990; Wilson and Ingram, 2003) but the functional effects of activated signaling pathways on behavior have been minimally investigated (Brutus et al., 1988). Here we show lack of robust *Adra2a* expression in *Penk*+ BNST cells in addition to lack of *Penk* expression in *Adra2a*+ BNST cells, suggesting a minimal direct interaction.

Next, we evaluated *Adra2a* transcript expression in and co-localization between the BNST neuronal populations positive for the transcripts encoding corticotropin releasing factor (*Crf*) and neuropeptide Y (*Npy*). In general, the CRF system has been heavily implicated as a key mediator of stress- and addiction-related behaviors in rodents and humans (Le et al., 2000; Marinelli et al., 2007; Lowery et al., 2010; Henckens et al., 2016; Pomrenze et al., 2017). The extended amygdala has been shown to be a key nexus for these actions (Erb and Stewart, 1999; Erb et al., 2001; Olive et al., 2002; Silberman and Winder, 2013; Micioni Di Bonaventura et al., 2014; Dedic et al., 2018a). Unexpectedly, *Adra2a* expression is intermediate-to-high in *Crf*+ BNST cells, suggesting potential modulation of neuronal activity by guanfacine and other α_2-AR agonists. Here we additionally show that guanfacine enhances inhibitory transmission in CRF+ BNST neurons, extending prior data showing inhibitory effects on excitatory drive. Future studies should aim to classify α_{2A}-AR receptor subpopulations in CRF+ BNST neruons and determine functional effects of modulation.

Neuropeptide Y (NPY) and CRF signaling pathways have generally been shown to have competing effects on both behavior and neuronal activity (Kash and Winder, 2006; Gilpin, 2012a; Ide et al., 2013). While the effects of CRF induce anxiety-like behaviors and promote

stress-induced addictive behaviors, NPY induces long-term resilience to stress-related behaviors (Sajdyk et al., 2008; Sah and Geracioti, 2012; Sabban et al., 2015; Reichmann and Holzer, 2016; Tasan et al., 2016) and blocks the transition to alcohol dependence and related behaviors in rodent models of addiction (Gilpin et al., 2008, 2011; Gilpin, 2012b; Sparrow et al., 2012). Some of these effects have similarly been localized to the BNST (Pleil et al., 2012, 2015b). Direct interactions between α_{2A}-AR agonism and NPY+ neuronal modulation is unlikely given relatively low expression of *Adra2a* in *Npy*+ BNST cells and *Npy* in *Adra2a*+ BNST cells. Supporting the hypothesis of CRF and NPY having complementary roles in physiology and behavior, *Npy* was minimally expressing in *Crf*+ BNST cells (9.4±1.9%) and *Crf* was similarly minimally expressed in *Npy*+ BNST cells (16.1±6.2%).

Together, these data suggest that *Adra2a* and resultant α_{2A}-AR expression is variable among populations of BNST neurons defined by expression of genetic markers. To determine the physiological and behavioral relevance of expression within these various subpopulations, future studies should utilize the floxed *Adra2a* mouse line that knocks down expression in specific neuronal populations after exposure to Cre recombinase (Caron et al., 2018). Using Cre driver lines for the genes described here or viral injection of Cre-encoding constructs will allow for cell- and subpopulation-specific contributions of *Adra2a* and α_{2A}-AR expression to physiology and behaviors of interest to be ascertained.

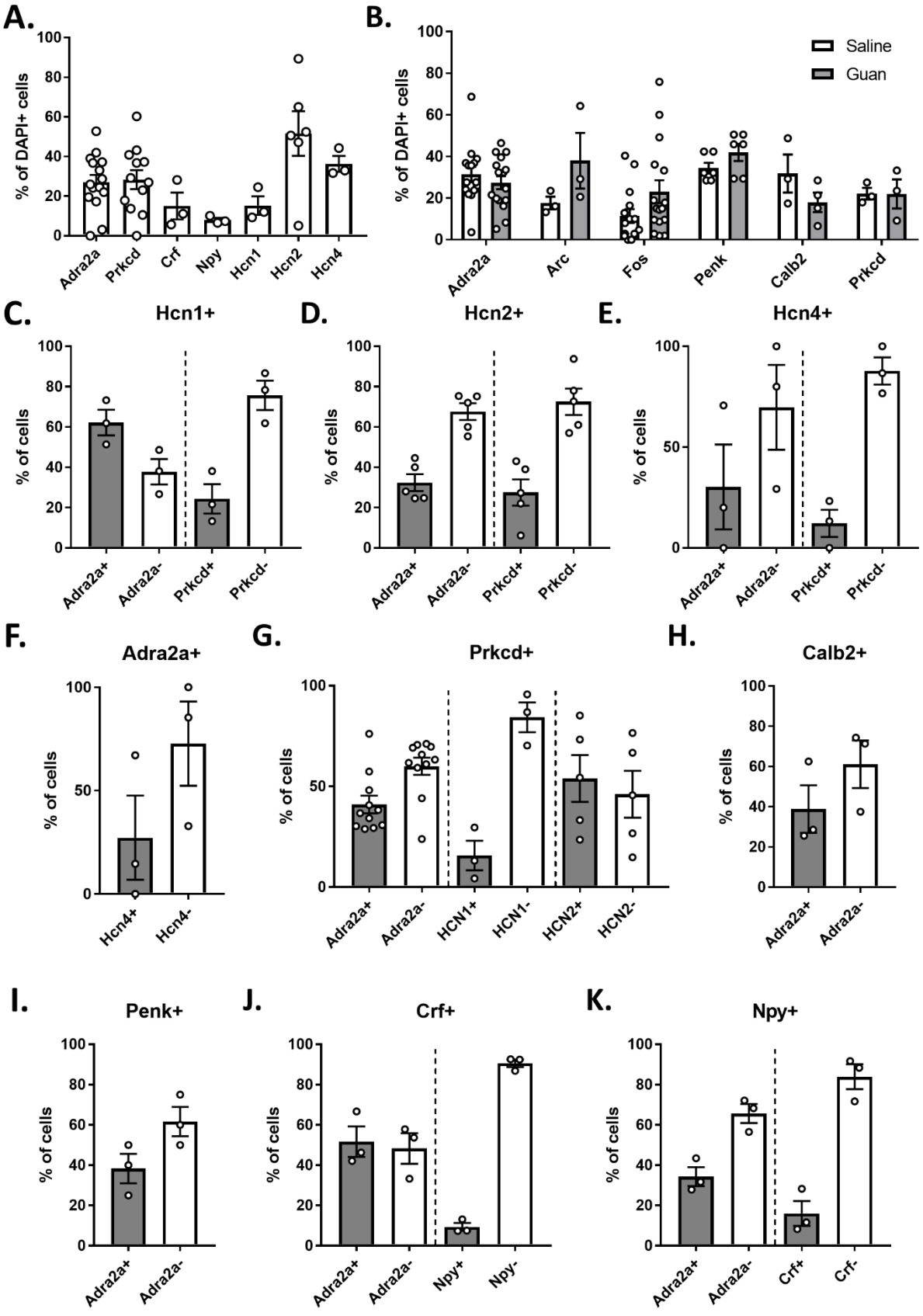
A.
% of DAPI+ cells
Adra2a
Prkcd
Crf
Npy
Hcn1
Hcn2
Hcn4
B.
Saline
Guan
% of DAPI+ cells
Adra2a
Arc
Fos
Penk
Calb2
Prkcd
C.
Hcn1+
% of cells
Adra2a+
Adra2a-
Prkcd+
Prkcd-
D.
Hcn2+
% of cells
Adra2a+
Adra2a-
Prkcd+
Prkcd-
E.
Hcn4+
% of cells
Adra2a+
Adra2a-
Prkcd+
Prkcd-
F.
Adra2a+
% of cells
Hcn4+
Hcn4-
G.
Prkcd+
% of cells
Adra2a+
Adra2a-
HCN1+
HCN1-
HCN2+
HCN2-
H.
Calb2+
% of cells
Adra2a+
Adra2a-
I.
Penk+
% of cells
Adra2a+
Adra2a-
J.
Crf+
% of cells
Adra2a+
Adra2a-
Npy+
Npy-
K.
Npy+
% of cells
Adra2a+
Adra2a-
Crf+
Crf-

Figure 29: Transcript analysis in BNST neuronal subpopulations. (A) Percentage of DAPI+ cells that express the transcripts *Adra2a*, *Prkcd*, *Crf*, *Npy*, *Hcn1*, *Hcn2*, and *Hcn4*. (B) Guanfacine-responsivity of transcript expression relative to saline injection for the transcripts *Adra2a*, Arc, *Fos*, *Penk*, *Calb2*, and *Prkcd*. Only *Fos* showed a significant upregulation in response to guanfacine injection. (C-K) Transcript analysis showing extent of expression of alternative transcripts in *Hcn1*+ (C), *Hcn2*+ (D), *Hcn4*+ (E), *Adra2a*+ (F), *Prkcd*+ (G), *Calb2*+ (H), *Penk*+ (I), *Crf*+ (J) and *Npy*+ (K) BNST cells.

Additionally, we evaluated guanfacine responsivity of transcript co-localization within subpopulations of BNST neurons (Figure 30). Previously, we showed that *Adra2a*+ cells increasingly express *Fos* after guanfacine injection, suggesting an intracellular-mediated mechanism (Figure 30A). Here we show that guanfacine treatment does not affect co-expression of *Prkcd* (saline: 22.2±1.8%; guanfacine: 30.2±2.6%; unpaired t-test, p=0.07), *Calb2* (saline: 23.9±9.7%; guanfacine: 38.4±17.8%; unpaired t-test, p=0.56), *Penk* (saline: 25.6±8.5%; guanfacine: 45.4±5.5%; unpaired t-test, p=0.13), or *Arc* (saline: 30.6±7.3%; guanfacine: 70.0±12.2%; unpaired t-test, p=0.06) in these cells in a statistically significant manner, although interesting trends emerged that should be followed up with additional statistical power. Specifically, upregulation of *Arc*, an immediate early gene that encodes for the activity-regulated cytoskeleton-associated protein (Arc) that has been previously implicated in synaptic plasticity and learning and memory (Lyford et al., 1995; McIntyre et al., 2005), could have functional implications for the molecular effects of long term drug use on plasticity within the BNST.

Similar analyses were performed on *Fos*+, *Arc*+, *Prkcd*+, *Calb2*+, and *Penk*+ BNST cells. There were no statistically significant changes among any of these populations, potentially due to lack of statistical power, but interesting trends are suggested by the data. Here we will report the directionality of the trends for the sake of clarity even without statistical trends being present in all cases. *Fos*+ neurons trend towards being more likely to express *Adra2a* (saline: 37.3±7.6%; guanfacine: 49.7±9.0; unpaired t-test; p=0.31), *Prkcd* (saline: 10.7±10.7%;

guanfacine: 29.0±10.0%; p=0.28), *Calb2* (saline: 24.1±11.0%; guanfacine: 57.3±17.3%; p=0.26) and *Arc* (saline: 29.5±6.8%; guanfacine: 61.8±15.7%; p=0.17) after guanfacine relative to saline injection while slightly less likely to express *Penk* (saline: 48.3±15.9%; guanfacine: 35.9±18.3%; p=0.63) (Figure 30B). Similarly, *Arc*+ BNST neurons show increased value but no statistical difference relative to saline injection with respect to co-localization with *Adra2a* (saline: 40.7±12.4%; guanfacine: 59.3±12.4%; p=0.35) and *Fos* (saline: 33.3±21.5%; guanfacine: 63.5±10.1%; p=0.30) (Figure 30C). As more work is done to identify, isolate and study guanfacine-activated neurons, transcript co-localization such as this may inform our understanding of both guanfacine-activated neurons and those that are active at baseline.

We also evaluated the effect of guanfacine exposure on activity within three genetically defined subpopulations of neurons: *Prkcd*+, *Calb2*+, and *Penk*+. All three populations responded similarly to guanfacine injection, with minimal changes in *Adra2a* expression (*Prkcd*: saline=35.3±2.3%, guanfacine=31.4±12.7%, p=0.79; *Calb2*: saline=38.9±11.8%, guanfacine=52.5±26.6%, p=0.70; *Penk*: saline=24.2±6.5%, guanfacine=33.9±6.6%, p=0.35) and nonsignificant upregulation of *Fos* (*Prkcd*: saline=8.9±8.9%, guanfacine=53.8±19.8%, p=0.14; *Calb2*: saline=21.4±5.1%, guanfacine=45.7±16.1%, p=0.36; *Penk*: saline=4.9±0.9%, guanfacine=9.3±5.2%, p=0.48) within the population. Interestingly, *Penk*+ BNST cells appear to be minimally active under both saline- and guanfacine-injected conditions. These results will hopefully inform future experiments as more recordings and behavioral manipulations are done on these genetically-defined subpopulations of BNST neurons.

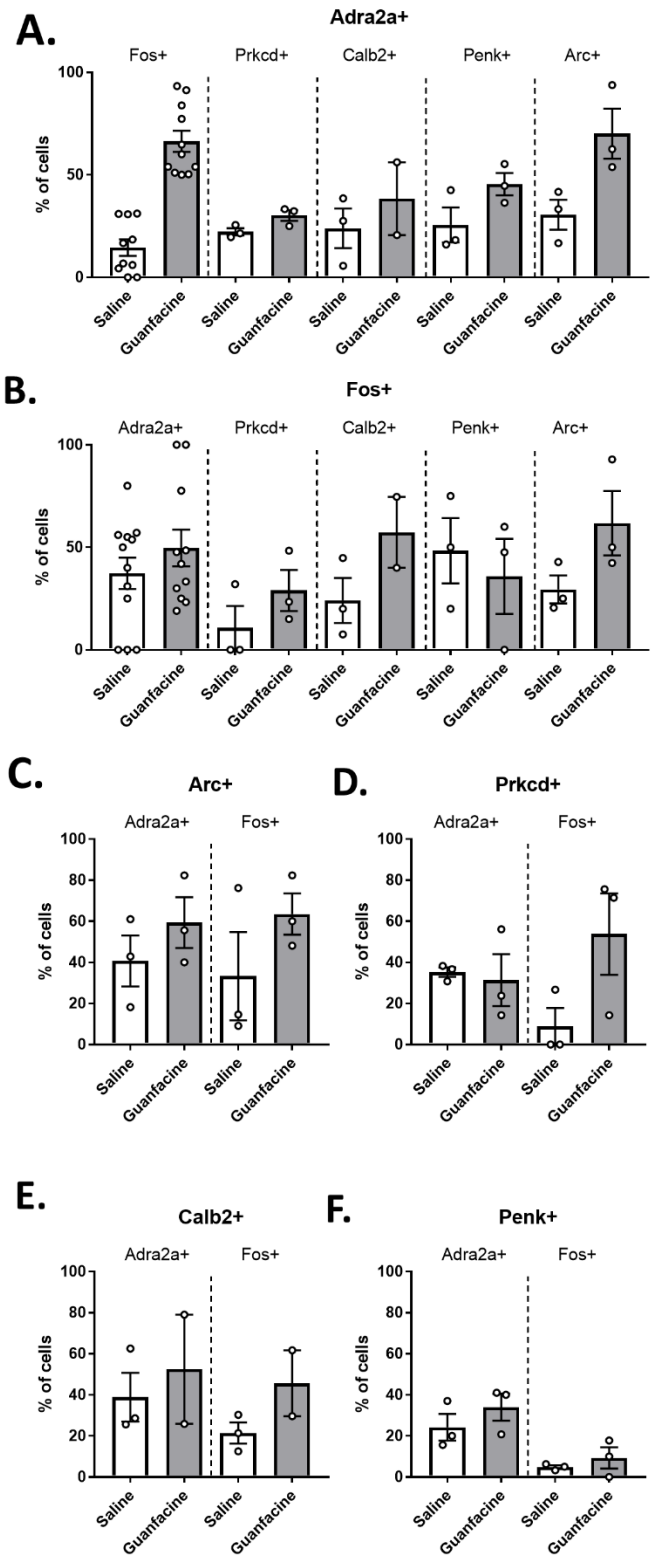

Figure 30: Guanfacine-initiated changes in transcription across different BNST subpopulations. (A-E) Guanfacine-induced transcriptional changes were minimal across co-localization in

Adra2a+ (A), *Fos+* (B), *Arc+* (C), *Prkcd+* (D), *Calb2+* (E), and *Penk+* (F) BNST cells. Specific changes in expression of *Adra2a, Prkcd, Calb2, Penk, Arc,* and *Fos* are shown in a subset of these cells.

This experimental data set, although limited in statistical power and conclusions, informs our understand of transcript expression and co-localization within the BNST. As our understanding of the molecular changes that occur in the BNST after chronic stress or drug use, identifying cell-specific targets and transcriptional changes will aid the development of targeted interventions to correct for deranged molecular signaling pathways. The work presented here represents a stepping stone towards that end goal.

Appendix XIII

Preliminary data suggests that non-validated ablation of CGRP+ parabrachial nucleus neurons does not affect BNST electrically-evoked field potential inhibition by guanfacine

Calcitonin gene related peptide (CGRP) is a neuropeptide that has been shown to be involved in pain, vasodilation, metabolism, and itch (Russell et al., 2014; Iyengar et al., 2017; Hendrikse et al., 2018). The parabrachial nucleus (PBN) contains neurons that express CGRP and is similarly implicated in physiological processes such as pain, thirst, fear, and feeding (Campos et al., 2018; Palmiter, 2018). The PBN is one of only a few regions of the brain that express the neuropeptide calcitonin gene-related peptide (CGRP). CGRP+ projections from the PBN to the BNST are hypothesized to play a role in anxiety-like behaviors, as CGRP injection into the BNST elicits anxiogenesis (Sink et al., 2011, 2013a) and CGRP receptor antagonists block these effects (Sink et al., 2013b). CGRP+ positive neurons from the PBN project to the extended amygdala and form axosomatic synapses that are hypothesized to be analogous to the detonator synapses between climbing fibers and Purkinje neurons in the cerebellum (Shimada et al., 1989; Dobolyi et al., 2005). This projection bidirectionally modulates BNST neuronal

activity, with half of neurons showing monosynaptic excitation and half showing feedforward inhibition (Flavin et al., 2014). Interestingly, guanfacine inhibits PBN stimulation-induced excitation but variably affects inhibition. Similarly to optically-evoked excitatory postsynaptic currents (oEPSCs) elicited from stimulation of PBN terminals within the BNST, guanfacine inhibits nonspecific electrically-evoked EPSCs (eEPSCs). We hypothesize that PBN inhibition drives inhibition of excitatory neurotransmission due to the axosomatic and instructive nature of these synapses. To test this hypothesis, we utilized a transgenic mouse line that expresses the diphtheria toxin receptor (DTR) downstream of the CGRPα promoter upon exposure to Cre recombinase (McCoy et al., 2012). After systemic injection of diphtheria toxin (DTX), cell-specific ablation will occur in CGRP+ neurons expressing Cre. The necessity of CGRP+ PBN neurons for guanfacine inhibition of electrically-evoked excitatory field potentials within the BNST could thus be assessed.

Viral injections and electrically evoked field potential recordings were performed as described above. Briefly, CGRPα-GFP-*fl*-stop-*fl*-DTR mice were unilaterally injected with AAV9-CMV-Cre:GFP into one parabrachial nucleus and sham injected into the other parabrachial nucleus (AP: -5.34 mm, ML: +/-1.31 mm, DV: -3.37 mm) (Paxinos and Franklin, 2004), both at a 15.03° angle. Three weeks after surgery, mice were injected with DTX (100 mg/kg) three times over a period of five days and then given at least one week to recover. BNST coronal brain slices (300 µm thick) were then prepared and allowed to recover for one hour before recording. All experiments were done in the presence of picrotoxin (25 µM) to isolate excitatory transmission. Electrical stimulation was passed through a nichrome wire in the stria terminalis, eliciting a response consisting of a fiber volley potential (N1) and a synaptic potential

(N2). Stimulation occurred every 10 seconds. Data was excluded if the N1 changed by >20% during the experiment.

Unilateral ablation of the PBN minimally affected guanfacine inhibition of electrically evoked excitatory field potentials recorded in the BNST (two-way ANOVA; treatment: effect $F(479,3360)=1.0$, $p=0.32$; time effect: $F(479,3360)=1.3$, $p=0.0002$; interaction effect: $F(479,3360)=0.7146$, $p>0.999$; Figure 31). In recordings from BNST where CGRP+ PBN input is unaltered, guanfacine inhibited N2 amplitude to 89.6±9.3% of baseline, although this effect did not reach statistical significance (paired t-test, $p=0.36$. In recordings from BNST where CGRP+ PBN input is ablated, guanfacine inhibited the N2 amplitude to 83.9±5.6% of baseline (paired t-test, $p=0.01$). The difference between slices where CGRP+ PBN was ablated or maintained was not statistically different (unpaired t-test, $p=0.59$). Due to the endogenous GFP expressed in CGRP+ cell bodies and the exogenous virally-expressed GFP, we were unable to validate the ablation of these terminals, so all conclusions drawn from this data must be tentative and replicated.

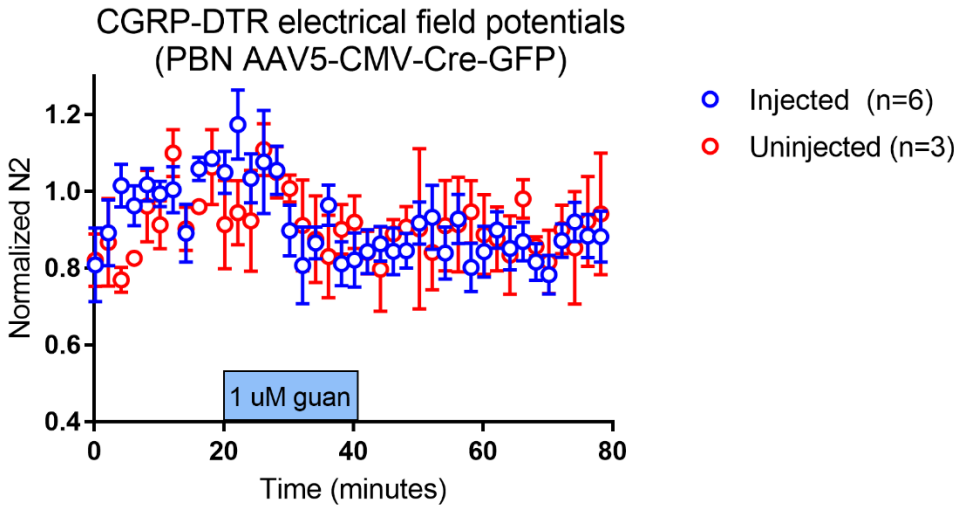

Figure 31: Ablation of CGRP+ parabrachial nucleus does not affect guanfacine-induced inhibition of electrically evoked excitatory field potentials in the BNST. Viral introduction of Cre recombinase (AAV9-CMV-Cre:GFP) to one parabrachial nucleus of mice expressing a floxed

stop codon upstream of the coding sequence for diphtheria toxin receptor leads to expression of this receptor in these neurons and subsequent ablation in the presence of diphtheria toxin. Ablation of these CGRP+ neurons in the parabrachial nucleus did not affect electrically evoked excitatory field potentials observed in the BNST, although validation of knockdown was not performed and the experiment may require additional statistical power.

A lack of effect in this experiment suggests that our hypothesis regarding the recruitment and inhibition of parabrachial nucleus afferents by α_{2A}-AR agonism after electrical stimulation is incorrect. If true, this would mean that other guanfacine-sensitive glutamatergic inputs to the BNST are recruited by electrical stimulation of the stria terminalis. The glutamatergic input from the basolateral amygdala is guanfacine-insensitive while that from the insular cortex is guanfacine-sensitive and thus a candidate region for this effect (Flavin, 2014; Flavin et al., 2014). Alternatively, experimental limitations may preclude a confident rejection of the null hypothesis. First, validation of ablation needs to be confirmed. This can be done by introduction of a Cre recombinase with an alternative fluorophore (AAV5-CaMKII-Cre:mCherry). Second, additional experiments need to be performed on effects on electrophysiological measures in the BNST to have appropriate statistical power. Only after these additions can the hypothesis of parabrachial recruitment can be confidently assessed.

Appendix XIV

Pharmacological effects on optically evoked excitatory postsynaptic and field potentials in the Thy1-COP4 transgenic mouse line

The Thy1-COP4 transgenic mouse line (line 9) expresses a transgene encoding channelrhodopsin-2 (ChR2) under the control of the thymus cell antigen 1 (Thy1) promoter randomly inserted into the genome, which as a result leads to expression within subsets of projection neurons across the brain, including neurons from the cortex, hippocampus, thalamus, midbrain, brainstem, cerebellar mossy fibers, and retinal ganglion cells (Arenkiel et al., 2007).

Importantly, this mouse line has been shown to minimally express ChR2 in dBNST neurons and shows little to no co-localization of ChR2 with calcitonin gene-related peptide (CGRP), a high fidelity marker of the guanfacine-inhibited parabrachial nucleus afferents within the dBNST (Flavin et al., 2014). This unique expression profile allowed for us to determine effects of α_{2A}-AR beyond inhibition of glutamate release from parabrachial nucleus terminals and unmask excitatory actions from postsynaptic receptor subpopulations (Flavin et al., 2014). Further, HCN inhibition by ZD7288 mimicked guanfacine action and enhanced excitatory field potential responses to optical stimulation in the BNST of these mice. We aimed to further characterize guanfacine responsivity in this mouse line and test mechanism by pharmacological manipulations design to block or mimic excitatory effects.

Optically evoked postsynaptic and field potential recordings were performed as described above. Thy1COP4 mice were used for all electrophysiological recordings. In the subset of mice that underwent stereotaxic surgery, mice were injected with AAV5-CaMKII-hM4Di:mCherry into one BNST and sham injected into the other (AP: 0.14, ML: +/-0.88, DV: -4.24) (Paxinos and Franklin, 2004), both at a 15.03° angle. Electrophysiological recordings were performed a minimum of three weeks after injection. Picrotoxin (25 μM) was used to isolate excitatory transmission. Light stimulation was passed through a GFP filter cube to produce blue light. For observation of optically-evoked postsynaptic potentials (oEPSPs), cells were equilibrated for 2-5 minutes after achieving whole cell configuration prior to recording. Optically-evoked postsynaptic potentials were observed as positive deflections while optically-evoked field potentials were observed as negative deflections with dual N1 (oN1) and N2 (oN2) components. Data was excluded if the oN1 changed by >20% during the experiment.

We first aimed to determine whether the optically evoked field potential response to guanfacine translated into excitatory activity within single cells. Previously, guanfacine was shown to inhibit optically evoked excitatory postsynaptic currents (oEPSCs) recorded in voltage clamp mode (Flavin, 2014). However, HCN involvement would be limited in this experimental design due to lack of hyperpolarizing voltages required to activate the channel (Wahl-Schott and Biel, 2009). Here, we show that twenty minute application of guanfacine (1 µM) reduces oEPSP amplitude to 62.5±14.1% of baseline values (paired t-test, p=0.03; Figure 32A), suggesting inhibitory actions. Lack of translation between guanfacine enhancement of optically evoked field potentials and inhibition of optically evoked postsynaptic currents and potentials could be due to heterogeneous effect within BNST neurons, cell dialysis preclusion of HCN channel-dependent mechanisms, or alternative mechanisms underlying the excitatory effects of α_{2A}-AR agonism on field potential responses in BNST.

Next, we aimed to determine whether guanfacine enhancement of excitatory transmission also occurred in the ventral BNST, where postsynaptic α_{2A}-ARs are also expressed but have been minimally evaluated on a functional level (Herr et al., 2012; Park et al., 2012) . Here we see that bath application of guanfacine does not affect oN2 amplitude (98.7±4.8%; Figure 32B), suggesting either no effect of guanfacine in this region or competing excitatory and inhibiting effects. Norepinephrine innervation is denser in the ventral than dorsal BNST and desensitization from norepinephrine released during the brain slice preparation process may preclude observations of receptor-dependent effects (Miles et al., 2002). This hypothesis could be tested by using norepinephrine receptor antagonists during brain slice preparation and observation of guanfacine effects thereafter.

Guanfacine enhancement of optically-evoked field potentials is hypothesized to occur through HCN inhibition via intermediate decreases in intracellular cAMP levels after canonical Gαi-mediated inhibition of adenylate cyclase (Wang et al., 2007). To test this hypothesis, we bath applied the non-hydrolyzable cAMP analogue 8-Br-cAMP (Figure 32C). Interestingly, 8-Br-cAMP incrementally but consistently inhibited optically evoked field potentials from 30-40 minutes to 91.6±4.0% of baseline values (paired t-test, p=0.02). This transient inhibition is suggestive of inhibition at Thy1+ synapses but requires further investigation due to nonspecificity of 8-Br-cAMP actions.

Similarly, we aimed to determine the effects of isoproterenol on Thy1-COP4 optically evoked excitatory field potentials to determine whether endogenous production of cAMP would have the opposite effect of guanfacine-mediated destruction. Isoproterenol enhances electrically evoked field potentials in the BNST (Egli et al., 2005), spontaneous excitatory postsynaptic currents in BNST neurons (Kash et al., 2008b), and depolarizes CRF+ BNST neurons (Silberman et al., 2013). Upon selective stimulation of afferents in Thy1COP4 BNST, though, isoproterenol did not affect the amplitude of optically evoked field potentials (94.9±4.3% baseline; Figure 32D). This result suggests either that the beta-adrenergic receptors are not expressed on Thy1+ afferents stimulated in this mouse line, or that competing inhibitory and excitatory effects preclude observation of either. Future studies should aim to determine what other G_s-coupled GPCRs are expressed in putative guanfacine-activated neurons such that endogenous cAMP levels could be increased through stimulating those pathways.

Further investigating the pathways connecting α_{2A}-AR agonism to enhancement of neuronal activity, we aimed to determine whether HCN inhibition would occlude guanfacine enhancement. To do this, we preincubated slices in the nonspecific HCN channel inhibitor

ZD7288 for one hour prior to recording optically evoked field potential responses to guanfacine (Figure 32E). Although guanfacine application without ZD7288 preincubation increased optically evoked field potential amplitude to 107.4±17.1% of baseline while guanfacine application with ZD7288 preincubation yielded a final amplitude of 99.1±10.9% of baseline, there were no statistically significant differences between each treatment and its baseline (paired t-test) or observed between the groups (unpaired t-test, p=0.68). The effect size of guanfacine in this experiment is smaller than previously observed, possibly due to increased slice handling as required for the preincubation protocol. This experiment should be re-attempted with minimal movement of slices to maximize effect size.

Finally, we aimed to determine whether CNO activation of the designer receptor hM4Di could mimic guanfacine induced enhancement of neuronal activity after agonism of the α_{2A}-AR. Bath application of CNO to hM4Di+ slices increased the oN2 amplitude to 107.8±7.5% of baseline while application to sham-injected slices inhibited slices to 90.7%. The effect of neither treatment was statistically significant relative to baseline (paired t-test; hM4Di, p=0.28; sham, p=0.34); or relative to each other (p=0.15). Cell-specific expression of hM4Di may allow for an unmasking of either a larger effect size or a more consistent effect in future experiments.

Through these experiments, we obtained preliminary data regarding the mechanism of guanfacine enhancement of optically evoked field potential responses, although additional experiments with more statistical power are needed. Future experiments should continue to attempt to block or mimic guanfacine-induced enhancement and investigate the inhibitory effects of 8-Br-cAMP. Further, identifying the afferents excited in this experimental protocol and utilizing alternative means of recording activity in the absence of cell dialysis (i.e. perforated

patch) may inform our understanding of the electrophysiological effects observed in the BNST of these mice.

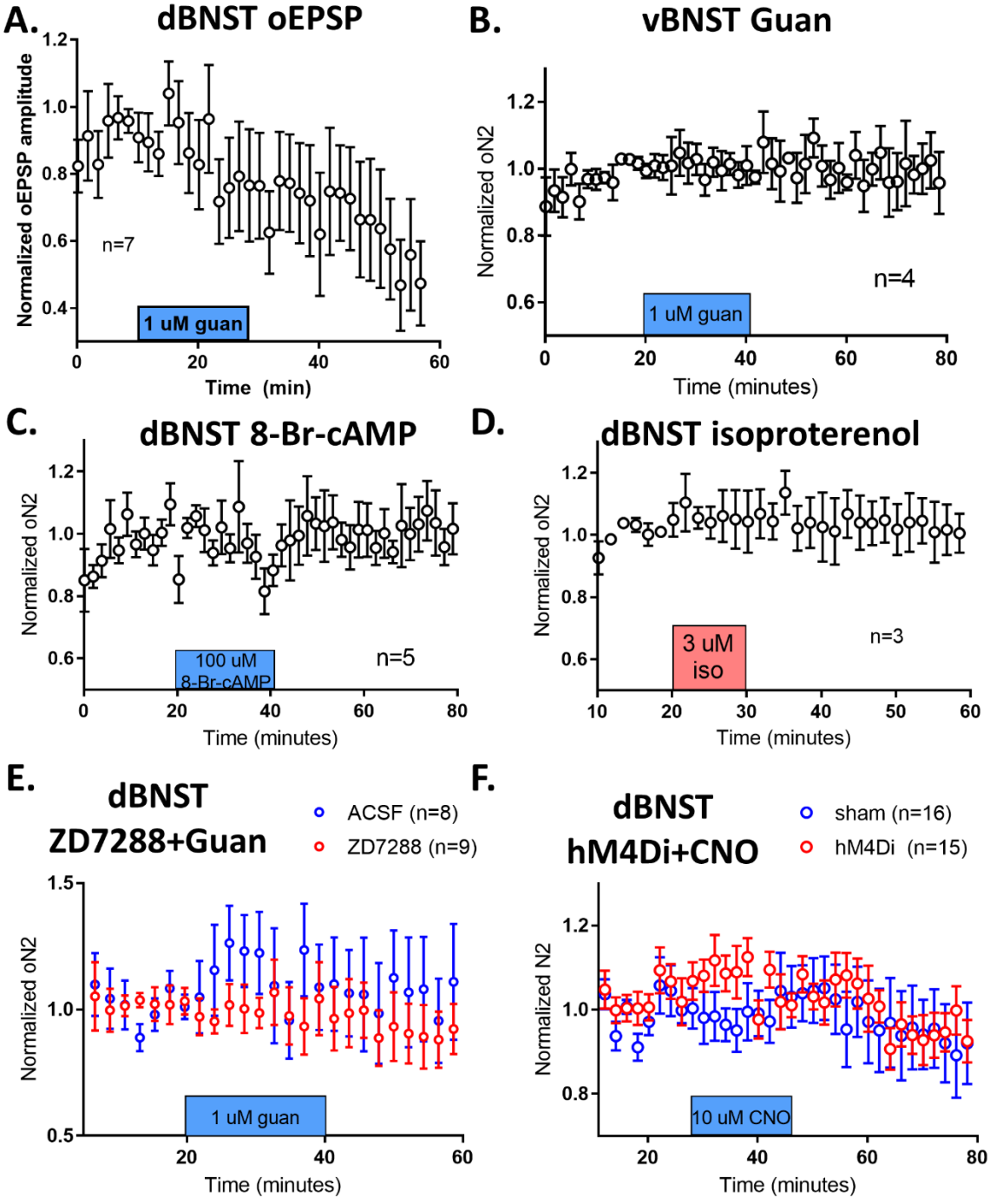

Figure 32: Pharmacological investigations of optically evoked field potentials in the BNST of Thy1-COP4 transgenic mice. (A) Guanfacine inhibits optically evoked excitatory postsynaptic potentials in Thy1COP4 BNST. (B) Guanfacine does not affect optically evoked field potentials

in the ventral BNST. (C) 8-Br-cAMP transiently inhibits optically evoked field potentials in the BNST of Thy1COP4 mice. (D) Isoproterenol does not affect optically evoked field potentials in the BNST of Thy1COP4 mice. (E) ZD7288 preincubation may reduce guanfacine enhancement of optically evoked field potentials. (F) CNO activation of BNST-expressed hM4Di may enhance optically evoked field potentials in the BNST of Thy1COP4 mice.

Bibliography

Abdolahi A, Williams GC, Benesch CG, Wang HZ, Spitzer EM, Scott BE, Block RC, van Wijngaarden E (2015a) Smoking cessation behaviors three months following acute insular damage from stroke. Addict Behav 51:24–30.

Abdolahi A, Williams GC, Benesch CG, Wang HZ, Spitzer EM, Scott BE, Block RC, van Wijngaarden E (2015b) Damage to the insula leads to decreased nicotine withdrawal during abstinence. Addiction 110:1994–2003.

Adekunbi DA, Li XF, Lass G, Shetty K, Adegoke OA, Yeo SH, Colledge WH, Lightman SL, O'Byrne KT (2018) Kisspeptin neurones in the posterodorsal medial amygdala modulate sexual partner preference and anxiety in male mice. J Neuroendocrinol 30:e12572.

Adhikari A (2014) Distributed circuits underlying anxiety. Front Behav Neurosci 8:112.

Aghajanian GK, Andrade R, Aghajanian GK (1985) Opiate and alpha2-adrenoceptor-induced hyperpolarizations of Locus Ceruleus Neurons in Brain Slices : Reversal by Cyclic Adenosine. J Neurosci 5:2359–2364.

Aghajanian GK, Vandermaelen CP (1982) alpha2-Adrenoceptor-Mediated Hyperpolarization of Locus Coeruleus Neurons : Intracellular Studies in vivo. Science 215:1394–1396.

Aghajanian GK, Wang Y-Y (1986) Pertussis toxin blocks the outward currents evoked by opiates and alpha-2 agonists in locus coeruleus neurons. Brain Res 371:390–394.

Aghajanian GK, Wang YY (1987) Common α2- and opiate effector mechanisms in the locus coeruleus: intracellular studies in brain slices. Neuropharmacology 26:793–799.

Ahmed SH, Koob GF (1997) Cocaine- but not food-seeking behavior is reinstated by stress after extinction. Psychopharmacology 132:289–295.

Albrechet-Souza L, Viola TW, Grassi-Oliveira R, Miczek KA, de Almeida RMM (2017) Corticotropin releasing factor in the bed nucleus of the stria terminalis in socially defeated and non-stressed mice with a history of chronic alcohol intake. Front Pharmacol 8:1–15.

Alheid GF (2003) Extended amygdala and basal forebrain. Ann N Y Acad Sci 985:185–205.

Alheid GF, Heimer L (1988) New perspectives in basal forebrain organization of special relevance for neuropsychiatric disorders: The striatopallidal, amygdaloid, and corticopetal components of substantia innominata. Neuroscience 27:1–39.

Ali Z, Ringkamp M, Hartke T V., Chien HF, Flavahan NA, Campbell JN, Meyer RA (1999) Uninjured C-Fiber Nociceptors Develop Spontaneous Activity and α-Adrenergic Sensitivity Following L6 Spinal Nerve Ligation in Monkey. J Neurophysiol 81:455–466.

Alvarez RP, Chen G, Bodurka J, Kaplan R, Grillon C (2011) Phasic and sustained fear in humans elicits distinct patterns of brain activity. Neuroimage 55:389–400.

Andero R, Dias BG, Ressler KJ (2014) A Role for Tac2 , NkB , and Nk3 Receptor in Normal and Dysregulated Fear Memory Consolidation. Neuron 83:444–454.

Andrade R (1993) Enhancement of beta-adrenergic responses by Gi-linked receptors in rat hippocampus. Neuron 10:83–88.

Arenkiel BR, Peca J, Davison IG, Feliciano C, Augustine GJ, Ehlers MD, Feng G (2007) In Vivo Light Induced Activation of Neural Circuitry in Transgenic Mice Expressing Channelrhodopsin-2. Neuron 54:205–218.

Arnold FJL, de Lucas Bueno M, Shiers H, Hancock DC, Evan GI, Herbert J (1992) Expression of c-fos in regions of the basal limbic forebrain following intra-cerebroventricular corticotropin-releasing factor in unstressed or stressed male rats. Neuroscience 51:377–390.

Arnsten AFT (2009) Stress signalling pathways that impair prefrontal cortex structure and

function. Nat Rev Neurosci 10:410–422.
Atkins AL, Mashhoon Y, Kantak KM (2008) Hippocampal regulation of contextual cue-induced reinstatement of cocaine-seeking behavior. Pharmacol Biochem Behav 90:481–491.
Avery SN, Clauss JA, Winder DG, Woodward N, Heckers S, Blackford JU (2014) BNST neurocircuitry in humans. Neuroimage 91:311–323.
Barth AL, Gerkin RC, Dean KL (2004) Alteration of neuronal firing properties after in vivo experience in a FosGFP transgenic mouse. J Neurosci 24:6466–6475.
De Bellis MD, Clark DDB, Beers SR, Soloff PH, Boring AM, Hall J, Kersh A, Keshavan MS, Bellis M De, Clark DDB (2000) Hippocampal volume in adolescent-onset alcohol use disorders. Am J Psychiatry 157:737–744.
Benegal V, Antony G, Venkatasubramanian G, Jayakumar PN (2007) Gray matter volume abnormalities and externalizing symptoms in subjects at high risk for alcohol dependence. Addict Biol 12:122–132.
Benson DL, Isackson PJ, Gall CM, Jones EG (1992) Contrasting patterns in the localization of glutamic acid decarboxylase and Ca2+/calmodulin protein kinase gene expression in the rat central nervous system. Neuroscience 46:825–849.
Birder LA, Perl ER (1999) Expression of α_2 -adrenergic receptors in rat primary afferent neurones after peripheral nerve injury or inflammation. J Physiol 515:533–542.
Blackmer T (2001) G Protein beta gamma Subunit – Mediated Presynaptic Inhibition : Regulation of Exocytotic Fusion Downstream of Ca 2+ Entry. Science 292:293–297.
Blaine SK, Milivojevic V, Fox HC, Sinha R (2016) Alcohol effects on stress pathways: Impact on craving and relapse risk. Can J Psychiatry 61:145–153.
Blaxall HS, Murphy TJ, Baker JC, Ray C, Bylund DB (1991) Characterization of the alpha-2C adrenergic receptor subtype in the opossum kidney and in the OK cell line. J Pharmacol Exp Ther 259:323–9.
Bonson KR, Grant SJ, Contoreggi CS, Links JM, Metcalfe J, Weyl HL, Kurian V, Ernst M, London ED (2002) Neural Systems and Cue-Induced Cocaine Craving. Neuropsychopharmacology 26:376–386.
Botta P, Demmou L, Kasugai Y, Markovic M, Xu C, Fadok JP, Lu T, Poe MM, Xu L, Cook JM, Rudolph U, Sah P, Ferraguti F, Lüthi A (2015) Regulating anxiety with extrasynaptic inhibition. Nat Neurosci 18:1493–1500.
Brown SA, Vik PW, Patterson TL, Grant I, Schuckit MA (1995) Stress, vulnerability and adult alcohol relapse. J Stud Alcohol 56:538–545.
Brown ZJ, Tribe E, D'Souza NA, Erb S (2009) Interaction between noradrenaline and corticotrophin-releasing factor in the reinstatement of cocaine seeking in the rat. Psychopharmacology 203:121–130.
Brownell KD, Marlatt GA, Lichtenstein E, Wilson GT (1986) Understanding and preventing relapse. Am Psychol 41:765–782.
Browning JR, Jansen HT, Sorg BA (2014) Inactivation of the paraventricular thalamus abolishes the expression of cocaine conditioned place preference in rats. Drug Alcohol Depend 134:387–390.
Bruijnzeel AW (2017) Neuropeptide systems and new treatments for nicotine addiction. Psychopharmacology 234:1419–1437.
Brutus M, Zuabi S, Siegel A (1988) Effects of D-Ala2-Met5-enkephalinamide microinjections placed into the bed nucleus of the stria terminalis upon active defence behaviour in the cat. Brain Res 473:147–152.

Buczek Y, Le AD, Wang AG, Stewart J, Shaham Y (1999) Stress reinstates nicotine seeking but not sucrose solution seeking in rats. Psychopharmacology 144:183–188.
Buffalari DM, Baldwin CK, See RE (2012) Treatment of cocaine withdrawal anxiety with guanfacine: relationships to cocaine intake and reinstatement of cocaine seeking in rats. Psychopharmacology 223:179–190.
Caffino L, Frankowska M, Giannotti G, Miszkiel J, Sadakierska-Chudy A, Racagni G, Filip M, Fumagalli F (2014) Cocaine-induced glutamate receptor trafficking is abrogated by extinction training in the rat hippocampus. Pharmacol Reports 66:198–204.
Cai H, Haubensak W, Anthony TE, Anderson DJ (2014) Central amygdala PKC-δ+ neurons mediate the influence of multiple anorexigenic signals. Nat Neurosci 17:1–11.
Caille S, Guillem K, Cador M, Manzoni OJ, Georges F (2009) Voluntary nicotine consumption triggers in vivo potentiation of cortical excitatory drives to midbrain dopaminergic neurons. J Neurosci 29:10410–10415.
Calipari ES, Bagot RC, Purushothaman I, Davidson TJ, Yorgason JT, Peña CJ, Walker DM, Pirpinias ST, Guise KG, Ramakrishnan C, Deisseroth K (2016) In vivo imaging identifies temporal signature of D1 and D2 medium spiny neurons in cocaine reward. 113:2–7.
Camille L, Hooper A, Yang X, Moss SJ, Maguire J (2018) Psychoneuroendocrinology Inability to suppress the stress-induced activation of the HPA axis during the peripartum period engenders de fi cits in postpartum behaviors in mice. Psychoneuroendocrinology 90:182–193.
Campeau S, Watson SJ (1997) Neuroendocrine and Behavioral Responses and Brain Pattern of c-fos Induction Associated with Audiogenic Stress. J Neuroendocrinol 9:577–588.
Campos CA, Bowen AJ, Roman CW, Palmiter RD (2018) Encoding of danger by parabrachial CGRP neurons. Nature 555:617–622.
Capriles N, Rodaros D, Sorge RE, Stewart J (2003) A role for the prefrontal cortex in stress- and cocaine-induced reinstatement of cocaine seeking in rats. Psychopharmacology 168:66–74.
Carboni E, Silvagni A, Rolando MTP, Di Chiara G (2000) Stimulation of in vivo dopamine transmission in the bed nucleus of stria terminalis by reinforcing drugs. J Neurosci 20:RC102.
Cardenas CG, Mar LP Del, Vysokanov A V, Arnold PB, Cardenas LM, Surmeier DJ, Scroggs RS (1999) Serotonergic modulation of hyperpolarization-activated current in acutely isolated rat dorsal root ganglion neurons. J Physiol 518:507–523.
Caron A, Lemko HMD, Castorena CM, Fujikawa T, Lee S, Lord CC, Ahmed N, Lee CE, Holland WL, Liu C, Elmquist JK (2018) POMC neurons expressing leptin receptors coordinate metabolic responses to fasting via suppression of leptin levels. Elife 7:1–18.
Chen S, Wang J, Siegelbaum SA (2001) Properties of Hyperpolarization-Activated Pacemaker Current Defined by Coassembly of HCN1 and HCN2 Subunits and Basal Modulation by Cyclic Nucleotide. J Gen Physiol 117:491–504.
Chiu R, Boyle WJ, Meek J, Smeal T, Hunter T, Karin M (1988) The c-fos protein interacts with c-Jun AP-1 to stimulate transcription of AP-1 responsive genes. Cell 54:541–552.
Christianson JP, Jennings JH, Ragole T, Flyer JGN, Benison AM, Barth DS, Watkins LR, Maier SF (2011) Safety signals mitigate the consequences of uncontrollable stress via a circuit involving the sensory insular cortex and bed nucleus of the stria terminalis. Biol Psychiatry 70:458–464.
Cohen S, Janicki-Deverts D, Miller GE (2007) Psychological stress and disease. JAMA - J Am Med Assoc 298:1685–1687.

Cole JC, Burroughs GJ, Laverty CR, Sheriff NC, Sparham EA, Rodgers RJ (1995) Anxiolytic-like effects of yohimbine in the murine plus-maze: strain independence and evidence against alpha2-adrenoceptor mediation. Psychopharmacology 118:425–436.
Conrad KL, Davis AR, Silberman Y, Sheffler DJ, Shields AD, Saleh SA, Sen N, Matthies HJG, Javitch JA, Lindsley CW, Winder DG (2012) Yohimbine depresses excitatory transmission in BNST and impairs extinction of cocaine place preference through orexin-dependent, norepinephrine-independent processes. Neuropsychopharmacology 37:2253–2266.
Conrad KL, Louderback KM, Gessner CP, Winder DG (2011) Stress-induced alterations in anxiety-like behavior and adaptations in plasticity in the bed nucleus of the stria terminalis. Physiol Behav 104:248–256.
Conrad KL, Louderback KM, Milano EJ, Winder DG (2013) Assessment of the impact of pattern of cocaine dosing schedule during conditioning and reconditioning on magnitude of cocaine CPP, extinction, and reinstatement. Psychopharmacology 227:109–116.
Conrad KL, Winder DG (2011) Altered anxiety-like behavior and long-term potentiation in the bed nucleus of the stria terminalis in adult mice exposed to chronic social isolation, unpredictable stress, and ethanol beginning in adolescence. Alcohol 45:585–593.
Contreras M, Billeke P, Vicencio S, Madrid C, Perdomo G, González M, Torrealba F (2012) A role for the insular cortex in long-term memory for context-evoked drug craving in rats. Neuropsychopharmacology 37:2101–2108.
Contreras M, Ceric F, Torrealba F (2007) Inactivation of the interoceptive insula disrupts drug craving and malaise induced by lithium. Science 318:655–658.
Cornil CA, Ball GF (2008) Interplay among catecholamine systems: Dopamine binds to α 2-adrenergic receptors in birds and mammals. J Comp Neurol 511:610–627.
Cosme C V., Gutman AL, LaLumiere RT (2015) The Dorsal Agranular Insular Cortex Regulates the Cued Reinstatement of Cocaine-Seeking, but not Food-Seeking, Behavior in Rats. Neuropsychopharmacology 40:2425–2433.
Crestani CC, Alves FHF, Correa FMA, Guimarães FS, Joca SRL (2010) Acute reversible inactivation of the bed nucleus of stria terminalis induces antidepressant-like effect in the rat forced swimming test. Behav Brain Funct 6:1–8.
Criado M, Gil a, Viniegra S, Gutiérrez LM (1999) A single amino acid near the C terminus of the synaptosomeassociated protein of 25 kDa (SNAP-25) is essential for exocytosis in chromaffin cells. Proc Natl Acad Sci U S A 96:7256–7261.
Crombag HS, Bossert JM, Koya E, Shaham Y (2008) Context-induced relapse to drug seeking: a review. Philos Trans R Soc B Biol Sci 363:3233–3243.
Cui G, Jun SB, Jin X, Pham MD, Vogel SS, Lovinger DM, Costa RM (2013) Concurrent activation of striatal direct and indirect pathways during action initiation. Nature 494:238–242.
Cullinan WE, Herman JP, Battaglia DF, Akil H, Watson SJ (1995) Pattern and time course of immediate early gene expression in rat brain following acute stress. Neuroscience 64:477–505.
Cullinan WE, Herman JP, Watson SJ (1993) Ventral subicular interactions with the hypothalamic paraventricular nucleus: evidence for a relay in the bed nucleus of the stria terminalis. J Comp Neurol 332:1–20.
Cummings S, Elde R, Ells J, Lindall a (1983) Corticotropin-releasing factor immunoreactivity is widely distributed within the central nervous system of the rat: an immunohistochemical study. J Neurosci 3:1355–1368.

Dabrowska J, Hazra R, Guo J-DD, Li C, Dewitt S, Xu J, Lombroso PJ, Rainnie DG (2013a) Striatal-enriched protein tyrosine phosphatase - STEPs toward understanding chronic stress-induced activation of corticotrophin releasing factor neurons in the rat bed nucleus of the stri aterminalis. Biol Psychiatry 74:817–826.

Dabrowska J, Hazra R, Guo JD, DeWitt S, Rainnie DG (2013b) Central CRF neurons are not created equal: Phenotypic differences in CRF-containing neurons of the rat paraventricular hypothalamus and the bed nucleus of the stria terminalis. Front Neurosci 7:1–14.

Dalsass M, Siegel a (1990) Opioid peptide regulation of neurons in the bed nucleus of the stria terminalis: a microiontophoretic study. Brain Res 531:346–349.

Daniel SE, Guo J, Rainnie DG (2017) A comparative analysis of the physiological properties of neurons in the anterolateral bed nucleus of the stria terminalis in the Mus musculus, Rattus norvegicus, and Macaca mulatta. J Comp Neurol 525:2235–2248.

Davies MF, Tsui J, Flannery JA, Li X, DeLorey TM, Hoffman BB (2004) Activation of α2Adrenergic Receptors Suppresses Fear Conditioning: Expression of c-Fos and Phosphorylated CREB in Mouse Amygdala. Neuropsychopharmacology 29:229–239.

Davies MF, Tsui JY, Flannery JA, Li X, DeLorey TM, Hoffman BB (2003) Augmentation of the noradrenergic system in alpha-2 adrenergic receptor deficient mice: anatomical changes associated with enhanced fear memory. Brain Res 986:157–165.

Day HEW, Curran EJ, Watson SJ, Akil H (1999) Distinct neurochemical populations in the rat central nucleus of the amygdala and bed nucleus of the stria terminalis: evidence for their selective activation by interleukin-1beta. J Comp Neurol 413:113–128.

Day HEW, Masini C V., Campeau S (2004) The pattern of brain c-fos mRNA induced by a component of fox odor, 2,5-dihydro-2,4,5-Trimethylthiazoline (TMT), in rats, suggests both systemic and processive stress characteristics. Brain Res 1025:139–151.

Day M, Carr DB, Ulrich S, Ilijic E, Tkatch T, Surmeier DJ (2005) Dendritic Excitability of Mouse Frontal Cortex Pyramidal Neurons Is Shaped by the Interaction among HCN , Kir2 , and K leak Channels. J Neurosci 25:8776–8787.

Debacker J, Hawken ER, Normandeau CP, Jones AA, Di Prospero C, Mechefske E, Gardner Gregory J, Hayton SJ, Dumont EC (2015) GluN2B-containing NMDA receptors blockade rescues bidirectional synaptic plasticity in the bed nucleus of the stria terminalis of cocaine self-administering rats. Neuropsychopharmacology 40:394–405.

Dedic N et al. (2018a) Chronic CRH depletion from GABAergic, long-range projection neurons in the extended amygdala reduces dopamine release and increases anxiety. Nat Neurosci 21:1.

Dedic N, Chen A, Deussing JM (2018b) The CRF Family of Neuropeptides and their Receptors - Mediators of the Central Stress Response. Curr Mol Pharmacol 11:4–31.

Degenhardt L, Whiteford HA, Ferrari AJ, Baxter AJ, Charlson FJ, Hall WD, Freedman G, Burstein R, Johns N, Engell RE, Flaxman A, Murray CJ, Vos T (2013) Global burden of disease attributable to illicit drug use and dependence: findings from the Global Burden of Disease Study 2010. Lancet 382:1564–1574.

Delaney AJ, Crane JW, Sah P (2007) Noradrenaline modulates transmission at a central synapse by a presynaptic mechanism. Neuron 56:880–892.

Delfs J, Zhu Y, Druhan JP, Aston-Jones G (2000) Noradrenaline in the ventral forebrain is critical for opiate withdrawal-induced aversion. Nature 403:430–434.

Deneux T, Kaszas A, Szalay G, Katona G, Lakner T, Grinvald A, Rozsa B, Vanzetta I (2016) Accurate spike estimation from noisy calcium signals for ultrafast three-dimensional

imaging of large neuronal populations in vivo. Nat Commun 7:1–17.
Dobolyi A, Irwin S, Makara G, Usdin TB, Palkovits M (2005) Calcitonin gene-related peptide-containing pathways in the rat forebrain. J Comp Neurol 489:92–119.
Dodson JD (1915) The relation of strength of stimulus to rapidity of habit-formation in the kitten. J Anim Behav 5:330–336.
Dolphin AC (1998) Mechanisms of modulation of voltage-dependent calcium channels by G proteins. J Physiol 506:3–11.
Dolphin AC, Scott RH (1987) Calcium channel currents and their inhibition by (-)-baclofen in rat sensory neurones: modulation by guanine nucleotides. J Physiol 386:1–17.
Dong HW, Petrovich GD, Swanson LW (2000) Organization of projections from the juxtacapsular nucleus of the BST: A PHAL study in the rat. Brain Res 859:1–14.
Dong HW, Petrovich GD, Swanson LW (2001) Topography of projections from amygdala to bed nuclei of the stria terminalis. Brain Res Rev 38:192–246.
Dong X, Li S, Kirouac GJ (2017) Collateralization of projections from the paraventricular nucleus of the thalamus to the nucleus accumbens, bed nucleus of the stria terminalis, and central nucleus of the amygdala. Brain Struct Funct 222:3927–3943.
Douglass AM, Kucukdereli H, Ponserre M, Markovic M, Gründemann J, Strobel C, Alcala Morales PL, Conzelmann K-KK, Lüthi A, Klein R (2017) Central amygdala circuits modulate food consumption through a positive-valence mechanism. Nat Neurosci 20:1384–1394.
Droutman V, Read SJ, Bechara A (2015) Revisiting the role of the insula in addiction. Trends Cogn Sci 19:414–420.
Dumont EC, Mark GP, Mader S, Williams JT (2005) Self-administration enhances excitatory synaptic transmission in the bed nucleus of the stria terminalis. Nat Neurosci 8:413–414.
Dumont EC, Rycroft BK, Maiz J, Williams JT (2008) Morphine produces circuit-specific neuroplasticity in the bed nucleus of the stria terminalis. Neuroscience 153:232–239.
Duvarci S, Bauer EP, Pare D (2009) The Bed Nucleus of the Stria Terminalis Mediates Inter-individual Variations in Anxiety and Fear. J Neurosci 29:10357–10361.
Egli RE, Kash TL, Choo K, Savchenko VL, Matthews RT, Blakely RD, Winder DG (2005) Norepinephrine modulates glutamatergic transmission in the bed nucleus of the stria terminalis. Neuropsychopharmacology 30:657–668.
Ehlinger DG, Bergstrom HC, McDonald CG, Smith RF (2012) Nicotine-induced dendritic remodeling in the insular cortex. Neurosci Lett 516:89–93.
Eiler WJA, Seyoum R, Foster KL, Mailey C, June HL (2003) D1 dopamine receptor regulates alcohol-motivated behaviors in the bed nucleus of the stria terminalis in alcohol-preferring (P) rats. Synapse 48:45–56.
Epping-Jordan MP, Markou A, Koob GF (1998) The dopamine D-1 receptor antagonist SCH 23390 injected into the dorsolateral bed nucleus of the stria terminalis decreased cocaine reinforcement in the rat. Brain Res 784:105–115.
Erb S, Ph D, Hitchcott PK, Phil D, Rajabi H, Sc B, Mueller D, Shaham Y, Ph D, Stewart J, Ph D (1998) Alpha-2 Adrenergic Receptor Agonists Block Stress-Induced Reinstatement of Cocaine Seeking. Neuropsychopharmacology 23:138–150.
Erb S, Salmaso N, Rodaros D, Stewart J (2001) A role for the CRF-containing pathway from central nucleus of the amygdala to bed nucleus of the stria terminalis in the stress-induced reinstatement of cocaine seeking in rats. Psychopharmacology 158:360–365.
Erb S, Shaham Y, Stewart J (1996) Stress reinstates cocaine-seeking behavior after prolonged

extinction and a drug-free period. Psychopharmacology 128:408–412.
Erb S, Stewart J (1999) A role for the bed nucleus of the stria terminalis, but not the amygdala, in the effects of corticotropin-releasing factor on stress-induced reinstatement of cocaine seeking. J Neurosci 19:RC35.
Faravelli C (1985) Life events preceding the onset of panic disorder. J Affect Disord 9:103–105.
Farrant M, Nusser Z (2005) Variations on an inhibitory theme: Phasic and tonic activation of GABAAreceptors. Nat Rev Neurosci 6:215–229.
Federman AD, Conklin BR, Schrader KA, Reed RR, Bourne HR (1992) Hormonal stimulation of adenylyl cyclase through Gi-protein beta-gamma subunits. Nature 356:159–161.
Felitti V (1998) Relationship of childhood abuse and household dysfunction to many of the leading causes of death in adults: The Adverse Childhood Experiences. Am J Prev Med 14:245–258.
Figueiredo HF, Bruestle A, Bodie B, Dolgas CM, Herman JP (2003) The medial prefrontal cortex differentially regulates stress-induced c-fos expression in the forebrain depending on type of stressor. Eur J Neurosci 18:2357–2364.
Flak JN, Solomon MB, Jankord R, Krause EG, Herman JP (2012) Identification of chronic stress-activated regions reveals a potential recruited circuit in rat brain. Eur J Neurosci 36:2547–2555.
Flavin SA (2014) The Effects of α2A-Adrenergic Receptors on Glutamatergic Signaling in the Bed Nucleus of the Stria Terminalis (Doctoral Dissertation).
Flavin SA, Matthews RT, Wang Q, Muly EC, Winder DG (2014) α2A-Adrenergic Receptors Filter Parabrachial Inputs to the Bed Nucleus of the Stria Terminalis. J Neurosci 34:9319–9331.
Flavin SA, Winder DG (2013) Noradrenergic control of the bed nucleus of the stria terminalis in stress and reward. Neuropharmacology 70:324–330.
Fleischmann A, Hvalby O, Jensen V, Strekalova T, Zacher C, Layer LE, Kvello A, Reschke M, Spanagel R, Sprengel R, Wagner EF, Gass P (2003) Impaired long-term memory and NR2A-type NMDA receptor-dependent synaptic plasticity in mice lacking c-Fos in the CNS. J Neurosci 23:9116–9122.
Flügge G, Van Kampen M, Meyer H, Fuchs E (2003) α2A and α2C-adrenoceptor regulation in the brain: α2A changes persist after chronic stress. Eur J Neurosci 17:917–928.
Flügge G, Van Kampen M, Mijnster MJ (2004) Perturbations in brain monoamine systems during stress. Cell Tissue Res 315:1–14.
Forget B, Pushparaj A, Le Foll B (2010) Granular insular cortex inactivation as a novel therapeutic strategy for nicotine addiction. Biol Psychiatry 68:265–271.
Fosque BF, Sun Y, Dana H, Yang C, Ohyama T, Tadross MR, Patel R, Zlatic M, Kim DS, Ahrens MB, Jayaraman V, Looger LL, Schreiter ER (2015) Labeling of active neural circuits in vivo with designed calcium integrators. Science 347:755–760.
Fox HC, Morgan PT, Sinha R (2014) Sex differences in guanfacine effects on drug craving and stress arousal in cocaine-dependent individuals. Neuropsychopharmacology 39:1527–1537.
Fox K, Stryker M (2017) Integrating Hebbian and homeostatic plasticity: Introduction. Philos Trans R Soc B Biol Sci 372.
Francesconi W, Berton F, Koob GF, Sanna PP (2009a) Intrinsic neuronal plasticity in the juxtacapsular nucleus of the bed nuclei of the stria terminalis (jcBNST). Prog Neuro-Psychopharmacology Biol Psychiatry 33:1347–1355.
Francesconi W, Berton F, Repunte-Canonigo V, Hagihara K, Thurbon D, Lekic D, Specio SE,

Greenwell TN, Chen SA, Rice KC, Richardson HN, O'Dell LE, Zorrilla EP, Morales M, Koob GF, Sanna PP (2009b) Protracted withdrawal from alcohol and drugs of abuse impairs long-term potentiation of intrinsic excitability in the juxtacapsular bed nucleus of the stria terminalis. J Neurosci 29:5389–5401.

Francesconi W, Szücs A, Berton F, Koob GF, Vendruscolo LF, Sanna PP (2017) Opiate dependence induces cell type-specific plasticity of intrinsic membrane properties in the rat juxtacapsular bed nucleus of stria terminalis (jcBNST). Psychopharmacology 234:3485–3498.

Fuchs RA, Evans KA, Ledford CC, Parker MP, Case JM, Mehta RH, See RE (2005) The role of the dorsomedial prefrontal cortex, basolateral amygdala, and dorsal hippocampus in contextual reinstatement of cocaine seeking in rats. Neuropsychopharmacology 30:296–309.

Funk D, Li Z, Lê AD (2006) Effects of environmental and pharmacological stressors on c-fos and corticotropin-releasing factor mRNA in rat brain: Relationship to the reinstatement of alcohol seeking. Neuroscience 138:235–243.

Gamache K, Pitman RK, Nader K (2012) Preclinical evaluation of reconsolidation blockade by clonidine as a potential novel treatment for posttraumatic stress disorder. Neuropsychopharmacology 37:2789–2796.

Gamo NJ, Lur G, Higley MJ, Wang M, Paspalas CD, Vijayraghavan S, Yang Y, Ramos BP, Peng K, Kata A, Boven L, Lin F, Roman L, Lee D, Arnsten AFT (2015) Stress Impairs Prefrontal Cortical Function via D1 Dopamine Receptor Interactions with Hyperpolarization-Activated Cyclic Nucleotide-Gated Channels. Biol Psychiatry:1–11.

Gantz SC, Bunzow JR, Williams JT (2013) Spontaneous inhibitory synaptic currents mediated by a g protein-coupled receptor. Neuron 78:807–812.

Ganzel BL, Morris PA, Wethington E (2010) Allostasis and the Human Brain: Integrating Models of Stress From the Social and Life Sciences. Psychol Rev 117:134–174.

Garcia MM, Gilster J, Harlan RE (1996) Chronic morphine decreases calbindin D(28k) immunoreactivity in a subset of cerebellar Purkinje neurons of rat brain. Brain Res 734:123–134.

Garner AR, Rowland DC, Hwang SY, Baumgaertel K, Roth BL, Kentros C, Mayford M (2012) Generation of a Synthetic Memory Trace. Science 254:1513–1517.

Gaszner B, Kormos V, Kozicz T, Hashimoto H, Reglodi D, Helyes Z (2012) The behavioral phenotype of pituitary adenylate-cyclase activating polypeptide-deficient mice in anxiety and depression tests is accompanied by blunted c-Fos expression in the bed nucleus of the stria terminalis, central projecting Edinger-Westphal nucleu. Neuroscience 202:283–299.

George MS, Abbott LF, Siegelbaum S a. (2009) HCN hyperpolarization-activated cation channels inhibit EPSPs by interactions with M-type K(+) channels. Nat Neurosci 12:577–584.

George O, Le Moal M, Koob GF (2012) Allostasis and addiction: Role of the dopamine and corticotropin-releasing factor systems. Physiol Behav 106:58–64.

Gerachshenko T, Schwartz E, Bleckert A, Photowala H, Seymour A, Alford S (2009) Presynaptic G-Protein-Coupled Receptors Dynamically Modify Vesicle Fusion, Synaptic Cleft Glutamate Concentrations, and Motor Behavior. J Neurosci 29:10221–10233.

Ghamari-Langroudi M, Digby GJ, Sebag JA, Millhauser GL, Palomino R, Matthews R, Gillyard T, Panaro BL, Tough IR, Cox HM, Denton JS, Cone RD (2015) G-protein-independent coupling of MC4R to Kir7.1 in hypothalamic neurons. Nature 520:94–98.

Gilpin NW (2012a) Corticotropin-releasing factor (CRF) and neuropeptide Y (NPY): Effects on inhibitory transmission in central amygdala, and anxiety- & alcohol-related behaviors. Alcohol 46:329–337.
Gilpin NW (2012b) Neuropeptide Y (NPY) in the extended amygdala is recruited during the transition to alcohol dependence. Neuropeptides 46:253–259.
Gilpin NW, Misra K, Herman MA, Cruz MT, Koob GF, Roberto M (2011) Neuropeptide y opposes alcohol effects on gamma-aminobutyric acid release in amygdala and blocks the transition to alcohol dependence. Biol Psychiatry 69:1091–1099.
Gilpin NW, Misra K, Koob GF (2008) Neuropeptide Y in the central nucleus of the amygdala suppresses dependence-induced increases in alcohol drinking. Pharmacol Biochem Behav 90:475–480.
Gilsbach R, Hein L (2012) Are the pharmacology and physiology of α 2adrenoceptors determined by α 2-heteroreceptors and autoreceptors respectively? Br J Pharmacol 165:90–102.
Gilsbach R, Ro C, Beetz N, Brede M, Hadamek K, Haubold M, Leemhuis J, Philipp M, Schneider J, Urbanski M, Szabo B, Weinshenker D, Hein L (2009) Genetic Dissection of alpha2-Adrenoceptor Functions in Adrenergic versus Nonadrenergic Cells. 75:1160–1170.
Gilsbach R, Schneider J, Lother A, Schickinger S, Leemhuis J, Hein L (2010) Sympathetic α2-adrenoceptors prevent cardiac hypertrophy and fibrosis in mice at baseline but not after chronic pressure overload. Cardiovasc Res 86:432–442.
Glangetas C, Fois GRR, Jalabert M, Lecca S, Valentinova K, Meye FJJ, Diana M, Faure P, Mameli M, Caille S, Georges F (2015) Ventral Subiculum Stimulation Promotes Persistent Hyperactivity of Dopamine Neurons and Facilitates Behavioral Effects of Cocaine. Cell Rep 13:2287–2296.
Glangetas C, Girard D, Groc L, Marsicano G, Chaouloff F, Georges F (2013) Stress Switches Cannabinoid Type-1 (CB1) Receptor-Dependent Plasticity from LTD to LTP in the Bed Nucleus of the Stria Terminalis. J Neurosci 33:19657–19663.
Glangetas C, Massi L, Fois GR, Jalabert M, Girard D, Diana M, Yonehara K, Roska B, Xu C, Lüthi A, Caille S (2017) In vivo single-cell homeostatic plasticity in the Bed Nucleus of the Stria terminalis triggers long-term anxiolysis. Nat Commun 8:1–7.
Glitsch M (2006) Selective Inhibition of Spontaneous But Not Ca2+-Dependent Release Machinery by Presynaptic Group II mGluRs in Rat Cerebellar Slices. J Neurophysiol 96:86–96.
Goeders NE (2003) The impact of stress on addiction. Eur Neuropsychopharmacol 13:435–441.
Gomez JL, Bonaventura J, Lesniak W, Mathews WB, Sysa-Shah P, Rodriguez LA, Ellis RJ, Richie CT, Harvey BK, Dannals RF, Pomper MG, Bonci A, Michaelides M (2017) Chemogenetics revealed: DREADD occupancy and activation via converted clozapine. Science 357:503–507.
Gos T, Schulkin J, Gos A, Bock J, Poeggel G, Braun K (2014) Paternal deprivation affects the functional maturation of corticotropin-releasing hormone (CRH)- and calbindin-D28k-expressing neurons in the bed nucleus of the stria terminalis (BNST) of the biparental Octodon degus. Brain Struct Funct 219:1983–1990.
Griebel G, Holmes A (2013) 50 Years of Hurdles and Hope in Anxiolytic Drug Discovery. Nat Rev Drug Discov 12:667–687.
Grigoryan G, Ardi Z, Albrecht A, Richter-Levin G, Segal M (2015) Juvenile stress alters LTP in ventral hippocampal slices: Involvement of noradrenergic mechanisms. Behav Brain Res

278:559–562.
Grimm JW, See RE (2000) Dissociation of primary and secondary reward-relevant limbic nuclei in an animal model of relapse. Neuropsychopharmacology 22:473–479.
Gros C, Pradelles P, Humbert J, Dray F, Le Gal la Salle G (1978) Regional distribution of met-enkephalin within the amygdaloid complex and bed nucleus of the stria terminalis. Neurosci Lett 10:193–196.
Grueter BA, Gosnell HB, Olsen CM, Schramm-Sapyta NL, Nekrasova T, Landreth GE, Winder DG (2006) Extracellular-signal regulated kinase 1-dependent metabotropic glutamate receptor 5-induced long-term depression in the bed nucleus of the stria terminalis is disrupted by cocaine administration. J Neurosci 26:3210–3219.
Grueter BA, Mcelligott ZA, Robison AJ (2008a) In vivo mGluR5 antagonism prevents cocaine-induced disruption of postsynaptically-maintained mGluR5-dependent long-term depression. J Neurosci 28:9261–9270.
Grueter BA, McElligott ZA, Robison AJ, Mathews GC, Winder DG (2008b) In vivo metabotropic glutamate receptor 5 (mGluR5) antagonism prevents cocaine-induced disruption of postsynaptically maintained mGluR5-dependent long-term depression. J Neurosci 28:9261–9270.
Grueter BA, Winder DG (2005) Group II and III metabotropic glutamate receptors suppress excitatory synaptic transmission in the dorsolateral bed nucleus of the stria terminalis. Neuropsychopharmacology 30:1302–1311.
Grupe DW, Oathes DJ, Nitschke JB (2013) Dissecting the anticipation of aversion reveals dissociable neural networks. Cereb Cortex 23:1874–1883.
Guenthner CJ, Miyamichi K, Yang HH, Heller HC, Luo L (2013) Permanent genetic access to transiently active neurons via TRAP: Targeted recombination in active populations. Neuron 78:773–784.
Gungor NZ, Pare D (2014) CGRP Inhibits Neurons of the Bed Nucleus of the Stria Terminalis: Implications for the Regulation of Fear and Anxiety. J Neurosci 34:60–65.
Gungor NZ, Pare D (2016) Functional Heterogeneity in the Bed Nucleus of the Stria Terminalis. J Neurosci 36:8038–8049.
Guzowski JF (2002) Insights into immediate-early gene function in hippocampal memory consolidation using antisense oligonucleotide and fluorescent imaging approaches. Hippocampus 12:86–104.
Halazonetis TD, Georgopoulos K, Greenberg ME, Leder P (1988) c-Jun dimerizes with itself and with c-Fos, forming complexes of different DNA binding affinities. Cell 55:917–924.
Hamid E, Church E, Wells C a, Zurawski Z, Hamm HE, Alford S (2014) Modulation of neurotransmission by GPCRs is dependent upon the microarchitecture of the primed vesicle complex. J Neurosci 34:260–274.
Hammack SE, Mania I, Rainnie DG (2007) Differential expression of intrinsic membrane currents in defined cell types of the anterolateral bed nucleus of the stria terminalis. J Neurophysiol 98:638–656.
Han JS (2005) Critical Role of Calcitonin Gene-Related Peptide 1 Receptors in the Amygdala in Synaptic Plasticity and Pain Behavior. J Neurosci 25:10717–10728.
Han JS, Adwanikar H, Li Z, Ji G, Neugebauer V (2010) Facilitation of synaptic transmission and pain responses by CGRP in the amygdala of normal rats. Mol Pain 6:1–14.
Han S, Soleiman M, Soden M, Zweifel LS, Palmiter RD (2015) Elucidating an Affective Pain Circuit that Creates a Threat Memory. Cell 162:363–374.

Han Y, Heuermann RJ, Lyman KA, Fisher D, Ismail Q-AA, Chetkovich DM (2017) HCN-channel dendritic targeting requires bipartite interaction with TRIP8b and regulates antidepressant-like behavioral effects. Mol Psychiatry 22:458–465.
Han Y, Noam Y, Lewis AS, Gallagher JJ, Wadman WJ, Baram TZ, Chetkovich DM (2011) Trafficking and Gating of Hyperpolarization-activated Cyclic Nucleotide-gated Channels Are Regulated by Interaction with Tetratricopeptide Repeat-containing Rab8b-interacting Protein (TRIP8b) and Cyclic AMP at Distinct Sites. J Biol Chem 286:20823–20834.
Haney M, Maccari S, Le Moal M, Simon H, Piazza P (1995) Social stress increases the acquisition of cocaine self-administration in male and female rats. Brain Res 698:46–52.
Harris EP, Abel JM, Tejada LD, Rissman EF (2016) Calbindin knockout alters sex-specific regulation of behavior and gene expression in amygdala and prefrontal cortex. Endocrinology 157:1967–1979.
Haubensak W, Kunwar PS, Cai H, Ciocchi S, Wall NR, Ponnusamy R, Biag J, Dong H-W, Deisseroth K, Callaway EM, Fanselow MS, Lüthi A, Anderson DJ (2010) Genetic dissection of an amygdala microcircuit that gates conditioned fear. Nature 468:270–276.
Hausen AC, Ruud J, Jiang H, Hess S, Varbanov H, Kloppenburg P, Hausen AC, Ruud J, Jiang H, Hess S, Varbanov H, Kloppenburg P (2016) Insulin-Dependent Activation of MCH Neurons Impairs Locomotor Activity and Insulin Sensitivity in Report Insulin-Dependent Activation of MCH Neurons Impairs Locomotor Activity and Insulin Sensitivity in Obesity. Cell Rep 17:2512–2521.
Hazra R, Guo J-DD, Ryan SJ, Jasnow AM, Dabrowska J, Rainnie DG (2011) A transcriptomic analysis of type I-III neurons in the bed nucleus of the stria terminalis. Mol Cell Neurosci 46:699–709.
Hazra R, Guo JD, Dabrowska J, Rainnie DG (2012) Differential distribution of serotonin receptor subtypes in BNSTALG neurons: Modulation by unpredictable shock stress. Neuroscience 225:9–21.
Heilig M, Egli M (2006) Pharmacological treatment of alcohol dependence: Target symptoms and target mechanisms. Pharmacol Ther 111:855–876.
Heilig M, Egli M, Crabbe JC, Becker HC (2010) Acute withdrawal, protracted abstinence and negative affect in alcoholism: Are they linked? Addict Biol 15:169–184.
Heim C, Nemeroff CB (2001) The role of childhood trauma in the neurobiology of mood and anxiety disorders: Preclinical and clinical studies. Biol Psychiatry 49:1023–1039.
Henckens MJAG, Deussing JM, Chen A (2016) Region-specific roles of the corticotropin-releasing factor–urocortin system in stress. Nat Rev Neurosci 17:636–651.
Hendrikse ER, Bower RL, Hay DL, Walker CS (2018) Molecular studies of CGRP and the CGRP family of peptides in the central nervous system. Cephalalgia 0:1–17.
Henry MS, Bisht K, Vernoux N, Gendron L, Torres-Berrio A, Drolet G, Tremblay M-È (2018) Delta Opioid Receptor Signaling Promotes Resilience to Stress Under the Repeated Social Defeat Paradigm in Mice. Front Mol Neurosci 11:100.
Henry MS, Gendron L, Tremblay ME, Drolet G (2017) Enkephalins: Endogenous Analgesics with an Emerging Role in Stress Resilience. Neural Plast 27:1546125.
Herr NR, Park J, McElligott ZA, Belle AM, Carelli RM, Wightman RM (2012) In vivo voltammetry monitoring of electrically evoked extracellular norepinephrine in subregions of the bed nucleus of the stria terminalis. J Neurophysiol 107:1731–1737.
Hess J (2004) AP-1 subunits: quarrel and harmony among siblings. J Cell Sci 117:5965–5973.
Highfield D, Yap J, Grimm JW, Shalev U, Shaham Y (2001) Repeated lofexidine treatment

attenuates stress-induced, but not drug cues-induced reinstatement of a heroin-cocaine mixture (speedball) seeking in rats. Neuropsychopharmacology 25:320–331.
Hill SY, De Bellis MD, Keshavan MS, Lowers L, Shen S, Hall J, Pitts T (2001) Right amygdala volume in adolescent and young adult offspring from families at high risk for developing alcoholism. Biol Psychiatry 49:894–905.
Hiraoka K, Motomura K, Yanagida S, Ohashi A, Ishisaka-Furuno N, Kanba S (2017) Pattern of c-Fos expression induced by tail suspension test in the mouse brain. Heliyon 3:e00316.
Holleran KM, Wilson HH, Fetterly TL, Bluett RJ, Centanni SW, Gilfarb RA, Rocco LERR, Patel S, Winder DG (2016) Ketamine and MAG Lipase Inhibitor-Dependent Reversal of Evolving Depressive-Like Behavior During Forced Abstinence From Alcohol Drinking. Neuropsychopharmacology 41:2062–2071.
Van Hook MJ, Babai N, Zurawski Z, Young Yim Y, Hamm HE, Thoreson WB (2017) A presynaptic group III mGluR recruits Gβγ/SNARE interactions to inhibit synaptic transmission by cone photoreceptors in the vertebrate retina. J Neurosci 37:4618–4634.
Huang AS, Mitchell JA, Haber SN, Alia-Klein N, Goldstein RZ (2018) The thalamus in drug addiction: from rodents to humans. Philos Trans R Soc Lond B Biol Sci 373:20170028.
Huang Z, Lujan R, Kadurin I, Uebele VN, Renger JJ, Dolphin AC, Shah MM (2011) Presynaptic HCN1 channels regulate Cav3.2 activity and neurotransmission at select cortical synapses. Nat Neurosci 14:478–486.
Iacopino AM, Christakos S (1990) Corticosterone regulates calbindin-D28k mRNA and protein levels in rat hippocampus. J Biol Chem 265:10177–10180.
Ide S, Hara T, Ohno A, Tamano R, Koseki K, Naka T, Maruyama C, Kaneda K, Yoshioka M, Minami M (2013) Opposing Roles of Corticotropin-Releasing Factor and Neuropeptide Y within the Dorsolateral Bed Nucleus of the Stria Terminalis in the Negative Affective Component of Pain in Rats. J Neurosci 33:5881–5894.
Inturrisi CE, Umans JG, Wolff D, Stern AS, Lewis R V, Stein S, Udenfriend S (1980) Analgesic activity of the naturally occurring heptapeptide [Met]enkephalin-Arg6-Phe7. Proc Natl Acad Sci U S A 77:5512–5514.
Iremonger KJ, Bains JS (2009) Retrograde Opioid Signaling Regulates Glutamatergic Transmission in the Hypothalamus. J Neurosci 29:7349–7358.
Iyengar S, Ossipov MH, Johnson KW (2017) The role of CGRP in peripheral and central pain mechanisms including migraine.
James MH, Charnley JL, Jones E, Levi EM, Yeoh JW, Flynn JR, Smith DW, Dayas C V. (2010) Cocaine- and Amphetamine-Regulated Transcript (CART) signaling within the paraventricular thalamus modulates cocaine-seeking behaviour. PLoS One 5.
Janes AC, Gilman JM, Radoman M, Pachas G, Fava M, Evins AE (2017) Revisiting the role of the insula and smoking cue-reactivity in relapse: A replication and extension of neuroimaging findings. Drug Alcohol Depend 179:8–12.
Jasper JR, Lesnick JD, Chang LK, Yamanishi SS, Chang TK, Hsu S a, Daunt D a, Bonhaus DW, Eglen RM (1998) Ligand efficacy and potency at recombinant alpha2 adrenergic receptors: agonist-mediated [35S]GTPgammaS binding. Biochem Pharmacol 55:1035–1043.
Jennings JH, Sparta DR, Stamatakis AM, Ung RL, Pleil KE, Kash TL, Stuber GD (2013) Distinct extended amygdala circuits for divergent motivational states. Nature 496:224–228.
Ji MH, Jia M, Zhang MQ, Liu WX, Xie ZC, Wang ZY, Yang JJ (2014) Dexmedetomidine alleviates anxiety-like behaviors and cognitive impairments in a rat model of post-traumatic stress disorder. Prog Neuro-Psychopharmacology Biol Psychiatry 54:284–288.

Jimenez JC, Su K, Goldberg AR, Luna VM, Biane JS, Ordek G, Zhou P, Ong SK, Wright MA, Zweifel LS, Paninski L, Hen R, Kheirbek MA (2018) Anxiety Cells in a Hippocampal-Hypothalamic Circuit. Neuron 97:670–683.
Joffe ME, Grueter BA (2016) Cocaine Experience Enhances Thalamo-Accumbens N-Methyl-D-Aspartate Receptor Function. Biol Psychiatry 80:671–681.
Johnson SB, Emmons EB, Anderson RM, Glanz RM, Romig-Martin SA, Narayanan NS, LaLumiere RT, Radley JJ (2016) A Basal Forebrain Site Coordinates the Modulation of Endocrine and Behavioral Stress Responses via Divergent Neural Pathways. J Neurosci 36:8687–8699.
Johnston AL, Koening-Berard E, Cooper TA, File SE (1988) Comparison of the Effects of Clonidine , Rilmenidine , and Guanfacine in the Holeboard and Elevated Plus-Maze. Drug Dev Res 15:405–414.
Ju G, Swanson LW, Simerly RB (1989) Studies on the Cellular Architecture of the Bed Nuclei of the Stria Terminalis in the Rat: II. Chemoarchitecture. J Comp Neurol 280:603–621.
Kabbaj M, Norton CS, Kollack-Walker S, Watson SJ, Robinson T, Akil H (2001) Social defeat alters the acquisition of cocaine self-administration in rats: Role of individual differences in cocaine-taking behavior. Psychopharmacology 158:382–387.
Kantak KM, Black Y, Valencia E, Green-Jordan K, Eichenbaum HB (2002) Dissociable effects of lidocaine inactivation of the rostral and caudal basolateral amygdala on the maintenance and reinstatement of cocaine-seeking behavior in rats. J Neurosci 22:1126–1136.
Kash TL, Baucum AJ, Conrad KL, Colbran RJ, Winder DG (2009) Alcohol exposure alters NMDAR function in the bed nucleus of the stria terminalis. Neuropsychopharmacology 34:2420–2429.
Kash TL, Matthews RT, Winder DG (2008a) Alcohol inhibits NR2B-containing NMDA receptors in the ventral bed nucleus of the stria terminalis. Neuropsychopharmacology 33:1379–1390.
Kash TL, Nobis WP, Matthews RT, Winder DG (2008b) Dopamine Enhances Fast Excitatory Synaptic Transmission in the Extended Amygdala by a CRF-R1-Dependent Process. J Neurosci 28:13856–13865.
Kash TL, Winder DG (2006) Neuropeptide Y and corticotropin-releasing factor bi-directionally modulate inhibitory synaptic transmission in the bed nucleus of the stria terminalis. Neuropharmacology 51:1013–1022.
Kassel JD, Stroud LR, Paronis CA (2003) Smoking, Stress, and Negative Affect: Correlation, Causation, and Context Across Stages of Smoking. Psychol Bull 129:270–304.
Katche C, Medina JH (2017) Requirement of an Early Activation of BDNF/c-Fos Cascade in the Retrosplenial Cortex for the Persistence of a Long-Lasting Aversive Memory. Cereb Cortex 27:1060–1067.
Kauer JA, Malenka RC (2007) Synaptic plasticity and addiction. Nat Rev Neurosci 8:844–858.
Kaufling J, Girard D, Maitre M, Leste-Lasserre T, Georges F (2017) Species-specific diversity in the anatomical and physiological organisation of the BNST-VTA pathway. Eur J Neurosci 45:1230–1240.
Kaupp UB, Seifert R (2001) Molecular Diversity of Pacemaker Ion Channels. Annu Rev Physiol 63:235–257.
Kawaura K, Karasawa JI, Chaki S, Hikichi H (2014) Stimulation of postsynapse adrenergic alpha2A receptor improves attention/cognition performance in an animal model of attention deficit hyperactivity disorder. Behav Brain Res 270:349–356.

Kemp A, Tischmeyer W, Manahan-Vaughan D (2013) Learning-facilitated long-term depression requires activation of the immediate early gene, c-fos, and is transcription dependent. Behav Brain Res 254:83–91.
Kendler KS, Karkowski LM, Prescott CA (1999) Causal Relationship Between Stressful Life Events and the Onset of Major Depression. Psychiatry Interpers Biol Process 156:837–841.
Keralapurath MM, Briggs SB, Wagner JJ (2017) Cocaine self-administration induces changes in synaptic transmission and plasticity in ventral hippocampus. Addict Biol 22:446–456.
Keralapurath MM, Clark JK, Hammond S, Wagner JJ (2014) Cocaine- or stress-induced metaplasticity of LTP in the dorsal and ventral hippocampus. Hippocampus 24:577–590.
Kerstetter KA, Wunsch AM, Nakata KG, Donckels E, Neumaier JF, Ferguson SM (2016) Corticostriatal Afferents Modulate Responsiveness to Psychostimulant Drugs and Drug-Associated Stimuli. Neuropsychopharmacology 41:1128–1137.
Kessler RC, Berglund P, Demler O, Jin R, Merikangas KR, Walters EE (2005a) Lifetime Prevalence and Age-of-Onset Distributions of DSM-IV Disorders in the National Comorbidity Survey Replicationset Distributions of DSM-IV Disorders in the National Comorbidity Survey Replication. Arch Gen Psychiatry 62:593–602.
Kessler RC, Berglund P, Demler O, Jin R, Walters EE (2005b) Lifetime prevalence and age-of-onset distributions' of DSM-IV disorders in the national comorbidity survey replication. Arch Gen Psychiatry 62:593–602.
Khoshbouei H, Cecchi M, Morilak D a (2002) Modulatory effects of galanin in the lateral bed nucleus of the stria terminalis on behavioral and neuroendocrine responses to acute stress. Neuropsychopharmacology 27:25–34.
Kim CKS, Brager DH, Johnston D (2017) Perisomatic changes in h-channels regulate depressive behaviors following chronic unpredictable stress. Mol Psychiatry 23:1–12.
Kim CS, Chang PY, Johnston D (2012) Article Enhancement of Dorsal Hippocampal Activity by Knockdown of HCN1 Channels Leads to Anxiolytic- and Antidepressant-like Behaviors. Neuron 75:503–516.
Kim S-Y, Adhikari A, Lee SY, Marshel JH, Kim CK, Mallory CS, Lo M, Pak S, Mattis J, Lim BK, Malenka RC, Warden MR, Neve R, Tye KM, Deisseroth K (2013) Diverging neural pathways assemble a behavioural state from separable features in anxiety. Nature 496:219–223.
Klumpers F, Kroes MCW, Baas J, Fernández G (2017) How human amygdala and bed nucleus of the stria terminalis may drive distinct defensive responses. J Neurosci 31:3830–16.
Kodani S, Soya S, Sakurai T (2017) Excitation of GABAergic Neurons in the Bed Nucleus of the Stria Terminalis Triggers Immediate Transition from Non-Rapid Eye Movement Sleep to Wakefulness in Mice. J Neurosci 37:7164–7176.
Koga K, Descalzi G, Collingridge GL, Zhuo M, Koga K, Descalzi G, Chen T, Ko H, Lu J, Li S, Son J (2015) Coexistence of Two Forms of LTP in ACC Provides a Synaptic Mechanism for the Interactions between Anxiety and Chronic Pain Article Coexistence of Two Forms of LTP in ACC Provides a Synaptic Mechanism for the Interactions between Anxiety and Chronic Pain. Neuron 85:377–389.
Koob GF (2009) Brain stress systems in the amygdala and addiction. Brain Res 1293:61–75.
Koob GF, Volkow ND (2010) Neurocircuitry of addiction. Neuropsychopharmacology 35:217–238.
Kosten TA, Miserendino MJD, Kehoe P (2000) Enhanced acquisition of cocaine self-administration in adult rats with neonatal isolation stress experience. Brain Res 875:44–50.

Koya E, Uejima JL, Wihbey KA, Bossert JM, Hope BT, Shaham Y (2009) Role of ventral medial prefrontal cortex in incubation of cocaine craving. Neuropharmacology 56:177–185.
Krashes MJ, Roth BL, Lowell BB, Koda S, Ye C, Rogan SC, Adams AC, Cusher DS, Maratos-flier E (2011) Rapid, reversible activation of AgRP neurons drives feeding behavior in mice Find the latest version : Brief report Rapid , reversible activation of AgRP neurons drives feeding behavior in mice. J Clin Invest 121:1424–1428.
Krawczyk M, DeBacker J, Mason X, Jones AA, Dumont EC (2014) Dopamine decreases NMDA currents in the oval bed nucleus of the stria terminalis of cocaine self-administering rats. Prog Neuro-Psychopharmacology Biol Psychiatry 51:83–88.
Krawczyk M, Georges FFF, Sharma R, Mason X, Berthet A, Bézard E, Dumont EC, Bezard E, Dumont ÉC, Bezard E, Dumont EC, Bézard E, Dumont EC (2011a) Double-Dissociation of the Catecholaminergic Modulation of Synaptic Transmission in the Oval Bed Nucleus of the Stria Terminalis. J Neurophysiol 105:145–153.
Krawczyk M, Sharma R, Mason X, DeBacker J, Jones AA, Dumont EC (2011b) A Switch in the Neuromodulatory Effects of Dopamine in the Oval Bed Nucleus of the Stria Terminalis Associated with Cocaine Self-Administration in Rats. J Neurosci 31:8928–8935.
Krüger O, Shiozawa T, Kreifelts B, Scheffler K, Ethofer T (2015) Three distinct fiber pathways of the bed nucleus of the stria terminalis to the amygdala and prefrontal cortex. Cortex 66:60–68.
Krugers HJ, Koolhaas JM, Medema RM, Korf J (1996) Prolonged subordination stress increases Calbindin-D28k immunoreactivity in the rat hippocampal CA1 area. Brain Res 729:289–293.
Kuhn BN, Klumpner MS, Covelo IR, Campus P, Flagel SB (2018) Transient inactivation of the paraventricular nucleus of the thalamus enhances cue-induced reinstatement in goal-trackers, but not sign-trackers. Psychopharmacology 235:999–1014.
Kumar R, Hazan A, Geron M, Steinberg R, Livni L, Matzner H, Priel A (2017) Activation of transient receptor potential vanilloid 1 by lipoxygenase metabolites depends on PKC phosphorylation. FASEB J 31:1238–1247.
Kupferschmidt DA, Cody PA, Lovinger DM, Davis MI (2015) Brain BLAQ: Post-hoc thick-section histochemistry for localizing optogenetic constructs in neurons and their distal terminals. Front Neuroanat 9:1–9.
Kupferschmidt DA, Juczewski K, Cui G, Johnson KA, Lovinger DM (2017) Parallel, but Dissociable, Processing in Discrete Corticostriatal Inputs Encodes Skill Learning. Neuron 96:476–489.e5.
Lahdesmaki J, Sallinen J, MacDonald E, Kobilka BK, Fagerholm V, Scheinin M (2002) Behavioral and neurochemical characterization of alpha2A-adrenergic receptor knockout mice. Neuroscience 113:289–299.
Lähdesmäki J, Sallinen J, MacDonald E, Scheinin M (2004) Alpha2A-adrenoceptors are important modulators of the effects of D-amphetamine on startle reactivity and brain monoamines. Neuropsychopharmacology 29:1282–1293.
Lakhlani PP, MacMillan LB, Guo TZ, McCool B a, Lovinger DM, Maze M, Limbird LE (1997) Substitution of a mutant alpha2a-adrenergic receptor via “hit and run” gene targeting reveals the role of this subtype in sedative, analgesic, and anesthetic-sparing responses in vivo. Proc Natl Acad Sci U S A 94:9950–9955.
Lampert R, Tuit K, Hong KI, Donovan T, Lee F, Sinha R (2016) Cumulative stress and autonomic dysregulation in a community sample. Stress 19:269–279.

Larkum ME, Launey T, Dityatev a, Lüscher HR (1998) Integration of excitatory postsynaptic potentials in dendrites of motoneurons of rat spinal cord slice cultures. J Neurophysiol 80:924–935.
Larriva-Sahd J (2004) Juxtacapsular nucleus of the stria terminalis of the adult rat: Extrinsic inputs, cell types, and neuronal modules: A combined golgi and electron microscopic study. J Comp Neurol 475:220–237.
Larzelere MM, Jones GN (2008) Stress and Health. Prim Care Clin Off Pract 35:839–856.
Lasseter HC, Xie X, Ramirez DR, Fuchs RA (2010) Sub-region specific contribution of the ventral hippocampus to drug context-induced reinstatement of cocaine-seeking behavior in rats. Neuroscience 171:830–839.
Le AD, Funk D, Coen K, Tamadon S, Shaham Y (2018) Role of Kappa Opioid Receptors in the Bed Nucleus of Stria Terminalis in Reinstatement of Alcohol Seeking. Neuropsychopharmacology 43:838–850.
Le AD, Harding S, Juzytsch W, Funk D, Shaham Y (2005) Role of alpha-2 adrenoceptors in stress-induced reinstatement of alcohol seeking and alcohol self-administration in rats. Psychopharmacology 179:366–373.
Le AD, Harding S, Juzytsch W, Watchus J, Shalev U, Shaham Y (2000) The role of corticotropin-releasing factor instress-induced relapse to alcohol-seeking behavior in rats. Psychopharmacology 150:317–324.
Lebow MA, Chen A (2016) Overshadowed by the amygdala: The bed nucleus of the stria terminalis emerges as key to psychiatric disorders. Mol Psychiatry 21:450–463.
Ledgerwood DM, Petry NM (2006) What do we know about relapse in pathological gambling? Clin Psychol Rev 26:216–228.
Leri F, Flores J, Rodaros D, Stewart J (2002) Blockade of stress-induced but not cocaine-induced reinstatement by infusion of noradrenergic antagonists into the bed nucleus of the stria terminalis or the central nucleus of the amygdala. J Neurosci 22:5713–5718.
Lewis AS, Schwartz E, Chan CS, Noam Y, Shin M, Wadman WJ, Surmeier DJ, Baram TZ, Macdonald RL, Chetkovich DM (2009) Alternatively Spliced Isoforms of TRIP8b Differentially Control h Channel Trafficking and Function. J Neurosci 29:6250–6265.
Lewis AS, Vaidya SP, Blaiss CA, Liu Z, Stoub TR, Brager DH, Chen X, Bender RA, Estep CM, Popov AB, Kang CE, Veldhoven PP Van, Bayliss DA, Nicholson DA, Powell CM, Johnston D, Chetkovich DM (2011) Deletion of the Hyperpolarization-Activated Cyclic Nucleotide-Gated Channel Auxiliary Subunit TRIP8b Impairs Hippocampal I h Localization and Function and Promotes Antidepressant Behavior in Mice. J Neurosci 31:7424–7440.
Li C, Sugam JA, Lowery-Gionta EG, McElligott ZA, McCall NM, Lopez AJ, McKlveen JM, Pleil KE, Kash TL (2016) Mu Opioid Receptor Modulation of Dopamine Neurons in the Periaqueductal Gray/Dorsal Raphe: A Role in Regulation of Pain. Neuropsychopharmacology 41:2122–2132.
Li JT, Xie XM, Yu JY, Sun YX, Liao XM, Wang XX, Su YA, Liu YJ, Schmidt M V., Wang XD, Si TM (2017) Suppressed Calbindin Levels in Hippocampal Excitatory Neurons Mediate Stress-Induced Memory Loss. Cell Rep 21:891–900.
Li S, Kirouac GJ, Seki T, Namba T, Mochizuki H, Onodera M (2008) Projections From the Paraventricular Nucleus of the Thalamus to the Forebrain, With Special Emphasis on the Extended Amygdala. J Comp Neurol 506:263–287.
Li X, Rubio FJ, Zeric T, Bossert JM, Kambhampati S, Cates HM, Kennedy PJ, Liu QR, Cimbro

R, Hope BT, Nestler EJ, Shaham Y (2015) Incubation of Methamphetamine Craving Is Associated with Selective Increases in Expression of Bdnf and Trkb, Glutamate Receptors, and Epigenetic Enzymes in Cue-Activated Fos-Expressing Dorsal Striatal Neurons. J Neurosci 35:8232–8244.
Lillethorup TP, Iversen P, Fontain J, Wegener G, Doudet DJ, Landau AM (2015) Electroconvulsive shocks decrease α2-adrenoceptor binding in the Flinders rat model of depression. Eur Neuropsychopharmacol 25:404–412.
Lloyd DA, Turner RJ (2008) Cumulative lifetime adversities and alcohol dependence in adolescence and young adulthood. Drug Alcohol Depend 93:217–226.
Lopez-Quintero C, Hasin DS, De Los Cobos JP, Pines A, Wang S, Grant BF, Blanco C (2011) Probability and predictors of remission from life-time nicotine, alcohol, cannabis or cocaine dependence: Results from the National Epidemiologic Survey on Alcohol and Related Conditions. Addiction 106:657–669.
Lörincz A, Notomi T, Tamás G, Shigemoto R, Nusser Z (2002) Polarized and compartment-dependent distribution of HCN1 in pyramidal cell dendrites. Nat Neurosci 5:1185–1193.
Louderback KM, Wills TA, Muglia LJ, Winder DG (2013) Knockdown of BNST GluN2B-containing NMDA receptors mimics the actions of ketamine on novelty-induced hypophagia. Transl Psychiatry 3:e331.
Lovinger DM, Kash TL (2015) Mechanisms of Neuroplasticity and Ethanol's Effects on Plasticity in the Striatum and Bed Nucleus of the Stria Terminalis. Alcohol Res 37:109–124.
Lowery EG, Spanos M, Navarro M, Lyons AM, Hodge CW, Thiele TE (2010) CRF-1 antagonist and CRF-2 agonist decrease binge-like ethanol drinking in c57bl/6j mice independent of the HPA axis. Neuropsychopharmacology 35:1241–1252.
Lu H, Cheng P lin, Lim BK, Khoshnevisrad N, Poo M ming (2010) Elevated BDNF after Cocaine Withdrawal Facilitates LTP in Medial Prefrontal Cortex by Suppressing GABA Inhibition. Neuron 67:821–833.
Lu L, Grimm JW, Hope BT, Shaham Y (2004) Incubation of cocaine craving after withdrawal: A review of preclinical data. Neuropharmacology 47:214–226.
Lu R, Li Y, Zhang Y, Chen Y, Shields AD, Winder DG, Angelotti T, Jiao K, Limbird LE, Zhou Y, Wang Q (2009) Epitope-tagged receptor knock-in mice reveal that differential desensitization of α2-adrenergic responses is because of ligand-selective internalization. J Biol Chem 284:13233–13243.
Lüscher C, Malenka RC (2011) Drug-Evoked Synaptic Plasticity in Addiction: From Molecular Changes to Circuit Remodeling. Neuron 69:650–663.
Lyford GL, Yamagata K, Kaufmann WE, Barnes CA, Sanders LK, Copeland NG, Gilbert DJ, Jenkins NA, Lanahan AA, Worley PF (1995) Arc, a growth factor and activity-regulated gene, encodes a novel cytoskeleton-associated protein that is enriched in neuronal dendrites. Neuron 14:433–445.
Lyman KA, Han Y, Heuermann RJ, Cheng X, Kurz JE, Lyman RE, Van Veldhoven PP, Chetkovich DM (2017) Allostery between two binding sites in the ion channel subunit TRIP8b confers binding specificity to HCN channels. J Biol Chem 292:17718–17730.
MacLennan SJ, Luong LA, Jasper JR, To ZP, Eglen RM (1997) Characterization of α2-adrenoceptors mediating contraction of dog saphenous vein: Identity with the human α(2A) subtype. Br J Pharmacol 121:1721–1729.
Madisen L et al. (2015) Transgenic mice for intersectional targeting of neural sensors and

effectors with high specificity and performance. Neuron 85:942–958.
Magee JC (1998) Dendritic Hyperpolarization-Activated Currents Modify the Integrative Properties of Hippocampal CA1 Pyramidal Neurons. J Neurosci 18:7613–7624.
Magee KEA, Madden Z, Young EC (2015) HCN Channel C-Terminal Region Speeds Activation Rates Independently of Autoinhibition. J Membr Biol 248:1043–1060.
Mahler S V., Vazey EM, Beckley JT, Keistler CR, McGlinchey EM, Kaufling J, Wilson SP, Deisseroth K, Woodward JJ, Aston-Jones G (2014) Designer Receptors Show Role for Ventral Palladium Input to Ventral Tegmental Area in Cocaine Seeking. Nat Neurosci 17:577–585.
Makino S, Gold PW, Schulkin J (1994) Effects of corticosterone on CRH mRNA and content in the bed nucleus of the stria terminalis; comparison with the effects in the central nucleus of the amygdala and the paraventricular nucleus of the hypothalamus. Brain Res 657:141–149.
Malikowska N, Fijałkowski Ł, Nowaczyk A, Popik P, Sałat K (2017) Antidepressant-like activity of venlafaxine and clonidine in mice exposed to single prolonged stress – A model of post-traumatic stress disorder. Pharmacodynamic and molecular docking studies. Brain Res 1673:1–10.
Mantsch JR, Weyer A, Vranjkovic O, Beyer CE, Baker D a, Caretta H (2010) Involvement of noradrenergic neurotransmission in the stress- but not cocaine-induced reinstatement of extinguished cocaine-induced conditioned place preference in mice: role for β-2 adrenergic receptors. Neuropsychopharmacology 35:2165–2178.
Marcinkiewcz CA, Mazzone CM, D'Agostino G, Halladay LR, Hardaway JA, DiBerto JF, Navarro M, Burnham N, Cristiano C, Dorrier CE, Tipton GJ, Ramakrishnan C, Kozicz T, Deisseroth K, Thiele TE, McElligott ZA, Holmes A, Heisler LK, Kash TL (2016) Serotonin engages an anxiety and fear-promoting circuit in the extended amygdala. Nature 537:97–101.
Marinelli PW, Funk D, Juzytsch W, Harding S, Rice KC, Shaham Y, Lê AD (2007) The CRF1receptor antagonist antalarmin attenuates yohimbine-induced increases in operant alcohol self-administration and reinstatement of alcohol seeking in rats. Psychopharmacology 195:345–355.
Martinez M, Phillips PJ, Herbert J (1998) Adaptation in patterns of c-fos expression in the brain associated with exposure to either single or repeated social stress in male rats. Eur J Neurosci 10:20–33.
Matzeu A, Weiss F, Martin-Fardon R (2015) Transient inactivation of the posterior paraventricular nucleus of the thalamus blocks cocaine-seeking behavior. Neurosci Lett 608:34–39.
Mazzone CM, Pati D, Michaelides M, DiBerto J, Fox JH, Tipton G, Anderson C, Duffy K, McKlveen JM, Hardaway JA, Magness ST, Falls WA, Hammack SE, McElligott ZA, Hurd YL, Kash TL (2018) Acute engagement of Gq-mediated signaling in the bed nucleus of the stria terminalis induces anxiety-like behavior. Mol Psychiatry 23:143–153.
McCormick DA, Pape H-C (1990) Properties of a hyperpolarization-activated cation current and its role in rhythmic oscillation in thalamic relay neurons. J Physiol 431:291–318.
McCoy ES, Taylor-Blake B, Zylka MJ (2012) CGRPα-expressing sensory neurons respond to stimuli that evoke sensations of pain and itch. PLoS One 7:e36355.
McCune SK, Voigt MM, Hill JM (1993) Expression of multiple alpha adrenergic receptor subtype messenger RNAs in the adult rat brain. Neuroscience 57:143–151.
Mcdonald AJ, Mascagni F, Guo L (1996) Projections of the medial and lateral prefrontal cortices

to the amygdala: A Phaseolus vulgaris leucoagglutinin study in the rat. Neuroscience 71:55–75.
McElligott ZA, Klug JR, Nobis WP, Patel S, Grueter BA, Kash TL, Winder DG (2010) Distinct forms of Gq-receptor-dependent plasticity of excitatory transmission in the BNST are differentially affected by stress. Proc Natl Acad Sci U S A 107:2271–2276.
McElligott ZA, Winder DG (2008) Alpha1-adrenergic receptor-induced heterosynaptic long-term depression in the bed nucleus of the stria terminalis is disrupted in mouse models of affective disorders. Neuropsychopharmacology 33:2313–2323.
McElligott ZA, Winder DG (2009) Modulation of glutamatergic synaptic transmission in the bed nucleus of the stria terminalis. Prog Neuropsychopharmacol Biol Psychiatry 33:1329–1335.
McEwen BS (1998) Protective and damaging effects of stress mediators. N Engl J Med 338:171–179.
McEwen BS (2004) Protection and damage from acute and chronic stress: Allostasis and allostatic overload and relevance to the pathophysiology of psychiatric disorders. Ann N Y Acad Sci 1032:1–7.
McEwen BS (2007) Physiology and neurobiology of stress and adaptation: Central role of the brain. Physiol Rev 87:873–904.
McEwen BS (2012) Brain on stress: How the social environment gets under the skin. Proc Natl Acad Sci 109:17180–17185.
McFarland K, Davidge SB, Lapish CC, Kalivas PW (2004) Limbic and motor circuitry underlying footshock-induced reinstatement of cocaine-seeking behavior. J Neurosci 24:1551–1560.
McIntyre CK, Miyashita T, Setlow B, Marjon KD, Steward O, Guzowski JF, McGaugh JL (2005) Memory-influencing intra-basolateral amygdala drug infusions modulate expression of Arc protein in the hippocampus. Proc Natl Acad Sci 102:10718–10723.
Meil WM, See RE (1997) Lesions of the basolateral amygdala abolish the ability of drug associated cues to reinstate responding during withdrawal from self- administered cocaine. Behav Brain Res 87:139–148.
Melchior JR, Ferris MJ, Stuber GD, Riddle DR, Jones SR (2015) Optogenetic versus electrical stimulation of dopamine terminals in the nucleus accumbens reveals local modulation of presynaptic release. J Neurochem 134:833–844.
Melchior JR, Jones SR (2017) Chronic ethanol exposure increases inhibition of optically targeted phasic dopamine release in the nucleus accumbens core and medial shell ex vivo. Mol Cell Neurosci 85:93–104.
Meredith GE, Callen S, Scheuer DA (2002) Brain-derived neurotrophic factor expression is increased in the rat amygdala, piriform cortex and hypothalamus following repeated amphetamine administration. Brain Res 949:218–227.
Micioni Di Bonaventura M V., Ciccocioppo R, Romano A, Bossert JM, Rice KC, Ubaldi M, St. Laurent R, Gaetani S, Massi M, Shaham Y, Cifani C (2014) Role of Bed Nucleus of the Stria Terminalis Corticotrophin-Releasing Factor Receptors in Frustration Stress-Induced Binge-Like Palatable Food Consumption in Female Rats with a History of Food Restriction. J Neurosci 34:11316–11324.
Miles PR, Mundorf ML, Wightman RM (2002) Release and uptake of catecholamines in the bed nucleus of the stria terminalis measured in the mouse brain slice. Synapse 44:188–197.
Milivojevic V, Fox HC, Jayaram-Lindstrom N, Hermes G, Sinha R (2017) Sex differences in guanfacine effects on stress-induced stroop performance in cocaine dependence. Drug

Alcohol Depend 179:275–279.
Miller PM, Hersen M, Eisler RM, Hilsman G (1974) Effects of social stress on operant drinking of alcoholics and social drinkers. Behav Res Ther 12:67–72.
Miller RJ (1998) Presynaptic Receptors. Annu Rev Pharmacol Toxicol 38:201–227.
Miloyan B, Joseph Bienvenu O, Brilot B, Eaton WW (2018) Adverse life events and the onset of anxiety disorders. Psychiatry Res 259:488–492.
Mineur YS, Bentham MP, Zhou W-L, Plantenga ME, McKee SA, Picciotto MR (2015) Antidepressant-like effects of guanfacine and sex-specific differences in effects on c-fos immunoreactivity and paired-pulse ratio in male and female mice. Psychopharmacology:3539–3549.
Moaddab M, Mangone E, Ray MH, McDannald MA (2017) Adolescent alcohol drinking renders adult drinking BLA-dependent: BLA hyper-activity as contributor to comorbid alcohol use disorder and anxiety disorders. Brain Sci 7:11.
Mobbs D, Yu R, Rowe JB, Eich H, FeldmanHall O, Dalgleish T (2010) Neural activity associated with monitoring the oscillating threat value of a tarantula. Proc Natl Acad Sci 107:20582–20586.
Monteggia LM, Eisch AJ, Tang MD, Kaczmarek LK, Nestler EJ (2000) Cloning and localization of the hyperpolarization-activated cyclic nucleotide-gated channel family in rat brain. Mol Brain Res 81:129–139.
Mu D, Deng J, Liu K-F, Wu Z-Y, Shi Y, Guo W-M, Mao Q, Liu X-J, Li H, Sun Y (2017) A central neural circuit for itch sensation. Science 357:695–699.
Myers B, Meerveld BG (2010) Elevated corticosterone in the amygdala leads to persistant increases in anxiety-like behavior and pain sensitivity. Behav Brain Res 214:465–469.
Nagano Y, Kaneda K, Maruyama C, Ide S, Kato F, Minami M (2015) Corticotropin-releasing factor enhances inhibitory synaptic transmission to type III neurons in the bed nucleus of the stria terminalis. Neurosci Lett 600:56–61.
Nakabeppu Y, Ryder K, Nathans D (1988) DNA binding activities of three murine Jun proteins: Stimulation by Fos. Cell 55:907–915.
Naqvi N, Rudrauf D, Damasio H, Bechara A (2007) Damage to the Insula Disrupts Addition to Cigarette Smoking. Science 315:531–535.
Neisewander JL, Baker D a, Fuchs R a, Tran-Nguyen LT, Palmer A, Marshall JF (2000) Fos protein expression and cocaine-seeking behavior in rats after exposure to a cocaine self-administration environment. J Neurosci 20:798–805.
Nestler EJ (2001) Molecular basis of neural plasticity underlying addiction . Nat Rev Neurosci 2:119–128.
Nestler EJ, Hope BT, Widnell KL (1993) Drug addiction: A model for the molecular basis of neural plasticity. Neuron 11:995–1006.
Neumann PA, Wang Y, Yan Y, Wang Y, Ishikawa M, Cui R, Huang YH, Sesack SR, Schlüter OM, Dong Y (2016) Cocaine-induced synaptic alterations in thalamus to nucleus accumbens projection. Neuropsychopharmacology 41:2399–2410.
Nguyen AQ, Dela Cruz JAD, Sun Y, Holmes TC, Xu X, Cruz JAD Dela, Sun Y, Holmes TC, Xu X (2016) Genetic cell targeting uncovers specific neuronal types and distinct subregions in the bed nucleus of the stria terminalis. J Comp Neurol 524:2379–2399.
Nguyen NK, Keck ME, Hetzenauer A, Thoeringer CK, Wurst W, Deussing JM, Holsboer F, Müller MB, Singewald N (2006) Conditional CRF receptor 1 knockout mice show altered neuronal activation pattern to mild anxiogenic challenge. Psychopharmacology 188:374–

385.
Nicholas AP, Pieribone V, Hokfelt T (1993) Distributions of mRNAs for alpha-2 adrenergic receptor subtypes in rat brain: an in situ hybridization study. J Comp Neurol 328:575–594.
Niswender CM, Conn PJ (2010) Metabotropic Glutamate Receptors: Physiology, Pharmacology, and Disease. Annu Rev Pharmacol Toxicol 50:295–322.
Nobis WP, Kash TL, Silberman Y, Winder DG (2011) Beta-Adrenergic receptors enhance excitatory transmission in the bed nucleus of the stria terminalis through a corticotrophin-releasing factor receptor dependent and cocaine-regulated mechanism. Biol Psychiatry 69:1083–1090.
Normandeau CP, Dumont EC (2017) Cocaine and Dysregulated Synaptic Transmission in the Bed Nucleus of the Stria Terminalis. Neurosci Cocaine:537–543.
Notomi T, Shigemoto R (2004) Immunohistochemical Localization of Ih Channel Subunits, HCN1-4, in the Rat Brain. J Comp Neurol 471:241–276.
Nowak B, Zadrozna M, Ossowska G, Sowa-Kućma M, Gruca P, Papp M, Dybała M, Pilc A, Nowak G (2010) Alterations in hippocampal calcium-binding neurons induced by stress models of depression: A preliminary assessment. Pharmacol Reports 62:1204–1210.
O'Shea EK, Rutkowskia R, Stafford WFI, Kim PS (1989) Preferential Heterodimer Formation by Isolated Leucine Zippers from Fos and Jun. Science 245:646–648.
Ognjanovski N, Schaeffer S, Wu J, Mofakham S, Maruyama D, Zochowski M, Aton SJ (2017) memory consolidation. Nat Commun 8:1–13.
Okamoto T, Harnett MT, Morikawa H, Harnett MT, Morikawa H (2018) Hyperpolarization-Activated Cation Current (I h) Is an Ethanol Target in Midbrain Dopamine Neurons of Mice. J Neurophysiol 95:619–626.
Okutsu Y, Takahashi Y, Nagase M, Shinohara K, Ikeda R, Kato F (2017) Potentiation of NMDA receptor-mediated synaptic transmission at the parabrachial-central amygdala synapses by CGRP in mice. Mol Pain 13:1–11.
Olive MF, Koenig HN, Nannini MA, Hodge CW (2002) Elevated extracellular CRF levels in the bed nucleus of the stria terminalis during ethanol withdrawal and reduction by subsequent ethanol intake. Pharmacol Biochem Behav 72:213–220.
del Olmo N, Miguéns M, Higuera-Matas A, Torres I, García-Lecumberri C, Solís JM, Ambrosio E (2006) Enhancement of hippocampal long-term potentiation induced by cocaine self-administration is maintained during the extinction of this behavior. Brain Res 1116:120–126.
Olsen CM, Winder DG (2010) Operant Sensation Seeking in the Mouse. J Vis Exp:4–7.
Ostrander MM, Richtand NM, Herman JP (2003) Stress and amphetamine induce Fos expression in medial prefrontal cortex neurons containing glucocorticoid receptors. Brain Res 990:209–214.
Pacak K, McCarty R, Palkovits M, Kopin IJ, Goldstein DS (1995) Effects of immobilization on in vivo release of norepinephrine in the bed nucleus of the stria terminalis in conscious rats. Brain Res 688:242–246.
Palij P, Stamford J a (1993) Real-time monitoring of endogenous noradrenaline release in rat brain slices using fast cyclic voltammetry. 2. Operational characteristics of the alpha 2 autoreceptor in the bed nucleus of stria terminalis, pars ventralis. Brain Res 607:134–140.
Palmiter RD (2018) The Parabrachial Nucleus: CGRP Neurons Function as a General Alarm. Trends Neurosci 41:280–293.
Park J, Kile BM, Wightman RM (2009) In vivo voltammetric monitoring of norepinephrine

release in the rat ventral bed nucleus of the stria terminalis and anteroventral thalamic nucleus. Eur J Neurosci 30:2121–2133.
Park J, Wheeler R a., Fontillas K, Keithley RB, Carelli RM, Wightman RM (2012) Catecholamines in the bed nucleus of the stria terminalis reciprocally respond to reward and aversion. Biol Psychiatry 71:327–334.
Park K, Hyun J, Kim H, Choi K, Jung S, Soon K (2011) Biochemical and Biophysical Research Communications HCN channel activity-dependent modulation of inhibitory synaptic transmission in the rat basolateral amygdala. Biochem Biophys Res Commun 404:952–957.
Park K, Lee S (2007) Hyperpolarization-activated currents control the excitability of principal neurons in the basolateral amygdala. Biochem Biophys Res Commun 361:718–724.
Partridge JG, Forcelli PA, Luo R, Cashdan JM, Schulkin J, Valentino RJ, Vicini S (2016) Stress increases GABAergic neurotransmission in CRF neurons of the central amygdala and bed nucleus stria terminalis. Neuropharmacology 107:239–250.
Patriarchi T, Cho JR, Merten K, Howe MW, Marley A, Xiong W, Folk RW, Broussard GJ, Liang R, Jang MJ, Zhong H, Dombeck D, Zastrow M Von, Nimmerjahn A, Gradinaru V, Williams JT, Tian L (2018) Ultrafast neuronal imaging of dopamine dynamics with designed genetically encoded sensors. Science 360:1–15.
Paxinos G, Franklin B (2004) The Mouse Brain in Stereotaxic Coordinates.
Pelham WE, Lang a R, Atkeson B, Murphy D a, Gnagy EM, Greiner a R, Vodde-Hamilton M, Greenslade KE (1997) Effects of deviant child behavior on parental distress and alcohol consumption in laboratory interactions. J Abnorm Child Psychol 25:413–424.
Phelix CF, Liposits Z, Paull WK (1992) Monoamine innervation of bed nucleus of stria terminalis: an electron microscopic investigation. Brain Res Bull 28:949–965.
Pian P, Bucchi A, Robinson RB, Siegelbaum SA (2006) Regulation of Gating and Rundown of HCN Hyperpolarization-activated Channels by Exogenous and Endogenous PIP $_2$. J Gen Physiol 128:593–604.
Piatkevich KD et al. (2018) A robotic multidimensional directed evolution approach applied to fluorescent voltage reporters. Nat Chem Biol 14:352–360.
Piazza PV, Deminiere JM, Le Moal M, Simon H (1990) Stress and pharmacologically induced behavioral sensitization increases to acquisition of amphetamine self-administration. Brain Res 514:22–26.
Pierce RC, Kumaresan V (2006) The mesolimbic dopamine system: The final common pathway for the reinforcing effect of drugs of abuse? Neurosci Biobehav Rev 30:215–238.
Pina MM, Cunningham CL (2017) Ethanol-seeking behavior is expressed directly through an extended amygdala to midbrain neural circuit. Neurobiol Learn Mem 137:83–91.
Pina MM, Young EA, Ryabinin AE, Cunningham CL (2015) The bed nucleus of the stria terminalis regulates ethanol-seeking behavior in mice. Neuropharmacology 99:627–638.
Pleil KE, Lopez A, McCall N, Jijon AM, Bravo JP, Kash TL (2012) Chronic stress alters neuropeptide y signaling in the bed nucleus of the stria terminalis in DBA/2J but not C57BL/6J mice. Neuropharmacology 62:1777–1786.
Pleil KE, Lowery-Gionta EG, Crowley NA, Li C, Marcinkiewcz CA, Rose JH, McCall NM, Maldonado-Devincci AM, Morrow AL, Jones SR, Kash TL, Morrow LA, Jones SR, Kash TL (2015a) Effects of chronic ethanol exposure on neuronal function in the prefrontal cortex and extended amygdala. Neuropharmacology 99:735–749.
Pleil KE, Rinker JA, Lowery-Gionta EG, Mazzone CM, McCall NM, Kendra AM, Olson DP, Lowell BB, Grant KA, Thiele TE, Kash TL (2015b) NPY signaling inhibits extended

amygdala CRF neurons to suppress binge alcohol drinking. Nat Neurosci 18:545–552.
Pomerlau OF, Pomerlau CS (1991) Research on stress and smoking: progress and problems. Br J Addict 86:599–603.
Pomrenze MB, Fetterly TL, Winder DG, Messing RO (2017) The Corticotropin Releasing Factor Receptor 1 in Alcohol Use Disorder: Still a Valid Drug Target? Alcohol Clin Exp Res 41:1986–1999.
Puente N, Cui Y, Lassalle O, Lafourcade M, Georges F, Venance L, Grandes P, Manzoni OJ (2011) Polymodal activation of the endocannabinoid system in the extended amygdala. Nat Neurosci 14:1542–1547.
Pushparaj A, Le Foll B (2015) Involvement of the caudal granular insular cortex in alcohol self-administration in rats. Behav Brain Res 293:203–207.
Pushparaj A, Hamani C, Yu W, Shin DS, Kang B, Nobrega JN, Le Foll B (2013) Electrical stimulation of the insular region attenuates nicotine-taking and nicotine-seeking behaviors. Neuropsychopharmacology 38:690–698.
Pushparaj A, Kim AS, Musiol M, Trigo JM, Le Foll B (2015) Involvement of the rostral agranular insular cortex in nicotine self-administration in rats. Behav Brain Res 290:77–83.
Radley JJ, Anderson RM, Hamilton BA, Alcock JA, Romig-Martin SA (2013) Chronic Stress-Induced Alterations of Dendritic Spine Subtypes Predict Functional Decrements in an Hypothalamo-Pituitary-Adrenal-Inhibitory Prefrontal Circuit. J Neurosci 33:14379–14391.
Radley JJ, Gosselink KL, Sawchenko PE (2009) A Discrete GABAergic Relay Mediates Medial Prefrontal Cortical Inhibition of the Neuroendocrine Stress Response. J Neurosci 29:7330–7340.
Radley JJ, Sawchenko PE (2011) A Common Substrate for Prefrontal and Hippocampal Inhibition of the Neuroendocrine Stress Response. J Neurosci 31:9683–9695.
Rainnie DG, Hazra R, Dabrowska J, Guo JD, Li CC, Dewitt S, Muly EC (2014) Distribution and functional expression of Kv4 family α subunits and associated KChIP β subunits in the bed nucleus of the stria terminalis. J Comp Neurol 522:609–625.
Rauscher FJ, Voulalas PJ, Franza BR, Curran T (1988) Fos and Jun bind cooperatively to the AP-1 site: reconstitution in vitro. Genes Dev 2:1687–1699.
Reichmann F, Holzer P (2016) Neuropeptide Y: A stressful review. Neuropeptides 55:99–109.
Reisiger A-R, Kaufling J, Manzoni OJ, Cador M, Georges F, Caille S (2014) Nicotine Self-Administration Induces CB1-Dependent LTP in the Bed Nucleus of the Stria Terminalis. J Neurosci 34:4285–4292.
Resstel LBM, Alves FHF, Reis DG, Crestani CC, Corrêa FMA, Guimarães FS (2008) Anxiolytic-like effects induced by acute reversible inactivation of the bed nucleus of stria terminalis. Neuroscience 154:869–876.
Reynolds MW, Frank C (2000) Smoking and adverse childhood experiences. JAMA J Am Med Assoc 283:1958–1959.
Rinker JA, Marshall SA, Mazzone CM, Lowery-gionta EG, Gulati V, Pleil KE, Kash TL, Navarro M, Thiele TE (2017) Extended Amygdala to Ventral Tegmental Area Corticotropin-Releasing Factor Circuit Controls Binge Ethanol Intake. Biol Psychiatry 81:930–940.
Rogers JL, See RE (2007) Selective inactivation of the ventral hippocampus attenuates cue-induced and cocaine-primed reinstatement of drug-seeking in rats. Neurobiol Learn Mem 87:688–692.
Rosin DL, Talley EM, Lee AMY, Stornetta RL, Gaylinn BD, Guyenet PG, Lynch KR (1996)

Distribution of cwzc -Adrenergic Receptor-Like Immunoreactivity in the Rat Central Nervous System. 165:135–165.
Roth BL (2016) Primer DREADDs for Neuroscientists. Neuron 89:683–694.
Russell FA, King R, Smillie S-J, Kodji X, Brain SD (2014) Calcitonin Gene-Related Peptide: Physiology and Pathophysiology. Physiol Rev 94:1099–1142.
Sabban EL, Serova LI, Alaluf LG, Laukova M, Peddu C (2015) Comparative effects of intranasal neuropeptide Y and HS014 in preventing anxiety and depressive-like behavior elicited by single prolonged stress. Behav Brain Res 295:9–16.
Sah R, Geracioti TD (2012) Neuropeptide Y and posttraumatic stress disorder. Mol Psychiatry 18:646–655.
Sajdyk TJ, Johnson PL, Leitermann RJ, Fitz SD, Dietrich A, Morin M, Gehlert DR, Urban JH, Shekhar A (2008) Neuropeptide Y in the Amygdala Induces Long-Term Resilience to Stress-Induced Reductions in Social Responses But Not Hypothalamic-Adrenal-Pituitary Axis Activity or Hyperthermia. J Neurosci 28:893–903.
Sanders J (2016) Data on Arc and Zif268 expression in the brain of the alpha-2A adrenergic receptor knockout mouse. Data Br 7:8–11.
Santoro B, Piskorowski RA, Pian P, Hu L, Liu H, Siegelbaum SA (2009) Article TRIP8b Splice Variants Form a Family of Auxiliary Subunits that Regulate Gating and Trafficking of HCN Channels in the Brain. Neuron 62:802–813.
Saper CB, Loewy AD (1980) Efferent connections of the parabrachial nucleus in the rat. Brain Res 197:291–317.
Sartor GC, Aston-Jones G (2012) Regulation of the ventral tegmental area by the bed nucleus of the stria terminalis is required for expression of cocaine preference. Eur J Neurosci 36:3549–3558.
Savchenko VL, Boughter JD (2011) Regulation of neuronal activation by alpha2A adrenergic receptor agonist. Neurotox Res 20:226–239.
Schmidt H (2012) Three functional facets of calbindin D-28k. Front Mol Neurosci 5:1–7.
Schramm NL, McDonald MP, Limbird LE (2001) The alpha(2a)-adrenergic receptor plays a protective role in mouse behavioral models of depression and anxiety. J Neurosci 21:4875–4882.
Schuckit MA, Hesselbrock V (1994) Alcohol Dependence and Anxiety Disorders: What is the relationship? Am J Psychiatry 151:1723–1734.
Schuckit MA, Irwin M, Brown SA (1990) The history of anxiety symptoms among 171 primary alcoholics. J Stud Alcohol 51:34–41.
Schuckit MA, Monteiro MG (1988) Alcoholism, anxiety and depression. Br J Addict 83:1373–1380.
Schweimer J, Fendt M, Schnitzler H-U (2005) Effects of clonidine injections into the bed nucleus of the stria terminalis on fear and anxiety behavior in rats. Eur J Pharmacol 507:117–124.
Scott KM, Korff M Von, Alonso J, Angermeyer MC, Benjet C, Bruffaerts R, Girolamo G De, Haro JM, Kessler RC, Kovess V, Ono Y, Ormel J, Posada-Villa J (2008) Childhood adversity, early-onset depressive/anxiety disorders, and adult-onset asthma. Psychosom Med 70:1035–1043.
See RE, Kruzich PJ, Grimm JW (2001) Dopamine, but not glutamate, receptor blockade in the basolateral amygdala attenuates conditioned reward in a rat model of relapse to cocaine-seeking behavior. Psychopharmacology 154:301–310.

Selye H (1936) A Syndrome produced by Diverse Nocuous Agents. Nature 138:32.
Seoane A, Tinsley CJ, Brown MW (2012) Interfering with Fos expression in rat perirhinal cortex impairs recognition memory. Hippocampus 22:2101–2113.
Shackman AJ, Fox AS, Oler JA, Shelton SE, Oakes TR, Davidson RJ, Kalin NH (2017) Heightened extended amygdala metabolism following threat characterizes the early phenotypic risk to develop anxiety-related psychopathology. Mol Psychiatry 22:724–732.
Shah MM (2012) HCN1 Channels : A New Therapeutic Target for Depressive Disorders ? Sci Signal 5:1–4.
Shaham Y, Erb S, Stewart J (2000a) Stress-induced relapse to heroin and cocaine seeking in rats: A review. Brain Res Rev 33:13–33.
Shaham Y, Highfield D, Delfs J, Leung S, Stewart J (2000b) Clonidine blocks stress-induced reinstatement of heroin seeking in rats: An effect independent of locus coeruleus noradrenergic neurons. Eur J Neurosci 12:292–302.
Shaham Y, Shalev U, Lu L, De Wit H, Stewart J (2003) The reinstatement model of drug relapse: History, methodology and major findings. Psychopharmacology 168:3–20.
Shaham Y, Stewart J (1994) Exposure to mild stress enhances the reinforcing efficacy of intravenous heroin self-administration in rats. Psychopharmacology 114:523–527.
Shaham Y, Stewart J (1995) Stress reinstates heroin-seeking in drug-free animals: An effect mimicking heroin, not withdrawal. Psychopharmacology 119:334–341.
Shalev U (2002) Neurobiology of Relapse to Heroin and Cocaine Seeking: A Review. Pharmacol Rev 54:1–42.
Shalev U, Erb S, Shaham Y (2010) Role of CRF and other neuropeptides in stress-induced reinstatement of drug seeking. Brain Res 1314:15–28.
Shalev U, Morales M, Hope BT, Yap J, Shaham Y (2001) Time-dependent changes in extinction behavior and stress-induced reinstatement of drug seeking following withdrawal from heroin in rats. Psychopharmacology 156:98–107.
Sharma S, Powers A, Bradley B, Ressler KJ (2016) Gene × Environment Determinants of Stress- and Anxiety-Related Disorders. Annu Rev Psychol 67:239–261.
Sharp FR, Sagar SM, Hicks K, Lowenstein D, Hisanaga K (1991) c-fos mRNA, Fos, and Fos-related antigen induction by hypertonic saline and stress. J Neurosci 11:2321–2331.
Shen W, Plotkin JL, Francardo V, Bezard E, Cenci MA, Surmeier DJ, Shen W, Plotkin JL, Francardo V, Ko WKD, Xie Z, Li Q, Fieblinger T (2015) M4 Muscarinic Receptor Signaling Ameliorates Striatal Plasticity Deficits in Models of L-DOPA- Induced Dyskinesia Article M4 Muscarinic Receptor Signaling Ameliorates Striatal Plasticity Deficits in Models of L-DOPA-Induced Dyskinesia. :762–773.
Shields AD, Wang Q, Winder DG (2009) alpha2A-adrenergic receptors heterosynaptically regulate glutamatergic transmission in the bed nucleus of the stria terminalis. Neuroscience 163:339–351.
Shimada S, Inagaki S, Kubota Y, Kito S, Funaki H, Takagi H (1989) Light and electron microscopic studies of calcitonin gene-related peptide-like immunoreactive terminals in the central nucleus of the amygdala and the bed nucleus of the stria terminalis of the rat. Exp Brain Res 77:217–220.
Shin KS, Rothberg BS, Yellen G (2001) Blocker state dependence and trapping in hyperpolarization-activated cation channels: evidence for an intracellular activation gate. J Gen Physiol 117:91–101.
Shinohara K, Watabe AM, Nagase M, Okutsu Y, Takahashi Y, Kurihara H, Kato F (2017)

Essential role of endogenous calcitonin gene-related peptide in pain-associated plasticity in the central amygdala. EurJNeurosci 46:2149–2160.
Sigurdsson T, Doyère V, Cain CK, LeDoux JE (2007) Long-term potentiation in the amygdala: A cellular mechanism of fear learning and memory. Neuropharmacology 52:215–227.
Silberman Y, Fetterly TL, Awad EK, Milano EJ, Usdin TB, Winder DG (2015) Ethanol Produces Corticotropin-Releasing Factor Receptor-Dependent Enhancement of Spontaneous Glutamatergic Transmission in the Mouse Central Amygdala. Alcohol Clin Exp Res 39:2154–2162.
Silberman Y, Matthews RT, Winder DG (2013) A corticotropin releasing factor pathway for ethanol regulation of the ventral tegmental area in the bed nucleus of of the stria terminalis. J Neurosci 33:950–960.
Silberman Y, Winder DG (2013) Corticotropin releasing factor and catecholamines enhance glutamatergic neurotransmission in the lateral subdivision of the central amygdala. Neuropharmacology 70:316–323.
Silinsky EM (1984) On the mechanism by which adenosine receptor activation inhibits the release of acetylcholine from motor nerve endings. J Physiol 346:243–256.
Singewald N, Salchner P, Sharp T (2003) Induction of c-Fos expression in specific areas of the fear circuitry in rat forebrain by anxiogenic drugs. Biol Psychiatry 53:275–283.
Sinha R, Catapano D, O'Malley S (1999) Stress-induced craving and stress response in cocaine dependent individuals. Psychopharmacology 142:343–351.
Sinha R, Fuse T, Aubin LR, O'Malley SS (2000) Psychological stress, drug-related cues and cocaine craving. Psychopharmacology 152:140–148.
Sinha R, Li CSR (2007) Imaging stress- and cue-induced drug and alcohol craving: Association with relapse and clinical implications. Drug Alcohol Rev 26:25–31.
Sinha R, Shaham Y, Heilig M (2011) Translational and reverse translational research on the role of stress in drug craving and relapse. Psychopharmacology 218:69–82.
Sink KS, Chung A, Ressler KJ, Davis M, Walker DL (2013a) Anxiogenic effects of CGRP within the BNST may be mediated by CRF acting at BNST CRFR1 receptors. Behav Brain Res 243:286–293.
Sink KS, Davis M, Walker DL (2013b) CGRP antagonist infused into the bed nucleus of the stria terminalis impairs the acquisition and expression of context but not discretely cued fear. Learn Mem 20:730–739.
Sink KS, Walker DL, Yang Y, Davis M (2011) Calcitonin gene-related peptide in the bed nucleus of the stria terminalis produces an anxiety-like pattern of behavior and increases neural activation in anxiety-related structures. J Neurosci 31:1802–1810.
Smith HR, Beveridge TJR, Nader MA, Porrino LJ (2016) Effects of abstinence from chronic cocaine self-administration on nonhuman primate dorsal and ventral noradrenergic bundle terminal field structures. Brain Struct Funct 221:2703–2715.
Smithers HE, Terry JR, Brown JT, Randall AD (2017) Aging-Associated Changes to Intrinsic Neuronal Excitability in the Bed Nucleus of the Stria Terminalis Is Cell Type-Dependent. Front Aging Neurosci 9:424.
Somerville LH, Wagner DD, Wig GS, Moran JM, Whalen PJ, Kelley WM (2013) Interactions between transient and sustained neural signals support the generation and regulation of anxious emotion. Cereb Cortex 23:49–60.
Somerville LH, Whalen PJ, Kelley WM (2010) Human bed nucleus of the stria terminalis indexes hypervigilant threat monitoring. Biol Psychiatry 68:416–424.

Sørensen AT, Cooper YA, Baratta M V, Weng F, Zhang Y, Ramamoorthi K, Fropf R, Laverriere E, Xue J, Young A, Schneider C, Rene C, Hemberg M, Yin JCP, Maier SF, Lin Y (2016) A robust activity marking system for exploring active neuronal ensembles. Elife 5:e13918.
Sørensen JB, Nagy G, Varoqueaux F, Nehring RB, Brose N, Wilson MC, Neher E (2003) Differential control of the releasable vesicle pools by SNAP-25 splice variants and SNAP-23. Cell 114:75–86.
Sparrow AM, Lowery-Gionta EG, Pleil KE, Li C, Sprow GM, Cox BR, Rinker JA, Jijon AM, Peňl J, Navarro M, Kash TL, Thiele TE (2012) Central neuropeptide y modulates binge-like ethanol drinking in C57BL/6J mice via Y1 and Y2 receptors. Neuropsychopharmacology 37:1409–1421.
Spencer SJ, Buller KM, Day TA (2005) Medial prefrontal cortex control of the paraventricular hypothalamic nucleus response to psychological stress: Possible role of the bed nucleus of the stria terminalis. J Comp Neurol 481:363–376.
Stein MB, Sareen J (2015) Generalized Anxiety Disorder. N Engl J Med 373:2059–2068.
Sterling P, Eyer J (1981) Biological basis of stress-related mortality. Soc Sci Med Part E Med Psychol 15:3–42.
Sterling P, Eyer J (1988) Allostasis: A New Paradigm to Explain Arousal Pathology. In: Handbook of Life Stress, Cognition and Health, pp.629–639.
Sterrenburg L, Gaszner B, Boerrigter J, Santbergen L, Bramini M, Roubos EW, Peeters BWMM, Kozicz T (2012) Sex-dependent and differential responses to acute restraint stress of corticotropin-releasing factor-producing neurons in the rat paraventricular nucleus, central amygdala, and bed nucleus of the stria terminalis. J Neurosci Res 90:179–192.
Stone LS, Vulchanova L, Riedl MS, Wang J, Williams FG, Wilcox GL, Elde R (1999) Effects of peripheral nerve injury on alpha-2A and alpha-2C adrenergic receptor immunoreactivity in the rat spinal cord. Neuroscience 93:1399–1407.
Strawn JR, Compton SN, Robertson B, Albano AM, Hamdani M, Rynn MA (2017) Extended Release Guanfacine in Pediatric Anxiety Disorders: A Pilot, Randomized, Placebo-Controlled Trial. J Child Adolesc Psychopharmacol 27:29–37.
Sugimura YK, Takahashi Y, Watabe AM, Kato F (2016) Synaptic and network consequences of monosynaptic nociceptive inputs of parabrachial nucleus origin in the central amygdala. J Neurophysiol 115:2721–2739.
Sun W, Rebec G V (2003) Lidocaine inactivation of ventral subiculum attenuates cocaine-seeking behavior in rats. J Neurosci 23:10258–10264.
Szücs A, Berton F, Nowotny T, Sanna P, Francesconi W (2010) Consistency and diversity of spike dynamics in the neurons of bed nucleus of stria terminalis of the rat: A dynamic clamp study. PLoS One 5.
Szücs A, Berton F, Sanna PP, Francesconi W (2012) Excitability of jcBNST neurons is reduced in alcohol-dependent animals during protracted alcohol withdrawal. PLoS One 7:1–11.
Taepavarapruk P, Phillips AG (2003) Neurochemical correlates of relapse to D-amphetamine self-administration by rats induced by stimulation of the ventral subiculum. Psychopharmacology 168:99–108.
Takahashi T, Forsythe ID, Tsujimoto T, Barnes- M, Takahashi T, Forsythe ID, Tsujimoto T, Barnes-davies M, Onodera K (1996) Presynaptic Calcium Current Modulation by a Metabotropic Glutamate Receptor. Science 274:594–597.
Tamagaki S, Suzuki T, Hagihira S, Hayashi Y, Mashimo T (2010) Systemic daily morphine enhances the analgesic effect of intrathecal dexmedetomidine via up-regulation of alpha 2

adrenergic receptor subtypes A, B and C in dorsal root ganglion and dorsal horn. J Pharm Pharmacol 62:1760–1767.
Taniguchi H, He M, Wu P, Kim S, Paik R, Sugino K, Kvitsani D, Fu Y, Lu J, Lin Y, Miyoshi G, Shima Y, Fishell G, Nelson SB, Huang ZJ (2011) A Resource of Cre Driver Lines for Genetic Targeting of GABAergic Neurons in Cerebral Cortex. Neuron 71:995–1013.
Tasan RO, Verma D, Wood J, Lach G, Hörmer B, de Lima TCM, Herzog H, Sperk G (2016) The role of Neuropeptide Y in fear conditioning and extinction. Neuropeptides 55:111–126.
Tedford HW, Zamponi GW (2006) Direct G Protein Modulation of Ca v 2 Calcium Channels. Pharmacol Rev 58:837–862.
Teicher MH, Anderson CM, Polcari A (2012) Childhood maltreatment is associated with reduced volume in the hippocampal subfields CA3, dentate gyrus, and subiculum. Proc Natl Acad Sci 109:E563–E572.
Thompson AM, Swant J, Gosnell BA, Wagner JJ (2004) Modulation of long-term potentiation in the rat hippocampus following cocaine self-administration. Neuroscience 127:177–185.
Thuault J, Constantinople CM, Nicholls R, Chen I, Zhu J, Panteleyev A, Vronskaya S, Nolan MF, Bruno R, Siegelbaum SA, Kandel ER (2013) Prefrontal Cortex HCN1 Channels Enable Intrinsic Persistent Neural Firing and Executive Memory Function. J Neurosci 33:13583–13599.
Tidey JW, Miczek KA (1997) Acquisition of cocaine self-administration after social stress: role of accumbens dopamine. Psychopharmacology 130:203–212.
Tillman RM, Stockbridge MD, Nacewicz BM, Torrisi S, Fox AS, Smith JF, Shackman AJ (2018) Intrinsic functional connectivity of the central extended amygdala. Hum Brain Mapp 39:1291–1312.
Tirumalai PS, Howells RD (1994) Regulation of calbindin-D2s K gene expression in response to acute and chronic morphine administration. Mol Brain Res 23:144–150.
Toda C, Kim JD, Impellizzeri D, Cuzzocrea S, Liu Z, Toda C, Kim JD, Impellizzeri D, Cuzzocrea S, Liu Z (2016) UCP2 Regulates Mitochondrial Fission and Ventromedial Nucleus Control of Glucose Article UCP2 Regulates Mitochondrial Fission and Ventromedial Nucleus Control of Glucose Responsiveness. Cell 164:872–883.
Torrisi S, O'Connell K, Davis A, Reynolds R, Balderston N, Fudge JL, Grillon C, Ernst M (2015) Resting state connectivity of the bed nucleus of the stria terminalis at ultra-high field. Hum Brain Mapp 36:4076–4088.
Tsay D, Dudman JT, Siegelbaum S a. (2007) HCN1 Channels Constrain Synaptically Evoked Ca2+ Spikes in Distal Dendrites of CA1 Pyramidal Neurons. Neuron 56:1076–1089.
Tully K, Li Y, Tsvetkov E, Bolshakov VY (2007) Norepinephrine enables the induction of associative long-term potentiation at thalamo-amygdala synapses. Proc Natl Acad Sci 104:14146–14150.
Turner R, Tjian R (1989) Leucine repeats and an adjacent DNA binding domain mediate the formation of functional cFos-cJun heterodimers. Science 243:1689–1694.
Turner RJ, Lloyd D a (2003) Cumulative adversity and drug dependence in young adults : racial / ethnic contrasts. Addiction 98:305–315.
Ulens C, Tytgat J (2001) Functional Heteromerization of HCN1 and HCN2 Pacemaker Channels. J Biol Chem 276:6069–6072.
Unnerstall JR, Kopajiq TA, Kuhar MJ (1994) Distribution of a2 agonist binding sites in the rat and human central nervous system: Analysis of some functional, antomic correlates of the pharmacologic effects of clonidine and related adrenergic agents. Brain Res Res Rev 7:69–

101.
Uzsoki B, Tóth M, Hernádi I (2011) Novelty response of rats determines the effect of prefrontal alpha-2 adrenoceptor modulation on anxiety. Neurosci Lett 499:219–223.
Vacher B, Funes P, Chopin P, Cussac D, Heusler P, Tourette A, Marien M (2010) Rigid analogues of the α2-adrenergic blocker atipamezole: Small changes, big consequences. J Med Chem 53:6986–6995.
Vardy E et al. (2015) A New DREADD Facilitates the Multiplexed Chemogenetic Interrogation of Behavior. Neuron 86:936–946.
Vazey EM, Aston-Jones G (2014) Designer receptor manipulations reveal a role of the locus coeruleus noradrenergic system in isoflurane general anesthesia. Proc Natl Acad Sci U S A 111:3859–3864.
Volkow ND, Fowler JS, Wolf AP, Hitzemann RJ, Dewey SS, Bendriem B, Alpert R, Hoff A (1991) Changes in brain glucose metabolism in cocaine dependence and withdrawal. Am J Psychiatry 148:621–626.
Vranjkovic O, Gasser PJ, Gerndt CH, Baker D a, Mantsch JR (2014) Stress-induced cocaine seeking requires a beta-2 adrenergic receptor-regulated pathway from the ventral bed nucleus of the stria terminalis that regulates CRF actions in the ventral tegmental area. J Neurosci 34:12504–12514.
Vranjkovic O, Hang S, Baker D a, Mantsch JR (2012) B-Adrenergic Receptor Mediation of Stress-Induced Reinstatement of Extinguished Cocaine-Induced Conditioned Place Preference in Mice: Roles for B1 and B2 Adrenergic Receptors. J Pharmacol Exp Ther 342:541–551.
De Vries TJ, Binnekade R, Mulder AH, Vanderschuren LJMJ (1998) Drug - induced reinstatement of heroin - and cocaine - seeking behaviour following long - term extinction is associated with expression of behavioural sensitization. Eur J Neurosci 10:3565–3571.
Vucicevic J, Srdic-Rajic T, Pieroni M, Laurila JMM, Perovic V, Tassini S, Azzali E, Costantino G, Glisic S, Agbaba D, Scheinin M, Nikolic K, Radi M, Veljkovic N (2016) A combined ligand- and structure-based approach for the identification of rilmenidine-derived compounds which synergize the antitumor effects of doxorubicin. Bioorganic Med Chem 24:3174–3183.
Waeber B, Nussberger J, Brunner H (1984) Effect of centrally acting antihypertensive drugs on the renin- angiotensin system and vasopressin . J Cardiovasc Pharmacol 6:799–802.
Wahl-Schott C, Biel M (2009) HCN channels: structure, cellular regulation and physiological function. Cell Mol Life Sci 66:470–494.
Walker DL, Davis M (1997) Double dissociation between the involvement of the bed nucleus of the stria terminalis and the central nucleus of the amygdala in startle increases produced by conditioned versus unconditioned fear. J Neurosci 17:9375–9383.
Walker DL, Davis M (2008) Role of the extended amygdala in short-duration versus sustained fear: A tribute to Dr. Lennart Heimer. Brain Struct Funct 213:29–42.
Walker DL, Toufexis DJ, Davis M (2003) Role of the bed nucleus of the stria terminalis versus the amygdala in fear, stress, and anxiety. Eur J Pharmacol 463:199–216.
Walton J, Byrum M, Shumaker A, Coury DL (2014) Prolonged Bradycardia and Hypotension Following Guanfacine Extended Release Overdose. J Child Adolesc Psychopharmacol 24:463–465 Available at: http://online.liebertpub.com/doi/abs/10.1089/cap.2014.0022.
Wanat MJ, Hopf FW, Stuber GD, Phillips PEM, Bonci a (2008) Corticotropin-releasing factor increases mouse ventral tegmental area dopamine neuron firing through a protein kinase C-

dependent enhancement of Ih. J Physiol 586:2157–2170.
Wang J, Chen S, Nolan MF, Siegelbaum SA (2002) Activity-dependent regulation of HCN pacemaker channels by cyclic AMP: Signaling through dynamic allosteric coupling. Neuron 36:451–461.
Wang J, Fang Q, Liu Z, Lu L (2006) Region-specific effects of brain corticotropin-releasing factor receptor type 1 blockade on footshock-stress-or drug-priming-induced reinstatement of morphine conditioned place preference in rats. Psychopharmacology 185:19–28.
Wang M, Ramos BP, Paspalas CD, Shu Y, Simen A, Duque A, Vijayraghavan S, Brennan A, Dudley A, Nou E, Mazer J a, McCormick D a, Arnsten AFT (2007) Alpha2A-adrenoceptors strengthen working memory networks by inhibiting cAMP-HCN channel signaling in prefrontal cortex. Cell 129:397–410.
Wang R, Macmillan LB, Fremeau RT, Magnus MA, Lindner J, Limbird LE (1996) Expression of alpha2-adrenergic receptor subtypes in the mouse brain: evaluation of spatial and temporal information imparted by 3 kb of 5' regulatory sequence for the alpha2a-AR-receptor gene in transgenic animals. Neuroscience 74:199–218.
Wang W, Wildes CP, Pattarabanjird T, Sanchez MI, Glober GF, Matthews GA, Tye KM, Ting AY (2017) A light- and calcium-gated transcription factor for imaging and manipulating activated neurons. Nat Biotechnol 35:864–871.
Wang X, Cen X, Lu L (2001) Noradrenaline in the bed nucleus of the stria terminalis is critical for stress-induced reactivation of morphine-conditioned place preference in rats. Eur J Pharmacol 432:153–161.
Weber T, Zemelman B V., McNew JA, Westermann B, Gmachl M, Parlati F, Söllner TH, Rothman JE (1998) SNAREpins: Minimal machinery for membrane fusion. Cell 92:759–772.
Weitlauf C, Egli RE, Grueter BA, Winder DG (2004) High-Frequency Stimulation Induces Ethanol-Sensitive Long-Term Potentiation at Glutamatergic Synapses in the Dorsolateral Bed Nucleus of the Stria Terminalis. J Neurosci 24:5741–5747.
Weitlauf C, Honse Y, Auberson YP, Mishina M, Lovinger DM, Winder DG (2005) Activation of NR2A-Containing NMDA Receptors Is Not Obligatory for NMDA Receptor-Dependent Long-Term Potentiation. J Neurosci 25:8386–8390.
Wells CA, Zurawski Z, Betke KM, Yim YY, Hyde K, Rodriguez S, Alford S, Hamm HE (2012) G Inhibits Exocytosis via Interaction with Critical Residues on Soluble N-Ethylmaleimide-Sensitive Factor Attachment Protein-25. Mol Pharmacol 82:1136–1149.
Westheimer G (1981) Postsynaptic inhibitory actions of catecholamines and opioid peptides in the bed nucleus of the stria terminalis. Exp Brain Res 41:264–270.
Wightman RM, Amatorh C, Engstrom RC, Hale PD, Kristensen EW, Kuhr WG, May LJ (1988) Real-time characterization of dopamine overflow and uptake in the rat striatum. Neuroscience 25:513–523.
Will MJ, Watkins LR, Maier SF (1998) Uncontrollable stress potentiates morphine's rewarding properties. Pharmacol Biochem Behav 60:655–664.
Willcocks AL, Mcnally GP (2013) The role of medial prefrontal cortex in extinction and reinstatement of alcohol-seeking in rats. Eur J Neurosci 37:259–268.
Williams JT, Henderson G, North RA (1985) Characterization of a2-adrenoreceptors which increase potassium conducance in rat locus coeruleus neurones. Neuroscience 14:95–101.
Williams SR, Mitchell SJ (2008) Direct measurement of somatic voltage clamp errors in central neurons. Nat Neurosci 11:790–798.

Wills TA, Klug JR, Silberman Y, Baucum AJ, Weitlauf C, Colbran RJ, Delpire E, Winder DG (2012) GluN2B subunit deletion reveals key role in acute and chronic ethanol sensitivity of glutamate synapses in bed nucleus of the stria terminalis. Proc Natl Acad Sci U S A 109:E278-87.

Wilson BC, Ingram CD (2003) Convergent effects of oxytocin and a δ-opioid agonist in the bed nuclei of the stria terminalis of the peripartum rat. Brain Res 991:267–270.

Winder DG, Conn PJ (1993) Activation of metabotropic glutamate receptors increases cAMP accumulation in hippocampus by potentiating responses to endogenous adenosine. J Neurosci 13:38–44.

Winder DG, Sweatt J (2001) Roles of serine/threonine phosphatases in hippocampel synaptic plasticity. Nat Rev Neurosci 2:461–474.

Wunsch AM, Yager LM, Donckels EA, Le CT, Neumaier JF, Ferguson SM (2017) Chemogenetic inhibition reveals midline thalamic nuclei and thalamo-accumbens projections mediate cocaine-seeking in rats. Eur J Neurosci 46:1850–1862.

Xia L, Nygard SK, Sobczak GG, Hourguettes NJ, Michael R, Bruchas MR (2017) Dorsal-CA1 Hippocampal Neuronal Ensembles Encode Nicotine-Reward Contextual Associations. Cell Rep 19:2143–2156.

Yasoshima Y, Sako N, Senba E, Yamamoto T (2006) Acute suppression, but not chronic genetic deficiency, of c-fos gene expression impairs long-term memory in aversive taste learning. Proc Natl Acad Sci U S A 103:7106–7111.

Yassa MA, Hazlett RL, Stark CEL, Hoehn-Saric R (2012) Functional MRI of the amygdala and bed nucleus of the stria terminalis during conditions of uncertainty in generalized anxiety disorder. J Psychiatr Res 46:1045–1052.

Yasui Y, Breder CD, Saper CB, Al YET (1991) Autonomic Responses and Efferent Pathway From the Insular Cortex in the Rat. J Comp Neurol 303:355–374.

Yin HS, Lai CC, Tien TW, Han SK, Pu XL (2010) Differential changes in cerebellar transmitter content and expression of calcium binding proteins and transcription factors in mouse administered with amphetamine. Neurochem Int 57:288–296.

Yiu AP, Mercaldo V, Yan C, Richards B, Rashid AJ, Hsiang HL, Pressey J, Mahadevan V, Tran MM, Kushner SA, Woodin MA, Frankland PW, Josselyn SA (2014) Article Neurons Are Recruited to a Memory Trace Based on Relative Neuronal Excitability Immediately before Training. Neuron 83:722–735.

Yoon E-J, Hamm HE, Currie KPM (2008) G protein betagamma subunits modulate the number and nature of exocytotic fusion events in adrenal chromaffin cells independent of calcium entry. J Neurophysiol 100:2929–2939.

Yoon E, Gerachshenko T, Spiegelberg BD, Alford S, Hamm HE (2007) Gby Interferes with Ca2+ -Dependent Binding of Synaptotagmin to the Soluble N -Ethylmaleimide-Sensitive Factor Attachment Protein Receptor (SNARE) Complex. Mol Pharmacol 72:1210–1219.

Zhang X lei, Upreti C, Stanton PK (2011) Gβγ and the C terminus of SNAP-25 are necessary for long-term depression of transmitter release. PLoS One 6:e20500.

Zhang Y, Jiang Y, Shao S, Zhang C, Liu F, Wan Y (2017) Inhibiting medial septal cholinergic neurons with DREADD alleviated anxiety-like behaviors in mice. Neurosci Lett 638:139–144.

Zhao Y, Fang Q, Straub SG, Lindau M, Sharp GWG (2010) Noradrenaline inhibits exocytosis via the G protein beta-gamma subunit and refilling of the readily releasable granule pool via the alphai1/2 subunit. J Physiol 588:3485–3498.

Zhong P, Vickstrom CR, Liu X, Hu Y, Yu L, Yu H, Liu Q (2018) HCN2 channels in the ventral tegmental area regulate behavioral responses to chronic stress. Elife 7:e32420.
Zhu Y, Wienecke CFR, Nachtrab G, Chen X (2016) A thalamic input to the nucleus accumbens mediates opiate dependence. Nature 530:219–222.
Zirlinger M, Anderson DJ (2003) Molecular dissection of the amygdala and its relevance to autism. Genes Brain Behav 2:282–294.
Zirlinger M, Kreiman G, Anderson DJ (2001) Amygdala-enriched genes identified by microarray technology are restricted to specific amygdaloid subnuclei. Proc Natl Acad Sci U S A 98:5270–5275.
Zislis G, Desai T V., Prado M, Shah HP, Bruijnzeel AW (2007) Effects of the CRF receptor antagonist d-Phe CRF(12-41) and the α2-adrenergic receptor agonist clonidine on stress-induced reinstatement of nicotine-seeking behavior in rats. Neuropharmacology 53:958–966.
Zurawski Z, Rodriguez S, Hyde K, Alford S, Hamm HE (2016) G beta gamma binds to the extreme C terminus of SNAP25 to mediate the action of G(i/o)-coupled G protein-coupled receptors. Mol Pharmacol 89:75–83.